Preferred Skin Colour Reproduction

Huanzhao Zeng

Submitted in accordance with the requirements for the degree of
Doctor of Philosophy

The University of Leeds
Department of Colour Science

September, 2011

The candidate confirms that the work submitted is his own and that appropriate credit has
been given where reference has been made to the work of others.

This copy has been supplied on the understanding that it is copyright material and that no
quotation from the thesis may be published without proper acknowledgement.

Acknowledgements

Abstract

The memory colour reproduction is an important factor in judging image quality of photographic images of real life scenes. As the most important memory colour category, skin tone was extensively studied for preferred colour reproduction in this research. The methodology to study skin colour preference was then applied to study the colour preference of two other important colour categories: green foliage and blue sky.

There are three essential parts for preferred skin colour enhancement: 1) building a skin colour model to detect skin colours or skin pixels; 2) finding a preferred skin colour region or a preferred skin colour centre; and 3) developing an algorithm to morph skin colours toward the preferred skin colour region. This study for skin colour enhancement started with the mathematical modelling of the skin colour region for skin colour detection. The modelling of skin colours was then applied to adjust skin colours of test images for psychophysical experiments that were to determine a preferred skin colour region. Finally, the skin colour modelling and the preferred skin colour centres were applied to adjust skin colours of digital photographic images for preferred colour reproduction.

Two approaches were developed to model the skin colour distribution for skin colour detection. The first approach was to model a local colour region for general applications. A convex hull is constructed to fit the geometrical shape of a local region, and then the convex hull is approximated with mathematical formulae. The formulations and data fitting are adjusted with interactive 3-D visualization. The approach is flexible for fitting data gamut with various mathematical forms for different purposes.

The other approach was to model skin colours with elliptical shapes. Three elliptical skin colour models were developed for skin colour detection. The first one is to model the skin colour cluster using a single ellipse ignoring the lightness (or luminance) dependency. It is simple and efficient, and the skin colour detection accuracy may be adequate for many applications. In the second model, the skin colour ellipse is adapted to different lightness so that the shape of the ellipse fits the skin colour cluster more accurately. The model is more complex to train and is less efficient in computation, but it is more accurate in skin colour detection. In the third method, an ellipsoid is trained to fit the skin colour cluster. It is almost as simple to train as the first model, but the skin colour detection accuracy is improved. Finally, these models were applied to train mixed skin colours, African skin colours, Caucasian skin colours, and Asian skin colours.

The results of skin colour modelling were applied to guide psychophysical experiments to determine preferred skin colours for skin colour enhancement. A series of psychophysical experiments were conducted to study skin colour preference of mixed culture background; skin colour preference by ethnicity and skin colour preference across ethnicities. The results reveal that preferred skin colours are more chromatic than real skin colours; observer variances in skin colour preference are larger in chroma than in hue; the preferred skin colour centre for mixed skin colours is about (21, 24) for CIE a*b* with a hue angle of 49° in D50 illuminant; Orientals prefer slightly less chromatic skin colours than Africans and Caucasians; and preferred skin colour variations in Africans are higher than the variations in Caucasians and the variations in Orientals. In cross-culture preference, Orientals consistently prefer slight less chromatic Oriental, Caucasian, and African skin colours than Caucasians and Africans, and Africans prefer more chromatic Caucasian and Oriental skin colours than Caucasians and Orientals. Comparison of preferred skin colour ellipses in CIELAB and CAM02-UCS reveals that CAM02-UCS is more uniform than CIELAB in the skin colour region.

Preferred skin colour enhancement algorithms were developed for skin colour enhancement in this research. The first method applies a static skin colour model to detect skin colours, and morphs skin colours toward a preferred skin colour centre. Psychophysical experimental results validate that the method of preferred skin colour enhancement effectively identifies skin colours without face recognition, improves the skin colour preference, and does not objectionably affect preferred skin colours in original images. The second method, skin colour enhancement using face box information, was proposed to further improve the result of skin colour enhancement. The skin colour distribution of face boxes were used to adjust the skin colour modelling and to adjust the coefficients for skin colour enhancement. The latter approach is more effective for enhancing skin colours that are far off from normal skin colours. Lastly, a new algorithm to morph skin colours was proposed.

The method to build elliptical skin colour models was further applied to model colour regions of green foliages and blue skies of photographic images for colour detection and enhancement. Elliptical colour models for these two colour regions were trained and were used to detect green foliage and blue sky colours.

The training results of the elliptical colour modelling of skin, green foliage, and blue sky of photographic images in CIELAB and CAM02-UCS were analysed to study these three memory colour objects and to study the colour space uniformity between CIELAB and CAM02-UCS.

Abbreviations

CMT   Colour Masker Tool

CRT   Cathode Ray Tube

ICC   International Color Consortium

LCD   Liquid Crystal Display

LUT   Lookup Table

PCS   Profile Connection Space (in ICC Colour Management System)

PSCC Preferred Skin Colour Centre

SPD   Spectral Power Distribution

UCS   Uniform Colour Space

ROC   Receiver Operating Characteristics

Contents

List of Figures

List of Tables

Chapter 1
Introduction

With the widespread availability of digital imaging devices to replace conventional analog devices, coupled with the meteoric growth of the Internet, colour imaging is experiencing a major revolution. People are finding more and more innovative ways to create and share digital images. The transformation from analog imaging to digital imaging makes colour image processing easier and easier. Due to exponential increasing volumes in digital photos, automatic colour image enhancement becomes an essential role for improving image quality. One aspect to improve the perceived image quality of daily life photos is to improve the colour rendering of images. Preferred colour rendering to appreciate observers is an important factor in enhancing the image quality of photographic images. In judging the colour reproduction of a photographic image, people compare memory colours of the image with memory colours of objects instead of comparing memory colours of the image with their real colours. Memory colours, especially skin tones, play an important role for preferred colour reproduction.

Since preferred colours are different from their original colours, preferred colour reproduction should be deviated from colorimetric colour reproduction. This is especially true for memory colours. To understand how to enhance memory colours for preferred colour reproduction, extensive studies on important memory colour categories were undertaken. This research was focused on the study of skin colour preference that included modelling skin colours for skin colour detection; determining preferred skin colours for preferred skin colour enhance of photographic images; and applying skin colour detection models and preferred skin colours for skin colour enhancement of photographic images. Colour detection and enhancement of green foliage and blue sky were briefly studied as well.

1.1 Aims and Scope

The goal of the research is to investigate the colour preference of memory colours, to find out preferred skin colours for preferred colour reproduction, to develop algorithms for automatic preferred skin colour reproduction, and to apply the methodology of skin colour preference to study colour preferences of green foliage and blue sky.

To achieve this goal, the following specific aims were established:

1. To establish a skin colour detection model to detect skin colours for studying skin colour enhancement;

2. To study skin colour preference of mixed culture background;

3. To investigate the differences of skin colour preferences among Africans, Caucasians, and Orientals;

4. To develop algorithms to automatically detect skin colours and to enhance skin colours for preferred skin colour reproduction; and

5. To study whether the method of skin colour preferencing can be applied to green foliage and blue sky colours.

1.2 Thesis Structure

This thesis includes seven further chapters which are organised as below:

Chapter 2: Literature Survey

Literatures relevant to this research were reviewed in five subject areas (human colour perception, numerical colour, colour appearance model, colour reproduction of digital images, preferred memory colour reproduction). At the end of the review, areas for research were determined.

Chapter 3: Modelling Skin Colours for Skin Colour Enhancement

Skin colour models for skin colour detection and skin colour enhancement were developed.

Chapter 4: Psychophysical Experiments to Study Preferred Skin Colours

Psychophysical experiments were conducted to study skin colour preferences of different ethnical backgrounds. The results were to be applied to automatic skin colour enhancement.

Chapter 5: Developing Preferred Skin Colour Enhancement Algorithms

Algorithms for preferred skin colour enhancement were presented.

Chapter 6: Verifying Preferred Skin Colour Enhancement

Psychophysical experiments were conducted to verify the effectiveness of skin colour enhancements.

Chapter 7: Green Foliage and Blue Sky Colours

The elliptical model for skin colour detection was applied to train colour detection models for detecting green foliage and blue sky.

<u>Chapter 8: Conclusions</u>

A summary of the findings of modelling skin colours from chapter 3, preferred skin colours for colour enhancement of photographic images from chapter 4, skin colour enhancement and verification from chapters 5 and 6, and foliage and sky colour detection from chapter 7 were given together with suggestions for future work.

1.3 Summary of Contributions to Knowledge

The present work made significant contributions to the study of skin colour preference and industry applications. These are summarised below:

- Established a robust and novel method for constructing memory colour databases to study memory colours including skin colours of three ethnic types, grass and sky;

- Proposed a new method to model memory colours using convex hull and 3-D gamut visualisation;

- Developed new skin colour models (lightness-dependent ellipse model and ellipsoid model) and trained them for skin colour detection and enhancement;

- Conducted experiments that lead to findings of preferred skin colours of different culture backgrounds;

- Developed new skin colour enhancement algorithms to apply in practice;

- Successfully applied the method of elliptical skin colour modelling to model green foliage colours and blue sky colours.

Following publications were produced in the course of this research:

1. Huanzhao Zeng and Ronnier Luo, "Chinese Skin Color Preference for Preferred Color Reproduction of Photographic Images", to be published. Referred to Section 4.3.

2. Huanzhao Zeng and Ronnier Luo, "Green grass and blue sky colour modelling and preferred colour adjustment for printing", to be published. Referred to Chapter 7.

3. Huanzhao Zeng and Ronnier Luo, "A New Preferred Skin Color Enhancement Method for Photographic Colour Reproduction", IS&T/SPIE 2012 Electronic Imaging Conference: Color Imaging:

Device-Independent Color, Color Hardcopy, and Graphic Arts. Referred to Section 5.2.

4. Huanzhao Zeng and Ronnier Luo, "Preferred Skin Colours of African, Caucasian, and Oriental", IS&T/SID 19th Color Imaging Conference, 2011. Referred to Section 4.4.

5. Huanzhao Zeng and Ronnier Luo, "Colour and Tolerance of Preferred Skin Colours on Digital Photographic Images", to appear in Color Research and Application, 2011. Referred to Sections 4.2 and 4.3.

6. Huanzhao Zeng and Ronnier Luo, "A Preferred Skin Color Enhancement Method for Photographic Colour Reproduction", Proc. SPIE: Color Imaging: Device-Independent Color, Color Hardcopy, and Graphic Arts, 786613 1-9, (2011). Referred to Section 5.1.

7. Huanzhao Zeng and Ronnier Luo, "Skin Color Modeling of Digital Photographic Images", Journal of Imaging Science and Technology, 55(3): 030201 – 1-12, 2011. Referred to Sections 3.3 to 3.8.

8. Huanzhao Zeng and Ronnier Luo, "Colour and Tolerance for Preferred Skin Colours", IS&T/SID 18th Color Imaging Conference, 190-195 (2010). Referred to Section 4.2.

9. Huanzhao Zeng and Ronnier Luo, "Modelling Memory Color Region for Preference Color Reproduction", Proc. SPIE: Color Imaging: Device-Independent Color, Color Hardcopy, and Graphic Arts XV, Vol. 7528, 752808 1-11, (2010). Referred to Section 3.2.

10. Huanzhao Zeng and Ronnier Luo, "Modelling Skin Colours for Preferred Colour Reproduction", IS&T/SID 17th Color Imaging Conference, 175-180 (2009). Referred to Sections 3.3 to 3.7.

Chapter 2
Literature Survey

This chapter provides background information and extensive overview of research that is relevant to the thesis. It is divided into following sections:

2.1. Human colour perception

2.2. The Numerical Colour

2.3. Colour Appearance Model: CIECAM02

2.4. Preferred Colour Reproduction of Digital Images

2.5. Conclusion Remark

The sections 2.1 to 2.3 are the overview of human colour perception and colour science theories. Section 2.4 explores the progress in the research related to preferred colour reproduction, where skin colour reproduction is the focus of the topic. Summary of the research in the field of memory colour reproduction and discussion of topics that are most relevant to the research in the field is followed in the final section.

2.1 Human colour perception

2.1.1 The Nature of Light

Light is the basis for human vision. Without light, we are all left in the dark. But what is light? The light (or visible spectrum) is the portion of the electromagnetic spectrum that is visible to the human eye. A typical human eye responds to wavelengths in air from about 380 to 730 nanometres (nm). Our visual system perceives this range of light wave frequencies as a smoothly varying rainbow of colours from shortest to longest wavelength: violet, blue, green, yellow, orange, and red. Although the spectrum is continuous and there are no clear boundaries between one colour and the next, the ranges may be used as an approximation. Ultraviolet radiation has a shorter wavelength than the visible violet light. Infrared radiation has a longer wavelength than visible red light. The white light is a mixture of the colours of the visible spectrum. A total absence of light is sensed as black.
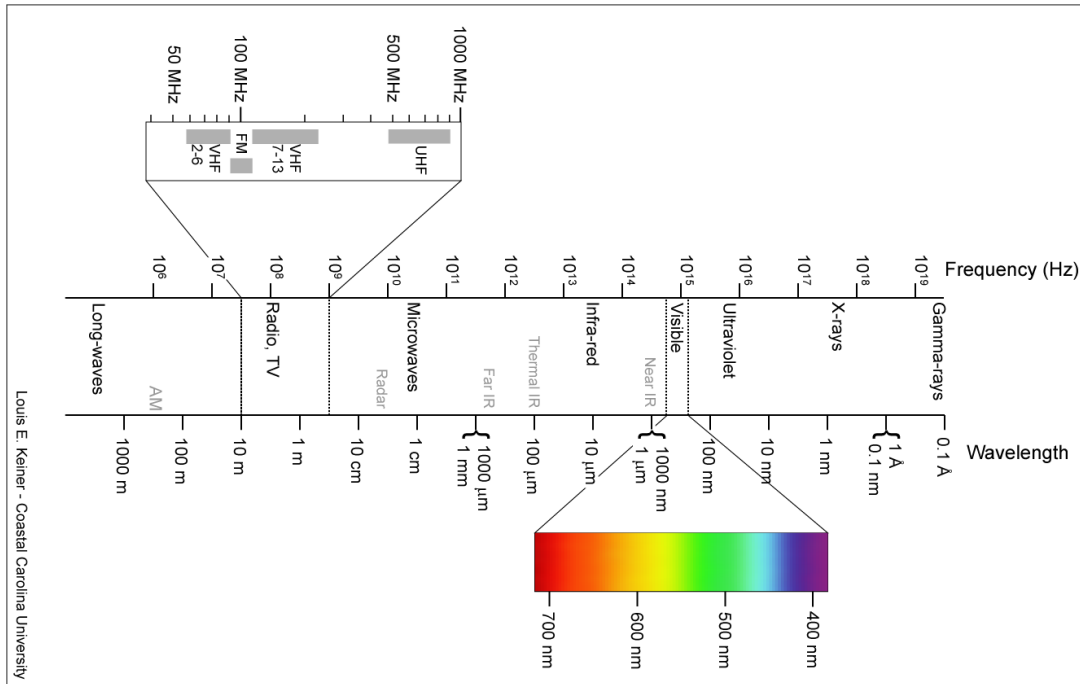
Fig. 2.1.1-1 The electromagnetic spectrum
(http://scipp.ucsc.edu/~haber/ph5B/Electromagnetic-Spectrum-3.png)

All light travels at the same speed in a vacuum. The speed of light within a material is lower than the speed of light in vacuum, and the ratio of speeds is known as the refractive index of the material. Because the refractive index (and thus the speed) of a wave in a material depends on its frequency, light consisting of multiple frequencies - for instance white light - will be dispersed at the interface between the material and air or vacuum. Both water and glass can be used to demonstrate dispersion; a glass prism yields an optical spectrum from white light, and rainbows are an ideal example of natural refraction of the visible spectrum.

2.1.2 The Human Colour Vision

2.1.2.1 Colour Perception by Eye

A sketch of the anatomical components of the human eye is shown in Fig. 2.1.2.1-1. The human eye has a simple two element lens. The cornea is the front or outer element and the lens is the back or inner element. The amount of light entering the eye is controlled by the iris which lies in between the two. The light passes through a clear gel called the vitreous humour and creates an inverted image on the retina at the back of the eyeball. The retina is the light sensitive part of the eye. Its surface has millions of photoreceptors. These photoreceptors sense the light and pass electrical signals indicating its presence through the optic nerve to stimulate the brain.
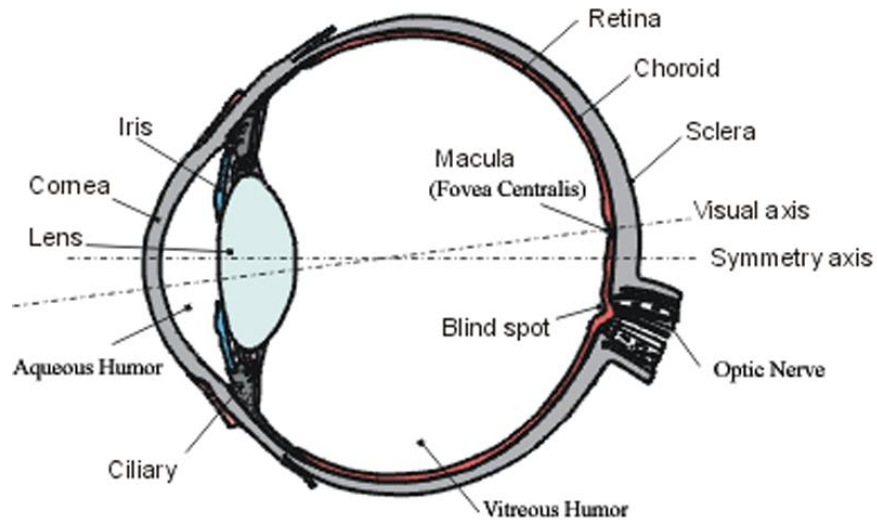
Fig. 2.1.2.1-1 A sketch of a cross section of the human eye (modified from http://info.tuwien.ac.at/iflt/safety/gif/s1_fig35.gif)

There are two types of photoreceptors, rods and cones. The rod vision is coarse but acute. It does not provide a sharp image. The rods are sensitive to very low levels of light but are monochromatic and cannot see colour. This is the reason that at very low light levels, humans see things in black and white.

The retina contains three types of cones. Different light sensitive pigments within each of these three types responds to different wavelengths of light. The three cones are maximally receptive to short, medium, and long wavelengths of light and are therefore usually called S-, M-, and L-cones (short, medium, and long cones). Cones operate only in relatively bright light, but they provide us with sharp images and enable us to see colours.
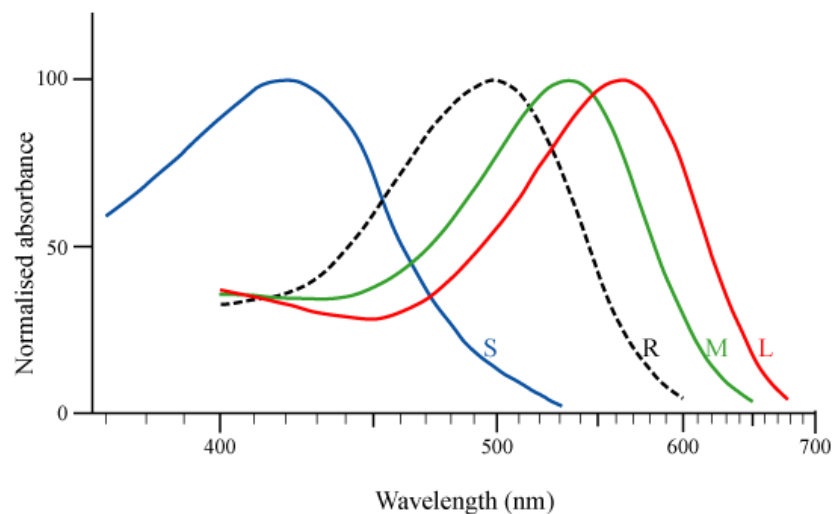
Fig. 2.1.2.1-2 Normalised absorbance of S, M, and L cones, and rods (http://www.jpse.co.uk/sensory/images/Cone-response.png)

At the centre of the retina is an area called the fovea, which has no blood vessels. Primarily cones are packed tightly in the fovea, so that it has the highest visual resolution.

2.1.2.2 Colour Perception by Brain

The eye flips the image of the world. The retina distorts the image that falls on the fovea. The images from the two eyes are combined and processed by a part of the brain known as visual cortex, which is part of the outermost layer of the brain. Visual cortex is broken down into five areas, labelled V1, V2, V3, V4, and MT (or V5). V1 is sometimes called striate cortex, primary visual cortex, or area 17. The other visual areas are referred to as extrastriate cortex. The visual cortex is located at the dorsal pole of the occipital lobe; more simply put, at the lower rear of the brain. An overall pathway of the human visual pathway is shown in Fig. 2.1.2.2-2.
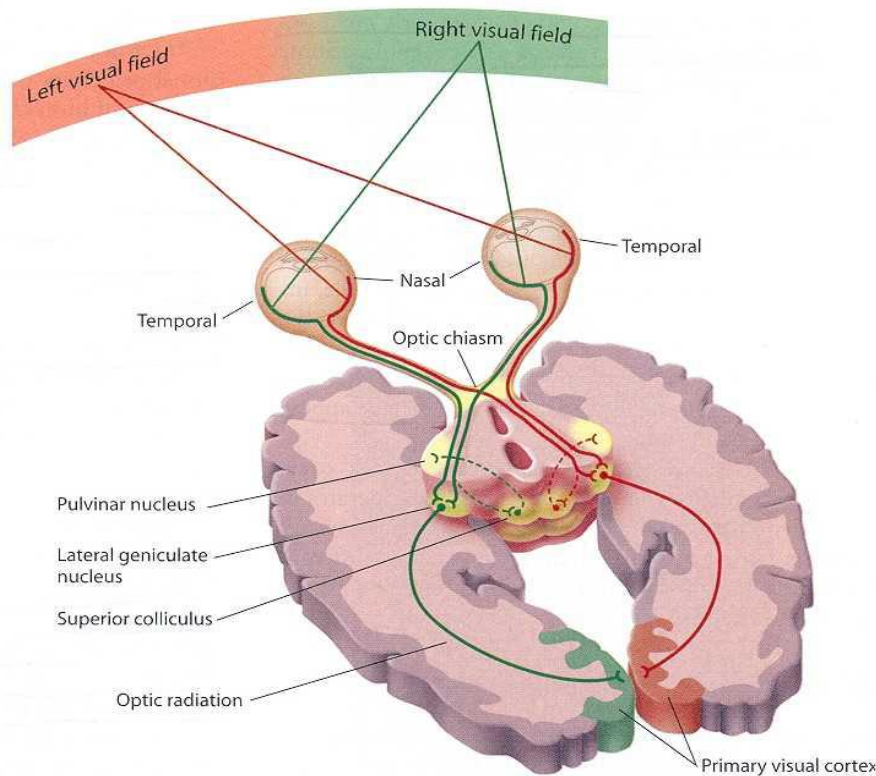
Fig. 2.1.2.2-1 A sketch diagram of the visual pathway
(http://thebrain.mcgill.ca/flash/index_i.html)

From the V1 blobs, colour information is sent to cells in the second visual area, V2. Neurons in V2 then synapse onto cells in area V4. Besides colour sensitivity, V4 neurons have been shown to be very sensitive to the shape of stimuli, curvature, and stereo-scopic depth. Neurons in V4 provide input to the inferior temporal lobe, "IT" cortex which is thought to integrate colour information with shape and form, although it has been difficult to define the appropriate criteria for

this claim. Despite this murkiness, it has been useful to characterise this pathway (V1 > V2 > V4 > IT) as the ventral stream or the "what pathway", distinguished from the dorsal stream ("where pathway") that is thought to analyse motion, among many other features (Lamme et al. 1998).
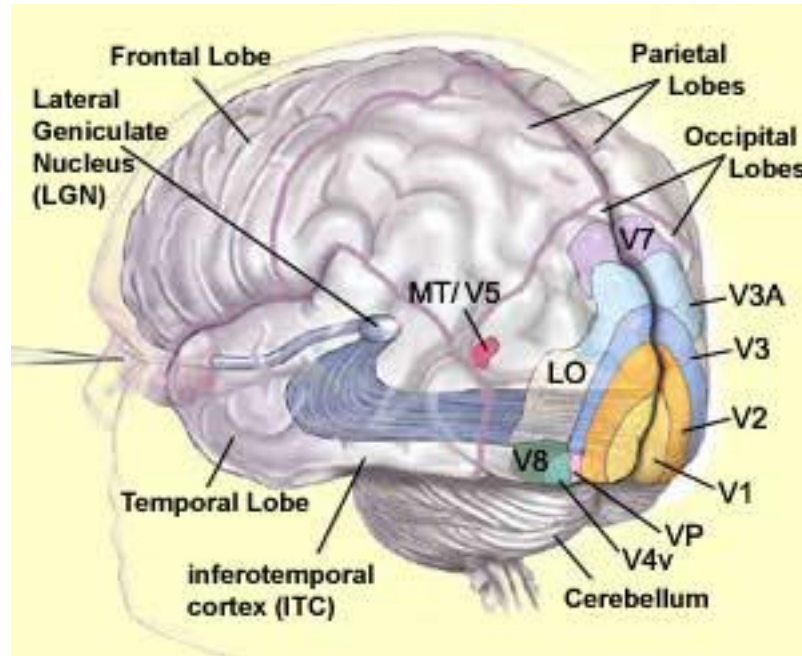
Fig. 2.1.2.2-2 The visual pathway (http://thebrain.mcgill.ca/flash/index_i.html)

Some controversy still exists regarding the exact extent of area V3, with some researchers proposing that the cortex located in front of V2 may include two or three functional subdivisions (Rosa and Tweedale 2000, Braddick et al. 2001).

Visual area V5, also known as visual area MT (middle temporal), is thought to play a major role in the perception of motion, the integration of local motion signals into global perceptions and the guidance of some eye movements (Born and Bradley 2005). MT is connected to a wide array of cortical and subcortical brain areas. Its inputs include the visual cortical areas V1, V2, and dorsal V3 (dorsomedial area) (Felleman and Essen 1991, Ungerleider and Desimone 1986), the koniocellular regions of the LGN, and the inferior pulvinar (Sincich et al. 2004).

2.1.3 Theories of Colour Vision

Two complementary theories of colour vision are the trichromatic theory and the opponent process theory. The Young–Helmholtz theory, proposed in the 19th century by Thomas Young and Hermann von Helmholtz, is a theory of trichromatic colour vision - the manner in which the photoreceptors in the eyes of humans and other primates work to enable colour vision (Goldstein 2007). In 1802, Young

postulated the existence of three types of photoreceptors (now known as cone cells) in the eye, each of which was sensitive to a particular range of visible light (Young 1802, Young et al. 1845). Hermann von Helmholtz developed the theory further in 1850: that the three types of cone photoreceptors could be classified as short-preferring (blue), middle-preferring (green), and long-preferring (red), according to their response to the wavelengths of light striking the retina (Helmholtz 1850). The relative strengths of the signals detected by the three types of cones are interpreted by the brain as a visible colour. The theory was proved over a century later in a 1983 experiment by Dartnall, Bowmaker, and Mollon, when microspectro-photopic readings of single eye cone cells were obtained (Eysenck and Keane 2005).

Hering proposed the opponent process theory in 1872 (Hering 1964). Hering looked more at qualitative aspects of colour and said there were six primary colours, coupled in three pairs: red-green, yellow-blue and white-black. Any receptor that is turned off by one of these colours is excited by its coupled colour. This results in six different receptors. The theory also explains afterimages. It was rehabilitated in the 1970s when Edwin Land developed the Retinex theory stating that whereas Helmholtz's colours hold for the eye, in the brain the three colours are translated into six (Land 1977).

The trichromatic theory and the opponent theory are complementary and explain processes that operate at different levels of the visual system. In summary, the trichromatic theory and the opponent theory are both correct. The human colour perception initials with the trichromatic vision in photo receptors, and later enters higher levels of opponent process in brain. Both theories describe different stages in visual physiology.

2.1.4 Basic Perceptual Colour Attributes

There are three basic perceptual attributes, brightness, hue, and colourfulness, and two relative colour attributes, lightness and chroma. According to Hunt (1998), these are defined as:

Brightness: Attribute of a visual sensation according to which an area appears to exhibit more or less light.

Hue: Attribute of a visual sensation according to which an area appears to be similar to one, or to proportions of two, of the perceived colours red, yellow, green, and blue.

Colourfulness: Attribute of a visual sensation according to which an area appears to exhibit more or less of its hue.

Lightness: The brightness of an area judged relative to the brightness of a similarly illuminated area that appears to be white or highly transmitting.

Chroma: The colourfulness of an area judged in proportion to the brightness of a similarly illuminated area that appears to be white or highly transmitting.

Lightness and chroma reflect visual strengths as the human visual perception adapts to a white point.

2.1.5 Adaptation and Colour Appearance Phenomena

2.1.5.1 Light/Dark Adaptation

Adaptation is a remarkable ability of the visual system to automatically adjust its sensitivity to accommodate a range of illumination greater than 10 orders of magnitude from dim to bright sunlight (Boynton 1979). In a quick first step, adaptation begins with the control of the light entering the eye by the iris. While the main purpose of the iris is to control the spatial quality of an image formed by the lens on the retina, its opening and closing does provide a crude adaptation mechanism over a range of only 4:1 to about 16:1 on a time scale of seconds (Fulton 2005). In a second step, the receptive cells on the retina of the eye change their actual sensitivity. This step is a slower process. The change between rod and cone vision is one factor. At low levels of illumination (<0.1 lux), the rods is more sensitive and more numerous than cones and may function alone. At high level of illumination (>10 lux), the response is only by cones. It takes up to about 30 minutes to complete dark adaptation. By contrast, it takes in the order of minutes to adapt from scotopic vision to photopic vision (Chien et al. 2000). Gain control in retinal photoreceptors and cells, and retinal pigment bleaching are also mechanisms for adaptation. The complex neural reaction in the visual cortex might play higher level of mechanism for adaptation.

2.1.5.2 Chromatic Adaptation

Chromatic adaptation is the ability of the human visual system to discount the colour of a light source and to approximately preserve the appearance of an object (Fairchild 1998). For example, a white piece of paper appears to be white whenever viewed under sky light and tungsten light.

Since there are several types of receptive cells in the eye, which are sensitive to different bands in the visible spectrum, the adaptation also manages the "white balance" of the eye, by chromatic adaptation. If the new lighting situation has a different colour temperature (e.g. there is an increased amount of red light relative to the total amount of light), the cells responsible for sensing red light will reduce their

sensitivity relative to the sensitivity of the other cells. As a result, a white surface will again appear white to the observer after a certain time, although it reflects a proportionally increased amount of red light.

2.1.5.3 Basic Colour Appearance Phenomena

The colour appearance of a test stimulus is influenced by changing the luminance, colours, and special properties of the background and surround. A few basic phenomena are briefly described here.

Simultaneous contrast and Induction: Two colours, side by side, interact with one another and change our perception accordingly. The effect of this interaction is called simultaneous contrast (Luo et al. 1995). Since we rarely see colours in isolation, simultaneous contrast affects our sense of the colour that we see. Fig. 2.1.5.3-1 shows several examples of the perceptual effect of simultaneous contrast. In (a), three small gray boxes have the same brightness. Surround a colour with a lighter colour and it will appear darker. Surround a colour with a darker colour and it will appear lighter. In (b), two smaller boxes have the same colour value. Surround a colour with a less saturated colour and it will appear more saturated. Surround a colour with a more saturated colour and it will appear less saturated. In (c), three smaller pink rectangles have the same colour value. Surround a colour with different colour backgrounds and it will appear different. Krauskopf et al. (1986) developed a method to measure simultaneous contrast, or chromatic induction. However, the method did not predict the outcome of their experiments. They concluded that simultaneous contrast was a consequence of interaction within higher-level chromatic mechanisms. Harrar and Vienot (2005) studied the spatio-chromatic induction by the neighbouring image and found that the induction differed from different neighbouring images.

Crispening: Crispening is the effect that causes an increase in perceived colour-difference when the background of the two stimuli is close to the colour of the stimuli. For example, the visual colour difference between two grey patches looks larger if they are on the grey background than they are on white or black background (Cui et al. 2001).

Hunt Effect: Hunt (1952) found that the colourfulness of an object increases due to the increase of luminance. For example, a typical outdoor scene appears more colourful in bright sunlight than it does on a dull day.

Stevens Effect: Stevens and Stevens (1963) found an increase in brightness (or lightness) contrast with an increasing luminance. As the luminance level increases, darker colours appear darker and lighter colours appear lighter.

Surround Effect: Bartleson and Breneman (1967) found that the perceived contrast in colourfulness and brightness increased with increasing luminance level of the surround. This effect is very important for cross-media colour reproduction.

Helmholtz-Kohlrausch effect: Helmholtz-Kohlrausch effect shows that brightness changes as a function of saturation (Wyszecki and Stiles 1982, Nayatani and Nakajima 1996). As a stimulus becomes more saturated at a constant luminance, its perceived brightness increase. Helmholtz-Kohlrausch effect is a function of hue angle as well (Fairchild 1998). It is less noticeable for yellows than for purples, for instance.
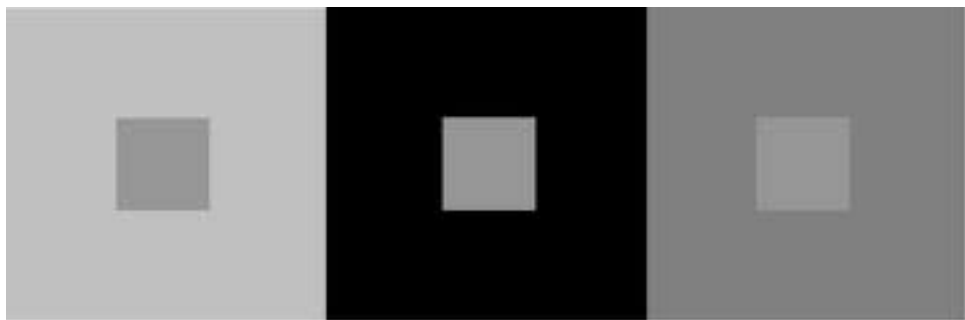
(a)
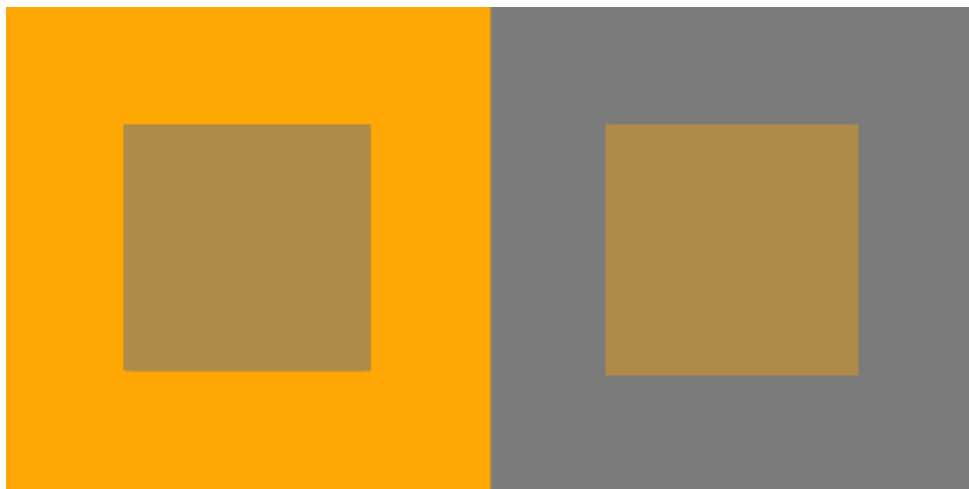
(b)
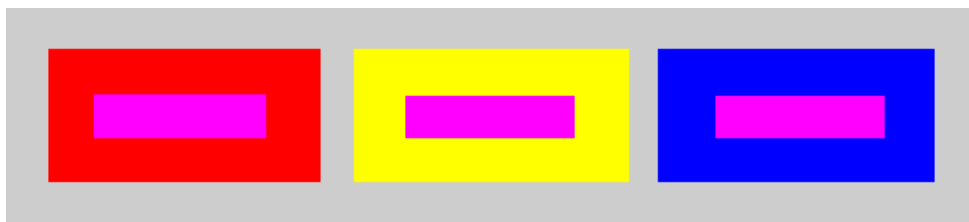
(c)

Fig. 2.1.5.3-1 Examples of simultaneous Contrast

2.2 The Numerical Colour

A human perceived colour may be expressed mathematically using three numbers: the extents to which each of the three types of cones is stimulated. Thus a human perceived colour may be thought of as a point in 3-dimensional Euclidean space. Since each wavelength λ stimulates each of the three types of cone cells to a known extent, these extents may be represented by three functions, $s(\lambda)$, $m(\lambda)$, $l(\lambda)$ corresponding to the response of the S, M, and L cone cells, respectively.

Finally, since a beam of light can be composed of many different wavelengths, to determine the extent to which a physical light $C(\lambda)$ stimulates each cone cell, we must calculate the integral (with respect to λ) over the interval $[\lambda_{min}, \lambda_{max}]$:

$$S = \int_{\lambda_{min}}^{\lambda_{max}} C(\lambda) \cdot s(\lambda) d\lambda$$
$$M = \int_{\lambda_{min}}^{\lambda_{max}} C(\lambda) \cdot m(\lambda) d\lambda \qquad (2.2\text{-}1)$$
$$L = \int_{\lambda_{min}}^{\lambda_{max}} C(\lambda) \cdot l(\lambda) d\lambda$$

In practice, it would be quite difficult to measure an individual's cones' responses, S, M, and L, to various physical colour stimuli. In order to simplify the problem, the CIE (Commission Internationale de l'Eclairage) defined a standard colour space, CIE 1931 XYZ colour space, in 1931. In the CIEXYZ colour space, the tristimulus values are not the S, M, and L responses of the human eye, but rather a set of tristimulus values called X, Y, and Z, which are roughly red, green and blue, respectively. Due to the nature of the distribution of cones in the eye, the tristimulus values depend on the observer's field of view. To eliminate this variable, the CIE defined the standard (colorimetric) observer (see CIE 2004 document). Originally this was taken to be the chromatic response of the average human viewing through a 2° angle, due to the belief that the colour-sensitive cones resided within a 2° arc of the fovea. Thus the CIE 1931 Standard Colorimetric Observer is also known as the CIE 1931 2° Standard Colorimetric Observer. In 1964, CIE defined a 10° Standard Colorimetric Observer, which is recommended to be used for more than about a 4° field of view.

2.2.1 CIE Standard Observers and XYZ Colour Space

The colour matching functions are the numerical description of the chromatic response of the observer (described above). The CIE has defined a set of three colour-matching functions, called $\overline{x}(\lambda)$, $\overline{y}(\lambda)$, and $\overline{z}(\lambda)$, which can be thought of as the spectral sensitivity curves of three linear light detectors that yield the CIEXYZ tristimulus values X, Y, and Z. The tabulated numerical values of these functions are known collectively as the CIE standard observer. The tristimulus

values for a colour with a colour stimulus Φ(λ) are given in terms of the standard observer by:

$$X = k\sum_{\lambda} \Phi(\lambda) \cdot \bar{x}(\lambda) \cdot \Delta\lambda$$

$$Y = k\sum_{\lambda} \Phi(\lambda) \cdot \bar{y}(\lambda) \cdot \Delta\lambda \qquad (2.2.1\text{-}1)$$

$$Z = k\sum_{\lambda} \Phi(\lambda) \cdot \bar{z}(\lambda) \cdot \Delta\lambda$$

where k is a constant to normalize the Y channel, λ is the wavelength of the equivalent monochromatic light, Φ(λ) is the colour stimulus function of the light seen by the observer, $\bar{x}(\lambda)$, $\bar{y}(\lambda)$, and $\bar{z}(\lambda)$ are the colour-matching functions of the CIE 1931 standard colorimetric observer, and Δλ is the wavelength sampling interval.

For non-self-luminous objects, the colour-stimulus function is given by

$$\Phi(\lambda) = R(\lambda)S(\lambda) \text{ or } \Phi(\lambda) = T(\lambda)S(\lambda) \qquad (2.2.1\text{-}2)$$

where R(λ) is the spectral reflectance factor of the object, T(λ) is the spectral transmission factor, and S(λ) is the relative spectral power distribution of the illuminant. The k in equation (2.2.1-1) is chosen such that the tristimulus value Y yields a value of 100 for a perfect reflecting diffuser (R(λ) = 1.0 for all λ).

For a self-luminous object, a photometric quantity can be calculated using equation (2.2.1-1) by setting k = 683 lm/W. Because $\bar{y}(\lambda)$ was chosen to be the CIE V(λ) luminosity function, the Y tristimulus value is corresponding to a photometric quantity.
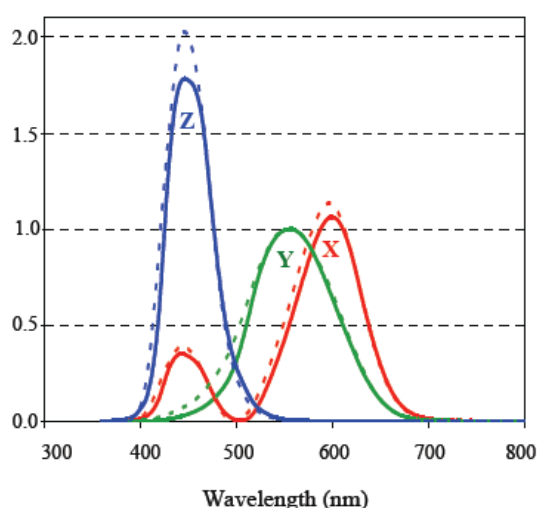
Fig. 2.2.1-1 CIE 1931 Standard Colorimetric Observer (full-line) and CIE 1964 Standard Colorimetric Observer (dash-line)

For the 10° observer, $\bar{x}(\lambda)$, $\bar{y}(\lambda)$, and $\bar{z}(\lambda)$ in above equations are replaced with the corresponding 1964 10° Standard Observer, $\bar{x}_{10}(\lambda)$, $\bar{y}_{10}(\lambda)$, and $\bar{z}_{10}(\lambda)$, respectively. Fig. 2.2.1-1 shows the colour matching functions of both 2° and 10° observers.

The dependence of luminance entirely on the Y value in the XYZ system means that the $\bar{y}(\lambda)$ colour-matching function represents the relative luminances of the colours of the spectrum; this is an important function in photometry, where it is known as the spectral luminous efficiency function, $V(\lambda)$.

2.2.2 CIE xy Chromaticity Diagram and CIE xyY Colour Space

Since the human eye has three types of colour sensors that respond to different ranges of wavelengths, a full plot of all visible colours is a three-dimensional figure. However, the concept of colour can be divided into two parts: brightness and chromaticity. The CIE XYZ colour space was deliberately designed so that the Y parameter was a measure of the brightness or luminance of a colour. The chromaticity of a colour was then specified by the two derived parameters x and y, two of the three normalised values which are functions of all three tristimulus values X, Y, and Z:

$$x = \frac{X}{X+Y+Z}$$
$$y = \frac{Y}{X+Y+Z}$$
$$z = \frac{Z}{X+Y+Z} = 1 - x - y$$

(2.2.2-1)

The derived colour space specified by x, y, and Y is known as the CIE xyY colour space and is widely used to specify colours in practice. Fig. 2.2.2-1 shows the related chromaticity diagram (a diagram for 10° is slightly different). The outer curved boundary is the spectral locus, with wavelengths shown in nanometres. The diagram represents all of the chromaticities visible to the average person. These are shown in colour and this region is called the gamut of human vision.
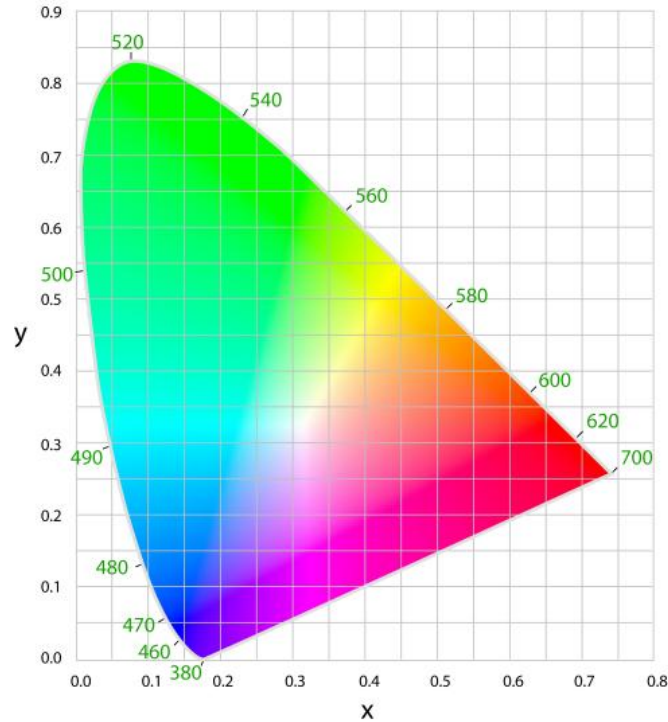
Fig. 2.2.2-1 The CIE 1931 colour space chromaticity diagram. The outer curved boundary is the spectral (or monochromatic) locus, with wavelengths shown in nanometres (http://www.rp-photonics.com/img/cie1931.png).

2.2.3 CIE Uniform Colour Spaces and Colour Difference Models

With CIE XYZ colour space (or CIE xy chromaticity space with equal luminance), the equal colour differences computed by Euclidean distance in different regions are not perceptually equal (Wright 1941). Several colour spaces have been developed to improve the visual uniformity. The mostly widely used uniform colour space is the CIELAB colour space as shown below:

$$L* = 116 f(Y/Y_n) - 16$$
$$a* = 500[f(X/X_n) - f(Y/Y_n)] \tag{2.2.3-1}$$
$$b* = 200[f(Y/Y_n) - f(Z/Z_n)]$$

where

$$f(t) = t^{1/3} \text{ for } t > (24/116)^3 \text{ or}$$

$$f(t) = (841/108)t + 16/116 \text{ otherwise,}$$

XYZ are the tristimulus values of a colour and $X_n Y_n Z_n$ are the tristimulus values of the reference white being used. L* represents the lightness, a* and b* represent the chroma coordinates.

The chroma is computed as $C* = \sqrt{a*^2 + b*^2}$. And colour difference is given by the formula:

$$\Delta E *_{ab} = \sqrt{\left(\Delta L *\right)^2 + \left(\Delta a *\right)^2 + \left(\Delta b *\right)^2} \qquad (2.2.3\text{-}2)$$

where $\Delta L*$, $\Delta a*$, and $\Delta b*$ are the differences of L*, a*, and b* between two colours, respectively.

The CIE 1976 L*a*b* colour space is not a perfectly uniform colour space. To further improve the uniformity of the colour difference metric, CIE defined a colour difference equation, ΔE_{94}, for small colour difference (CIE 1995). Since then, CIE refined the equation to further improve the perceptual uniformity, and emerged with CIEDE2000 (Luo et al. 2001).

2.2.4 Metamerism

Metamerism is the matching of apparent colour of objects with different spectral power distributions (Hunt 1998). Colours that match this way are called metamers. In practice, the word metamerism is often used to indicate a metameric failure rather than a match.

A spectral power distribution describes the proportion of total light emitted, transmitted, or reflected by a colour sample at every visible wavelength; it precisely defines the light from any physical stimulus. However, the human eye contains only three colour receptors (cone cells), which means that all colours are reduced to three sensory quantities, called the tristimulus values. Metamerism occurs because each type of cone responds to the cumulative energy from a broad range of wavelengths, so that different combinations of light across all wavelengths can produce an equivalent receptor response and the same tristimulus values or colour sensation.

The term illuminant metameric failure is sometimes used to describe situations where two material samples match when viewed under one light source but not another.

The difference in the spectral compositions of two metameric stimuli is often referred to as the degree of metamerism. The sensitivity of a metameric match to any changes in the spectral elements that form the colours depend on the degree of metamerism. Two stimuli with a high degree of metamerism are likely to be very sensitive to any changes in illuminant, material composition, observer, field of view, etc.

Using metameric colour matching rather than spectral colour matching is a problem in industries where colour matching or colour tolerances are important. A classic example is in automobiles: the interior fabrics, plastics and paints may be manufactured to provide a good colour match under a standard light source (such as the sun), but the matches can disappear under different light sources (fluorescent or halide lights). Similar problems can occur in apparel manufactured from different

types of dye or using different types of fabric, or in quality colour printing using different types of inks. Papers manufactured with brighteners are especially susceptible to colour changes when lights differ in their short wavelength radiation, which can cause some papers to fluoresce.

Metamerism is a factor that must be considered in non-spectral (metameric) colour imaging. The human visual system integrates spectral data with three types of cone receptors to produce a three-channel colour image. It is considered metameric since an infinite variety of potential spectral power distributions in the scene can produce the same colour response in the three integrated channels (Fairchild et al. 2001). The colour matching between two imaging systems in an illuminant condition may be invalidated under a different illuminant condition. For example, a colour printer that is tuned for the D50 illuminant will not produce same colours as viewed under the average office lighting condition because the relative spectral power distribution of two illuminants are different. Hence, the result of colour reproduction may be unexpected. There are many factors that influence the degree of metamerism, such as the spectral absorption of inks and media, the combination of inks, the tradeoffs of illuminants to modelling the colour mapping. The metamerism must be considered for preference colour reproduction, because the colours for preferred colour reproduction are likely to be affected by metamerism.

2.2.5 Illuminants

Except for self-luminous objects, at least a light source must be provided to light up an object. The spectral power distribution (SPD) of the light source is one of the factors to determine the colour of the object (see equation 2.2.1-1). It is therefore clear that an essential step in specifying colour is to accurately define the illuminants involved. To simplify the problem, CIE specified a serial of Standard Illuminants: A, B, C, D, E, and F (CIE 2004a).

The D series of illuminants are constructed to represent natural daylight. A D Illuminant has SPD of a black body in a certain temperature, so it has a colour temperature (see the section of Colour Temperature). They are difficult to produce artificially, but are easy to characterise mathematically.

Illuminant E is an equal-energy radiator; it has a constant SPD inside the visible spectrum. It is useful as a theoretical reference illuminant that gives equal weight to all wavelengths. It also has equal CIE XYZ tristimulus values, thus its chromaticity coordinates are $(x,y)=(1/3,1/3)$.

The F series of illuminants represent various types of fluorescent lighting.

The spectrum of a standard illuminant, like any other profile of light, can be converted into tristimulus values. The set of three tristimulus coordinates of an illuminant is called a white point. If the profile is normalised, then the white point can equivalently be expressed as a pair of chromaticity coordinates.

2.2.6 Colour Temperature

Without a light source, we cannot see anything. The colour temperature of a light source is determined by comparing its chromaticity with that of an ideal black-body radiator (Planckian radiator). The temperature (measured in Kelvin, K) at which the heated black-body radiator matches the colour of the light source is the source's colour temperature. For a black body source, it is directly related to Planck's law (Rybicki and Lightman 1979) and Wien's displacement law (Rybicki and Lightman 1976). Yellow-red colours are considered warm, and blue-green colours are considered cool. Confusingly, higher Kelvin temperatures (3600–5500 K) are considered cool and lower colour temperatures (2700–3000 K) are considered warm. Cool light produces higher contrast and is considered better for visual tasks. Warm light is preferred for living spaces because it is considered more flattering to skin tones and clothing.
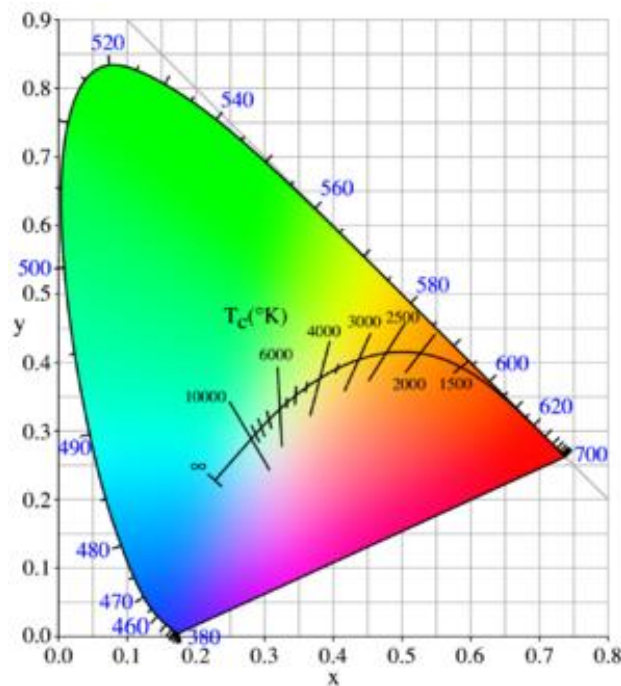
Fig. 2.2.6-1 The chromaticities of black-body light sources of various temperatures (Planckian locus) on the CIE 1931 x-y chromaticity space, and lines of constant correlated colour temperature (http://www.juliantrubin.com/encyclopedia/engineering/colour_temperature_files/300px-PlanckianLocus.png).

The chromaticity of a light source may not be on the chromaticity curve of the Planckian radiator. If that is the case, a term, correlated colour temperature (CCT) is applied. CCT is the temperature of the Planckian radiator whose perceived colour most closely resembles that of a given stimulus at the same brightness and under specified viewing conditions. CCT's calculation is performed using CIE 1960 uniform colour space coordinates u and v. Fig. 2.2.6-1 shows the colour temperature line and the constant CCT lines.

2.3 Colour Appearance Model: CIE CAM02

Colour appearance models are capable of predicting colour appearance under a variety of viewing conditions, including different light sources, luminance levels, surrounds, and lightness of backgrounds. They are particularly useful for cross-media colour reproduction. The CIECAM02 colour appearance model was built upon the basic structure and form of the CIECAM97s colour appearance model (CIE 2004b). It provides a model to transform tristimulus values to or from perceptual attribute correlates under different viewing conditions. The two major pieces of this model are a chromatic adaptation transform and equations for computing correlates of perceptual attributes.

The visual observing fields are briefly described in the following sub-section, followed by the forward implementations of CIECAM02.

2.3.1 Visual Areas in the Observing Field

Hunt (1991 and 1998) defined five visual areas in the observing field for related colours as illustrates in Fig. 2.3.1-1. A brief description is followed (Choi 2008).
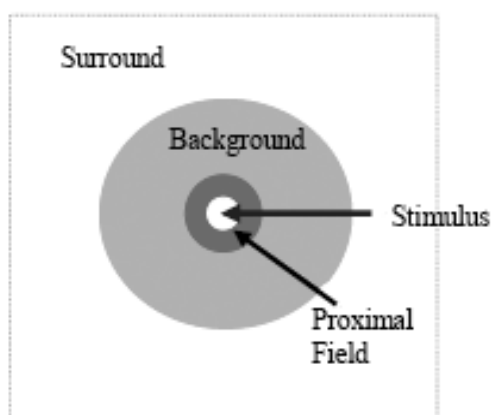
Fig. 2.3.1-1 The five defined visual areas

Stimulus: the colour element for which colour-appearance measurement is required. Typically, a stimulus is taken to be a uniform patch of about 2° angular subtends.

Proximal field: the immediate environment of the colour element considered, extending typically for about 2° from the edge of that colour element in all or most direction. It is normally specified to be equal to the background in CIECAM02.

Background: the environment of the colour element considered, extending typically for about 10° from the edge of the proximal field in all or most directions. The background is usually considered to be a neutral grey with 20% luminance factor.

Surround: a field beyond the background.

Adapting field: the total environment of the colour element considered, including the proximal field, the background, the surround, and extending to the limit of vision in all directions.

2.3.2 Setting Model Parameters

Fairchild (1998) and Luo and Hunt (1998) have both provided definitions of surround. A surround ratio is determined and then a surround is assigned. The surround ratio, S_R is computed by:

$$S_R = L_{SW}/L_{DW}$$

where L_{SW} is the luminance of the surround white and L_{DW} is the luminance of the device white. The luminance values are measured in cd/m^2. If S_R is 0 then a dark surround is appropriate. If S_R is less than 0.2 then a dim surround should be used while an S_R of greater than or equal to 0.2 corresponds to an average surround. A few examples of parameter settings are shown in Table 2.3.2-1, where L_A is the luminance of the adapting field in cd/m^2, which is computed as 20% of the device white (CIE TC 8-01).

Table 2.3.2-1 Example parameter settings

Example	Ambient Illumination in lux (or cd/m^2)	Scene or device white luminance	L_A in cd/m^2	Adopted white point	S_R	Surround
Surface colour evaluation in a light booth	1000 (318.3)	318.30 cd/m^2	63.66	Light booth WP	1	Average

Viewing self-luminous display at home	38 (12)	80 cd/m²	16	Between display WP and ambient WP	0.15	Dim
Viewing slides in dark room	0 (0)	150 cd/m²	30	Between Projector WP and E	0	Dark
Viewing self-luminous display under office illumination	500 (159.2)	80 cd/m²	16	Between display WP and CWF	2	Average

2.3.3 Implementation of the Forward Model

First the surround parameters F, c and Nc are selected from Table 2.3.3-1. For intermediate surrounds, these values can be linear interpolated.

Table 2.3.3-1 Categorical viewing condition settings for the model

Viewing Condition	F	c	Nc
Average surround	1.0	0.69	1.0
Dim surround	0.9	0.59	0.9
Dark surround	0.8	0.525	0.8

The sample CIE 1931 tristimulus values are converted to a long, medium and short wavelength sensitive space using the CAT02 forward matrix as shown below:

$$\begin{bmatrix} R \\ G \\ B \end{bmatrix} = M_{CAT02} \begin{bmatrix} X \\ Y \\ Z \end{bmatrix} \tag{2.3.3-1}$$

$$M_{CAT02} = \begin{bmatrix} 0.7328 & 0.4296 & -0.1624 \\ -0.7036 & 1.6975 & 0.0061 \\ 0.0030 & 0.0136 & 0.9834 \end{bmatrix} \tag{2.3.3-2}$$

The degree of adaptation to the white point, D, is computed by equation (2.3.3-3). The value ranges from 1 for complete adaptation to 0 for no adaptation.

$$D = F \left[1 - \left(\frac{1}{3.6} \right) e^{\left(\frac{-(L_A + 42)}{92} \right)} \right] \tag{2.3.3-3}$$

The chromatic adaptation is computed by equation (2.3.3-4).

$$R_c = [(Y_w D / R_w) + (1 - D)]R$$
$$G_c = [(Y_w D / G_w) + (1 - D)]G \qquad (2.3.3\text{-}4)$$
$$B_c = [(Y_w D / B_w) + (1 - D)]B$$

where R_w, G_w, B_w are the RGB values computed for the white point using equations (2.3.3-1) and (2.3.3-2).

The viewing condition dependent constants are computed below:

$$k = 1/(5L_A + 1) \qquad (2.3.3\text{-}5)$$

$$F_L = 0.2k^4(5L_A) + 0.1(1 - k^4)^2(5L_A)^{1/3} \qquad (2.3.3\text{-}6)$$

$$n = Y_b / Y_w \qquad (2.3.3\text{-}7)$$

$$N_{bb} = N_{cb} = 0.725(1/n)^{0.2} \qquad (2.3.3\text{-}8)$$

$$z = 1.48 + \sqrt{n} \qquad (2.3.3\text{-}9)$$

Convert to Hunt-Pointer-Estevez space for post-adaptation nonlinear compression:

$$\begin{bmatrix} R' \\ G' \\ B' \end{bmatrix} = M_{HPE} M_{CAT02}^{-1} \begin{bmatrix} R_c \\ G_c \\ B_c \end{bmatrix} \qquad (2.3.3\text{-}10)$$

$$M_{HPE} = \begin{bmatrix} 0.38971 & 0.68898 & -0.07868 \\ -0.22981 & 1.18340 & 0.04641 \\ 0 & 0 & 1 \end{bmatrix} \qquad (2.3.3\text{-}11)$$

Apply post-adaptation nonlinear compression:

$$R_a^{'} = \frac{400(F_L|R'|/100)^{0.42} sign(R')}{27.13 + (F_L|R'|/100)^{0.42}} + 0.1$$
$$G_a^{'} = \frac{400(F_L|G'|/100)^{0.42} sign(G')}{27.13 + (F_L|G'|/100)^{0.42}} + 0.1 \qquad (2.3.3\text{-}12)$$
$$B_a^{'} = \frac{400(F_L|B'|/100)^{0.42} sign(B')}{27.13 + (F_L|B'|/100)^{0.42}} + 0.1$$

Calculate temporary Cartesian representation (a and b) and hue before computing eccentricity factor and perceptual attributes:

$$a = R'_a - 12G'_a/11 + B'_a/11$$
$$b = \frac{1}{9}(R'_a + G'_a - 2B'_a) \qquad (2.3.3\text{-}13)$$

$$h = \tan^{-1}(b/a) \qquad (2.3.3\text{-}14)$$

The hue angle, h, should be computed in degrees.

Compute eccentricity factor:

$$e_t = \frac{1}{4}\left[\cos\left(h\frac{\pi}{180}+2\right)+3.8\right]$$

(2.3.3-15)

Hue quadrature or H can be computed from linear interpolation of the data shown in Table 2.3.3-2. If $h < h_1$, then H'=h+360; otherwise h'=h. Choose a value of I so that $h_i <= h' < h_{i+1}$.

Table 2.3.3-2 Unique hue data for the calculation of Hue Quadrature

	Red	*Yellow*	*Green*	*Blue*	*Red*
i	0	1	2	3	4
h_i	20.14	90.00	164.25	237.53	380.14
e_i	0.8	0.7	1.0	1.2	0.8
H_i	0.0	100.0	200.0	300.0	400.0

$$H = H_i + \frac{100(h'-h_i)/e_i}{(h'-h_i)/e_i + (h_{i+1}-h')/e_{i+1}}$$

(2.3.3-16)

Compute A, the achromatic response:

$$A = \left[2R'_a + G'_a + (1/20)B'_a - 0.305\right]N_{bb}$$

(2.3.3-17)

Lightness, J, is calculated from the achromatic signals of the stimulus, A, and white, A_w:

$$J = 100(A/A_a)^{cz}$$

(2.3.3-18)

Compute brightness, Q:

$$Q = \frac{4}{c}\sqrt{J/100}(A_s + 4)F_L^{0.25}$$

(2.3.3-19)

Compute a temporary magnitude quantity, t, which will be used to compute C.

$$t = \frac{(50000/13)N_c N_{cb}e_t(a^2+b^2)^{0.5}}{R'_a + G'_a + (21/20)B'_a}$$

(2.3.3-20)

Calculate chroma, C:

$$C = t^{0.9}\sqrt{J/100}(1.64 - 0.29^n)^{0.73}$$

(2.3.3-21)

Calculate colourfulness, M:

$$M = CF_L^{0.25}$$

(2.3.3-22)

Saturation, s, can be calculated by:

$$s = 100\sqrt{M/Q} \qquad\qquad (2.3.3\text{-}23)$$

The corresponding Cartesian coordinates are as followed:

$$\begin{aligned} a_C &= C\cos(h) \\ b_C &= C\sin(h) \end{aligned} \qquad\qquad (2.3.3\text{-}24)$$

$$\begin{aligned} a_M &= M\cos(h) \\ b_M &= M\sin(h) \end{aligned} \qquad\qquad (2.3.3\text{-}25)$$

$$\begin{aligned} a_s &= s\cos(h) \\ b_s &= s\sin(h) \end{aligned} \qquad\qquad (2.3.3\text{-}26)$$

Attributes of CAM02-UCS (Luo et. al. 2006), a uniform colour space based on CIECAM02, are computed below:

$$\begin{aligned} J' &= \frac{(1+100\cdot c_1)J}{1+c_1\cdot J} \\ M' &= (1/c2)\ln(1+c_2\cdot M) \\ a' &= M'\cdot\cos(h) \\ b' &= M'\cdot\sin(h) \end{aligned}$$

where $c_1 = 0.007$, $c_2 = 0.0228$.

2.3.4 Examples Using CIECAM02 for Device Colour Characterisation

Two examples below demonstrate how to use CIECAM02 colour appearance model for device colour characterization. The first example illustrates an ideal method to display sRGB (Stoke et al. 1996) colour images (or RGB colours from the standard sRGB monitor) on an LCD monitor. Prior to the colour transformation, an sRGB data set sampled in entire sRGB gamut is prepared to generate a source gamut for gamut mapping. The data set in sRGB colour space are converted to CIE XYZ colour space. CIECAM02 colour appearance model is used to convert XYZ to CAM02 Jab or JCh. A source gamut in Jab or JCh space is constructed. Similarly, a destination gamut in Jab or JCh space is constructed as well. Now, a gamut mapping object is constructed using the source gamut and the destination gamut. As shown in Fig. 2.3.4-1, the steps to convert a colour from sRGB to LCD device RGB are: 1) the sRGB colour is converted to CIEXYZ; 2) the CIECAM02 forward transformation of the source is applied to convert XYZ to Jab or JCh; 3) gamut mapping is applied to map Jab or JCh from the source gamut to the destination gamut; 4) the new Jab or JCh colour is converted to XYZ using the inverse transformation of the CIECAM02 colour appearance model of the destination; and 5) the colour in CIE XYZ space is finally transformed to the LCD device RGB space using the LCD monitor device colour model.
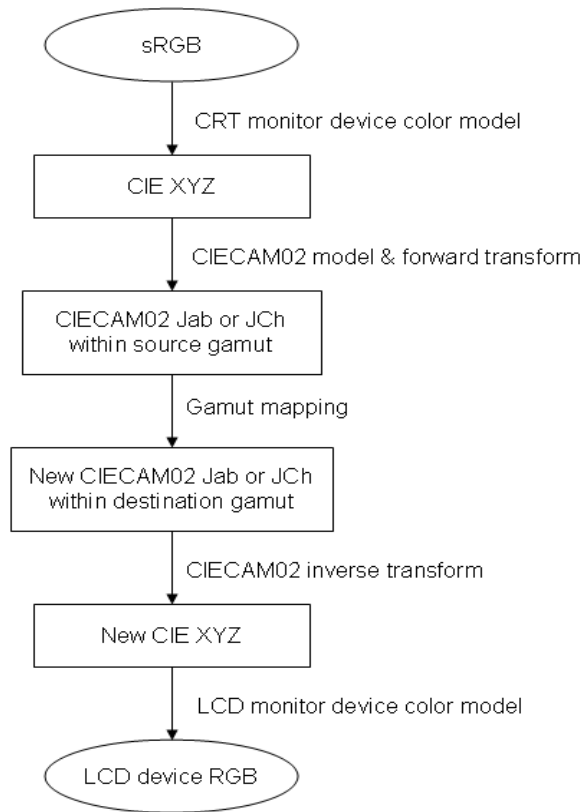
Fig. 2.3.4-1 A block diagram for the colour characterisation to transform sRGB to an LCD device RGB colour space
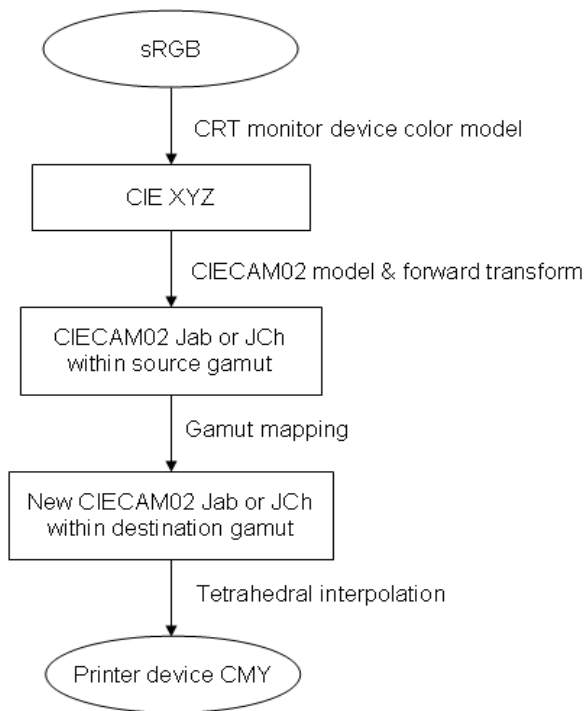
Fig. 2.3.4-2 A block diagram for the colour characterisation to transform sRGB to a printer device CMY colour space

Another example is the colour characterisation to transform sRGB to a printer device CMY(K) colour space. Fig. 2.3.4-2 illustrates a typical approach a block diagram for the colour characterisation. The process is similar to that in the earlier example except that an inverse transformation of the CIECAM02 model in the destination viewing environment is avoided. After the gamut mapping, a colour in Jab or JCh within the destination is converted to the printer CMY(K) space directly through tetrahedral interpolation.

Depending on the algorithms or the implementation for cross-media colour reproduction, an inverse transformation from CIECAM02 attributes to CIE XYZ may be required (example 1) or may never occur (example 2).

2.4 Preferred Colour Reproduction of Digital Images

An image may be captured with a digital camera, scanned with a scanner, or created using computer graphics. It may then be displayed on a monitor display, projected on a screen, sent to somewhere else as a digital file, or printed as a hardcopy. The colour and image content of an image may be edited before being displayed or printed. A simple imaging flow may be abstracted as three components: an input component to create the image, an enhancement component to process or edit the image, and an output component to reproduce the image on display, hardcopy, or as a digital file.

In an open workflow, an input component typically produces an image with a certain reference standard. For example, a digital camera captures a scene in a raw data form with the scene-referred state and typically transforms it to a display-referred sRGB image. Besides re-rendering the image to a specific output device (e.g. a LCD display or a printer), an output component may perform specific colour and imaging rendering for certain objectives. Some of the renderings may be performed in a separate component between the input and the output component. In a complex workflow, there may be more variable and more uncertainties for the colour rendering, depending on the objective of the colour reproduction.

Hunt (1974, 2006) categorised the objective of colour reproduction into six types: spectral colour reproduction, colorimetric, exact, equivalent, corresponding, and preferred. Some of these rendering types can be correlated with the rendering intents in ICC (International Color Consortium) colour management system (http://www.color.org).

Section 2.4.1 provides an overview of the six types of colour reproduction. Since the preferred colour reproduction is the interest in this research, it is discussed further in Section 2.4.2. A subset of preferred colour reproduction, memory colour

reproduction of familiar objects, which is the centre of this research, is discuss in detail in Section 2.4.3. Sections 2.4.4 to 2.4.6 briefly explore colour enhancement of skin, green plants, and blue sky, respectively. Section 2.4.7 summaries the survey of the preferred colour reproduction.

2.4.1 Hunt's Colour Reproduction Intents

If the purpose of colour reproduction is to reproduce the colours of the original and to have the reproduced colours match the original colours independent of the illuminant, the spectral reflectance curves of the original and reproduced colours must be identical. For self-luminous colours, this has to be defined as equality of relative spectral power distributions. This is call spectral colour reproduction. The spectral colour reproduction (Hardeberg 2001, Berns et al. 1998, Tzeng and Berns 1999 and 2000, Murakami and Ishii 2004, Chorin et al. 2007, Yamamoto et al. 2007, Derhak et al. 2006) is promising, but it is mostly not available for general digital image colour reproduction, especially in consumer digital imaging. A 3-channel display is not able to produce the same relative spectral power distributions as those of the original colour. Colour images are mostly not represented with spectral reflectance, either. A camera, a scanner, or a printer is mostly not able to produce the same spectral reflectance as that of the originals.

Since spectral colour reproduction is mostly impractical, a metameric match to have the same CIE chromaticities and relative luminances between the original and the reproduction colours may be characterised. This is called colorimetric colour reproduction (Clapper and DeMarsh 1969). The colorimetric calculation is usually carried out relative to a well-lit reference white in the original, and relative to the illuminant white of its reproduction. This makes absolute luminances between the original and the reproduction independent of each other. This simplification may have its limitation, since the illuminance intensity affects the colour appearance. For the rendering from a physical world to a digital image using a digital camera, this method may not produce colour appearance match satisfactorily, due to more extended dynamic ranges of the physical world. Colorimetric colour reproduction (equality of chromaticities and relative luminances) is a useful criterion when the original and reproduction have the same viewing conditions and uses illuminants of the same colour. The colorimetric colour reproduction closely matches the absolute-colorimetric colour rendering intent in ICC colour management. In ICC colour management, the absolute-colorimetric colour rendering intent may be used for colour proofing of a print hardcopy on a display or using a different printer.

On the top of the colorimetric colour reproduction, if the absolute luminances of the colours in the original and in the picture are also equal, the reproduction of a

colour in a picture is exactly the same as that in the original in chromaticity and absolute luminance. This is called exact colour reproduction. In this case, the equality of colour appearance is guaranteed only if the viewing conditions between the two are the same. Exact colour reproduction (equality of chromaticities, relative luminances, and absolute luminances) ensures equality of appearance for original and reproduction if the viewing conditions between the two are the same.

In many situations (e.g. different lighting conditions), colorimetric and exact colour reproduction may not produce similar colour appearance. Another approach, equivalent colour reproduction, is defined as the reproduction in which the chromaticities, relative luminances, and absolute luminances of the colours are such that, when seen in the reproduction-viewing conditions, they have the same appearance as the colours in the original scene. The illuminants (spectral distribution and intensity) and surrounds are of practical importance in modelling the equivalent colour reproduction. These effects can be modelled using CIECAM02 colour appearance model. Equivalent colour reproduction (chromaticities, relative luminances, and absolute luminances such as to ensure equality of appearance) allows for adjustments to compensate the differences in viewing conditions.

Corresponding colour reproduction is defined as reproduction in which the chromaticities and relative luminances of the colours are such that, when seen in the picture-viewing conditions, they have the same appearance as those colours in the original would have had if they had been illuminated to produce the same average absolute luminance level as that of the reproduction. Corresponding colour reproduction has the same advantage over equivalent colour reproduction as colorimetric colour reproduction has over exact colour reproduction: by relating the colours both in the original and in the reproduction to a reference white, allowance is made for the fact that observers tend to perceive not in isolation but with reference to a framework provided by the environment. Corresponding colour reproduction (chromaticities and relative luminances such as to ensure equality of appearance when the original and reproduction luminance levels are the same) allows for all effects of viewing conditions except absolute luminance levels, and provides a realistic criterion for general application.

The colour reproductions described above are aimed to reproduce colour perception of the original scene in certain conditions. There are evidences that people might prefer to see an image in which the colour appearances of some familiar objects to be shifted slightly away from their original colours. For example, Caucasian skin colour is generally preferred to be a sun-tanned appearance; yet Asian skin colour may prefer to be slightly desaturated. Blue sky is generally

preferred to be more saturated. It may also be desirable to introduce other distortions of colour rendering to create mood or atmosphere in a picture. In this context, preferred colour reproduction is defined as reproduction in which colours depart from equality of appearance to those in the original, either absolutely or relative to white, in order to achieve a more pleasing result to the viewer (Hunt 2006). In ICC colour management system, the perceptual rendering intent is an intent that allows preference rendering; however, it is not equivalent to the preferred colour reproduction defined by Hunt. According to Hunt, the preferred colour reproduction can be applied on top of any other five colour reproduction intents. Preferred colour reproduction is an appropriate aim for consumer colour imaging, such as consumer printing and consumer digital photography.

Except for the spectral colour reproduction, a comparison of the major properties of the other five colour reproduction methods is listed in Table 2.4.1-1.

Table 2.4.1-1 A comparison of 5 non-spectral colour reproduction intents

	chromaticities	*relative luminances*	*absolute luminances*	*appearance*
Colorimetric Colour Reproduction	equal	equal		
Exact Colour Reproduction	equal	equal	equal	
Equivalent Colour Reproduction	same appearance	same appearance	same appearance	same
Corresponding Colour Reproduction	same appearance	same appearance	equal	same
Preferred Colour Reproduction				more pleasing

2.4.2 Preferred Colour Reproduction

To simplify the problem yet adequate for the current research, the non-spectral colour reproduction objectives may be regrouped into three categories: colorimetric (relative and absolute colorimetric), perceptual, and preferred. The colorimetric colour reproduction covers Hunt's Colorimetric and Exact colour reproduction. The perceptual colour reproduction includes Hunt's equivalent and corresponding colour reproduction. Preferred colour reproduction is the perceptual colour reproduction, plus preference colour adjustment.

In digital colour reproduction, the colorimetric colour reproduction is used for colour proofing, and is also used as a baseline colour reproduction. Without the capability of colorimetric colour characterization, the objective of perceptual colour characterisation may be difficult to achieve. Fernandez et al. (2005) investigated preferred colour reproduction versus colorimetric colour reproduction, and concluded that colorimetric intention of image reproduction was a good first step, and observer colour preference incorporated into image reproduction techniques should be viewed as an enhanced or customized version of the colorimetric reproduction objective.

Previous research efforts for preferred colour reproduction can be traced back more than half a century. According to Bartleson (1960), people might prefer to see an image in which the colour appearance of a familiar object agrees with its memory colour rather than with the actual colorimetric content of the original scene. Hunt et al. (1974), although indicated that colorimetric type of colour reproductions should be used as a baseline of colour reproduction, concluded that observers would prefer object colours to be reproduced with greater saturation in comparison to the original, and that certain memory colours such as grass, sky, and skin are preferred to be produced with slightly different hues and with greater purity. It is well known that observers are able to rate the quality of an image with or without the original image presented. Without the original image, observers rate the quality of the image with an idealized image in the memory (Janssen and Blommaert 2000).

Apparently, the colour sensations evoked by a reproduction are compared with a mental recollection of the colour sensations previously experienced when looking at objects similar to the ones being appraised (Yendrikhovskij et al. 1999). Since most of the object colours found in nature are subject to considerable variations in hue, saturation, and lightness, the precision with which their mental recollections are stored in memory is low, and generally leads to substantial subjective tolerances for colour reproduction errors. And, since the appreciation is based on the mental recollections of similar objects, the correctness of the colour rendering can be estimated in pictures taken by other people.

Boust et al. (2006) compared how experts and naïves judge the colour preference of digital images. They found that both experts and naïves did not focus on objects if no memory colours were associated with them. Both experts and naïve observers used memory colours to adjust image or to judge image quality. An image was preferred if the colours of the elements in the scene match the colours observers had stored in their memory. The findings reveal that preference memory colour reproduction is crucial for the colour quality of images.

Koh et al. (2006) studied colour preference and perceived colour naturalness of television quality digital videos, and found maximum scores for both attributes usually occurred at videos with higher chroma than the original videos. However, the naturalness scores peaked at lower mean chroma than the preferred chroma. They also found that the chroma boosting for both attributes were video content dependent. Koh et al. (2007) then added another parameter, 'annoyance', to study compressed video IQ (image quality). Besides the same conclusion for colour preference and naturalness, annoyance scores decrease to a minimum and then increase as mean chroma increased.

Colour preference enhancement is to improve the perceived image quality. Yendrikhovskij et al. (1998, 1999) used naturalness to determine the fidelity of reproduced object colours. A GUN space is proposed to model image quality. The three coordinates are: Genuineness (G), Usefulness (U), and Naturalness (N). Genuineness is referred to as the degree of apparent similarity of reproduced image & environment with the external reference, i.e. original image & environment. Ideally, an image with highest degree of genuineness should give an impression of 'real'. The genuineness is crucial for proofs, catalogues, fine art, etc. Usefulness is referred to as the degree of apparent correspondence of the reproduced image & environment with the observer & task activity. The main criterion of usefulness is the maximum discriminability. The usefulness requirement is crucial for medical images, military night-vision images, etc. Naturalness is referred to as the degree of apparent similarity between the reproduced image & environment and the internal references, i.e. memory prototypes. The influence of this attribute on the quality judgements becomes substantial when no external reference, i.e. the original, is available for observers: watching TV, looking at photos, browsing through the internet, etc. It gives a measure of the similarity between the colours of objects presented in an image and the prototypical colours of the corresponding object categories. They found naturalness of a whole picture was determined by the naturalness of the most critical objects in the picture. They proposed that images of good quality should at least be perceived as natural, implying a strong relationship between perceived naturalness and the quality of images of real-life scenes. To summarize, considering an over-saturated original picture that has to be reproduced by three colour devices, the Genuineness-device ('no lies' strategy) will reproduced the picture perceptually the same; the Usefulness-device ('see more' strategy) will try to increase the saturation further (considering colour attribute only); the Naturalness-device ('no surprise' strategy) will decrease the saturation down to the prototypical level.

Yendrikhovskij et al. further developed a colour quality index to evaluate the colour quality of natural images. The colour quality is the weighted combination of a naturalness index and a normalised colourfulness index. Yendrikhovskij analysed 78 images from two Photo CDs, and suggested that the distribution of colours could be roughly divided in four regions in CIE u'v' colour space: achromatic, orange-yellow, yellow-green, and blue. Those areas have no distinct borders and form a sort of triangle within the orange, green, and blue colours in corners. These three regions can be referred to as 'skin', 'grass', and 'sky' segments for convenience. They represent the three most familiar and frequently reproduced categories of colours: human faces, grass, and sky (Bartleson and Bray 1962, Hunt et al 1974). The naturalness of colour reproduction of natural images is estimated locally within these segments. Yendrikhovskij defined the naturalness of each segment by a Gaussian density function of the differences between the average saturation of the segment and a mean saturation which is the expected mean value of colours within the segment. The total naturalness index for an image is defined as the average naturalness indices of each pixel of the image. The colourfulness index of an image is defined as the combination of the average saturation of the image and the standard deviation of the saturation of the image. Finally, a colour quality index is proposed based on the naturalness index and colourfulness index. Yendrikhovskij's experimental results show very good agreement between the model and psychophysical values. However, in the experiment, Yendrikhovskij manipulated only the saturation of images in CIELUV colour space, and the lightness and hue angle are excluded from the modelling. Even if saturation is considered, it is difficult to model because the saturation for maximizing colour preference is not the same as that for maximizing naturalness.

Colour preference is different from either genuineness or naturalness. It seems that the colour preference is ignored in the GUN model. Although colour preference enhancement improves the image quality, it may degrade genuineness. Although both correlate with each other, their objectives are different. For example, an observer may prefer the blue sky of an image to be more saturated than that with optimized naturalness. Koh et al., in their study of colour preference and perceived colour naturalness of digital video, found naturalness scores peaked at lower mean chroma levels than preference.

Fernandez et al. (2005) studied the observer and cultural variability for preferred colour reproductions of pictorial images, and concluded that inter-observer variability was approximately twice the magnitude of intra-observer variability. When analysing the data set for image content variability, images that contained people (faces) were routinely less variable than images without people (faces).

Furthermore, despite the fact that preference variability due to observers' cultural background was found to be statistically significant, it was also demonstrated not to be visually significant. Finally, variability in preference due to image content and differences among observers were visually more significant than the variability due to cultural background.

While Fernandez's results show that the differences of colour preference among different cultures are not significant, there are other evidences that demonstrate difference in colour preference among different ethnic backgrounds. This will be discussed in Section 2.4.3. As a matter of fact, different preference colour reproductions for different geographical locations have been designed and implemented on many consumer printers, digital photo mini-labs, and movies.

To understand how colour preference works in an imaging workflow, a couple of colour pipeline examples are provided in sub-section 2.4.2.1. A few important components that affect colour preference are overviewed in sub-section 2.4.2.2.

2.4.2.1 Colour Preference in an Imaging Pipeline

There are many approaches to produce colour images. Colour imaging pipelines for different capturing approaches are different. Fig. 2.4.2.1-1 illustrates an example of a specific case, a typical digital camera processing pipeline. Since an image captured with a digital camera is to be viewed on a display screen or on a hardcopy, it is necessary to transform the image from the scene-referred state to the output-referred state such that the image appears pleasing on the output device and has the desired colour appearance of the image creator. Colour images produced from different approaches are usually converted to a common colour rendering state (usually in the output-referred state), and mostly are merged into a common colour space. Fig. 2.4.2.1-1 depicts an original scene captured with a digital camera sensor through optical lens, passing through a series of colour and image processing steps, and eventually becoming an output-referred colour encoding RGB image. Preferred colour enhancement in the colour rendering step is to produce colours that are preferred to human eyes.
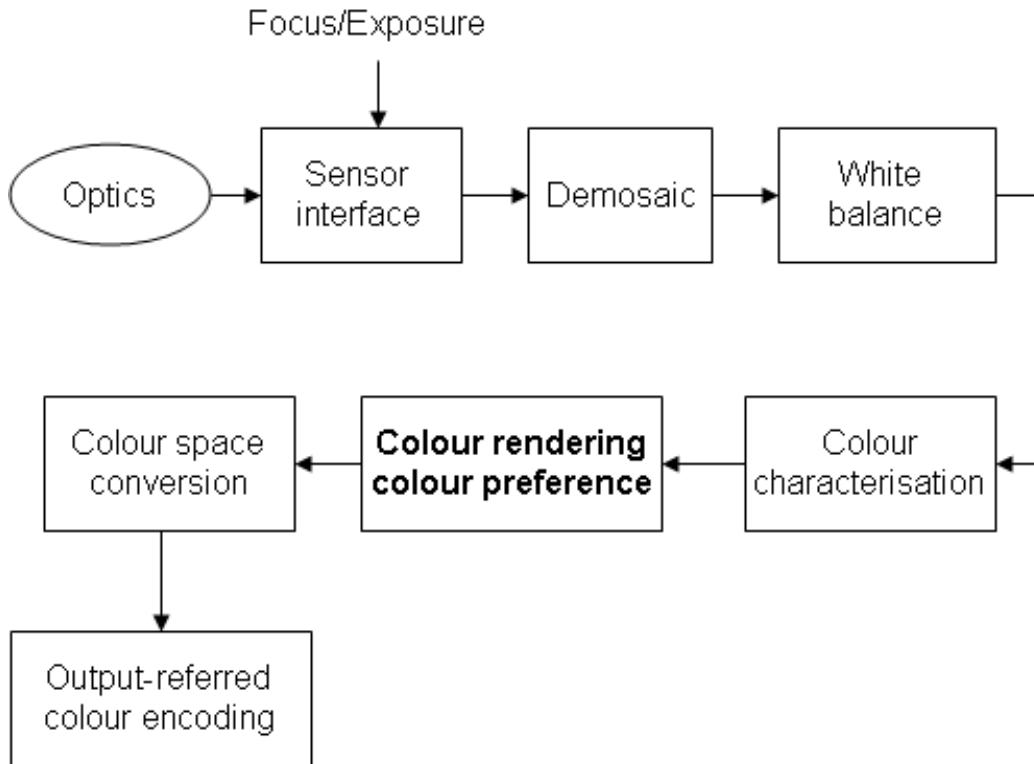
Fig. 2.4.2.1-1 A typical digital camera processing pipeline

Fig. 2.4.2.1-2 illustrates a colour processing pipeline that the author developed for the colour transformation from the output-referred state to a target device colour space (e.g. to display or to print). The image classifier is to classify images based on image objects, pages, or jobs. If an object is classified as photo, a series of colour and image enhancements may be applied. The order of the enhancements in the figure may be altered, depending on the implementation. Again, the step of preferred colour enhancement is to produce more pleasing colours. The object is then passed to a step for colour appearance adjustment aimed at a target device and at a target viewing condition, a step for gamut mapping to the target device, and a step for colour space transformation to a target device. If the gamut mapping is not image-dependent, this step may be performed through interpolation using a pre-generated colour lookup table. A computer application always generates computer graphics at the output-referred state, and an image scanner scans a colour hardcopy that is already at the output-referred state. Therefore there is no scene-referred to output-referred colour rendering in these two situations.
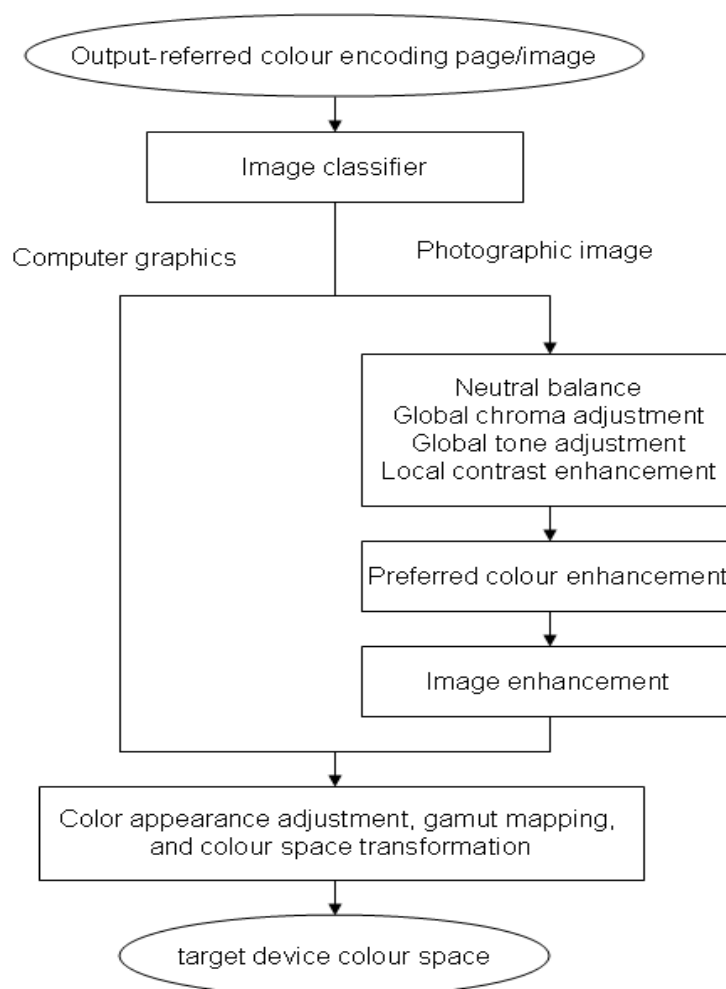
Fig. 2.4.2.1-2 A colour processing pipeline for the colour transformation of the output-referred encoding colours to a target device colour space.

An ideal process for the colour reproduction of output-referred images is to first perform object type segmentation. The purpose of this step is to apply different colour rendering intents and different image enhancements to different objects. Photographic images and business graphics (including text) have different characteristics and generally should be treated differently. For example, gamut mapping methods or parameters for printing these two types of images are quite different. A simple approach to classify an image (or object) into photo or graphics is to count the colours on the image. If the number of colours is small, the image is classified as graphics. Otherwise, it is a photo. This method is simple but false classification may be high. Prabhakar et al. (2002) used three low-level image features: texture, colour, and edge characteristics to classify a colour image into business graphics or natural picture. Naccari et al. (2005) developed a method to classify images into 'portrait', 'landscape', and 'other' for automat colour rendition of natural scene images. Besides applying different colour enhancement algorithms to these three types of objects as described in the reference, different colour maps may be used to further optimize the colour reproduction. Szummer and Picard

(1998) developed an indoor-outdoor image classification method using low-level image features. Hu et al. (2003) applied Bayesian framework and relevance feedback to improve the accuracy of indoor-outdoor image classification. The classification of indoor-outdoor images may be applied to process colours differently. For example, it may be used to aid detecting illuminant or neutral balance.

Automatic detecting grey (black and white) images is very useful in many applications. If RGB signals are the same among three channels (assuming the colour space is neutral balanced with R=G=B), the image may be treated a perfect grey image. However, scanning a grey image in a colour mode by a scanner will mostly not produce equal RGB signals for each pixel. The classification of colour v.s. grey images in this case may be scanner device dependent. The scanner neutral balance, scanner spectral sensitivity characteristics, and the image processing pipeline affect the neutral balance. Similarly, using a digital camera to capture a gray object will not produce a perfect gray image, because of non-perfect illumination detection. From the colour processing point of view, if a colour image has very low chroma (near grey), most of colour enhancement steps may be skipped (except for tone adjustment). However, knowing an image is a grey image may be very helpful for the neutral balance in colour transformation from one colour space to another.

The finer the image classification, the more it helps for colour enhancement. However, image classification in general is a difficult task and subject to false detection. EXIF (Exchangeable Image File Format) tags (http://www.exif.org/), if found within an image, may be helpful for classifying the image. Many tags (e.g. exposure time, F number, OECF, ISO speed rating, light source, scene capture type, etc) are useful for colour and image enhancement.

If an image contains different content types, it may be segmented to different objects and each object is assigned a proper object type for colour and image processing. This method has been used for image segmentation of scanned images, and for preference colour reproduction. For example, an image that contains text, pie-charts, faces, sky, and trees, may be segmented to sub-images (objects), in which each contains single object type. Text enhancement is applied to the text object, the business graphics colour map is applied to pie-charts, and memory colour enhancements are applied to skin tone, blue sky, and trees, and so on.

2.4.2.2 Colour Imaging Attributes that Affect Colour Preference

A few important colour imaging attributes that affect colour preference are briefly discussed below.

2.4.2.2.1 Global Tone Adjustment and Chroma Adjustment

Tone and colour processing are of major importance in producing excellent images. Tone mapping is a technique to modify colours through tone curves, such as to approximate the appearance of high dynamic range (HDR) images with a more limited dynamic range. Although a capturing device, such as a digital camera, performs tone mapping when captures images, the tone mapping may not be optimal for a specific reproduction device on a specific viewing condition, and thus a tone re-mapping may be necessary.

Histogram equalization is a technique to stretch an image to the full dynamic range. It effectively spreads out frequent intensity pixels. However, it may produce unrealistic visual effects for natural images. Improved techniques, such as local histogram equalization and adaptive histogram equalization were proposed to enhance image contrast and maintain the natural visual effect (Kim et al. 1998, Buzuloiu et al. 1999, Tian et al. 2007).

Holm (2003) developed a tone mapping method based on "zone" characteristics of an image. Zone 0 is full black, zone 10 is full white, and contents with shadings fall between 1 and 9. A tone curve is generated based on the re-mapping of the zones. The method requires extensive knowledge about the conditions that an image is captured. Zhang et al. (2006) developed a method for image tone mapping using an adaptive sigmoidal function, in which the sigmoidal function parameters are determined by original image statistics.

Besides global tone transformation to map original tone range into the reproduction medium, local contrast enhancement is another technique to preserve details.

Properly adjusting chroma may enhance the overall image quality. An image captured using a digital camera tends to perceptually lack of colourfulness. Because the colourfulness is related to brightness (Hunt 2006), if a physical world scene that usually has a higher luminance than that of a digital world is reproduced colorimetrically, the colourfulness will be reduced. To compensate the differences in brightness, chroma of the captured image should be boosted. To optimize the chroma adjustment, the image characteristics, the viewing condition, and the gamut of the device should be considered.

2.4.2.2.2 Colour Balance

Colour balance is another important factor in colour image enhancement. An important goal of this adjustment is to balance neutral colours correctly. Hence, the general method is sometimes called grey balance, neutral balance, or white balance.

Most digital cameras have a mean to select a colour correction based on the type of scene illumination, using either manual illuminant selection, or automatic white balance (AWB), or custom white balance. The algorithms are known as illuminant estimation and chromatic adaptation (Forsyth 1990, Finlayson 1996, Barnard 1999, Finlayson and Hordley 2000, Finlayson et al. 2001, Süsstrunk et at. 2001, Jiang and Fairchild 2005, Xiong and Funt 2006, Ebner 2007, Skaff and Clark 2007).

In printing world, colour balance is generally an effort to print a colour image that preserves the neutral balance of the original image. Colour separation or black generation is an important step to determine the neutral grey for printer colour characterisation (Zeng 2000 and 2001). CMYK 1- dimensional (1-D_ lookup tables (LUT) or multiple-dimensional LUT may be adjusted to compensate colour shift in printing (Zeng 2003).

The judgment of neutral balance is affected by the viewing condition. Furthermore, different persons may prefer neutral to be slightly different in colour tints, for example, one may prefer neutral to be slightly bluish while another one may prefer slightly yellowish. Hence, a colour temperature adjustment feature may be implemented in an imaging workflow to adjust the colour balance of images (Park 2003). This can also be used to compensate metamerism.

2.4.2.2.3 Local Contrast Enhancement

To produce a higher dynamic range image on a smaller dynamic range device, optimizing global tone mapping may not cope well with huge contrast ratios. Local contrast adjustment is generally capable of preserving local detail while the global tone range is compressed. Retinex models have been extensively used for local contrast enhancement (Brainard and Wandell 1986, McCann 2001, Moroney and Tastl 2004, Meylan and Süsstrunk 2006). There are rich sources of open source codes and references in this area. Moroney proposed a local contrast enhancement method using non-linear masking (Moroney 2000). iCAM is a sophisticated colour appearance model that is capable of performing high-dynamic range tone mapping and other colour appearance modelling (Fairchild and Johnson 2002, Kuang and Fairchild 2007). Local contrast enhancement is not only used for processing HDR images, but also used for processing images that lack of local contrast.

2.4.2.2.4 Device-Dependent and Image-Dependent Gamut Mapping

Due to the gamut limitation in reproducing colour, gamut mapping is essential for adapting colours from one device gamut to another (Morovic 2008). Device-dependent gamut mapping methods treat image-dependency very coarsely. An image, a page, or a document is categorised into a few groups, such as photo,

business graphics, and mixed contents. A gamut mapping method that is optimized for each group is applied to map the source device gamut to the destination device gamut.   Besides the dependency on image types, the reproduction objective (rendering intent) is another factor for consideration.   For example, a gamut mapping that minimizes a colour difference metric may be used for colorimetric rendering intent, and a geometric morphing method may be applied for the mapping of business graphics.

Gamut mapping may have interaction with other colour rendering attributes. For example, to display an sRGB image (or a video stream) on a large gamut display, such as an Adobe RGB display, the smaller source gamut may be expanded to the Adobe RGB gamut. As a result, the skin tone may become displeasing due to gamut expansion.

Image-dependent gamut mapping, although has many limitations, may be preferred in many situations (Bala et al. 2001, Morovic and Wang, 2003, Zolliker and Simon 2007). It uses the information of the image content (image gamut, image histogram, etc.) to perform gamut mapping. It may use the output device gamut more wisely than the device-dependent gamut mapping. If an edge-preserving gamut mapping method is applied, image details are preserved.

2.4.2.2.5 Imaging Attributes for Colour Enhancement

Besides enhancing the colour characteristics, a number of imaging attributes may be considered for image enhancement.

Sharpening is an important attribute. This attribute is image dependent, and medium dependent. A sharpness value on an image may be estimated to determine how much to sharpen or to smooth the image. A medium (a specific display or printer on a specific setting) dependent sharpening factor may be applied to optimise the final sharpening decision.   Local sharpening/smoothing may be applied to sharpen sharp edges, to smooth face and flat areas, etc. De-noise, scratch removal, and de-screening may be applied to further remove image noise. Other factors, such as 3-D boosting to increase the depth effect, face retouching to rejuvenate characters, teeth whitening, red-eye removal, may be applied to photographic images.

2.4.3 Preferred Colours and Memory Colours of Familiar Objects

As a subset of the preference colour reproduction, memory colour reproduction plays an important role in overall colour reproduction.   Memory colours, such as colours of skin tone, green grass, and blue sky are often categorised as special colour regions for subjective adjustment during colour enhancement or

gamut mapping. They may also be used for automatic image classification and image retrieval, and for pictorial image quality analysis. An overview of prototypical colours of skin tone, green plant, and blue sky is presented below.

2.4.3.1 MacAdam (1951)

In his study of the quality of colour reproduction, MacAdam used a series of colour prints to study optimum colour reproduction of skin colours. The colour prints of a portrait of a young lady (Caucasian) were made from well-exposed colour-separation negatives, with variations of balance from too red or yellow to too blue, and from too green to too pink. Sufficiently small steps of variation were used so as to obtain a number of satisfactory prints. These prints were presented to a number of judges who were asked to accept or reject each on the basis of balance alone. An ellipse encompassing forehead colours with 50% or greater acceptance levels was drawn. The print accepted by the most judges (83%) had the forehead colour (CIE x-y of about 0.434 and 0.396) located in the middle of the ellipse. The actual forehead colour of the lady (CIE x-y of about 0.437 and 0.384) was noticeably different from the acceptance colours within the ellipse. The measurement was based on the assumption of a 4000K blackbody source of illumination. The results led to two conclusions. First, optimum reproduction of skin colour is not "exact" reproduction. Second, the shape of the 50% acceptance zone is similar to the shape of the zone of equally noticeable differences.

2.4.3.2 Sanders (1959)

Sanders studied colour preferences for natural objects, including hand, face, tea, butter, raw beefsteak, and potato chips. A viewing booth with variable colour light was provided to change colours of test objects. The main illumination of the booth was provided by three pairs of fluorescent lamps with green, blue, and pink colours. The luminous flux from each pair of lamps could be controlled by means of a dimmer circuit. By adjusting each 21-step dimmer, light of variable colours could be produced. Additional tungsten lamps could be switched on or off as desired to achieve desirable colours. The colour light was mixed by a sheet of tracing paper and a diffusing screen. The background colour was controlled by a background box at the back of the booth. The box, which contained two fluorescent lamps, was painted white inside and was covered with tracing paper. The colour of the background could be altered by changing the fluorescent lamps. In this experiment, the background was confined to the chromaticity of either CIE Illuminant B or C. For each object investigated an attempt was made to provide a set of colours which included unsatisfactory colours on all sides of the acceptable ones. The colours in the set were then presented in random order to each observer who was asked to say

whether the colour presented was found to give "good", "fair to good", "fair", "fair to unsatisfactory", or "unsatisfactory" colour rendition to the sample. To average repeated observations, the judgments were given the weights 100, 75, 50, 25, and 0, respectively. It was found that the preferred colour of the face (CIE xy values under CIE Illuminant C are 0.441+/-0.011 and 0.379+/-0.007, respectively) is more saturated than the actual facial colour; the preferred colour for butter is considerably paler than the colour of the actual butter sample; the difference between the preferred colour and its actual colour for the remainder of the objects were not significant.

2.4.3.3 Bartleson

2.4.3.3.1 Bartleson (1959)

According to Bartleson, photographs typically do not compare a photo directly with its original scene. Photographers rely on their memory of the colours of objects in the original scene to judge the colour reproduction quality of memory colours. Bartleson printed a woman portrait using Kodak Flexichrome Process to study the preferred colour reproduction of flesh colours. Twelve 4x5-in. prints were produced in which chromaticities of the face area were systematically varied around and between the chromaticities for average natural flesh and the corresponding mean memory-colour. The prints were viewed in a viewing booth with neutral gray wall of approximately 18% reflectance and CIE Illuminant C simulated daylight. 10 observers who had moderate to advanced technical knowledge of colour photography evaluated the samples by paired-comparison, and then judged the acceptability one by one. Acceptability was defined as the condition in which an observer evidenced no displeasure when evaluating the reproduction. The experiment confirmed that memory flesh colours were warmer (or more yellowish) and more chromatic than actual flesh colours. The mean memory-colour and the optimum print were coincident in Munsell notation chart, i.e., both have the same chromaticness. Bartleson concluded that "preferred flesh-reproductions may be of virtually the same hue and saturation as the abstract memory-colour for flesh". Since the data was rather limited (only one image was used), the conclusion was considered "qualitative rather than quantitative".

2.4.3.3.2 Bartleson (1960)

Bartleson defined "memory colour" as colours that are recalled in association with familiar objects, that is, objects with which we have frequent visual experience. In this context, memory colour does not refer to the ability of sheer colour recollection which is generally termed "colour memory". Instead, memory colours

are considered to be an individual's standard recollection for familiar objects and, because of the frequency with which certain object-perceptions are repeated, these memory colours tend to be relatively stabilized. In his study of memory colours of ten familiar, naturally occurring objects, Bartleson placed 931 Munsell colour patches in a viewing booth and judged by 50 observers. The walls of the viewing booth were painted with a neutral gray of approximately 18% reflectance, and the colour temperature was 2700°K with an illumination level of approximately 200ft-c at the viewing plane. About half of the observers were "nontechnical" and the other half were "technical". The experimenter named an object or a substance and the observer examined the display of colour samples and then indicated the patch that best represented the colour of the object. Observers were allowed to interpolate between available patches. The ten object colours used were: red brick, green grass, dry grass, blue sky, flesh, tanned flesh, broad-leafed summer foliage, evergreen trees, inland soil, and beach sand. Each observer completed all ten judgments in about 15 minutes. The result indicates that chromaticities of the memory colours are different from those of the natural objects. In natural flesh, including suntan, varies mostly in luminance (for Caucasian) and somewhat in purity, the memory colours for flesh are dissimilar in dominant wavelength and both are distinctly more yellow than natural flesh. Green grass and deciduous foliage appear to be remembered as more blue green than yellow green, both memory colours having approximately the same dominant wavelength. Dry grass, in memory, falls at a dominant wavelength that is nearly common to both natural grass and deciduous foliage. The memory colour for blue sky is more cyan and of higher purity than the mean for natural skies. The standard deviation for the choice of memory-colour hue for flesh is the highest, excepting that resulting from the abnormal distribution of memory colours for sand. This may indicate that individuals have rather definite impressions of the colour of flesh, although a general tendency to remember flesh as being more yellow than it actually is. Overall, there is evidence of increased saturation in the memory colours. To compare his data with others, Bartleson converted his finding of memory colours from Illuminant A to Illuminant C. The CIE x-y values of mean memory colours of flesh, grass, and sky are listed in Table 2.4.3.3-1.

Table 2.4.3.3-1 Bartleson's result of mean memory colours (CIE xy) in Iluminant C (1960)

Memory colour	x	y
Flesh	0.3548	0.3441
Tan flesh	0.3593	0.3724
Green grass	0.2478	0.4149

Dry grass	0.3372	0.4059
Green foliage	0.2665	0.3681
Evergreens	0.3735	0.4049
Blue sky	0.2319	0.3012

2.4.3.3.3 Bartleson (1961)

Bartleson found that colour memory obtained from successive colour matching was significantly different from memory colour. Bartleson defined that colour memory was an observer's ability to remember and reproduce or recognize abstract colours. Short-term colour memory could be found through successive colour-matching experiments. To study whether there was significantly difference between colour memory and memory-colour, Bartleson conducted a successive colour-matching experiment using four 3- by 3-inch colour patches of natural flesh, blue sky, sand, and deciduous foliage, together with 931 Munsell patches. The viewing condition was exactly the same as the memory colour experiment described earlier. One object-colour patch was viewed by an observer for 15 second against a neutral surround of about Munsell Value 5. The patch was then removed and the observer searched the array of Munsell patches in order to find one that best matched the original patch. The process was repeated for all four object-colours. Experimental results of successive colour matching indicate that saturation and lightness tend to change in memory, but hue remains essentially the same. In general, there is an increase in saturation with memory and usually an increase in the lightness of light colours and a decrease in the lightness of dark colours. By contrast, memory-colours of familiar objects have statistically and perceptually significant hue shifts as well as changes in saturation and lightness with memory. The differences suggest that the processes of colour memory and memory-colour are significantly different. Therefore, colour-memory and memory-colour effects cannot be indiscriminately interchanged in considering colour reproduction requirements for photographic processes.

2.4.3.3.4 Bartleson and Bray (1962)

In their study of the preferred reproduction of flesh, blue-sky, and green-grass colours, Bartleson and Bray closely examined the differences among preferred colour, memory colour, and real colours of the three familiar objects. To study the tolerance for preferred Caucasian flesh reproduction in prints, nineteen 6- by 7.5-inch Kodak Dye Transfer Prints were made, all with the same colour balance, with variations only in the flesh chromaticities. Eleven experienced observers evaluated the prints in a viewing booth illuminated with CIE Illuminnt C. Each observer first

ranked 19 samples into two groups of 9 and 10 prints, respectively. Thus, there was forced consistency within each group, as was common in ranking experiments. Then, the observer fitted each print of the first group, randomly selected, into the group-two rank array. The individual observer consistency as evaluated by this procedure was somewhere between pair-comparison and the forced consistency of ranking. The data were fitted into a pair-comparison data matrix and therefore treated as pair-comparison data. An elliptical contour was constructed to approximate the locus of 50% acceptance (positive z-scores were treated as acceptable). The result shows that a) the centroids for the flesh memory-colour, b) several satisfactory reproductions of flesh, c) a preferred reproduction flesh colour determined in a different time, and d) the most preferred reproduction colour determined in this experiment all lie close to one another and at some distance from natural flesh. It indicates that preferred reproduction colours for flesh are distributed around the chromaticness of the mean flesh memory-colour rather than the average natural flesh colour. The preferred flesh (Caucasian) colour has CIE x-y values of about (0.436, 0.392) under 4000K illuminant. Probably due to the gamut limitation of the photographic colour reproduction, the preferred colour is a little pale compared to that in the modern colour photographic colour reproduction.

Their second phase of the experiment was to study preferred colour reproduction for blue sky. Two series of 14 and 9 prints were made of scenes containing large areas of blue sky in the same manner. Blue sky chromaticities were varied while the overall print balance remained constant. 20 experienced observers ranked each of the prints in order of merit according to their preferences for the colour of reproduced sky. The chromaticities of the prints which received acceptable ratings were plotted. The approximate area of natural sky chromaticities was plotted in the same figure. The mean memory colours determined by Bartleson (1960) and by Newhall et. al. (1957) lie at some distance from the centroid chromaticity of these preferred print colours. The most representative chromaticity for preferred reproduction of blue sky agreed well with the natural sky chromaticity but not with the mean memory colour chromaticity. There was no tendency of memory colours to be more preferred than natural colours. These results indicate that the preferred blue sky hue is the same as the real sky hue. However, due to the limitation of the print gamut, the preference in chroma may be unreliable.

The third phase of the experiment was to study the preferred colour reproduction for green grass. Again, a panel of 20 observers rated prints from two dissimilar scenes in which colours of grass areas had been controlled separately from the overall colour balance. 10 sample prints from Scene I and 20 from Scene II were selected for judgment. The chromaticities of prints found to be acceptable

were plotted, together with the hue locus of the mean natural grass colours. They found that the most preferred grass colour located at some distance from that of the mean memory colour. The difference in hue is such as to produce a preferred colour that is more "yellow-green" than the memory colour. The preferred chromaticities lie along the locus of the natural grass hue. The preferred reproduction colour appears to be more similar to the mean of the natural colour than to the mean of the memory colour.

2.4.3.4 Hunt et al. (1974)

Hunt et al. commented that the gamut of colours attainable in some of the systems used in earlier publications was much more limited than that produced with modern photographic systems, and such systems might be biased in favour of a somewhat lower level of colour saturation. Another bias from the previous studies was that most of the colour preferences were assessed in reflection prints using daylight. For these reasons, Hunt et al. undertook a fresh assessment of the preferred colour reproduction of blue sky, green grass, and Caucasian skin in colour photography using up-today colour photographic systems. A split-field technique was used to produce colour reflection prints and projected transparencies, in which one area could be altered in colour while keeping the rest of the picture constant. The variable area was arranged to contain only blue sky, green grass, or Caucasian skin. Colour pictures were judged by groups of observers for the quality of the reproduction in the test areas, and chromaticities corresponding to preferred and acceptable colour reproduction were obtained. In reflection prints, the preferred blue sky was found to have a higher purity than the average real blue sky, but the preferred green grass and the preferred Caucasian skin had similar purities but were slightly yellower than average real samples. In transparencies projected with tungsten-halogen lamps, the preferred and acceptable chromaticities were considerably more orange because of visual adaptation to the light of the projector. The authors compared the results with earlier studies by other researchers using photographic materials that had more limited colour gamuts and suggested that the limited gamuts might tend to reduce the purities of preference colours.

2.4.3.5 Sanger et al. (1994)

To adjust skin colours for preferred colour reproduction, the preferred skin colour region must be found. Sanger et al. measure offset printing samples of Mongoloid, Caucasoid, and Negroid skin colours, and modelled the colour regions of each type of skin colours in u'-v' axes with ellipses. They found that the Negroid distribution was wider than the distribution of other races; chroma of skin colour increased steadily in the order of Caucasoid, Mongoloid, and Negroid while the

lightness increased in the reverse order; the hues were similar and the dominant wavelength was about 590nm in all distributions. Three portrait photos of Mongoloid, Caucasoid, and Negroid were used to study preferred skin colours. Skin colours of each image were altered to produce a series of 50 to 60 copies of images with different facial tones. A preferred colour for each image was evaluated by an observer rating experiment. A panel of five naïve observers was asked to rate skin colours using five categories: excellent, good, acceptable, poor, and bad. Afterwards, chromaticities u' and v' of skin colours in sample images as excellent and good were measured and plotted in u'v' chromaticity diagram to analyse their distributions. The result shows that chroma of preferred skin colours increases steadily in the order of Caucasoid, Mongoloid, and Negroid, preferred hue angles among three groups are about the same, with dominant wavelength at about 590nm. The u'v' of preferred skin colour centres of Caucasoid, Mongoloid, and Negroid in D65 are approximately (0.218, 0.486), (0.221, 0.492), and (0.231, 0.501), respectively. The orientations of three preferred skin colour ellipses are similar, and the shape of each ellipse shows that hue tolerance is smaller than the chroma tolerance in preferred skin colours.

2.4.3.6 Yano and Hashimoto (1997)

Yano and Hashimoto used three female models to studying the preference for Japanese complexion. Each model's face was illuminated under 40 different illumination colours from a lighting box while the viewing adapting fields were illuminated by two other lighting boxes with correlated colour temperature the same as D65 (6100K), produced the combination of 120 facial colours under a constant viewing condition. Twenty-one Japanese women evaluated the preference of the skin colours using seven scales: excellent, good, fair, acceptable, poor, bad, and very bad. The skin colours rated as better than acceptable were used to draw a preferred skin colour ellipse in u'v' coordinate diagram for each model. Three preferred skin colour ellipses are very close, which indicates that the preferred complexions are about the same among different models. The real skin colours of the three models were measured, adapted to D65 and drawn on the same u'v' diagram to compare with their preferred complexions. It illustrates that the three real skin colours are more different than the three preferred skin colours. The average preferred Japanese complexion was (u', v') = (0.2425, 0.4895) corresponding to D65 illuminant. Compared with the real complexion of "Japanese Woman", the preferred skin colour is shifted to a slightly higher saturation and slightly more reddish in hue. The preferred Japanese complexion is quite different from the preferred complexion of Caucasian woman studied by Sanders (1959). Preferred Caucasian complexion is shifted to a much higher saturation level than the real

Caucasian complexion. They concluded that "Caucasian observers prefer a higher saturated complexion than do Japanese observers".

2.4.3.7 Yendrikhovskij (1999)

Yendrikhovskij discussed two interesting aspects of appraising colour reproductions. First, "although any colour photograph is always distorted relative to reality, the deviation from the colorimetrically perfect rendering is seldom conspicuous to observers". Second, "although items in a reproduction might never be experienced by observers directly, people usually do not have any problem in criticizing the realism of the reproduced colours". The reason is that the colour sensations evoked by a reproduction are compared with a mental recollection of the colour sensations previously experienced when looking at objects similar to the ones being appraised. Memory colours are quite consistent among different observers. And there is a tendency for memory colours to be more saturated compared with their actual object colours. People might prefer to see an image in which the colour appearance of a familiar object agrees with its memory colour rather than with their colorimetric content of the original scene. One of the important characteristics of the representation of colours in memory is the organization of colours into categories and prototypes. Prototypical colours are indeed more salient in perceptual and cognitive domains. They tend to be more rapidly and consistently perceived, remembered, and learned than non-prototypical colours. Skin, grass, and sky are the categories that are frequently seen in real-life images. "One can expect that observers are sensitive to colour manipulation of these categories, since they exhibit a limited gamut in nature. On the other hand, colour manipulations of objects from a category that does not exhibit certain stabilities in the outside world are not as critical for observers."

2.4.3.8 Bodrogi and Tarczali (2001)

Bodrogi and Tarczali studied the colour memory of various sky, skin, and plant colours. Observers memorise an original colour O in a first viewing situation. This becomes an instant memory colour M. After a given time interval t, observers compare their so-called later memory colour M' with an "actual" colour A. The colour A seen in a second viewing situation usually differs from the colour seen the first viewing situation. In the second viewing situation, observers may modify the colour A until it matches M'. The result of the modification of A is the colour C. The later is usually called corresponding colour. In their study, the two viewing situations were identical. Thus the difference between the colours O and C is completely due to memory effects. Bodrogi used photo-realistic images containing

sky, plant, and Caucasian skin colours, as well as standalone colour patches taken from the corresponding photo-realistic images to study the shift of memory colours.

In their experiment, all images were displayed in a dark room, on a calibrated EIZO F784 21'' colour monitor. The reference white (x=0.299, y=0.267, and Y=37cd/m^2) was always displayed on the left side and on the right side of the screen as two vertical stripes. An observer adapted to this viewing situation for at least 2 minutes. The observer watched a colour of the part of an image (or a uniform colour patch); memorize it in the next black frame; after 4 second of pause, tried to find the memory of the colour by adjusting three sliders at the top of the screen corresponding to lightness, hue, and saturation. In one of the task, the original colour O is a uniform patch on a uniform gray background. In another task, the original colour O is displayed with the image context. In a third task, the original colour O is part of a photo-realistic image containing an identifiable shapes and /or texture (e.g. grass, sky, or Caucasian skin). 11 observers participated in the experiment. In general, memory colour shift is larger in photo-realistic images than in standalone colour patches. In both cases, later memory colours M' tend to have higher chroma than the instant memory colour M. This is agreed with findings from many other researches. For skin and sky, the later memory colours M' tend to be darker than the instant memory colour M. For plant, the result is opposite. Hue shift depends on the original colours. For sky, instant memory colours M are shifted toward purple-blue. For skin, observers tend to find that M' colours contain more unique yellow than O. For plants, observers tend to find that M' colours contain more unique green than O. Bodrogi suggested that the findings of memory colour shift can be applied to gamut mapping to mimic the memory shift. Because the memory shift depends on the presence or absence of the image context, the context of image contents should be considered in the memory colour reproduction.

2.4.3.9 Kuang et al. (2005)

Kuang et al. (2005) conducted psychophysical experiments to study the influence of different factors on colour preference of photographic colour reproduction. 14 sRGB images were used to study colour preference of skin tone, green grass, and blue sky. The area of interest (people, green grass, or blue sky) is masked manually for colour adjustment. Each image was converted to CIELAB colour space, and then colours of the area of interest were adjusted in Lch (lightness, chroma, and hue) space. The Lch space was divided evenly into 12 by 12 by 6 small cubes. Therefore, there were 13, 13 and 7 steps in L*, C_{ab}* and h_{ab} respectively. Thus a total of 1183 colour adjusted images for each original image might be produced. In each comparison, three images were displayed on the CRT screen simultaneously. Forty-eight colour-normal observers took part in the colour

preference experiment. They were categorised into four groups: 14 Caucasian, 13 Asian/Pacific, 13 Indian and 8 African American observers. Of them, 17 were females and 31 were males. Observers were instructed to pick the preferred one by clicking that image directly. A preferred image was found in 14 comparisons from coarse to fine selection. The experimental result is summarized below: 1) background lightness has little influence on skin colour preference; 2) capturing illuminant has significant influence on skin colour preference; 3) the preference variances on Asian and Caucasian skin colours are smaller than those on Indian and African American; 4) background lightness has slight influence on the lightness preference while background chromaticity and image content have little influence for sky colour preference; 5) image contents have influence on grass colour preference both in lightness and chromaticity; and 6) no significant culture difference among different ethnic observers.

2.4.3.10 Topfer et al. (2006)

Topfer et al. studied the regional preference for the rendition of people. They argued that the preferred rendition of people was more complex than reproducing the preferred chromaticities of skin tones, because colour and tone attributes came into play, e.g., tone reproduction and colour and density balance. AgX systems in store fields were used to print samples. Near optimum rendition of the scenes presented in the experiment (in terms of tone reproduction and overall colour and density balance) was obtained with the help of local Kodak personnel. The selections were quantified using small Munsell N5 gray cards included in the images. Samples with different skin tone variations were produced. Print lightness was quantified based on five different CIELAB L* levels of a mid-tone neutral patch covering a total range of 25. In each experiment, observers were asked to rank-order 13 or 14 4 x 6-inch prints for each scene in terms of overall quality. All experiments were conducted under controlled lighting conditions using a Gretag Macbeth Judge II light booth with D50 Illuminant. In China, ten scenes captured on Kodak Gold 200 film and on three digital camera models were included in the skin tone and colour balance studies. Additional experiments on tone reproduction were carried out with five levels and 35 different scenes. At least 30 observers participated in each study. Ten labs in four large cities in China were chosen for the field study. Eight participants per lab were recruited, including three lab operators and five store customers, for a total of 80 observers (30 photofinishing operators and 50 consumers). In India, sixteen scenes captured on four different film types, including Kodak Gold 200 film, were presented in a combined skin colour and tone reproduction experiment. Three largest cities (Delhi, Chennai, and Mumbai) were selected for the study allowed to sample the full gamut of skin colours in India. The

rank-order technique was used for judgment. The proportions of selecting one sample over another in terms of quality were transformed to 50% just-noticeable differences (JNDs) of quality.

The experimental result demonstrates that preferences for the rendition of Caucasian and Asian skin tones differ substantially; more reddish and desaturated renditions of skin colour were preferred in India and China; the preferred skin colours for India and China overlap, which suggests that similar appearances of skin tones are preferred in both countries, however, Indian skin tones show a wider variety in lightness than Chinese skin tones, and are on average somewhat darker; the preferred overall print lightness, quantified by the Munsell N3.5 is highest in India, followed by China and the US; the orientation of the preferred skin colour ellipses changes by region; for Caucasian skin tones, hue is the most important attribute; wider variations in hue were tolerated in China; and individual preferences for the rendition of skin colour showed much less variation in China than in India and the US.

2.4.3.11 Summary

Various researches consistently concluded that preferred colour reproduction tends to produce more chromatic colours than original colours in general, although it may slightly distort the fidelity. Preferred colour reproduction has optimal chroma higher than that for natural colour reproduction.

The skin colour category is the most critical prototypical colour region in photographic colour images. There is a consistent conclusion that preferred skin colours are different from actual skin colours, and preferred Caucasian skin colour is more yellowish than real Caucasian skin colours.

A summary of preferred skin colours from various researches is listed in Table 2.4.3.11-1. Some colour values are estimated from plots of authors' publications. Parker et al. data are from their presentation slides.

Table 2.4.3.11-1 Mean preferred skin colours from various studies

Authors	Sample	Obs.	Ethnics	Viewing Condition	Colour
MacAdam 1951	Kodak print	n/a	Caucasian skin tone, Caucasian observers	4000K Illuminant	CIE xy: 0.434, 0.396
Sanders 1959	Physical people	n/a	Caucasian skin tone, Caucasian	C Illuminant	CIE xy: 0.441, 0.379

			observers		
Bartleson & Bray 1962	Kodak print	11	Caucasian skin tone, Caucasian observers	4000K Illuminant	CIE xy: 0.436, 0.392
Sanger 1994	Print	5	Caucasian skin tone, Japanese observers	D65	CIE xy: 0.355, 0.351
Sanger 1994	Print	5	Asian skin tone, Japanese observers	D65	CIE xy: 0.367, 0.360
Sanger 1994	Print	5	African skin tone, Japanese observers	D65	CIE xy: 0.387, 0.373
Yano & Hashimoto 1997	female model	21	Japanese skin tone Japanese observers	D65	CIE u'v': 0.2425, 0.4895
Bodrogi & Tarczali 2001	CRT display	11	Caucasian skin tone, Caucasian observers	Background: CIE Yxy: 37, 0.299, 0.267	CIE u'v': 0.27, 0.47
Kuang et al. 2005	CRT display	48	Asian skin tone, mixed observers	D65	CIE a*b*: 11.7 21.5
Kuang et al. 2005	CRT display	48	Caucasian skin tone, mixed observers	D65	CIE a*b*: 26.7, 38.0
Kuang et al. 2005	CRT display	48	Indian skin tone, mixed observers	D65	CIE a*b*: 23.0, 30.0
Kuang et al. 2005	CRT display	48	African skin tone, mixed observers	D65	CIE a*b*: 18.3, 29.0
Parker et al. 2006	TV	n/a	Asian skin tone	D65	YCbCr: 121.9, 104.6, 157.3
Parker et al. 2006	TV	n/a	Caucasian skin tone	D65	YCbCr: 157.2, 104.3, 153.1

Parker et al. 2006	TV	n/a	African skin tone	D65	YCbCr: 95.7, 111.6, 150.2
Parker et al. 2006	TV	n/a	Mixed skin tone	D65	YCbCr: 136.3, 105.6, 153.9

To compare results with each other, all colours are adapted to a common white point, D50, and converted to a common colour space, CIELAB. If an original adapted white point is not known, the viewing illuminant is assumed. Since MacAdam and Bartleson and Bray used an illuminant that is very different from D65 and their adapted white points are not known, their data are not used for comparison. If a mean preferred skin colour was provided in CIE xy or u'v' colour space, CIE Y value is set to be a value so that L* equals 60 for Caucasian and Asian skin tones or 50 for African skin tone. The skin colour from Bodrogi and Tarczali is a mean memory skin colour instead of a preferred skin colour. The results are listed in Table 2.4.3.11-2 and illustrated in Fig. 2.4.3.11-1.

Table 2.4.7-2 Mean preferred skin colours from various studies converted to CIELAB with D50 white point

Authors	Sample	Obs.	Ethnics	a*	b*
Sanders 1959	Physical people	n/a	Caucasian skin tone, Caucasian observers	22.5	34.8
Sanger 1994	Print	5	Caucasian skin tone, Japanese observers	7.8	11.2
Sanger 1994	Print	5	Asian skin tone, Japanese observers	8.9	15.1
Sanger 1994	Print	5	African skin tone, Japanese observers	9.8	18.6
Yano & Hashimoto 1997	female model	21	Japanese skin tone Japanese observers	19.0	15.3
Bodrogi & Tarczali 2001	CRT display	11	Caucasian skin tone, Caucasian observers	23.0	21.5
Kuang et al. 2005	CRT display	48	Asian skin tone, mixed observers	12.2	22.8

Kuang et al. 2005	CRT display	48	Caucasian skin tone, mixed observers	28.7	38.7
Kuang et al. 2005	CRT display	48	Indian skin tone, mixed observers	20.8	30.6
Kuang et al. 2005	CRT display	48	African skin tone, mixed observers	20.1	29.5
Parker et al. 2006	TV	n/a	Asian skin tone	19.8	24.8
Parker et al. 2006	TV	n/a	Caucasian skin tone	14.8	23.9
Parker et al. 2006	TV	n/a	African skin tone	16.3	18
Parker et al. 2006	TV	n/a	Mixed skin tone	16.6	23

The mean preferred skin colours spread in a large chroma range. The preferred colours obtained from print samples in 1950's to 1960's have smaller chroma, which may be the result of gamut limitation in producing image samples. The hue angles spread around a small hue range, with a hue centre at about 54°.
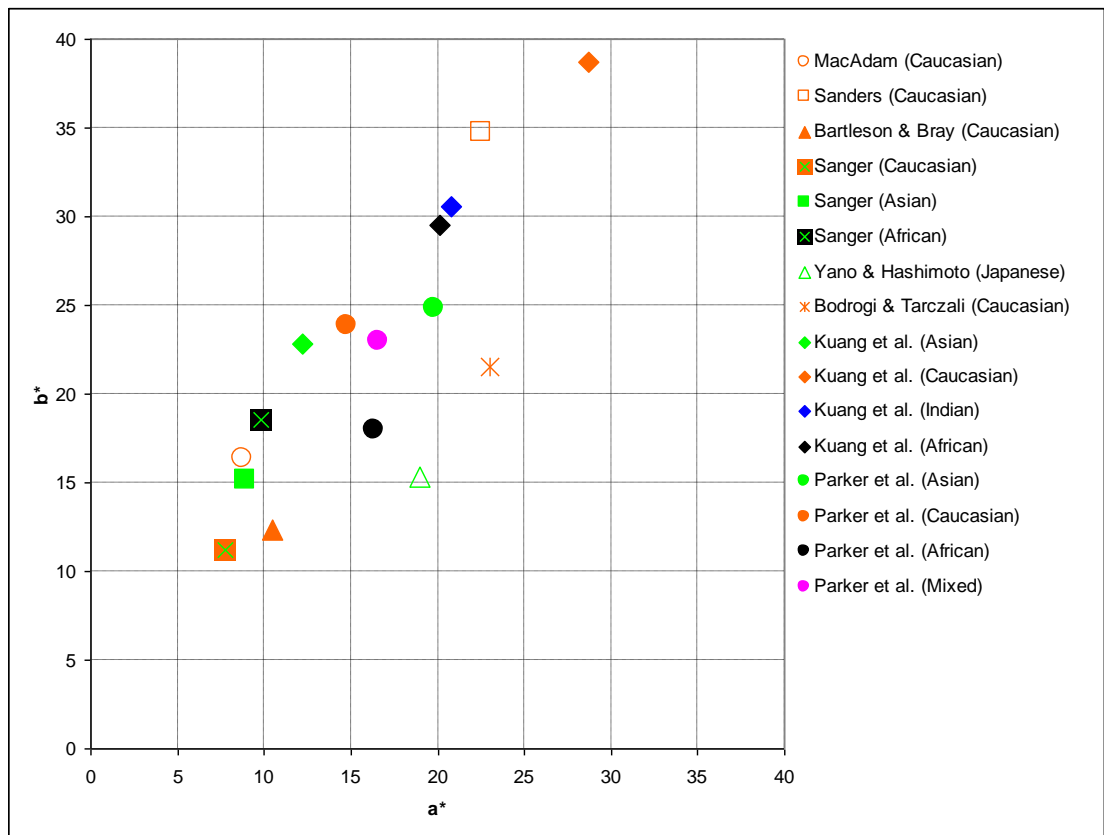
Fig. 2.4.3.11-1 Mean preferred skin colours from various studies

Green plants appear to be remembered as more blue green than yellow green. The memory colour for blue sky is more cyan and of higher purity than the mean for natural skies. Green plants and blue skies are preferred to be more chromatic than their memory colours.

2.4.4 Skin Colour Enhancement

Since preferred colour reproduction is to have colour look preferred to human eyes, the outcome of preference should be determined on the output-referred state. Say it more specifically, the optimization of the preferred colour reproduction should aim at the representation medium, such as a LCD display, a printed hardcopy, sRGB colour space, etc.

To perform special colour processing to a category of memory colours, the category of colours must be detected, and its boundary must be defined. There are two basic approaches for memory colour segmentation. One is feature-based and the other is pixel-based (ignoring spatial information). The feature-based technique is often used to detect blue sky, green grass, faces, lake/sea water, etc. It may be used to detect face, and therefore to determine the skin region of the face (Sanger et al. 1994, Qian 2001, Nallaperumal et al. 2006, Gasparini et al. 2008, Gallagher et al. 2008, Fredembach et al. 2008). It has been used extensively in red-eye removal. General speaking, this technique is computational expensive.

Detecting object's memory colours through their colour values is simpler than feature based approaches. If a colour belongs to the skin tone region, the relative position or probability of the colour is computed for proper adjustment. The major drawback of this approach is that it identifies any colour that belongs to a memory colour region regardless what the object is. For example, the skin colour of a wall is processed the same way as that of a face. A combination of feature-based and colour-based detections improves the detection accuracy.

A detail review of skin colour, skin colour detection, and skin colour enhancement is presented in next three sub-sections.

2.4.4.1 Skin Colour Overview

Each of us is unique in terms of the combination of tens of thousands of genetically determined characteristics that we possess. However, we clearly have some traits in common with other people. These traits can be affected by differential selective pressures and environmental influences.

Humans like to classify and use identity labels for people and things with which we come in contact. It satisfies our apparent need for a sense of order. In addition to gender and age, most of us readily classify each other into categories on

the basis of what we consider to be races. In North America, people usually think in terms of Black, White, Asian, Hispanic or Latino, and Indian or Native American. These are all archaic concepts of physical types that have little biological reality. Academics may use more sophisticated sounding terms for these perceived biological groupings, such as Negroid, Caucasoid or Caucasian, and Mongoloid. Fig. 2.4.4.1-1 shows the worldwide distribution of skin colour variation.
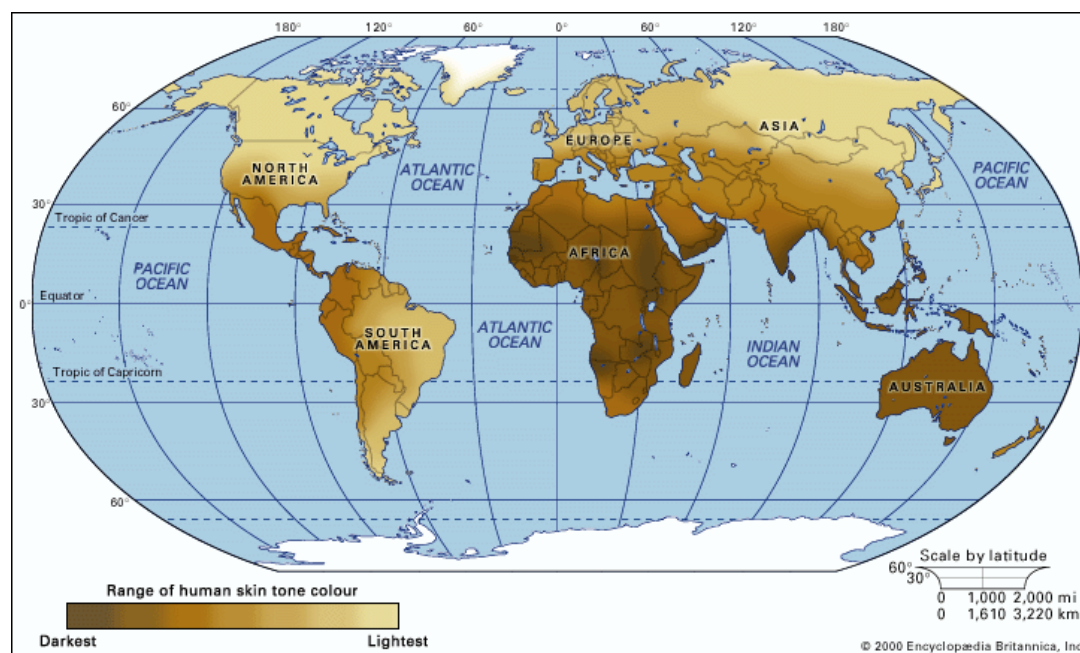
Fig. 2.4.4.1-1 Worldwide distribution of skin colour variation (Encyclopaedia Britannica, Inc.)

Human skin can be divided into two main regions, the epidermis and the dermis. The dermis is attached to the underlying hypodermis (see Fig. 2.4.4.1-2). The epidermis is the most superficial layer of the skin. The dermis is the inner layer of the skin. Hypodermis is a layer connects the skin to deeper structures. It is not part of the skin. The reflectance of the skin at various wavelengths is mainly determined by the chromophores present in the various layers of the skin, which includes melanin, keratin, carotene, collagen, and haemoglobin (Angelopoulou 1999 and 2001). Light incident on skin must first encounter the epidermis. The melanin in the epidermis acts as a filter whose transmission rate increase with wavelength. The light that is not absorbed by melanin penetrates the epidermis and reaches the dermis. In the dermis, the hemoblobin in the blood vessels causes selective absorptions. Heavily pigmented skin increases the amount of melanin which absorbs most of the light in the epidermis, allowing a much smaller percentage of the incident light to reach the vasculature of the dermis (Angelopoulou 2001). The spectral characteristics of difference races or different individuals are due only to variation in the amount of melanin present (Sun and Fairchild 2002).
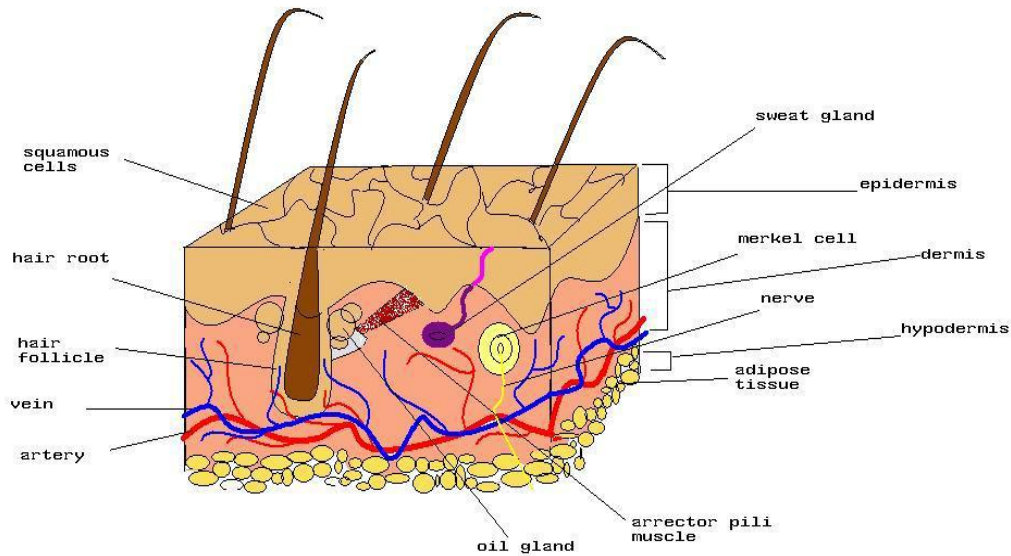
Fig. 2.4.4.1-2 A diagram of human skin (created by Crystal Mason, release under GNU Free Documentation License)

2.4.4.2 Skin Detection

When developing a system for skin colour detection and skin colour enhancement, three main problems are faced: what colour space to be used; how to model skin colour distribution; and how to adjust skin colours. Each of these three aspects is discussed in following subsections.

2.4.4.2.1 Colour Spaces for Skin Colour Modelling

In the scene-referred state, if the image capturing condition is known, the parameters of the capturing condition may be used to guide how to decide a skin colour region. The higher the confidence of the parameters (illuminant and other lighting parameters), the smaller a skin colour region can be determined for more accurate skin colour detection.

To detect skin colours in the output-referred state, a larger colour region should be defined to cover skin colours captured under different lighting conditions and with different sensors. Because the white balance may be incorrect or inaccurate, the skin colours may occupy slightly different regions. Colour editing or various colour enhancement may shift skin tones. For various reasons, a skin colour gamut larger than that in the scene-referred state should normally be used for the skin colour detection of general output-referred images. If the capturing condition is fixed or is known, the skin colour region will be confined in a smaller region.

Many colour spaces (e.g. RGB, r-g, YC_bC_r, HSV/HIS/HSL, YUV, YIQ, L*u*v*, L*a*b*, etc.) have been used to define a skin colour region for skin colour detection, face detection, and skin colour enhancement (Kakumanu 2007).

2.4.4.2.1.1 *RGB Colour Space*

Due to the fact that colour images are displayed in an RGB colour space, an RGB colour space may be used to detect skin colours efficiently. For general RGB images with an unknown RGB colour space, sRGB colour space may be assumed. If RGB colour space is treated as device-dependent, the parameters for the skin region must be modified for each RGB colour space. Gasparini et al. (2008) used RGB colour space for binary classification of skin pixels. Choudhury et al. (2008) applied RGB colour space in forensic investigations to search and identify pornographic images. Jones et al. (2002) developed a statistical colour model using RGB colour space to detect skin colours.

2.4.4.2.1.2 *r-g Colour Space*

To remove the effect of brightness, an RGB colour space may be normalized as an r-g chrominance space:

$$r = \frac{R}{R+G+B}$$

$$g = \frac{G}{R+G+B}$$
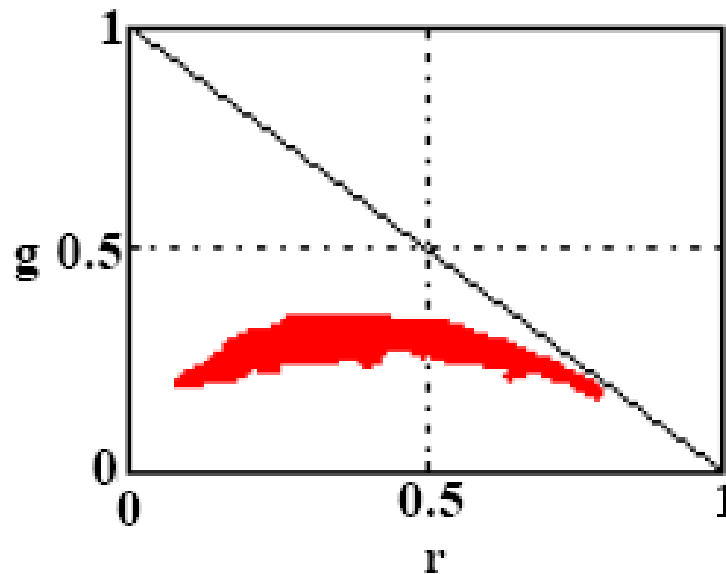
Fig. 2.4.4.2-1 Computed skin loci for a Sony digital camera

As a 2-D space, r-g chrominance space is efficient in computation, and it is approximately invariant to changes of surface orientation relative to the light source. The r-g colour space has been widely used for illumination detection and skin/face detection in scene-referred stage (Martinkauppi 2002). Fig. 2.4.4.2-1 (Martinkauppi 2002) shows the r-g gamut of skin colours (the red area) computed with the data captured using a Sony digital camera.

The r-g colour space is also used for skin/face detection in the output-referred stage. Qian (2001) applied r-g space to generate a binary map for face detection. Because of the high efficiency in using the r-g chrominance space, this approach can be used for real-time face detection for video and TV. Boussaid et al. (2003) applied r-g colour space on the on-chip skin detection for colour CMOS imagers. Almohair et al. (2007) used a Gaussian model for skin detection in r-g colour space. The r-g colour space was widely used for face detection (Gasparini 2008, Zarit 1999).

The ratios between two channels of RGB colour space may be directly applied for skin colour detection. The basic idea is similar to using r-g chrominance space. Brand and Mason (2000) used the ratio of R/G to determine skin colours (with additional ratios of R/B and G/B to improve accuracy).

In summary, representing skin gamut in the r-g colour space is efficient (downgrade colour space from 3-D to 2-D), simple, and compact. A basic assumption of using r-g colour space for skin colour detection is that the skin locus is luminance independent in r-g space. It has been found that the accuracy of skin colour detection is compromised based on this assumption (Hsu et al. 2002, Kovac et al. 2003).

2.4.4.2.1.3 YC_bC_r Colour Space

YC_bC_r is a colour space that is rotated from a nonlinear RGB colour space so that Y approximately represents brightness, and C_b and C_r represent chrominance coordinates. The colour space is used for image and video compression (JPEG, JPEG2000, and MPEG). Many hardware/firmware manipulates RGB images in YC_bC_r colour space. This makes YC_bC_r convenient and efficient to use. Furthermore, explicit separation of colour signals into luminance and chrominance makes it attractive for skin colour modelling.

The official YC_bC_r colour space is sometimes referred to as the CCIR 601 colour space. The recommendation 601 specifies 8-bit (i.e. 0 to 255) coding of YC_bC_r, whereby the luminance component Y has an excursion of 219 and an offset of +16. This coding places black at code 16 and white at code 235. In doing so, it reserves the extremes of the range for signal processing foot-room and headroom.

On the other hand, the chrominance components C_b and C_r have excursions of +/- 112 and offset of +128, producing a range from 16 to 240 inclusively. Similar colour spaces include YUV and YIQ. YC_bC_r is a digital colour system, while YUV and YIQ are analog spaces for their respective PAL and NTSC systems.

The YC_bC_r colour space used in different literatures may be slightly different. It may be the rotation of sRGB to sYCC with personal scaling range.

Chai et al. (2000) applied a Bayesian approach for skin colour classification in YC_bC_r colour space. Hsu et al. (2002) modified YC_bC_r such that chrominance of skin colours with the same C_bC_r were about the same for different luminance, i.e., to make the skin colour loci to be Y-component independent. Phung et al. (2002) modelled skin colours by a set of three Gaussian clusters, each of which was characterised by a centroid and a covariance matrix. Park et al. (2006) applied YC_bC_r colour space to model the distribution of skin colour in the C_b-C_r plane, in which the Mahalanobis distances of skin colours to the skin centre were used to compute the distribution of skin colours using a bivariate Gaussian probability density function. To remove the luminance (Y-coordinate) dependency on the decision for the skin colour detection, Kovac modified YC_bC_r colour space so that the 2-D chrominance ellipse of the skin colour region was about the same for different Y (Kovac et al. 2003). Many other literatures used YC_bC_r colour space for skin colour detection or face detection (Zarit 1999, Gasparini 2008, Menser and Wien 2000, Mahmoud 2008).

2.4.4.2.1.4 Perceptually Uniform Colour Spaces

CIE L*a*b* and L*u*v* are perceptually uniform colour spaces. The Jab coordinates based on CIECAM02 colour appearance model is reported to be reasonably uniform (Luo et al. 2006). Colour characterization and gamut mapping are mostly performed in a uniform colour space. If the skin colour detection is to be used for colour enhancement, a uniform colour space may be more appropriate.

Cai et al. (1998) used CIE L*a*b* colour space to determine the likelihood of a colour to be a skin colour. Kuang et al. (2005) studied the colour preference in photographic colour reproduction for skin tone, green, and blue sky under CIE L*a*b* colour space. They concluded that the capturing illuminant and the image content was an important factor that influenced the colour preference of human skin and grass. Braun (2006) performed memory colour enhancement in CIE L*a*b* colour space for colour mapping and ICC profiling. Yang and Ahuja (1998) applied the u*-v* coordinates of CIEL*u*v* colour space to detect human faces.

2.4.4.2.1.5 Other Colour Spaces

Converting a colour signal to luminance-chrominance coordinates, one separates the colour signal into a luminance and two chrominance coordinates. This generally simplifies the colour processing. Many other luminance-chrominance colour spaces (e.g. HSV, HSL, HSI, TSL) may be used for skin colour detection (Zarit 1999, Sigal et al. 2000, Jordao et al. 1999, Birchfield 1998, Huynh-Thu et al. 2002, Tomaz et al. 2003, Gasparini and Schettini 2006).

2.4.4.2.1.6 Discussion

Zarit et al. (1999) investigated five colour spaces (CIE L*a*b*, Fleck HS, HSV, r-g, and YC_rC_b) for skin detection. Their result shows that the goodness of a colour space depends on the implementation.

Albio et al. (2001) theoretically proved that "separability of the skin and no skin is independent of the colour space chosen". For every colour space, there exists an optimum skin detector scheme such that the performances of all these skin detector schemes are the same. However, some colour spaces may be easier to optimize while others are more difficult to optimize. Therefore Albio's conclusion may be theoretically correct but practically incorrect.

Shin et al. (2002) evaluated skin detection using RGB colour space and other eight colour spaces: normalized RGB, CIE XYZ, CIE L*a*b*, HIS, SCT, YC_rC_b, YIQ, and YUV, and concluded that the RGB colour space provided the best separability between skin and non-skin. However, this conclusion may be unreliable, since it only proves that their modelling in RGB colour space is better than in other colour spaces. The performance for difference colour spaces highly depends on the optimization or the training of parameter sets.

Lee and Yoo (2002) developed an elliptical boundary model for skin colour detection. They tested the model using six chrominance spaces (ignoring the luminance channel): r-g, CIE a*b*, CIE xy, CIE u*v*, C_bC_r, and IQ (IQ of YIQ). The model "gives the best performance in every chrominance space" compared with the single and mixture Gaussian models. One short coming of the model is that it assumes the skin boundary is luminance independent. Expanding the model to adapt the shape of ellipses to different luminance should further improve the performance of the model.

A good colour space for skin colour detection should well separate skin and non-skin colours. Some researchers modified existing colour spaces to improve the separation of skin and non-skin colours. However, modifying a colour space with such an approach distorts the uniformity of the colour space and therefore is not appropriate for skin colour enhancement.

In summary, the RGB colour space seems to be more suitable for fast detection on RGB images. Using a luminance-chrominance colour space for skin colour detection reduces the interaction between luminance and chrominance, therefore generally simplifies the process. For this reason, YC_rC_b and r-g colour spaces are widely used for skin colour detection. Using a uniform colour space (CIE L*a*b*, L*u*v*, or CAMJab) may improve the skin colour detection rate, however, the computation efficiency may be compromised. Skin colour detection using chrominance (e.g. rg, a*b*, or u*v*) ignoring the luminance-dependency simplifies the algorithm and improves the efficiency, but the detection rate may be lower.

2.4.4.2.2 Skin Decision Rules

Most of skin colour detection methods are aimed for face detection. The rules to determine skin colours for face detection and for skin colour enhancement may be different. However, it is no doubt that there are similarities and that methods for face detections would be useful for skin colour enhancement.

Fig. 2.4.4.2-2 shows an example of the skin colour distribution under two different colour spaces (Lee and Yoo 2000). The Compaq skin database (Jones and Rehg 1999) was used to generate the colour distribution. Lee and Yoo selected 2,000 skin images and 4,000 non-skin images from the database to compute histograms with 400x400 bin resolution. The distribution of skin densities looks like a normal distribution. Fig. 2.4.4.2-3 shows a side view of Fig. 2.4.4.2-2(a), where N denotes non-skin density peak and S denotes skin density peak. The figure show the peak of the skin skewed toward the grey point.

(a)   (b)
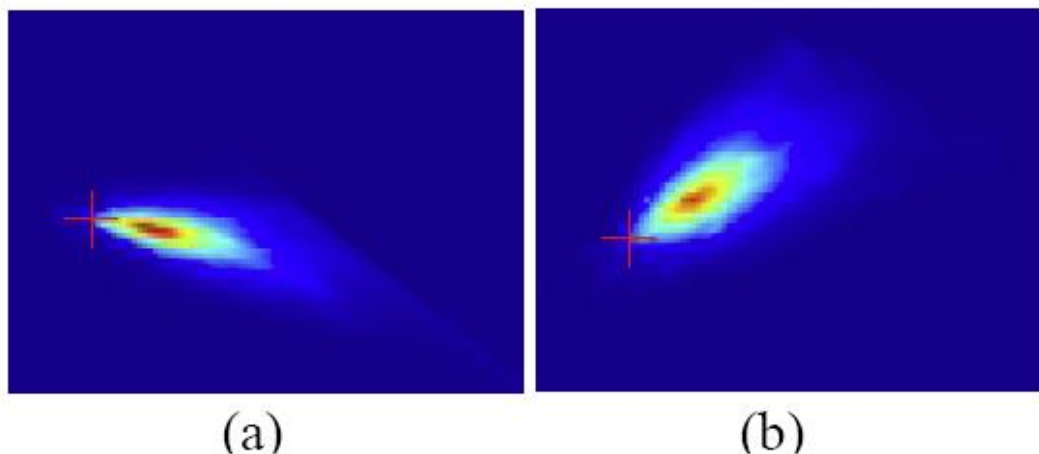
Fig. 2.4.4.2-2 Skin chrominance histograms in a) r-g and b) CIE-u*v* colour spaces. The cross mark denotes the grey point. (Lee and Yoo 2000)
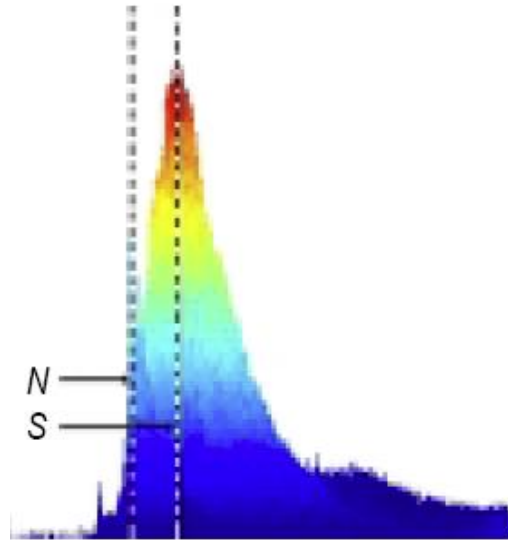
Fig. 2.4.4.2-3 A side view of Fig. 2.4.4.2-2(a), where N denotes non-skin density peak and S denotes skin density peak. (Lee and Yoo 2000)

2.4.4.2.2.1 Explicitly defined skin colour region

One method to define the skin colour region is explicitly defined the range in a specific colour space. For example, Kovac et al. (2003) determined the skin region in RGB colour space under D65 illuminant as shown below:

$$R > 95, G > 40, B > 20;$$

$$\text{Max}\{R, G, B\} - \min \{R, G, B\} < 15; \text{ and}$$

$$|R - G| > 15, R > G, R > B.$$

Chai et al. (1999) used C_b and C_r thresholds to determine skin colours in YC_bC_r colour space:

$$77 <= C_b <= 127 \text{ and } 133 <= C_r <= 173.$$

Phung et al. (2002) used slightly different ranges for skin colour detection in YC_bC_r colour space:

$$75 <= C_b <= 135 \text{ and } 130 <= C_r <= 180.$$

Following ranges was used for skin colour detection by Mahmoud (2008):

$$Y > 80, 85 < C_b < 135, 135 < C_r < 180.$$

Gomez and Morales (2002) applied skin colour decision rules in r-g colour space:

$$r/g > 1.185, r(1 - r - g) > 0.107, \text{ and } rg > 0.112.$$

Obviously, applying chrominance decision rules (C_bC_r or rg) do not take the luminance into account. To consider the range dependency on luminance, one approach is to modify the chrominance coordinate so that the space is invariant of luminance. Hsu et al. (2002) modified C_bC_r in YC_bC_r colour space, and defined skin colours in a modified C_bC_r ellipse that is not dependent on luma Y. This is achieved by fitting piecewise linear boundaries to the skin cluster using

$$C'_{i=b,r} = \begin{cases} C_i(Y) & K_l \leq Y \leq K_h \\ \left(C_i(Y) - \overline{C}_i(Y)\right) \cdot \dfrac{W_{C_i}}{W_{C_i}(Y)} + \overline{C}_i(K_h) & else \end{cases}$$

where i represents b or r, and

$$W_{C_i(Y)} = \begin{cases} WL_{Ci} + \dfrac{(Y - Y_{\min}) \cdot (W_{C_i} - WL_{Ci})}{K_l - Y_{\min}} & Y < K_l \\ WH_{Ci} + \dfrac{(Y_{\max} - Y) \cdot (W_{C_i} - WH_{Ci})}{Y_{\max} - K_h} & Y > K_h \end{cases}$$

$$\overline{C}_b(Y) = \begin{cases} 108 + \dfrac{(K_l - Y) \cdot (118 - 108)}{K_l - Y_{\min}} & Y < K_l \\ 108 + \dfrac{(Y - K_h) \cdot (118 - 108)}{Y_{\max} - K_h} & Y > K_h \end{cases}$$

$$\overline{C}_r(Y) = \begin{cases} 154 + \dfrac{(K_l - Y) \cdot (154 - 144)}{K_l - Y_{\min}} & Y < K_l \\ 154 + \dfrac{(Y - K_h) \cdot (154 - 132)}{Y_{\max} - K_h} & Y > K_h \end{cases}$$

with W_{Cb}=46.97, WL_{Cb}=23, WH_{Cb}=14, W_{Cr}=38.76, WL_{Cr}=20, WH_{Cr}=10, K_l=125, and K_h=188. These parameters are estimated from training samples of skin colours. $Y_{\min}$ and $Y_{\max}$ in the YC_rC_b colour space are 16 and 235, respectively. An elliptical model for the skin colours in the transformed $C'_bC'_r$ space is described as

$$\frac{(x - ec_x)^2}{a^2} + \frac{(y - ec_y)^2}{b^2} = 1$$

$$\begin{bmatrix} x \\ y \end{bmatrix} = \begin{bmatrix} \cos(\theta) & \sin(\theta) \\ -\sin(\theta) & \cos(\theta) \end{bmatrix} \begin{bmatrix} C'_b - c_x \\ C'_r - c_y \end{bmatrix}$$

where c_x =109.38, c_y=152.02, θ=2.53 (in radian), ec_x=1.60, ec_y=2.41, a=25.39, and b=14.03 are computed from the skin cluster in the $C'_bC'_r$ space.

Kovac et al. (2003) applied the same approach with slightly different piecewise linear fitting parameters.

The obvious advantage of these methods is its simplicity of the decision rules that leads to rapid constructing a classifier. The difficulty is to find a good colour space and adequate decision rules empirically.

2.4.4.2.2.2 Non-parametric skin distribution modelling

The key idea of the non-parametric skin colour modelling is to estimate skin colour distribution from the training data without deriving an explicit skin colour model (Vezhnevets et al. 2003). The process is sometimes referred to as the construction of skin probability map (SPM).

A colour space may be quantized to a number of bins, forming a 2D or 3D histogram that is formed as a lookup table (LUT). Each bin stores the number of times this particular colour occurred in the training images. The histogram may then be normalized and converted to a discrete probability distribution:

$$P_{skin}(c) = \frac{skin[c]}{Norm}$$

where *skin[c]* is the value of the histogram bin corresponding to colour vector *c*, and *Norm* is the normalization coefficient. $P_{skin}(c)$ can be stored in a LUT that constitutes the likelihood of colours corresponding to skin.

This method has been used for face detection and tracking by many researchers (Chen et al. 1995, Zarit et al. 1999, Brand et al. 2000, Sigal et al. 2000, Gomez 2002).

$P_{skin}(c)$ is actually a conditional probability *P(c/skin)*, a probability of observing colour *c*, knowing that a skin pixel is seen. Another conditional probability *P(c/-skin)*, the probability that a given colour belongs to non-skin class, can also be computed. Using Bayes maximum likelihood approach, a given image pixel can be classified as skin, if

$$\frac{P(c \mid skin)}{P(c \mid -skin)} \geq \rho ,$$

where $0 <= \rho <= 1$ is a threshold value which can be adjusted to trade-off between true positives and false positives using a ROC (receiver operating characteristics) curve calculated from a training data set.

Another appropriate measure for skin detection would be *P(skin/c)*, the probability of being a skin pixel given a colour value *c*. The Bayes rule to compute this probability is:

$$P(skin \mid c) = \frac{P(c \mid skin)P(skin)}{P(c \mid skin)P(skin) + P(c \mid -skin)P(-skin)}$$

where *P(c/skin)* are *P(c/-skin)* are directly computed from skin and non-skin colour histograms. The prior probability *P(skin)* and *P(-skin)* can be estimated from the overall number of skin and non-skin samples in the training set (Jones and Rehg 1999, Zarit et al. 1999, Chai et al. 2000)

Brown et al. (2000) applied Self-Organizing Map (SOM), which is an unsupervised artificial neural network, to skin detection.

In summary, the advantages of the non-parametric methods are fast in training and usage, and theoretically independent of the shape of skin distribution (it is not required for considering the shape of the skin colour cluster as a colour space is selected). The disadvantage is that a large storage space may be required. To reduce the amount of memory, a coarser sampling in the colour space must be used.

2.4.4.2.2.3 *Parametric skin distribution modelling*

It may be assumed that skin has a colour centre and skin colours spread around the centre due to different skin colours, various capturing conditions, and colour processing variations. The skin colour distribution may be described with a Gaussian like function.

Single Gaussian Model (SGM)

A multivariate normal distribution of a D-dimensional random variable x is defined as:

$$N(x;\mu,\Sigma) = \frac{1}{(2\pi)^{D/2}|\Sigma|^{1/2}} \exp\left[-\frac{1}{2}(x-\mu)^T\Sigma^{-1}(x-\mu)\right]$$

where μ is the mean vector and Σ the covariance matrix of the normally distributed random variable x. The model parameters are estimated from the training data using the following equations:

$$\mu = \frac{1}{n}n\sum_{i=1}c_i$$

$$\Sigma = \frac{1}{n-1}\sum_{i-1}^{n}(c_i-\mu)(c_i-\mu)^T$$

Either the *P(c/skin)* probability or the Mahalanobis distance from the *c* colour vector to mean vector μ can be used to measure the similarity of the pixel with the skin colour (Hsu et al. 2002, Yang and Ahuja 1998, Menser and Wien, 2000, Almohair et al. 2007, Park et al. 2006).

Gaussian Mixture Model (GMM)

SGM assumes a unimodal distribution which may cause intolerable error in estimation and discrimination. A better approximation can be obtained when the

values are generated by one of several randomly occurring independent sources. In this case the distribution function is a multimodal one which can be estimated using a finite number of mixed Gaussian or a Gaussian mixture model.

There are several facts that support the model of mixed Gaussian functions. The colour distribution is influenced by different lighting conditions or object movement. Different cameras, camera settings, or illuminants may produce different colour values. Human skin colours differ from person to person.

The GMM probability density function can be defined as a weighted sum of Gaussian as:

$$P(x;\theta) = \sum_{i=1}^{N} \alpha_i G(x;\mu_i,\alpha_i)$$

where α_i is the weight of ith component. The weight can be interpreted as a priori probability of a random variable in the ith group. G is a Gaussian probability density function with parameters μ and α. In addition, x is a sample input and N is the number of components. The parameter list of the GMM probability density function is given by:

$$\theta\{\alpha_i, \mu_i, \sigma_i\} \text{ for } i = 1, \ldots, N.$$

Estimation of model parameters is performed using a well known iterative method called Expectation Maximization (EM) which assumes that the number of components is known before hand (Yang and Ahuja 1999, Jones and Rehg 1999, Terrillon et al. 2000, Huynh-Thu et al. 2002, Hassanpour et al. 2008).

The choice of number of components, N, is quite important. While too low of number N may lead to poor fitting, too high a number may over-fit the data (fit the noise). The number of components used in literatures are from 2 (Yang and Ahuja 1999) to 16 (Jones and Rehg 1999).

Caetano et al. (2002) evaluated SGM and MGM. They concluded that: first, GMM behaves similarly over the whole range of the ROC curve; second, although the performance of SGM is similar to those of GMM for low false positive rates, it is significantly decreased for high true positive rates. The conclusion suggests that GMM may be more appropriate than SGM when a high correct detection rate is needed.

Elliptic Boundary Model

Using the single Gaussion model to detect skin, the boundary of each equal probability distribution locus is an ellipse, and the centre colour (the skin colour with the highest probability) is at the centre of the ellipse. If an elliptic model is

considered, there will be no restriction that the skin colour with the highest probability to be in the centre.

The mixed Gaussian model provides more freedoms for modelling the skin colour region. From the human perception point of view, the shape of each equal probability distribution locus should be smooth. Yet, this may be a difficult task for multiple Gaussian distributions. Nevertheless, a smooth curve fit of each equal probability distribution locus should still be an elliptic shape.

To develop a uniform colour space or a perceptual colour difference model, perceptual tolerance ellipses are often used to check the uniformity or goodness of the model (Macadam 1942, Wyszecki and Fielder 1971, Luo and Rigg 1986). The human perceptual colour tolerance to a colour in a perceptually uniform colour space can be modelled with an elliptic shape. The better the modelling of the uniformity of a uniform colour space correlate to human perception, the closer the tolerance ellipses is to spheres. Based on this observation, the colour tolerance to skin tone in a perceptually well correlated colour space should be an elliptic shape.

Yendrikhovskij et al. (1999) suggested that the colours of an object category were distributed with a probability density function around its prototypical colour. Based on this opinion, the single Gaussian model should be a perfect fit for skin colours. Due to various physical factors (illuminants, camera characteristics, human colour editing, etc.), the skin colour distribution deviates from the Gaussian distribution. However, the boundary of equal-distribution boundary should approximately be an elliptic shape.

By examining skin and non-skin distributions in six colour spaces, Lee and Yoo (2002) concluded that skin colour cluster, being approximately elliptic in shape is not well approximate by a SGM. Due to the asymmetry of the skin cluster with respect to its density peak, the usage of the symmetric Gaussian models may lead to high false positive rate. They proposed an "elliptical boundary model" which is as fast and simple in training and evaluation as SGM, gives superior detection results on the Compaq database compared to both SGM and MGM.

Kim et al. (2005) applied the elliptical boundary model for preferred skin colour reproduction. A set of skin colour regions in different luminance were modelled using ellipses in u'-v' chrominance space, and a set of corresponding ellipses were modelled for preferred skin colours. The colour adjustment was performed based on adaptive affine transform.

In Summary, SGM, MGM, and the elliptical model all operate in chrominance plane, ignoring the luminance information. Although the mathematical models to train parameters ignore the luminance information, the final parameters may be

tuned to fit for different luminance levels. Since the goodness fit depends on the shape of the skin colour cluster, the model performance varies from colour space to colour space (Terrillon et al. 2000, Lee and Yoo 2002). The SGM should fit well for strict physical conditions (fixed lighting condition, single camera and setting, etc.). Yang et al. (1998) has shown that the skin colour distribution of a single person under fixed lighting conditions in a normalized RGB space obeys Gaussian distribution. In reality, general skin colour distribution has asymmetric distributions that cannot be fitted with SGM. Employing mixture of Gaussians or several Gaussian clusters provides the flexibility to fit data with asymmetric distributions. Observing that the clouds of skin colours in chrominance spaces are of nearly elliptic shape, the elliptical boundary model should be promising.

2.4.4.2.2.4 Multispectral Approach

Storring et al. (2004) used a combination of standard RGB bands and three near infrared bands to detect human skin. With simulations under changing illumination conditions, their result shows an improved robustness over pure RGB based approaches. This approach may be generalized to detect the skin colours of multispectral images.

2.4.4.2.3 Summary of Skin Detection

Skin colour detection significantly depends on the training data. The aim of the skin colour detection determines how training data to be collected. For example, if the skin detection is under a specific lighting condition, the training data set should be collected under the same lighting condition. If the skin detection is for general purposes, the training data should be collected from various sources that cover varieties of capturing conditions and skin types.

The skin colour modelling depends on factors, such as accuracy, efficiency, and hardware capability. In general, using a simple explicit defined model is fast, hardware cost is low, yet the accuracy may be compromised.

The histogram based approach is fast in training and usage. Due to the table based property, it is independent of the shape of the skin colour distribution. The size of a LUT can be determined based on the requirement of accuracy, and affordability of the memory usage. The probability of a colour that is not located on a node may be quantized to the closest node or be computed through multi-dimensional interpolation.

SGM may be accurate enough under controlled environments, such as under a specific lighting condition and using a specific type of camera. For general

purposes, MGM may be used to improve the modelling accuracy in the expenses of more complex training process and higher computation complexity.

Due to the asymmetry of the skin colour cluster with respect to its density peak, the usage of symmetric Gaussian models may lead to high false positive detection rate. An elliptic boundary model may fit training data more accurately and may be easier to train, and it is more efficient in computation.

The goodness of a skin detection model is often evaluated using the true positive (TP) and false positive (FP) detection rates. Increasing the TP detection rate is generally at the cost of increasing the FP detection rate. The relationship between TP rate and FP rate is often drawn with a curve, called Receiver Operating Characteristics (ROC) curve. Fig. 2.4.4.2-4 shows an example. The horizontal axis is FP detection rate, and the vertical axis is TP detection rate. The curve is very helpful for determining a proper detection threshold.
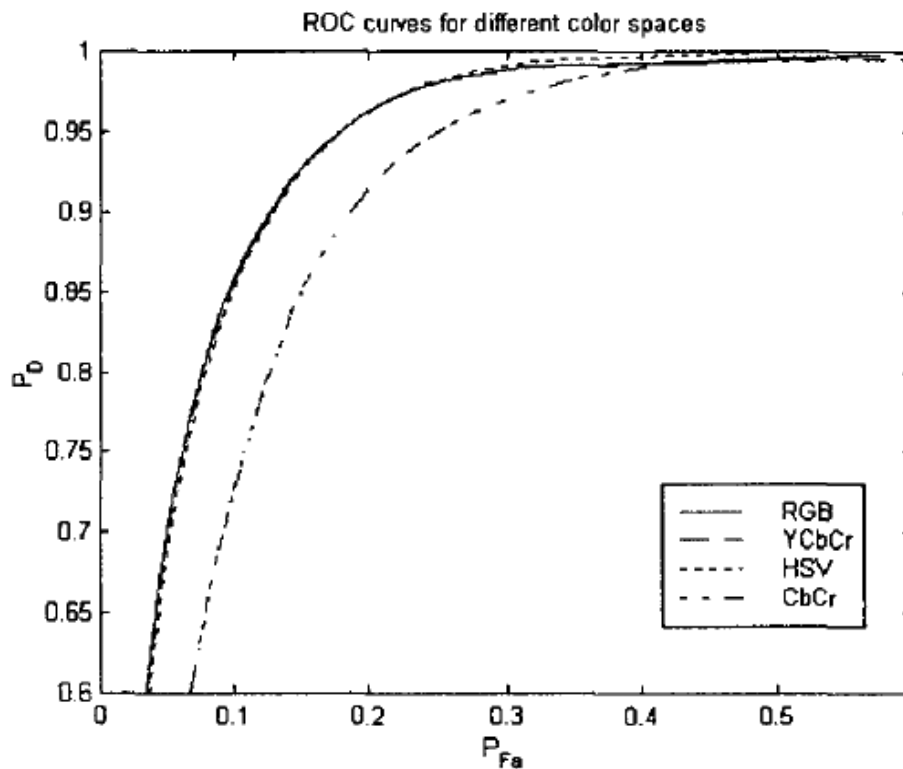
Fig. 2.4.4.2-4 ROC curves for different colour spaces (Albio et al. 2001)

There are a number of other skin detection methods that are not discussed here, because they are less relevant for colour adjustment. For example, Gomez (2002) constructed new colour spaces to cluster skin colours such that skin colours and non-skin colours are better separated. The method improves the skin detection rate. However, the colour space is distorted, which is not relevant for colour adjustment.

2.4.4.2.4 Discussion of Skin Detection Relevant to Skin Colour Reproduction

Most of skin colour detection methods discussed herein is used for face tracking. Typically, a colour space is selected, and a skin decision rule to separate colours as skin and non-skin colours is applied. A boundary must be determined to separate skin and non-skin.

A colour space that performs well for skin detection may be impropriate for colour enhancement. Important criteria of a good colour space for skin detection are: 1) the shape of the skin cluster can be easily formulated; and 2) the skin colours and non-skin colours are well separated. Important criteria for skin colour enhancement may be: 1) the shape of the skin colour cluster can be easily formulated; and 2) the colour space is perceptual uniformed.

The skin detection for face tracking sets a clear boundary to determine skin and non-skin. In skin colour enhancement, a skin likelihood value is computed for colour adjustment. There is no need to set a clear boundary for skin colour enhancement.

The method using skin probability distribution LUT may be a potentially useful method for skin colour adjustment. Smaller LUTs may be built if memory usage is limited, and probabilities may be computed through interpolation.

SGM is simple and is accurate under a controlled environment. If faces are detected in a single photo, it should be very accurate for modelling skin colours of one or few faces in the photo. For such reason, it may be useful for face detection aided skin colour enhancement.

Although the elliptical boundary model has the advantage over other skin detection models, it models skin colours in chrominance coordinates ignoring the luminance channel. Expanding it to model skin colours in 3-D colour space should further improve skin colour detection accuracy.

The shape of the skin colour cluster depending on luminance is not taken into account in many skin detection methods for face detection and skin colour enhancement. It has been found that the skin colour region in chromaticity space is luminance (or lightness) dependent. Ignoring the luminance-dependency, both face detection and skin colour enhancement suffer due to lowering accuracy in skin detection. To improve the accuracy for skin colour modelling, the luminance dependency should be further investigated.

The illuminant has a large effect on the skin colour locus. If the illuminant is known, the skin colour locus for the specific illuminant can be use for skin detection (Storring and Graunum 2002). On the other hand, if the illuminant is unknown but a skin region is detected (e.g. a face is detected), the illuminant can be derived

through analysing the skin locus (Martinkauppi 2002). Besides using skin detection for illumination detection and face recognition, the skin colour detection can be used for the colour adjustment beyond the skin colour adjustment. For example, it can be used for auto-exposure and auto-focus control such that skin tone is optimally captured in digital photography (Quan et al. 2005). It can be used to improve the white balance and to optimize the global tone curve or local contrast.

2.4.4.3 Skin Colour Enhancement Algorithms

Skin colours are different under different illuminant conditions. As flesh tones are captured with a digital camera, the raw RGB signals are recorded. If a digital camera detects the illuminant accurately, chromatic adaptation will be performed correctly to normalise the white point of the image and to produce an output-referred image with proper white balance. The output image is normally display preferred and it is mostly in sRGB colour space, in which D65 illuminant with IEC61966-2.1 (http://webstore.ansi.org/) specified viewing condition is assumed. In a professional mode, images may be encoded using Adobe RGB colour space. Except for working on the raw RGB stage, the illuminant detection and chromatic adaptation have mostly been applied. However, the illumination detection may be incorrect or inaccurate, and needs to be fine tune in skin colour enhancement.

To enhance skin colours, skin colour must be detected. A skin colour probability model or a face detection method may be used for skin colour detection and to compute a strength for skin colour adjustment. A following step is to morph skin colours to a preferred colour region.

Lee and Ha (1997) proposed a flesh tone enhancement approach for real-time TV display. Mongolian, Negroid, and Caucasian skin tones were detected based on the hue angle of each colour. The brightness and saturation of a skin colour was adjusted toward its ideal colour centre, and the hue angle was not adjusted.

Braun (2006) developed an algorithm that squeezes skin colours toward a preferred point. Squeezing is used rather than rotation since the input skin hue is unknown. The squeezing is applied to entire images to improve skin tones without the need for segmentation. It affects objects that are not skin but are with skin-colours. It was found that the colour modification of objects with skin colours was not objectionable since people focused mainly on colour adjustment of skin objects in images. The best results were found when the preferred point was specified by its CIELAB hue angle and chroma, and squeezed only in hue, but over a limited chroma range. The formula for the adjustment is shown below:

$$H_{out} = H_{in} - \Delta H \cdot w_H \cdot w_C$$

where $\Delta H = H_{in} - H_{pref}$, w_C is given by a Gaussian, and w_H is given by the addition of two Gaussian functions as shown below:

$$w_H = \frac{K \cdot w_{temp}}{\max(w_{temp})}$$

$$w_{temp} = e^{-0.5\left(\frac{H_{in}-M}{2H_{sigma}^2}\right)^2} + e^{-0.5\left(\frac{H_{in}+M}{2H_{sigma}^2}\right)^2}$$

$H_{pref}=45$, $C_{pref} = 25$

$H_{sigma} = 20$, $C_{sigma} = 10$

$M = 30$, $K = 0.6$

Images enhanced by this algorithm were reported to result in equal or improved rendition over the unadjusted originals.

Kim et al. (2005) developed a preferred skin colour adjustment method based on adaptive affine transform. The RGB signals of the input video are first transformed to Yu'v'. Skin colours are defined within an ellipse as given below:

$$\frac{[\Delta u'\cos\theta_s + \Delta v'\sin\theta_s]^2}{A_s^2} + \frac{[\Delta v'\cos\theta_s - \Delta u'\sin\theta_s]^2}{B_s^2} \leq 1$$

In the equation, $\Delta u' = u'-u'_s$ and $\Delta v' = v'-v'_s$. The (u'_s, v'_s) is the centre of the skin colour ellipse. θ_s, A_s, and B_s are the rotation angle, the major axis length, and the minor axis length of the skin colour ellipse, respectively.

A preferred skin colour region is noted with coefficients: the centre is $(u'_p v'_p)$, the rotation angle is θ_p, and the major and the minor axes are A_p and B_p. An input skin colour is converted into a preferred skin colour by the following equation

$$\begin{bmatrix} u'_p & v'_p & 1 \end{bmatrix}^T = M_T \begin{bmatrix} u'_s & v'_s & 1 \end{bmatrix}^T$$

where M_T is a 3x3 matrix for the skin colour transformation which is decomposed into five matrices as below:

$$M_T = M_{OTrans} M_{Orat} M_{Aff} M_{IRot} M_{ITrans}$$

where,

$$M_{ITrans} = \begin{bmatrix} 1 & 0 & u'_s \\ 0 & 1 & -v'_s \\ 0 & 0 & 1 \end{bmatrix}, \quad M_{IRot} = \begin{bmatrix} \cos\theta_s & \sin\theta_s & 0 \\ -\sin\theta_s & \cos\theta_s & 0 \\ 0 & 0 & 1 \end{bmatrix},$$

$$M_{OTrans} = \begin{bmatrix} 1 & 0 & u'_p \\ 0 & 1 & -v'_p \\ 0 & 0 & 1 \end{bmatrix}, \quad M_{ORot} = \begin{bmatrix} \cos\theta_p & \sin\theta_p & 0 \\ -\sin\theta_p & \cos\theta_p & 0 \\ 0 & 0 & 1 \end{bmatrix},$$

$$M_{Aff} = \begin{bmatrix} A_p & -A_p & 0 \\ 0 & 0 & B_p \\ 1 & 1 & 1 \end{bmatrix} \begin{bmatrix} A_s & -A_s & 0 \\ 0 & 0 & B_s \\ 1 & 1 & 1 \end{bmatrix}^{-1}.$$

Here, M_{ITrans} is a matrix to translate the centre (u'_p, v'_p) of the skin colour ellipse to the origin and M_{OTrans} is a matrix to convert the origin to the centre of the preferred skin colour ellipse. M_{IRot} is a matrix to rotate the skin colour ellipse to 0° and M_{ORot} is a matrix to rotate the ellipse to the angle of the preferred skin colour ellipse. M_{Aff} is an affine transform matrix to rescale the skin colour area to the preferred skin colour area.

The colour adjustment based on these math formulae is simple but is not smooth for the transition from original skin colours to preferred skin-colours due to boundary issues.

Park et al. (2006) proposed a method to optimize memory colours in YC_bC_r colour space for the colour reproduction on digital TV. Because images may be captured under various conditions, they suggested that "the skin colour boundary for practical purposes should be large enough to cover skin colours taken under various illuminants but small enough to avoid unintended colour transformation of non-skin areas in an image; and preferred skin colours should be included within the skin colour boundary". The skin colour data were collected from digital images in Corel Gallery 1,000,000. The 20x20 pixels of colour patches were taken from the skin area in these images. A total of 1196 skin samples were taken, including 365 from Oriental, 627 from Caucasians, and 202 from blacks. How these images were captured was unknown. It was assumed that various illuminants and capturing conditions were covered. They found that the skin colour distribution was Gaussian-liked. The skin colour distribution was therefore modelled with a bivariate Gaussian probability density function, f(x, y):

$$f(x, y) = \frac{1}{2\pi\sigma_x\sigma_y\left(1-\rho^2\right)^{1/2}} \exp\left[\frac{1}{2}q(x, y)\right],$$

where x and y represent C_b and C_r, μ_x and μ_y are the mean values of x and y, σ_x and σ_y are the variances of x and y, and

$$q(x, y) = \frac{1}{\rho^2}\left[\left(\frac{x-\mu_x}{\sigma_x}\right)^2 - 2\rho\left(\frac{x-\mu_x}{\sigma_x}\right)\left(\frac{y-\mu_y}{\sigma_y}\right)\right] + \left(\frac{x-\mu_x}{\sigma_x}\right)^2$$

is the squared Mahalanobis distance.

Park et al. found that the distribution among skin tones of different skin types was very similar except for the average luminance. However, the distributions of luminance were overlapped among skin types. They decided not to distinguish skin

types for colour transformation. The squared Mahalanobis distance, q(x, y), was used to determine the skin boundary. A small region with a boundary of a constant Mahalanobis distance around the centre (μ_x, μ_y) was determined as the prototypical colour region of the skin object. A larger region with a boundary of a constant Mahalanobis distance around the centre (μ_x, μ_y) was determined as the skin colour region.

Fig. 2.4.4.3-1 shows a prototypical colour of skin object M; an area, C, that belong to a "constant interval" of the skin object (the orange region); and an area detected as skin colours, A (grey + orange regions). According to Park et al., a skin colour that is within the orange region C is an ideal skin colour and therefore is not adjusted; a colour that is outside the boundary of A is not belong to a skin colour and therefore is not adjusted either; and a skin colour P is pushed closer to the ideal skin colour region C. A line is drawn between P and M, and P is reproduced as P', which is moved closer to the prototypical colour boundary, M'.
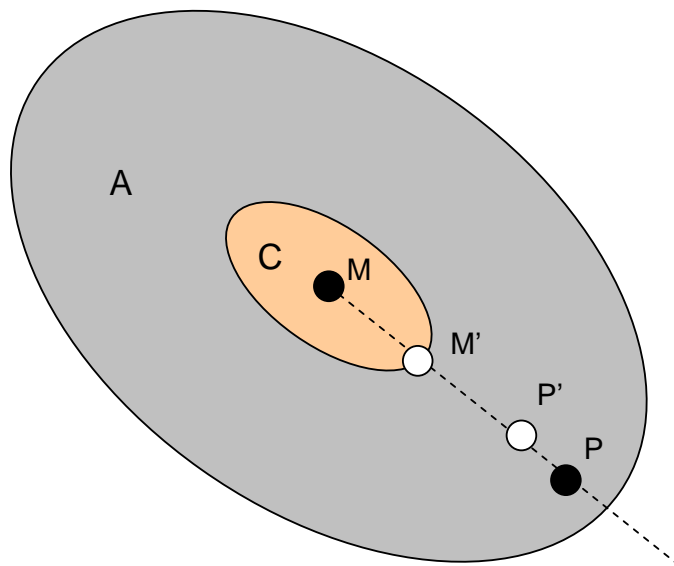
Fig. 2.4.4.3-1 Relationship among prototypical colour, constant interval, and boundary of a memory colour

Park's approach assumes that the preferred skin colour centre is the centre of the skin colour distribution, which is not true in reality.

Quan and Jin (2008) presented a method for memory colour based preferred colour reproduction. They applied following simple rules to segment green foliage, skin tone, and blue sky in YC_bC_r colour space:

Green: $C_b < C_r$ & $C_b > 10 * C_r$

Skin: $C_b < -0.1 * C_b$ & $C_b > -1/0.8*C_r$ & $R < 1.75*G$

Sky: $C_b < -1/0.4*C_r$ & $C_b > -0.6*C_r$

A nonlinear curve is used for contrast and saturation adjustment, and a tone mapping curve is applied to adjust the tone range. Following non-linear curve is used for contrast and saturation adjustment:

$$y = a^{1-\gamma} x^{\gamma} \qquad 0 \le x \le a;$$
$$y = 1 - (1-a)^{1-\gamma}(1-x)^{\gamma} \quad a \le x \le 1.$$

where a is a transition value and γ is to control the nonlinearity of the curve.

Saturation adjustments in their experiment are: $a = 0.2$; $\gamma = 2.0$ for foliage green cluster, $\gamma = 1.5$ for sky blue cluster, $\gamma = 1.0$ for skin colour cluster, and $\gamma = 1.25$ for all other colours that do not belong to these three memory colour clusters.

To stretch pixel values to the entire tone range, a confident black level (x0) and a confident white level (x1) are calculated by analysing the histogram of the image. Then the pixel range in the range of [x0, x1] is expanded to the full range of [0, 1] through following transformation in order to use the above nonlinear curve:

$$a = \frac{x0 + x1}{2}$$
$$x' = \min\{\max\{x - x0, 0\}/(x1 - x0), 1\}$$

γ is set to 1.2 in their experiment for contrast enhancement.

Their findings are: 1) for people scenes, high contrast decreases image quality and effect of saturation is small; 2) for non-people scenes, high contrast enhances image quality significantly and medium saturation is favoured compared to low and high levels; 3) for high light level scenes where noise is not an issue, enhancing contrast is in general good; 4) for low light level scenes, the treatment in colour and tone has only moderate effect on perceived image quality, because the scenes lack memory colours and tradeoffs need to be made between colour saturation, contrast, shadow details, and noise.

Nachlieli et al. (2009) presented an algorithm that used face detection and a global skin colour model to coarsely discriminate skin from non-skin pixels on faces. A statistical analysis of skin colours in each face was used to refine parameters of the skin colour model. The per-face colour models were used to compute the final skin probability map. The colours of skin pixels were shifted towards a "memory prototype" skin colour, while the magnitude of the shift was the function of the pixel's likelihood belonging to the skin tone area.

Initially, a Gaussian probability function for skin detection in LCH colour space is constructed as

$$P(skin \mid l,c,h) = Z \cdot e^{-\left(\frac{(l-\mu_l)^2}{2\sigma_l^2} + \frac{(c-\mu_c)^2}{2\sigma_c^2} + \frac{(h-\mu_h)^2}{2\sigma_h^2}\right)}$$

The skin probability map is adjusted based on the relative location of each pixel on a face map.

Ignoring the lightness dependency, the skin likelihood function of each person becomes:

$$P(skin \mid c,h) = Z \cdot e^{-\left(\frac{(c-\mu_c)^2}{2\sigma_c^2} + \frac{(h-\mu_h)^2}{2\sigma_h^2}\right)}$$

μ and σ of each person is computed from the person's probability map.

The (a^*_{orig}, b^*_{orig}) of a skin colour in L*a*b* space is corrected by following formulae:

$$a^*_{new} = a^*_{orig} + \Delta I_a k P\left(a^*_{orig}, b^*_{orig}\right)^\gamma$$

$$b^*_{new} = b^*_{orig} + \Delta I_b k P\left(a^*_{orig}, b^*_{orig}\right)^\gamma$$

where $P(a^*_{orig}, b^*_{orig})$ is the pre-calculated skin likelihood of this pixel, γ controls the smoothness of the transition between the corrected and uncorrected regions, and k is a factor that controls the magnitude for colour correction.

Xu and Pan (2010) presented a skin and sky colour detection and enhancement method for TV colour enhancement. A sigma filter decomposes the input image into a low-pass image (or primary image) and a high-pass image (or residue image). The sigma filter utilizes a 1-D or 2-D rectangular window, where the current pixel I(x,y) is at the centre of the window. The sigma filter compares the pixels I(i,j) in the window with the central pixel I(x,y), and averages those pixels whose value differences with the central pixel I(x,y) is within a threshold T. Because the sigma filter drops pixels that are not within the threshold, it is a nonlinear filter. Mathematically, the output from the sigma filter, $I_{LP}(x,y)$, may be calculated by

$$I_{LP}(x,y) = \frac{\sum\limits_{(i,j)\in E \,\&\, |I(i,j)-I(x,y)|<T} I(i,j)}{N(x,y)}$$

where E is the window, N(X, y) is the count of the pixels in E that satisfy the condition of $|I(I, j) - I(x, y)| < T$

The sigma filter generates the low-pass image, and the high-pass image is obtained by subtraction. Because the sigma filter is a smoothing filter preserving sharp edges, the low-pass image generated from a sigma filter contains limited details but maintains sharp edges, and the high-pass image contains details/noises/artifacts but relatively few sharp edges. In general, by separating the image into a pair of channels, the lower frequency channel will contain relatively

few artifacts and noise, and the higher frequency channel will contain relatively more artifacts and noise. By performing the enhancements primarily on the lower frequency channel, the artifacts and noise in the image will not tend to be enhanced in the final image.

A skin score LUT and a sky score LUT are pre-generated. Skin colour enhancement is expressed as:

$$c_{new} = skinScore(c) \cdot skinEnhance(c) + (1 - skinScore(c)) \cdot c$$

where c represents a pixel colour, skinScore(c) represents the skin colour likelihood for colour c, and skinEnhance(c) refers to enhanced skin colour for colour c, and c_{new} is the output colour.

Sky colour enhancement is performed in similar manner. The low-pass image, which contains no details or artifacts, goes through the detection and enhancement path. The high pass image, containing details and noise and artifacts, does not go through the detection and enhancement path and will be added back to the colour enhanced low pass image to generate the enhanced image. Therefore, the noise in the high pass image is not enhanced. The enhancement can take place in any colour space such as YC_bC_r, HSV, or IPT.

Hung et. Al. (2010) developed a skin colour enhancement method that modified hue and saturation of skin tone colours using linear interpolation in a triangle that encompasses skin colours to be adjusted. A 2-D colour space (the luminance or light channel is not considered) is divided into many triangular sub-regions. Knowing the colour mapping of each vertex from original colour values to enhanced/adjusted colour values, any colour is mapped to a corresponding location by linear interpolation within a triangle that encompasses the colour.

2.4.5 Colour Enhancement of Green Plants

The green plant colour region is another important memory colour category in natural scenes (Yendrikhovskij et al. 1999). The reproduction of green foliage is of importance in preferred colour reproduction.

Bartleson and Bray (1962) used Kodak Dye Transfer prints to produce two dissimilar green grass scenes. The grass areas were controlled separately from the overall colour balance. According to them, the most representative chromaticity for preferred reproduction is located at some distance from that of the mean memory colour. The difference in hue is such as to produce a preferred colour that is more "yellow-green" than the memory colour. The preferred colour appears to be more similar to the mean of the natural colour than to the mean of the memory colour. They found that the preferred chroma for green grass to be lower than that of the

natural mean, but the result might be due to the limit of the physical gamut. Hunt et al. (1974) found that the preferred grass colour lied on the yellowish side of typical average real grass, but the difference was small; and the purities were about the same. Kuang et al. (2005) found that preferred chroma for grass and sky was much higher than the original colours, i.e. observers preferred higher chromatic grass and sky colours than their actual colours. Bartleson and Bray and Hunt et al. concluded that the preferred green grass was slightly more yellowish than real green.

Determining a colour region by hue angles is simple and intuitive. Although this may not be very accurate, it has been widely used to determine green plant colours in colour enhancement (referred to the description of Quan's and Jin's method in Section 2.4.5). The feature based image segmentation is another approach to detect green plants (Fredembach et. al. 2008, Naccari et. al. 2005, Luo et. al. 2001, Herman et. al. 2004, Skarbek and Koschan 1994).

Fredembach et al. (2008) applied an eigenregion-based framework that used PCA-based features to segment three memory colour regions, skin, plants, and sky. Adding colour-based segmentation should further improve the segmentation accuracy.

Chromatic green colours displayed on display screens are much brighter than reproduced on hardcopies due to the gamut difference. How to optimize colours in this region for the preference colour reproductions from display to hardcopy and from hardcopy to display is yet to be known.

2.4.6 Colour Preference of Blue Sky

Similar to the green grass category, blue sky is another category among three important memory colour categories for natural scene images. The colour reproduction of blue sky is very important for photographic images of outdoor scenes. Bartleson and Bray (1962) found that the preferred reproduction of blue sky in colour prints corresponded to a more "purple-blue" colour than the memory colour, and the preferred hue was more like the hue of the natural colour. This is different from the preferred reproduction colour for flesh in which the preferred flesh colour is more like the mean memory flesh colour rather than the average natural flesh colour. Although the experimental results were derived from very limited data sets (two scenes only), they emphasized that there was "ample evidence that the sky reproductions having the hue of natural sky do tend to be preferred". The preferred reproduction for sky occurred at a generally higher purity than the natural colour.

Hunt et al. (1974) found that "for the blue sky colour, although the dominant wavelength of the preferred and the real colours are closely similar, the preferred colour has an appreciably higher purity".

Kuang et al. (2005) found preferred chroma for sky was much higher than the original colours, i.e. observers preferred high chromatic sky colours than their real colours. And observers preferred more cyan-ish blue sky colour. Koh et al. (2007) studied the colour preference and perceived colour naturalness of digital video, and also found that blue sky looked more pleasing when its colour was purer and deeper.

Detecting blue sky may be useful for colour enhancement. Luo and Etz (2002) proposed a model-based approach consisting of colour classification, region extraction, and physical-motivated sky signature validation. Gallagher et al. (2004) improved this detection algorithm based on a two-dimensional polynomial model of the image of blue sky. Initial sky detection is applied to establish high-confidence blue sky regions. A 2-D polynomial model is used to validate candidate sky regions.

Takahashi and Hirata (2006) proposed a sky detection method enabling robust region detection for cloudy sky by evaluating similarity of visual features between combined regions of segmented regions from an input image and sky region stored in a database.

Quach et al. (2007) implemented a blue-sky detection method for real-time blue sky detection, which can be used for the noise reduction and colour enhancement of blue sky for HDTV.

You and Chien (2008) proposed a method to segment the sky area and enhance the saturation of the region with a factor determined by an average saturation of the whole sky region and a weight computed from the relative pixel position as well as original saturation. The RGB values of an image are converted into HSV using following equations:

$$H_1 = \cos^{-1}\left\{\frac{0.5[(R-G)+(R-B)]}{\sqrt{(R-G)^2+(R-B)(G-B)}}\right\}$$

$$H = H_1 \qquad B \le G$$
$$H = 360^o - H1 \quad B > G$$

$$S = \frac{\max(R,G,B) - \min(R,G,B)}{\max(R,G,B)}$$

$$V = \frac{\max(R,G,B)}{255}$$

The boundary of sky is defined by

$180^o < H < 300^o, 0.1 < S <= 1, 0.4 < V <= 1.$

Similarly, Quan and Jin used hue angles to determine blue sky colours (referred to Section 2.4.5).

The sky region detected using above equations also includes blue parts from sea, lake, and buildings. Such regions are removed through efficient non-recursive flood-fill labelling algorithm.

Increasing the saturation of the whole sky without considering cloud regions can lead to lower contrast between sky and cloud. Since the B component is much higher than the R and G components in sky, and the R, G, and B are very close and with high values in cloud, the R/B ration can be used to extract cloud.

A saturation enhancement factor, E, is computed by:

$$S_{avg} = \frac{1}{N}\sum_{i=1}^{N} S_i \quad S_i \in sky$$

$$E = 3(1.0 - S_{avg}) \quad 0.2 \le S_{avg} \le 1.0,$$
$$E = 0.3 \quad\quad\quad S_{avg} < 0.2$$

where S_{avg} is the average saturation of the detected sky region. The saturation of the sky is increased by a factor of 0.3 if the average sky saturation is lower than 0.2, and is reduced if the average sky saturation is higher.

The saturation of a clear blue sky in daylight gradually increases as we look upward from the horizon to the zenith. Thus, a vertical position adjustment factor may be computed to gradually increase enhancement as the position moves up.

Similar to segmenting skin and green plants using PCA-based feature detection, blue sky may be segment in the same manner (Fredemback et al. 2008).

Displays (CRT, LCD, LED) are able to produce bright chromatic colours, while printers produce high chromatic colours with lower lightness. Chromatic blue colours represented on a display colour space tend to be mapped to darker colours on hardcopies. On the other hand, if dark blue sky colours scanned from a hardcopy are to be displayed on a display screen or to be translated into a display colour space, should the lightness be increased or be preserved? How the transformation between hardcopy and display affects the preferred colour reproduction on blue sky remains to be investigated.

2.5 Conclusion Remark

As a subset of preferred colour reproduction, memory colour reproduction plays an important role in overall colour reproduction. Memory colours of familiar

objects are the key clues to judge the colour quality. People usually judge the colour of a familiar object by comparing its colour appearance with its memory colour rather than with the real object. Three prototypical categories: skin, green foliage, and blue sky, are main memory colour categories for preferred colour reproduction.

To enhance colours locally through digital image processing, a region of interest must be determined. There are many approaches to determine the skin colour region for face detection. Determining skin colours explicitly for skin colour detection is simple but the detection rate may be low. This approach may be used in situations that hardware resource is limited. Modelling skin colour distribution using probability LUTs is expensive in memory usage. However, reducing the size of LUT and using it with interpolation may be an attractive approach for skin colour enhancement. SGM was found to be accurate under a strict condition. GMM may be used for unconstraint conditions for its ability to adapt to the shape of non-symmetric histograms. However, it is more complex to train and the computation efficiency is lower. The elliptical boundary model is simple, easy to train, and more accurate than SGM. The method has been used for colour adjustment in chrominance space. Ignoring the fact that the luminance (or lightness) affects the shape of the skin colour region, skin colour detection accuracy would be compromised. To achieve high modelling accuracies, the luminance dependency should be taken into account.

With colour-based skin colour detection for skin colour enhancement, all colours that belong to skin colours are adjusted. This has been found not to be a problem in general, because people focus on memory colours of familiar objects. To exclude these non-skin objects from skin colour enhancement, feature-based skin detection must be applied. However, feature-based approaches may detect and enhance faces only and miss to detect and enhance full body colours.

Many other colour transformations, such as global tone and local tone adjustment and global chroma adjustment, should be executed prior to memory colour enhancement. Skin colours captured with a digital camera highly depend on the lighting condition or the white balance. White balance should be performed prior to preferred colour enhancement. On the other hand, skin colour analysis from skin colour enhancement may be useful for rebalancing overall image colours that are shifted from inaccurate illuminant detection.

Green plants and blue sky are two other important memory colour categories of natural scene images. Methods that combine colour-based detections with feature-based detections were found to be more effective for blue sky colour enhancement.

A preferred colour centre must be determined for preference colour enhancement of the colour region. A preferred colour is different from a memory colour. The difference is smaller for some prototypical colours, and larger for some other prototypical colours. Improperly using a statistical skin colour centre, a preferred skin colour centre, or a memory skin colour centre for preferred colour enhancement will lead to suboptimal results.

Preferred skin colour has been extensively studied in the past half a century. However, these studies are not comprehensive due to the technical limitations in psychophysical experiments, and inconsistent results due to limited number of samples or observers or biased from experimental conditions. In order to have a solid understanding of skin colour preference for preferred colour reproduction, new psychophysical experiments should be designed and conducted to overcome these problems.

In a colour imaging chain, there may be different blocks where colours can be adjusted. Similar colour enhancement algorithms may be repeated in different blocks. For example, skin colour enhancement may be performed in the capturing step in a digital camera, in photo application software in the editing step, and in the printing step in a printer or in a displaying step in a display. Applying a skin colour enhancement algorithm multiple times may lead to excess adjustment and result in losing details or other artifacts. By analysing the colour distribution of the skin colours in an image, the amount of colour adjustment may be determined. If skin tones of an image have been in a preferred condition, the skin colour enhancement step should not degrade the preference of the skin tones.

Chapter 3
Modelling Skin Colours for Skin Colour Enhancement

3.1 Introduction

Colour rendering is an important factor to judge the perceived image quality of the colour reproduction of digital images. Skin tone, as the most important category among memory colours, plays an important role in preferred colour reproduction. Various skin colour detection models have been presented in the past. A simple method is to explicitly define the range of colours in a specific colour space. In general, this method is computationally efficient, low hardware cost, yet the accuracy may be compromised. Another method is to estimate skin colour distribution from the training data without deriving an explicit skin colour model. A skin probability map is constructed, and may be quantized and represented as a lookup table (LUT). The probability of a colour that is not located on a node may be quantized to the closest node or be computed through interpolation. While the method is fast in training and is theoretically independent of the shape of the skin colour distribution, a large storage space may be required.

With the assumption that skin colours spread around a skin colour centre due to variations in physical conditions (e.g. skin types, capturing conditions, etc.), the skin colour distribution may be approximated with a Gaussian-like function. The idea leads to the proposal of Single Gaussian Model (SGM), which is formulated by a multivariate normal distribution function. Although modelling reasonably accurate in a strict condition, SGM may cause intolerable error in estimation and discrimination of skin colours captured in complex environments. A better approximation can be obtained using Gaussian Mixture Model (GMM) which mixes a finite number of Gaussian functions. GMM may be more appropriate than SGM if high correct detection rates are desired. However, it is more complex to train and more expensive in computation.

Storring et al. (2004) and Fredembach et al. (2009) combined standard RGB bands and near-infrared bands to detect human skin. Their results demonstrate an improved robustness over pure RGB based approaches. The approach may be

generalized for the skin colour detection of multispectral images, yet it is not appropriate for general consumer imaging.

Sanger et al. (1994, 1997) applied an ellipse distribution function to express skin colours for face detection. Lee and Yoo (2002) concluded that the skin colour cluster could be well modelled using an ellipse. This is similar to the modelling of the human perceptual colour tolerance in a perceptually uniform colour space in which the visual colour tolerance can be well modelled with ellipses. Another evidence to support elliptical modelling is that colours of an object category distribute around its prototypical colour with a probability density function. Due to various physical disturbances (illuminations, camera characteristics, image editing, etc.), the skin colour distribution deviates from Gaussian distributions. However, the shape of equal-distribution contours should be approximately elliptical.

In a preliminary study, a limited amount of skin colours were used to construct a convex hull for the skin colour region, and the shape of the convex hull was analysed and fitted mathematically. It was confirmed that the shape of the skin colour cluster in chrominance space could be fitted with Gaussian distribution or ellipse (Zeng and Luo 2010). From the human perception point of view, the shape of each equal probability distribution locus of a skin colour boundary should be smooth and should be approximately elliptical. Furthermore, an elliptical shape is a natural choice for approximating the shape of a physical object. From all of these evidences, an elliptical boundary model was finally adapted, modified and expanded to compensate the lightness dependency in this study. The model was applied to guide psychophysical experiments to determine a preferred skin colour centre for skin colour enhancement.

This chapter is organized as below: the primary study of modelling a local colour region using a convex is presented in Section 3.2; a method to construct skin colour databases for elliptical modelling is presented in Section 3.3; the study of the skin colour region to justify of adopting an elliptical model is discussed in Section 3.4; the ellipse modelling and ellipsoid modelling are described in Section 3.5; the training results of skin colour modelling of digital images are presented in Section 3.6; the training results of skin colour modelling of colorimetric skin colours are presented in Section 3.7; and the final section is the conclusion remark.

3.2 Priminary Study of Skin Colour Modelling

As far as the shape of a colour region is convex, a convex hull can be constructed to represent the gamut of the region. It is fairly safe to assume that the shape of a local colour region (e.g. skin, grass, sky) for colour preference

enhancement is convex. Constructing a local colour region using a convex hull is flexible and universal (applicable to modelling skin colour boundary as well as modelling other local colour regions, such as green grass and blue sky). Assuming that the shape of a colour region is convex, a convex hull can be generated automatically to represent the region. Using skin tone as an example, a set of skin colours are collected to generate a convex hull that represents the skin tone region. In this study, two approaches are used to build a database for a colour region. One is to carefully hand-pick colour samples that are within a colour region (the skin colour region in this case) to be studied and to add them to a data set (noted "skin sample set" herein). No order sequence is required for adding colours into the skin sample set, and duplicating colours are allowed. A skin colour sample can be obtained from an image or through measurement. The other approach is to use a bitmap image or a set of images (noted "skin image set" herein). Fig. 3.2-1 shows a skin image set in which the sub-images were cropped from various images. A master image with uniform skin colour background was initially created in Photoshop. Skin tone images were cropped from various images and pasted to this image. Each sub-image was converted to the colour space of the master image before being pasted to the master image. Because images may have noisy pixels, noise removal operations were applied to remove noise. In Photoshop, Median and Depeckle filters were applied to remove noise.

Fig. 3.2-1 A skin colour combo image

All skin colours were converted to CIELAB colour space, adapted to D50 using the linear Bradford chromatic adaptation matrix. A convex hull was then generated. The skin colour loci in three lightness levels were created in CIE a*-b* coordinates with constant lightness as shown in Fig. 3.2-2. It illustrates that the skin

tone loci is lightness dependent in CIELAB colour space. The lightness dependency should be taken into account for skin colour modelling.
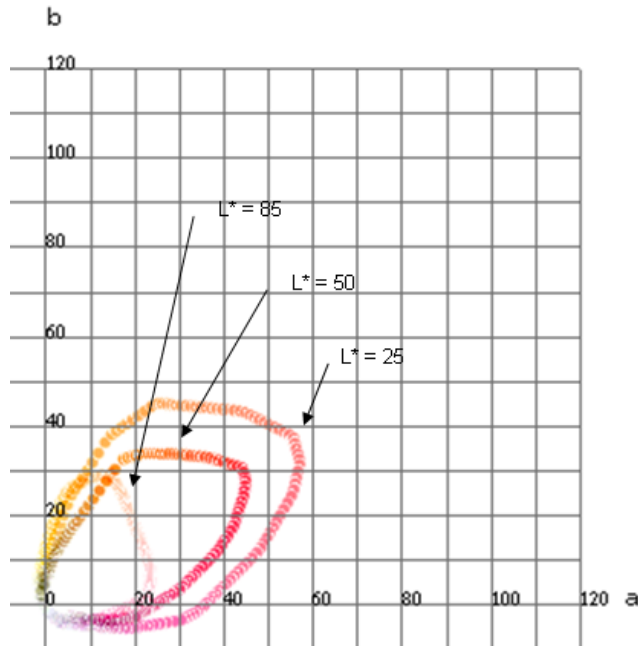
Fig. 3.2-2 A comparison of the skin tone convex hull in a*-b* coordinates with constant-lightness. The three lightness levels are 25, 50, and 85.
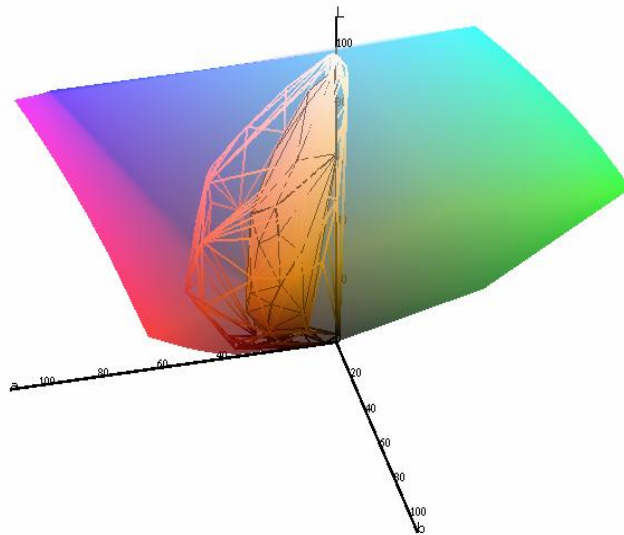
Fig. 3.2-3 Skin colour convex hulls generated using a skin image set (wireframe) and a skin sample set (solid) in CIE L*a*b* colour space, and the sRGB gamut (transparent)

Fig. 3.2-3 shows two convex hulls generated using two skin colour data sets, the skin sample set and the skin image set. The sRGB gamut is also drawn for visual comparison. The skin sample set was constructed by hand picking about 200 skin colour samples from many different images. Due to the inclusion of chromatic reds (such as lips) in the skin image set, its corresponding convex hull has richer

colours in the red region. Fig. 3.2-4 shows both skin tone convex hulls and sRGB gamut in a*-b* coordinates.
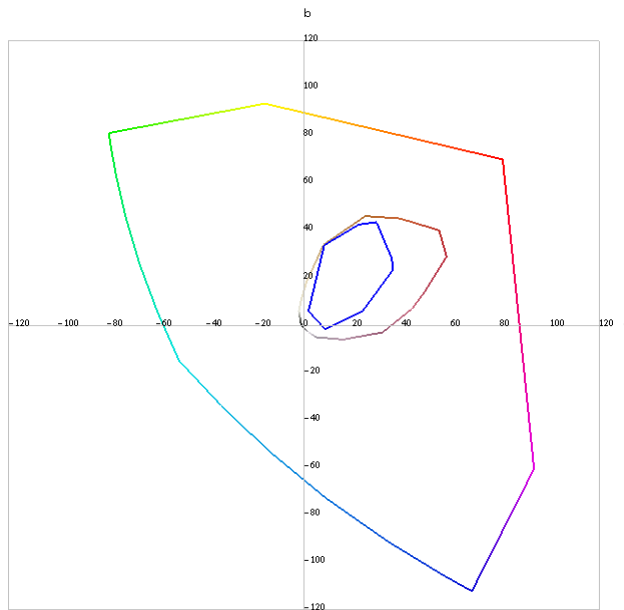
Fig. 3.2-4 Skin colour convex hulls generated using a skin image set (orange) and a skin sample set (blue), and the sRGB gamut (outskirt)

It is easy to add a lot of colours to a data set represented as images. However, it may be difficult to remove unwanted colours that may screw up the convex hull. Although it is laborious to hand-pick (or measure) a large amount of colours and add them to a skin sample set, it is easy to add carefully selected colours or to detect any colours that are entered incorrectly. As shown in figures 3.2-3 and 3.2-4, different data sets produce different convex hulls. It is important to visually check convex hulls for any errors that may exist in a database, because any noisy sample points may inflated a convex hull.

A green grass data set and a blue sky data set are prepared to construct grass and sky convex hulls as well. Fig. 3.2-5 shows the sRGB gamut, convex hulls of skin tones, green grass colours, and blue sky colours in CIELAB colour space. Fig. 3.2-6 is the projection of Fig. 3.2-5 in a*-b* coordinates (i.e. ignoring the L* coordinate).

To enhance memory colours, colours within the convex hull of the memory colour region are identified and adjusted accordingly. If a colour is out of the convex hull, preference adjustment is not performed. Otherwise, a weight to modulate the preferred colour adjustment is computed based on the relative location of the colour in the convex hull. If a colour is within a defined core region, full adjustment is performed. Otherwise, a distance to the boundary of the convex hull

and a distance to the core region are applied to compute a weight for colour adjustment.

To simplify colour adjustments, an equation based model may be built to approximate a colour region described with a convex hull. To model skin colours, the shape of 3-D skin colours is visualized to assist formulizing the region. Three formulations were developed in this study for skin colour modelling.
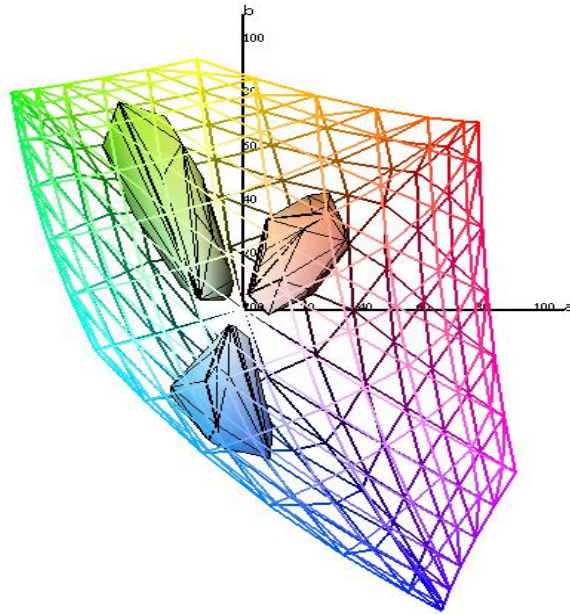
Fig. 3.2-5 Convex hulls of skin tones, green grass colours, and blue sky colours, and the sRGB gamut in CIELAB colour space
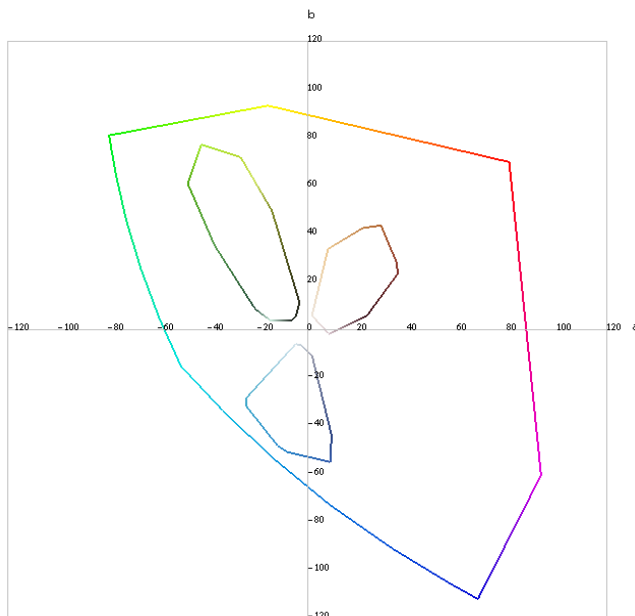
Fig. 3.2-6 Convex hulls of skin tones, green grass colours, and blue sky colours, and the sRGB gamut in a*-b* coordinates

3.2.1 Skin Colour Formulation 1

L* of skin tones is set to be in the range of [3, 97], and is scaled to the range of [0, 1]:

$$L_s = \frac{L^* - L^*_{dark}}{L^*_{light} - L^*_{dark}} \quad\quad (3.2.1-1)$$

where L* is lightness; L^*_{dark} and L^*_{light} are the lower end (=3) and higher end (=97) of lightness of the skin colours; and L_s is the scaled output.

A coefficient for lightness-dependent chroma adjustment is determined by Eq. (3.2.1-2) where a power of 0.4 is to adjust the curve so that w_L maximizes at a proper position.

$$w_L = \left(1 - \frac{|L_s - 0.5|}{0.5}\right)^{0.4} \quad\quad (3.2.1-2)$$

By visualizing each hue slice of the skin gamut in CIELAB colour space (adapted to D50), the relationship between hue angle in degrees and maximum chroma is obtained as listed in Table 3.2.1-1.

Table 3.2.1-1 Hue angle (in degrees) vs. chroma of skin colours

HUE ANGLE	CHROMA
0	35
10	45
20	55
30	65
40	60
50	52
60	40
70	40
80	25

A coefficient for chroma adjustment is computed by:

$$w_h = \left(1 - \frac{|h - h_{center}|}{0.5(h_{high} - h_{low})}\right)^{0.5} \quad\quad (3.2.1-3)$$

where w_h is the coefficient for hue-dependent chroma adjustment, h is the hue angle in degrees, h_{centre} is the hue centre of the skin tone, h_{high} and h_{low} are the higher end (78-degree) and lower end (0-degree) of the skin colours. $h_{centre} = (h_{high} + h_{low})/2$.

Two end points of the skin colour gamut on the lightness-chroma coordinates are (3, 3) and (97, 3), corresponding to the shadow end and the highlight end. With these parameters, a colour must have a chroma of 3 or higher to be classified as a skin colour. In other words, colour adjustment for skin colours starts with chroma that is equal to or greater than 3.

The minimum chroma of skin tone is computed by linear interpolation between two end points:

$$C_{\min} = C_{dark} + L_s \left(C_{light} - C_{dark} \right) \tag{3.2.1-4}$$

where $C_{\min}$ is the minimum chroma of skin colour for L* corresponding to L_s computed using Eq. (3.2.1-2); C_{dark} and C_{light} are the chroma of the shadow end and the highlight end, respectively. Since both C_{dark} and C_{light} are set to 3, $C_{\min}$ is always equal to 3. Eq. (3.2.1-4) is used only if C_{dark} and C_{light} are different.

The maximum chroma of skin colours is fitted with:

$$C_{\max} = C_{\min} + (35 \cdot w_h + 35) \cdot w_L \tag{3.2.1-5}$$

The skin colours are bounded by lightness between $[L_{low}, L_{high}]$, hue angle between $[h_{low}, h_{high}]$, and chroma between $[C_{\min}, C_{\max}]$.
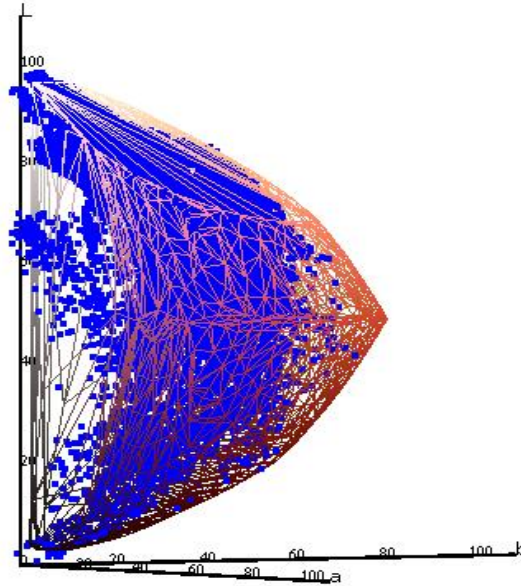
Fig. 3.2.1-1 The formulation of the skin colour boundary (wireframe) and the colours of the skin image set (blue dots)

A 129x129x129 uniformly sampled sRGB colours are converted to CIELAB colour space and adapted to D50 with the linear Bradford chromatic adaptation. The above skin colour formulation is applied to find skin colours. These sampled skin colours are used to construct a convex hull as shown in Fig. 3.2.1-1 for the parameter tuning and model verification. The skin image set is shown as blue dots

to visualize how well the model fits the image set. A gamut comparison of the skin colour formulation, the skin image set, and the skin sample set is drawn in CIE a*-b* coordinates with constant-lightness of 25, 50, and 70 from left to right as shown in Fig. 3.2.1-2. The gamut of the skin colour formulation (orange) is aimed to fit the skin image set (cyan). The model mimics the gamut of the image set closely. The gamut from the skin colour formulation covers a larger range of colours. The intention is to cover the nearby transition colours for preference adjustment. Depending on how the transition of the colour adjustment is performed from non-skin colours to skin colours, the skin colour formulation may be adjusted to slightly shrink or expand the skin colour region.
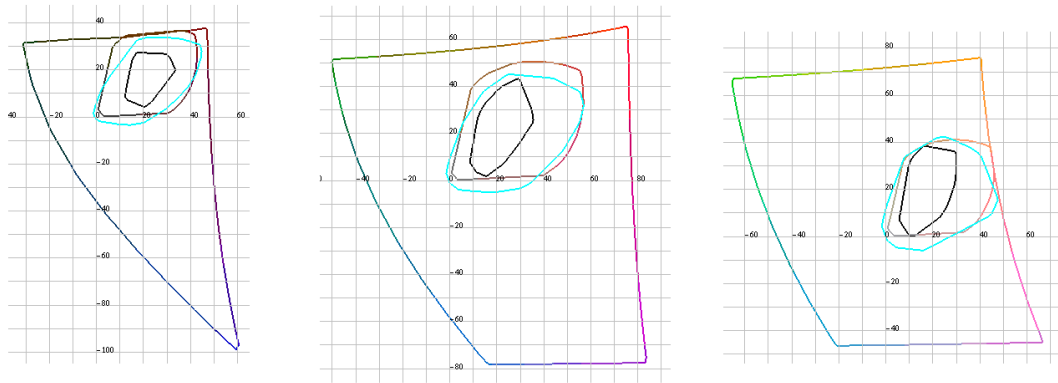
Fig. 3.2.1-2 A comparison of constant-lightness slices of the skin colour formulation (orange), the skin image set (cyan), and the skin colour sample set (black) in a*-b* coordinates with constant-lightness at 25, 50, and 70, from left to right, respectively. The outbound is the sRGB gamut.

3.2.2 Skin Colour Formulation 2

The skin colour boundary formulation 1 is developed by visualizing the shape of each hue slice. A different formulation is developed through visualizing the gamut in constant-lightness slices. Following equation is applied to fit the gamut shape in constant-lightness slices:

$$C = C_{max} \cdot [\sin(2\theta)]^{1/2} \qquad (3.2.2-1)$$

where C_{max} is the max chroma in each constant-lightness slice, and θ is a parameter scaled from hue angle. θ is in the range of [0°, 90°], or [0, $\pi/2$]. For different constant-lightness slices, C_{max} is different, i.e. C_{max} is lightness-dependent. Fig. 3.2.2-1 shows the curve of Eq. (3.2.2-1) with $C_{max} = 71$.

The hue range of skin colours is denoted [h_{low}, h_{high}]. In CIELAB colour space, h_{low} is about 0°, and h_{high} is about 80°. The hue angle, h, of a skin colour in the range of [h_{low}, h_{high}] is scaled to [0°, 90°] by:

$$\theta = \frac{h - h_{low}}{h_{high} - h_{low}} \cdot 90 \qquad (3.2.2\text{-}2)$$
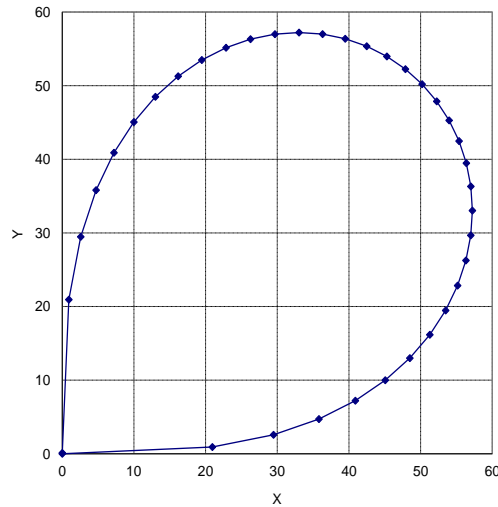
Fig. 3.2.2-1 A curve to formulate the skin colour boundary in a constant-lightness slice

The approximate relationship between lightness and maximum chroma of skin colours in CIE L*a*b* colour space is shown in Table 3.2.2-1.

Table 3.2.2-1 lightness versus chroma of skin colours

L^*	C_{max}
0	0
10	32
20	50
30	60
40	70
50	70
60	65
70	57
80	42
90	21
100	0

The maximum chroma is about 71 at lightness of about 46. The maximum chroma in each constant-lightness is computed by following equations:

$$L_s = \left(\frac{L^*}{100}\right)^{\gamma} \qquad (3.2.2\text{-}3)$$

$$w_L = 4 \cdot L_s \cdot (1 - L_s) \tag{3.2.2-4}$$

$$C = C_{max} \cdot [\sin(2\theta)]^{1/2} \cdot w_L \tag{3.2.2-5}$$

Eq. (3.2.2-3) is to readjust L* so that the mid-point, $L_s = 0.5$, corresponds to the constant-lightness slice in which the maximum chroma of skin colours is reached, i.e., a weight, w_L, reaches maximum of 1.0. Set L*=45.5 as the L* in which chroma reaches maximum, $\gamma = \log(0.5)/\log(0.455)$, which is about 0.88. The reasons to choose L*=45.5 for computing γ are: to maximize chroma on this lightness-slice; and to have chroma in Eq. (3.2.2-5) closely match the maximum chroma in Table 3.2.2-1 globally. C_{max} is a constant that is set to about 71.

To detect whether a colour is within the skin colour region, the hue angle is first computed. If the hue angle is within the range of [h_{low}, h_{high}], Eqs. (3.2.2-2) to (3.2.2-5) are applied to compute chroma, C. If the chroma of the colour is not larger than C, the colour is a skin colour.

With this formulation, neutral axis (chroma=0) becomes a natural boundary for skin colours. This is the intention to have colour adjustment stop at neutral axis. A minimum chroma may be set to exclude near-neutral colours.

The comparison of the skin colour formulations 1 and 2 is shown in Fig. 3.2.2-2. Again, a 129x129x129 uniformly sampled sRGB colours are converted to CIELAB colour space and adapted to D50 using the linear Bradford chromatic adaptation. Each skin colour formulation is applied to find skin colours. A convex hull is then constructed for the resulted skin colours obtained from each formulation. The gamut shapes of two formulations are very similar.
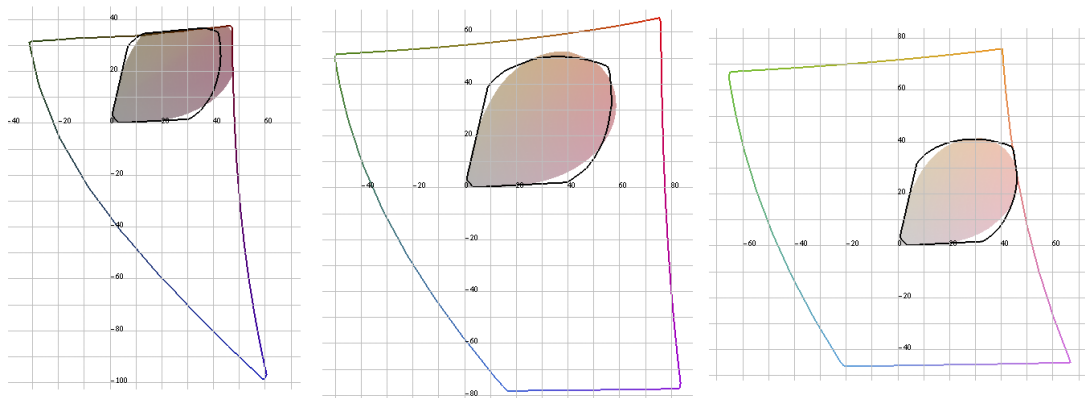
Fig. 3.2.2-2 A comparison of two skin colour formulations in a*-b* coordinates with constant-lightness (black wireframe for Formulation 1 and solid colour brush for Formulation 2). The lightness are 25, 50, and 70, from left to right, respectively. The outbound is the sRGB gamut.

3.2.3 Skin colour Formulation 3

Park, et al. (2006) formulated the boundary of skin colours in C_b-C_r colour space for preferred skin colour reproduction of displays. The boundary of skin colours is defined as an ellipse using a constant density contour having the same probability of a bivariate Gaussian function. Kim (2005) applied an elliptical model for skin colour enhancement. In this study, following formulae are applied to compute a constant density contour to describe the skin colour boundary in CIELAB colour space:

$$q = \left(\frac{a*-a_0}{r_a}\right)^2 - \rho \cdot \left(\frac{a*-a_0}{r_a}\right) \cdot \left(\frac{b*-b_0}{r_b}\right) + \left(\frac{b*-b_0}{r_b}\right)^2 \qquad (3.2.3\text{-}1)$$

$$P_{ab} = \exp(-0.5 \cdot q) \qquad (3.2.3\text{-}2)$$

where $(a_0\ b_0)$ is the centre of the skin chrominance; r_a and r_b are the variances of a* and b* of the skin colours, respectively; and ρ is a correlation coefficient. P_{ab} is the probability map of skin colours, which is used to determine the boundary of skin colours and how far a colour is from the skin colour centre. The formula was fitted with the skin image set. The coefficients are: $(a_0, b_0) = (27, 22)$; $(r_a, r_b) = (20, 18)$; and $\rho = 0.7$. $P_{ab} > 0.4$ is set to be the boundary for skin colours.

To take the attribute of lightness into account, an L*-dependent factor, w_L, computed from Eq. (3.2.2-4) is applied to modulate the coefficients, a_0, b_0, r_a, and r_b:

$$\begin{aligned}
a_0^{'} &= a_0 \cdot w_L \\
b_0^{'} &= b_0 \cdot w_L \\
r_a^{'} &= r_a \cdot w_L \\
r_b^{'} &= r_b \cdot w_L
\end{aligned} \qquad (3.2.3\text{-}3)$$

where $a_0^{'}$, $b_0^{'}$, $r_a^{'}$, and $r_b^{'}$ are used to replace a_0, b_0, r_a, and r_b in Eq. (3.2.3-1) for computing q.

The advantage of this model is the convenience for computing the distance of a colour to the skin colour centre, and therefore it is easy to compute a weight for skin colour adjustment.

3.2.4 Discussion

With 3-D gamut visualization, a convex hull generated from a colour region is fitted with different formulae. Although the approach lacks rigorous mathematical modelling, the formulations and data fitting can be adjusted with interactive visual inspection. In addition, it is flexible for fitting data gamut with various mathematical formulae for different purposes. The formulations 1 and 2 work directly in lightness, chroma, and hue angle coordinates, while the formulation 3

works directly in lightness-chromaticities space. Formulation 2 is convenient for skin colour adjustment that gradually fades off toward the neutral axis. Formulation 3 has the advantage for computing a distance to the gamut boundary and to use the distance as a weight for skin colour adjustment.

A limitation of the method is that the occurrence of a skin pixel in a database (or the probability of a colour to be a skin colour) can not be applied to affect the construction of the boundary. The probability of each colour may be applied to compute a weight to affect the gamut construction. With such an approach, noise colours and other colours that have very low probabilities can be removed. This will be explored in next few sections. The elliptical modelling as described in Section 3.2.3 will be further studied as well.

3.3 Constructing an Image Database to Train Skin Models

In this research, the preferred skin colour reproduction is aimed for processing general digital photographic images. Hence, images captured with different digital cameras under various conditions were collected for training skin colour models.

An image database, Halloween database, to train skin colour models is composed of about 2500 digital images that cover Caucasian, Asian, and African facial tones. About 60% of the images came from an HP internal image database. Since 1998, the HP Vancouver site organized a Halloween event for the kids of HP employees to have fun in the site. Taking photos for kids and families was part of the event. Two photo studios were set up each year to take pictures. Thus, there were two capturing conditions in which the lighting conditions, backgrounds, and digital cameras might be different each year. And these setting conditions and digital cameras were different year over year. The digital photos from 2001 to 2008 are used for our skin tone analysis. Since the photos captured prior to 2001 have lower image quality, they were decided not to be used. The main reason to use these images for this study was that the lighting conditions were well controlled, and therefore each image had proper white balance.

The images from the HP Halloween image source were captured under limited conditions (lighting conditions and camera types). To avoid bias on image capturing conditions, images from various other sources were added. Most of these images were captured outdoor in past few years using various professional and consumer digital cameras. Fig. 3.3-1 shows a few images from the database.

Fig. 3.3-1 Selected images from Halloween database

A colour masking tool (CMT) was developed to label skin colours in each image. Fig. 3.3-2 is a snapshot of the tool. The left window shows the original image. Once the mouse is pointed to a skin colour and clicked, the skin colour of this point is applied as the seed colour (colour centre) to grow the colour region. The span of the region is determined by a range slider that sets a colour difference threshold of each pixel to the seed colour. A colour difference value is scaled to an 8-bit mask value between 0 and 255. A seed colour has a colour difference of zero and is corresponded to a mask value of zero. A colour difference that is equal to or greater than the threshold set by the range slider corresponds to a mask value of 255. All other colour differences are scaled to the range of 0 and 255 accordingly. A mask value of 255 corresponds to non-skin colours. Pixels selected as skin colours are marked pink on the centre window.   The mask values of the image are represented as a gray-scale image shown on the right window.
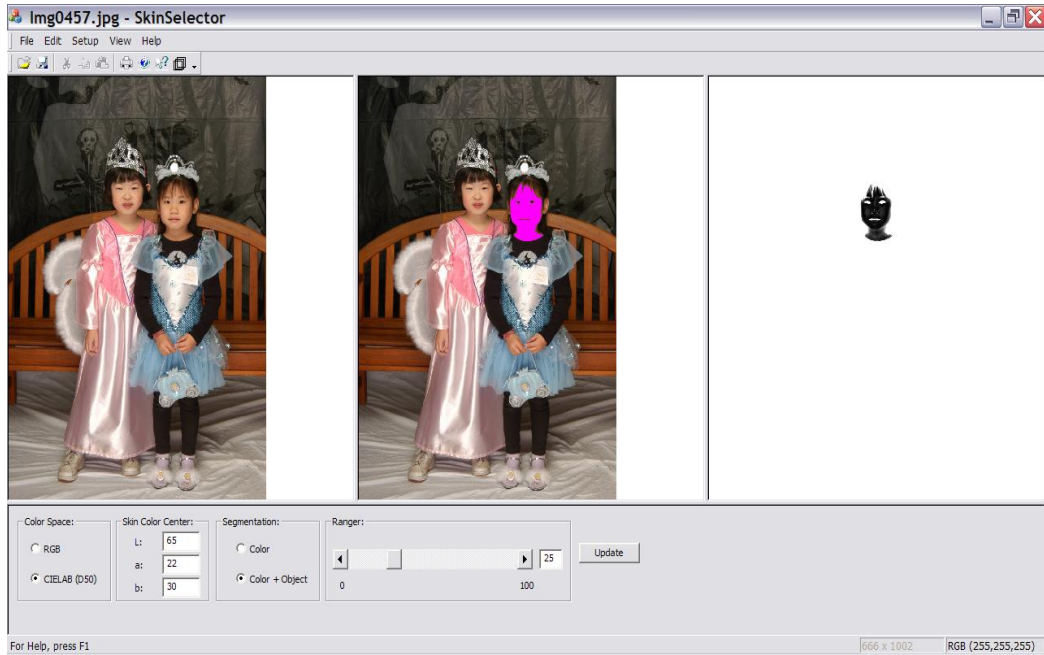
Fig. 3.3-2 The colour masking tool (CMT) to label skin colours

Although an RGB colour space can be used to grow a region, it was found that results produced in CIELAB colour space were more closely correlated to the human visual perception. Therefore, CIELAB colour space was selected in this study. RGB colour values are converted to L*a*b* using the embedded ICC profile of each image (or sRGB ICC profile if no embedded ICC profile exists).

If the segmentation method, "Colour + Object" in the tool, is selected, the regional growth subjects to the constraint that skin colours must be clustered together as a single object, which prohibits more than one isolated region. This method is used to construct the skin database for: 1) it prohibits growing similar colours to other objects; and 2) it enables labelling skins of different persons on an image with different colour centres.

After an object is labelled, the source image (on the left window), the image with a labelled skin object (on the centre window), the image of the skin mask (on the right window), and the setting parameters are saved. An image with very high resolution is re-sampled to a size of about 2-mega pixels to avoid that the image is weighted much higher than a lower resolution image.

Labelled pixels are used to analyse skin colours, and all other pixels that are not labelled (white pixels in the image on the right window) are ignored. As a result, labelling all skin pixels is not necessary.

After labelling all images, a script reads each image (the image on the left window) and its associated labelled image (image on the right window) and adds occurrences of skin colours to a 256x256x256 RGB LUT. The reason for using a

256^3 LUT is the convenience for counting occurrences of 8-bit RGB images. The number on each node of the LUT represents the occurrences of the RGB colour as a skin pixel. So the number on every non-skin node is zero. Each skin colour from an 8-bit/channel RGB image adds an occurrence count to the corresponding bin of the LUT. To remove noisy pixels and pixels that may be inaccurately selected as skin pixels, a small percentage of pixels with occurrences at the lower end are excluded from counting occurrences at the time each image is processed. In this study, 10% least occurring pixels were removed from each image.

The skin colours of the Halloween image database were labelled mostly by the author. The bias from the user selection should be insignificant for two reasons: first, during counting skin pixel occurrences from each image, a process was implemented to remove a small percentage of labelled skin pixels whose colour histograms were under a threshold; and secondly, a huge amount of skin pixels (in the order of billions) were collected from diversified images. Nevertheless, a second image database, RPS database, was created to verify the bias of skin labelling from different users and the dependency on training data sets. It is a collection of 626 proprietary photographic images that were collected from different sources, including indoor and outdoor images and covering different ethnic types. All images were sampled to a uniform resolution of 1200x1800. Fig. 3.3-3 shows a few images from this database. Again, the same colour selector tool was used to label skin pixels. The skin labelling was mostly done by a colour engineering when he and I worked on a join-project. A comparison of training results using these two databases is presented in the Discussion section.

Fig. 3.3-3 Selected images from RPS database

3.4 Gamut of Skin Colour Cluster of Digital Images

Fig. 3.4-1 shows the cluster of the selected skin colours of the Halloween database in CIELAB colour space. The right one is the projection in a*-b* coordinates, i.e., the top-down view of the cluster. The shapes of constant-lightness slices are close to ellipses, but the sizes and the locations of ellipses at different lightness are different. If an ellipse is used to fit the skin boundary on the a*-b* plane, it should be large enough to cover the dominant mid-tone skin colours, although smaller ellipses fit well for lighter and darker tones.
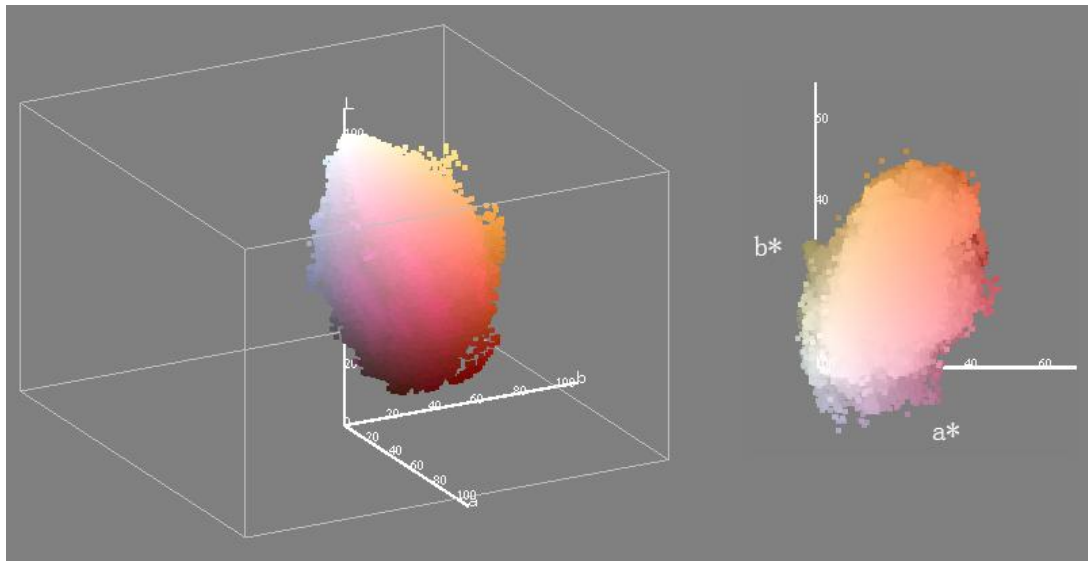
Fig. 3.4-1 3-D gamut of all labelled skin pixels of Halloween database

CIELAB colour space is selected to study skin colour modelling, because it is reasonably uniform in the skin colour region, its lightness and chrominance are separated by L* and a*b*, and the transformation between CIELAB and RGB is reasonably efficient.

To study how an ellipse fits skin colours on constant lightness slices, 2-D a*-b* convex hulls of skin colours were constructed for constant lightness at 0, 10, 20, …, 100. Since no skin sample colours were found on L* that was less than or equal to 10, no convex hulls could be constructed for these two L* levels. Convex hulls for other L* levels (20, 30, …, 90) are shown in Fig. 3.4-2. Except that extreme colours (noise, incorrectly selected pixels) skew the shape of the convex hull in highlight and shadow regions, the shapes of convex hulls in the mid-tone region look like ellipse. Dark colours subject to higher noise, and highlight colours may be influenced more heavily by the white balance and lighting conditions. These may be the reasons that the shapes of the convex hull in two end regions are less like ellipse. This is the reason that frequencies (f_i in elliptical modelling formulae) are used as weights to model the shape.
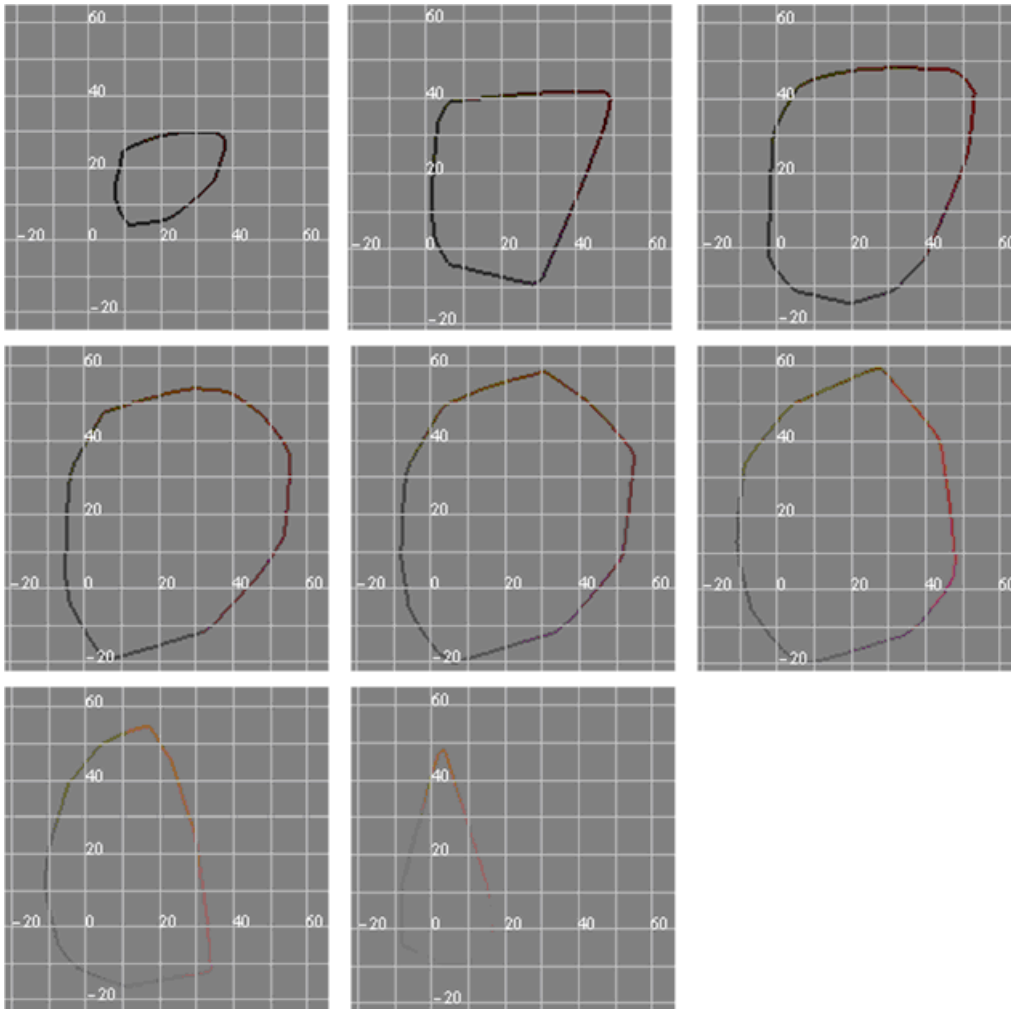
Fig. 3.4-2 2-D constant-lightness a*-b* slices of skin colours for L* at 20, 30, …, 90, from left to right, top to bottom.

Figs. 3.4-1 and 3.4-2 show a trend that ellipses to fit the gamut of skin colours in a*-b* coordinates should be lightness dependent. Would it be less luminance-dependent in CIE Yxy space? Fig. 3.4-3 shows the skin colour cloud of the same data set in Yxy space. The shapes and sizes of the skin colours at different Y levels are different. For images captured with a single camera or at the raw data state, the skin colour cluster under x-y or r-g space may take up a smaller region and be less luminance-dependent, but this is not the focus of this study.

The shape of the skin colour gamut in Fig. 3.4-1 shows that the skin colour boundary can be reasonably approximated with an ellipse. The variations of 2-D a*b* gamut in different lightness shows that modelling elliptical boundary that is adapted to different lightness should fit the skin colour cluster more accurately.
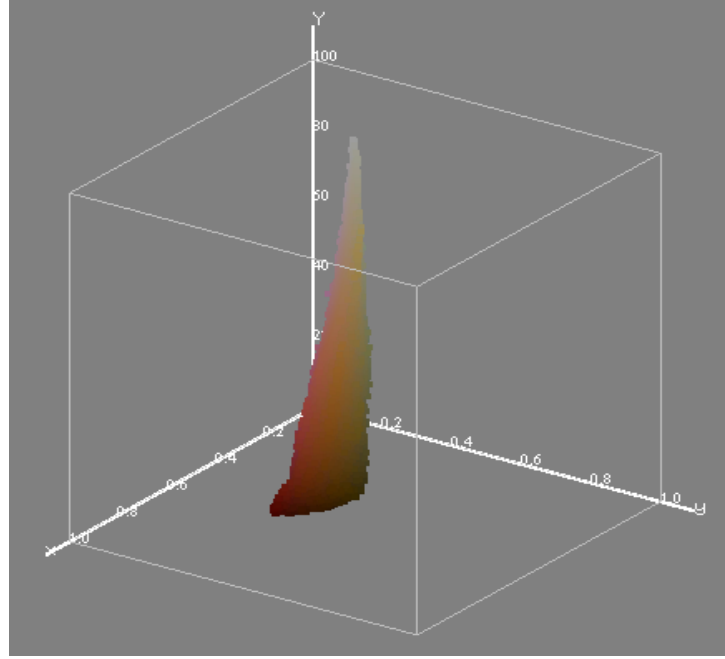
Fig. 3.4-3 3-D skin colour gamut in Yxy colour space (D50)

3.5 Elliptical Boundary Model

Since the shape of the skin colour cluster of digital images in CIELAB colour space is approximately elliptical, the skin colour cluster will be modelled with elliptical shapes. To generalize the model, let $X_1, \ldots, X_n$ be distinctive colours of a skin colour training data set and $f(X_i)=f_i$ $(i = 1, \ldots, n)$ be the occurrence counts of a colour, X_i. An elliptical boundary model $\Phi(X)=(X, \Psi, \Lambda)$ is defined as

$$\Phi(X) = [X - \Psi]^T \Lambda^{-1} [X - \Psi] \tag{3.5-1}$$

where the elliptical centre, Ψ, and the covariance matrix, Λ, are given by

$$\Psi = \frac{1}{n} \sum_{i=1}^{n} X_i \tag{3.5-2}$$

$$\Lambda = \frac{1}{N} \sum_{i=1}^{n} f_i (X_i - \mu)(X_i - \mu)^T \tag{3.5-3}$$

where $N = \sum_{i=1}^{n} f_i$ is the total number of samples in the training data set and the

vector $\mu = \frac{1}{N} \sum_{i=1}^{n} f_i X_i$ is the mean of chrominance vectors.

Given a threshold ρ and an input colour X of a pixel, X is classified as a skin colour if $\Phi(X) < \rho$ and as a non-skin colour otherwise. The threshold ρ trades off correct detections by false detections. As ρ increases, the correct detection rate increases, however, the false detection rate increases as well. $\Phi(X) = \rho$ defines an

elliptical boundary between skin and non-skin colours. The centre of the ellipse is given by ψ and the principal axes are determined by Λ.

3.5.1 Ellipse Skin Colour Modelling

In this study, an ellipse skin colour model represented in a matrix form and a polynomial form were derived. And a skin colour database was created to train coefficients of these two formulae.

Ignoring the lightness coordinate, the cluster of skin colours may be modelled with a single ellipse. In a 2-dimensional chrominance space, X is expressed as $X = \begin{pmatrix} x \\ y \end{pmatrix}$, and Λ^{-1} is represented in a matrix form

$$\Lambda^{-1} = \begin{pmatrix} \lambda_{00} & \lambda_{01} \\ \lambda_{10} & \lambda_{11} \end{pmatrix} \tag{3.5-4}$$

$\Phi(X)$ can be reorganized in the following form:

$$\Phi(X) = \lambda_{00}(x - x_0)^2 + (\lambda_{01} + \lambda_{10})(x - x_0)(y - y_0) + \lambda_{11}(y - y_0)^2 \tag{3.5-5}$$

where (x_0, y_0) is the centre and λ coefficients determines the covariance matrix.

The equation can be expressed by

$$\Phi(x, y) = u_0(x - x_0)^2 + u_1(x - x_0)(y - y_0) + u_2(y - y_0)^2 \tag{3.5-6}$$

where $u_0 = \lambda_{00}$, $u_1 = \lambda_{01} + \lambda_{10}$, and $u_2 = \lambda_{11}$.

The ellipse equation Eq. (3.5-6) has been widely used in colour difference modelling. With the elliptical model, the majority work is to find the matrix Λ. According the Eq. (3.5-3),

$$\Lambda = \frac{1}{N} \sum_{i=1}^{n} f(x_i, y_i) \begin{pmatrix} x_i - x_0 \\ y_i - y_0 \end{pmatrix} (x_i - x_0 \quad y_i - y_0)$$

This can be reformatted as

$$\Lambda = \frac{1}{N} \sum_{i=1}^{n} f(x_i, y_i) \begin{pmatrix} (x_i - x_0)^2 & (x_i - x_0)(y_i - y_0) \\ (x_i - x_0)(y_i - y_0) & (y_i - y_0)^2 \end{pmatrix} \tag{3.5-7}$$

Comparing Eqs. (3.5-4) and (3.5-7), it is obvious that $\lambda_{01} = \lambda_{10}$.

It will be easier to draw the ellipse, if the x-y coordinate system is translated to the ellipse's centre and then rotated to the principal axes of the ellipse. Let's rotate $X = \begin{pmatrix} x \\ y \end{pmatrix}$ to a new coordinate $X' = \begin{pmatrix} x' \\ y' \end{pmatrix}$ with an angle of θ,

$$\begin{pmatrix} x' \\ y' \end{pmatrix} = \begin{pmatrix} \cos(\theta) & -\sin(\theta) \\ \sin(\theta) & \cos(\theta) \end{pmatrix}, \text{ or } \begin{pmatrix} x \\ y \end{pmatrix} = \begin{pmatrix} \cos(\theta) & \sin(\theta) \\ -\sin(\theta) & \cos(\theta) \end{pmatrix} \begin{pmatrix} x' \\ y' \end{pmatrix}.$$

Eq. (3.2-1) can be written as

$$\Phi(X) = \begin{pmatrix} x - x_0 & y - y_0 \end{pmatrix} \begin{pmatrix} \lambda_{00} & \lambda_{01} \\ \lambda_{10} & \lambda_{11} \end{pmatrix} \begin{pmatrix} x - x_0 \\ y - y_0 \end{pmatrix}$$

where $\lambda_{01} = \lambda_{10}$. After translating the origin to (x_0, y_0), the above equation becomes

$$\Phi(X') = \begin{pmatrix} x' & y' \end{pmatrix} \begin{pmatrix} \lambda_{00} & \lambda_{01} \\ \lambda_{10} & \lambda_{11} \end{pmatrix} \begin{pmatrix} x' \\ y' \end{pmatrix}$$

By applying rotation, the equation becomes

$$\Phi(X'') = \begin{pmatrix} x'' & y'' \end{pmatrix} \begin{pmatrix} \cos(\theta) & -\sin(\theta) \\ \sin(\theta) & \cos(\theta) \end{pmatrix} \begin{pmatrix} \lambda_{00} & \lambda_{01} \\ \lambda_{10} & \lambda_{11} \end{pmatrix} \begin{pmatrix} \cos(\theta) & \sin(\theta) \\ -\sin(\theta) & \cos(\theta) \end{pmatrix} \begin{pmatrix} x'' \\ y'' \end{pmatrix} \quad (3.5\text{-}8)$$

or

$$\Phi(X'') = \begin{pmatrix} x'' & y'' \end{pmatrix} \begin{pmatrix} \lambda_{00}\cos^2(\theta) - \lambda_{01}\cdot\sin(2\theta) + \lambda_{11}\sin^2(\theta) & \lambda_{01}\cos(2\theta) - 0.5(\lambda_{11} - \lambda_{00})\sin(2\theta) \\ \lambda_{01}\cos(2\theta) - 0.5(\lambda_{11} - \lambda_{00})\sin(2\theta) & \lambda_{00}\sin^2(\theta) + \lambda_{01}\sin(2\theta) + \lambda_{11}\cos^2(\theta) \end{pmatrix} \begin{pmatrix} x'' \\ y'' \end{pmatrix}$$

$$(3.5\text{-}9)$$

By rotating the coordinate to the principal axes, the matrix in the middle becomes a diagonal matrix, i.e., the upper right and the lower left terms become zero:

$$\lambda_{01}\cos(2\theta) - 0.5(\lambda_{11} - \lambda_{00})\sin(2\theta) = 0.$$

Thus, the angle to rotate the major axis is

$$\theta = 0.5\arctan\left(\frac{2\lambda_{01}}{-\lambda_{00} + \lambda_{11}}\right) \quad (3.5\text{-}10)$$

Two parameters related to the principal axes are

$$A = \lambda_{00}\cos^2(\theta) - \lambda_{01}\cdot\sin(2\theta) + \lambda_{11}\sin^2(\theta)$$
$$B = \lambda_{00}\sin^2(\theta) + \lambda_{01}\sin(2\theta) + \lambda_{11}\cos^2(\theta) \quad (3.5\text{-}11)$$

The lengths of the semi-major and semi-minor axes are $\sqrt{\dfrac{1}{A}}$ and $\sqrt{\dfrac{1}{B}}$.

Rewrite Eq. (3.5-8) as

$$\begin{pmatrix} \cos(\theta) & -\sin(\theta) \\ \sin(\theta) & \cos(\theta) \end{pmatrix} \begin{pmatrix} \lambda_{00} & \lambda_{01} \\ \lambda_{10} & \lambda_{11} \end{pmatrix} \begin{pmatrix} \cos(\theta) & \sin(\theta) \\ -\sin(\theta) & \cos(\theta) \end{pmatrix} = \begin{pmatrix} A & 0 \\ 0 & B \end{pmatrix},$$

The equation can be reorganized as

$$\begin{pmatrix} \lambda_{00} & \lambda_{01} \\ \lambda_{10} & \lambda_{11} \end{pmatrix} = \begin{pmatrix} A\cdot\cos^2(\theta) + B\cdot\sin^2(\theta) & \dfrac{B-A}{2}\sin(2\theta) \\ \dfrac{B-A}{2}\sin(2\theta) & A\cdot\sin^2(\theta) + B\cdot\cos^2(\theta) \end{pmatrix} \quad (3.5\text{-}12)$$

The training result (see Section 3.6) shows that the centre, the size, and the orientation of a 2-D chrominance ellipse at different lightness levels are different. The colour modelling accuracy would be comprised if a single ellipse is derived to represent the skin colour region. To improve the modelling accuracy, a training data set is divided into many sub-sets, each containing pixels within a bin of lightness. For example, a data set represented in CIELAB colour space may be divided into twenty sub-sets, in which each sub-set spans 5 units of L*, and an ellipse is generated for each bin of lightness. The variations of the sequence of ellipses are analysed, abrupt changes are smooth out, and interpolations are applied to derive a lightness-adapted ellipse model. The details are described in Section 3.6.

3.5.2 Ellipsoid Skin Colour Modelling

A new skin colour model, the ellipsoid skin colour model, is proposed in this section to model the skin colour cluster in a 3-dimensional lightness-chrominance colour space. An advantage of this model over the ellipse model is that the lightness dependency of the shape of skin cluster is included in the modelling.

In a 3-D space, X is represented as $X = \begin{pmatrix} x \\ y \\ z \end{pmatrix}$. The Λ^{-1} is represented in a matrix form

$$\Lambda^{-1} = \begin{pmatrix} \lambda_{00} & \lambda_{01} & \lambda_{02} \\ \lambda_{10} & \lambda_{11} & \lambda_{12} \\ \lambda_{20} & \lambda_{21} & \lambda_{22} \end{pmatrix} \qquad (3.5\text{-}13)$$

$\Phi(X)$ in Eq. (3.5-1) is reorganized as

$$\begin{aligned}
\Phi(x, y, z) = {} & \lambda_{00}(x - x_0)^2 + (\lambda_{01} + \lambda_{10})(x - x_0)(y - y_0) + \\
& (\lambda_{02} + \lambda_{20})(x - x_0)(z - z_0) + \lambda_{11}(y - y_0)^2 + \\
& (\lambda_{12} + \lambda_{21})(y - y_0)(z - z_0) + \lambda_{22}(z - z_0)^2
\end{aligned} \qquad (3.5\text{-}14)$$

With the ellipsoid model, the main work is to find the matrix Λ. According to Eq. (3.5-7),

$$\Lambda = \frac{1}{N} \sum_{i=1}^{n} f(x_i, y_i, z_i) \begin{pmatrix} x_i - x_0 \\ y_i - y_0 \\ z_i - z_0 \end{pmatrix} \begin{pmatrix} x_i - x_0 & y_i - y_0 & z_i - z_0 \end{pmatrix}$$

This can be reformatted as

$$\Lambda = \frac{1}{N} \sum_{i=1}^{n} f(x_i, y_i, z_i) \begin{pmatrix} (x_i - x_0)^2 & (x_i - x_0)(y_i - y_0) & (x_i - x_0)(z_i - z_0) \\ (x_i - x_0)(y_i - y_0) & (y_i - y_0)^2 & (y_i - y_0)(z_i - z_0) \\ (x_i - x_0)(z_i - z_0) & (y_i - y_0)(z_i - z_0) & (z_i - z_0)^2 \end{pmatrix}$$

(3.5-15)

Comparing Eqs. (3.5-13) and (3.5-15), $\lambda_{01} = \lambda_{10}$ and $\lambda_{21} = \lambda_{12}$. The ellipsoid function (3.5-14) can be written as:

$$\Phi(x, y, z) =$$

$$u_0(x - x_0)^2 + u_1(x - x_0)(y - y_0) + u_2(y - y_0)^2 + u_3(x - x_0)(z - z_0) + u_4(y - y_0)(z - z_0) + u_5(z - z_0)^2$$

(3.5-16)

where $u_0 = \lambda_{00}$, $u_1 = \lambda_{01} + \lambda_{10}$, $u_2 = \lambda_{11}$, $u_3 = \lambda_{02} + \lambda_{20}$, $u_4 = \lambda_{12} + \lambda_{21}$, and $u_5 = \lambda_{22}$.

A general approach to find the three principal axes of the ellipsoid is to translate the origin of the coordinate to the centre of the ellipsoid, and then rotate the ellipsoid so that three principal axes overlapped with the three coordinates. After translating the origin of the coordinates to the centre of the ellipsoid, the coordinate X(x y z) becomes X'(x' y' z'), where

$$x' = x - x_0$$
$$y' = y - y_0 .$$
$$z' = z - z_0$$

Denote a 3x3 rotation matrix, M_r, which is a 3x3 matrix. $X'' = M_r X'$. Eq. (3.5-1) is rewritten as

$$\Phi(X'') = X''^T M_r^T \Lambda^{-1} M_r X''$$

(3.5-17)

Denoting $M = M_r^T \Lambda^{-1} M_r$, $\Phi(X'') = X''^T M X''$. To rotate X' to X'', M_r must be such that M becomes a diagonal matrix. A 3-dimensional rotation can be specified with three Euler angles.

Matrices for rotating α around the x-axis, β around the y-axis, and γ around the z-axis are expressed below:

$$R_x(\alpha) = \begin{pmatrix} 1 & 0 & 0 & 0 \\ 0 & \cos\alpha & -\sin\alpha & 0 \\ 0 & \sin\alpha & \cos\alpha & 0 \\ 0 & 0 & 0 & 1 \end{pmatrix}$$

$$R_y(\beta) = \begin{pmatrix} \cos\beta & 0 & \sin\beta & 0 \\ 0 & 1 & 0 & 0 \\ -\sin\beta & 0 & \cos\beta & 0 \\ 0 & 0 & 0 & 1 \end{pmatrix}$$

$$R_z(\gamma) = \begin{pmatrix} \cos\gamma & -\sin\gamma & 0 & 0 \\ \sin\gamma & \cos\gamma & 0 & 0 \\ 0 & 0 & 1 & 0 \\ 0 & 0 & 0 & 1 \end{pmatrix}$$

A general rotation matrix depends on the order of rotations. A matrix rotates about x, then y, and finally z is:

$$R_z R_y R_x(\alpha) = \begin{pmatrix} \cos\beta\cos\gamma & \cos\gamma\sin\alpha\sin\beta - \cos\alpha\sin\gamma & \cos\alpha\cos\gamma\sin\beta + \sin\alpha\sin\gamma & 0 \\ \cos\beta\sin\gamma & \cos\alpha\cos\gamma + \sin\alpha\sin\beta\sin\gamma & -\cos\gamma\sin\alpha + \cos\alpha\sin\beta\sin\gamma & 0 \\ -\sin\beta & \cos\beta\sin\alpha & \cos\alpha\cos\beta & 0 \\ 0 & 0 & 0 & 1 \end{pmatrix}$$

With such complexity, it is not trivial to derive α, β, and γ to meet the requirement that M becomes a diagonal matrix. Doing the math in a spherical coordinate system may simplify the expression slightly. However, finding three rotation angles are neither trivial.

An exhaustive search approach was then developed to solve the problem. Since two points on the surface that intercept the longest principal axis have the longest distance to the centre, this property was used to find the longest axis. Due to the symmetric behaviour, it is not necessary to search the entire gamut, and only a point on the ellipsoid surface needs to be found (the other point is the mirror from the centre). By exhaustive searching points within a portion of the ellipsoid, a point that has the longest distance to the centre is found. The vector connected the centre and this point is the longest principal semi-axis.

There are two points that the shortest principal axis intercepts with the ellipsoid surface. The distance of either point to the centre is shorter than the distance of any other surface point to the centre. This property is used to find the shortest principal axis. With exhaustive searching, if a point is not inside the ellipsoid, its distance to the centre is computed. A point that has the shortest distance to the centre is eventually found. Because principal axes are perpendicular to each other, this property can be used to reduce searching points. A vector connecting the resulted point and the centre is the shortest semi-axis.

A vector that passes the centre and is perpendicular to a plane constructed using the longest and the shortest principal axis is the vector of the third axis. This property is used to find the third axis. The direction of the third axis is the cross product of the vectors of the other two axes. By searching the points from the centre along the direction of the vector of the third axis, a point within the ellipsoid and has

the longest distance to the centre is the interception point between the third axis and the ellipsoid surface.

3.6 Training Results of Skin Colour Modelling of Digital Images

3.6.1 Ellipse Skin Colour Boundary Modelling

As described in Section 3.3, each labelled skin pixel in the database has a mask value between 0 and 255 to encode skin colour likelihood (the higher the value, the lower the likelihood). However, mask values were binarized to skin or non-skin colours for the skin colour modelling in this study. In other words, each colour was treated as a skin colour or a non-skin colour, and its likelihood value (colour difference to the central skin colour) was not applied for the modelling. Although some information about the likelihood of skin pixels are lost from binarisation the skin map, the binarised skin likelihood information may be more reliable from following two reason. First, skin pixels were labelled based on visual feedback from the binary mask shown on the right window using CMT. Second, since skin pixels were labelled mostly by a single operator, using binary mask might reduce biased from operators.

The RGB colour at each node of the RGB skin occurrence LUT was converted to CIE L*a*b* colour space and the white point was adapted to D50 using linear Bradford chromatic adaptation matrix (Luo and Hunt 1998) which was used to create the official sRGB ICC profile, (Nielsen and Stokes 1998). The LUT was used to train elliptical models, where the count in each bin of the LUT is the occurrence, f(X_i) or f_i, in Eq. (3.5-3), and the a*b* or L*a*b* of each bin location is the colour, X.

3.6.1.1 Lightness-Independent Ellipse Model (Single-Ellipse Model)

Projecting all colours to a*-b* coordinates (i.e., ignoring each colour's lightness value), an ellipse is trained. Although the accuracy to fit skin colour in an ellipse is sacrificed for simplicity and efficiency, it is adequate for some applications. Fig. 3.6.1-1 shows the modelled ellipse in a*-b* coordinates to cover 95% of the labelled skin colours of Halloween database. The centre coordinates are (19, 20), together with the ellipse parameters [A, A/B, θ] of [26.9, 1.8, -62°], where A and B are the semi-major axis and semi-minor axis, and θ is the orientation angle of the major axis (negative-degree means counter-clockwise rotation). See Appendix A for the detailed training result. For practical applications, the principle axes may be increased or decreased proportionally (equivalent to adjusting ρ of the elliptical model) to adjust the skin colour boundary. A method to choose a proper coverage

rate to achieve desired skin colour detection accuracy will be discussed in Section 3.6.3.
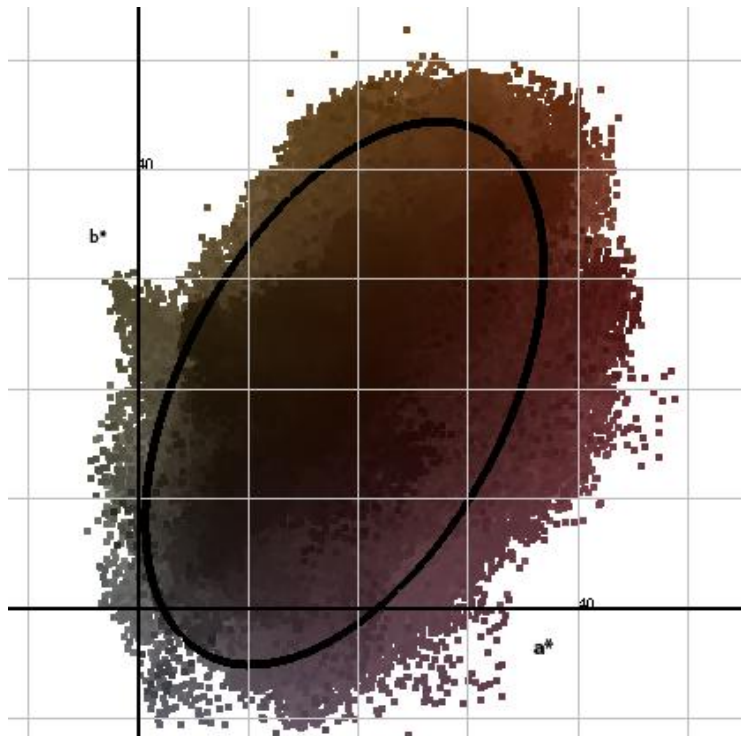
Fig. 3.6.1-1 The trained skin colour ellipse in CIELAB a*-b* coordinates

3.6.1.2 Lightness-Dependent Ellipse Model (Multi-Ellipse Model)

The centres, sizes, and orientations of 2-D chrominance ellipses of the skin colour cluster at different lightness levels are different. Training ellipses on different lightness separately should improve the skin colour modelling accuracy. To train lightness-dependent ellipses, the labelled skin colours of Halloween database were divided into many sub-sets, each containing pixels within a bin of lightness. In this study, the full range of L* from 0 to 100 was divided into 10 buckets, each occupying an L* of 10 units. The training data set was sorted into these 10 L* buckets. Ellipses in a*-b* coordinates trained for each bucket are shown in Fig. 3.6.1.2-1. Each ellipse was fitted to cover 90% of skin colours within the bucket. There is no ellipse at the bucket of L* within [0, 10]. The upper left one is for the L* bucket of [10, 20] and the last one is for L* bucket of [90, 100]. The L* bucket increases orderly from left to right and top to bottom in the figure. The skin colour centres, sizes of principal axes, and orientations of ellipses as functions of lightness are described in following sub-sections. See Appendix B for details of the training result.
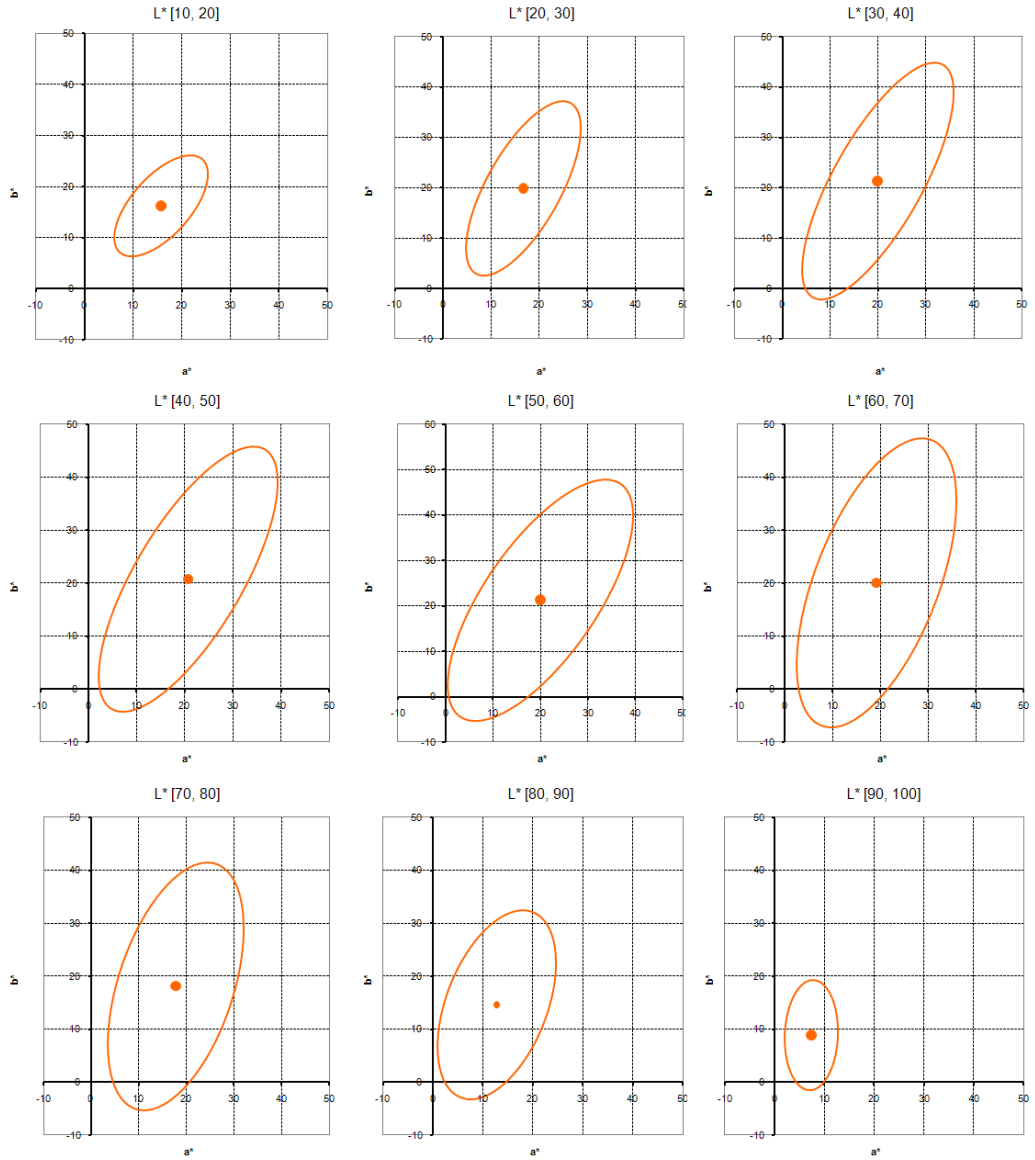
Fig. 3.6.1.2-1 Skin colour ellipses in different constant-lightness buckets

3.6.1.2.1 Skin Colour Centre

Chroma of each ellipse centre is plotted in Fig. 3.6.1.2-2. There is no data in the first bin where L* is in the range of 0 to 10. A curve to fit the trained points is plotted as well. The curve was fitted with an equation:

$$C* = -0.00004L*^3 - 0.00130L*^2 + 0.42260L* + 16.84800.$$
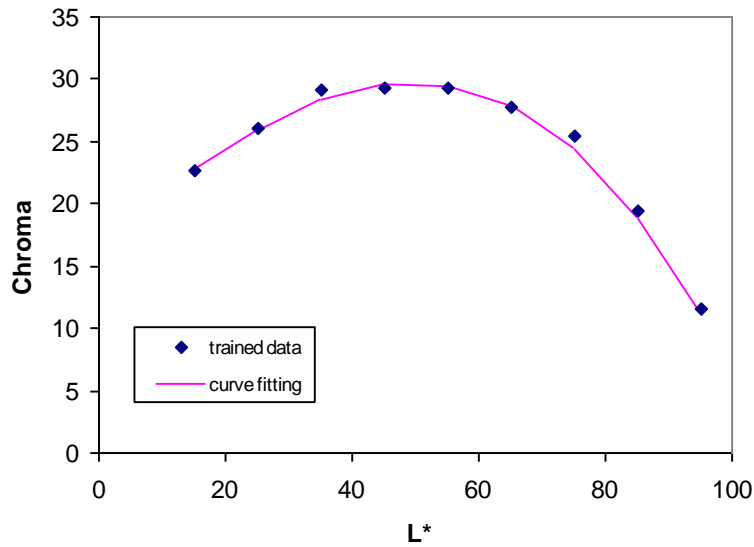
Fig. 3.6.1.2-2 Chroma of the skin colour centres
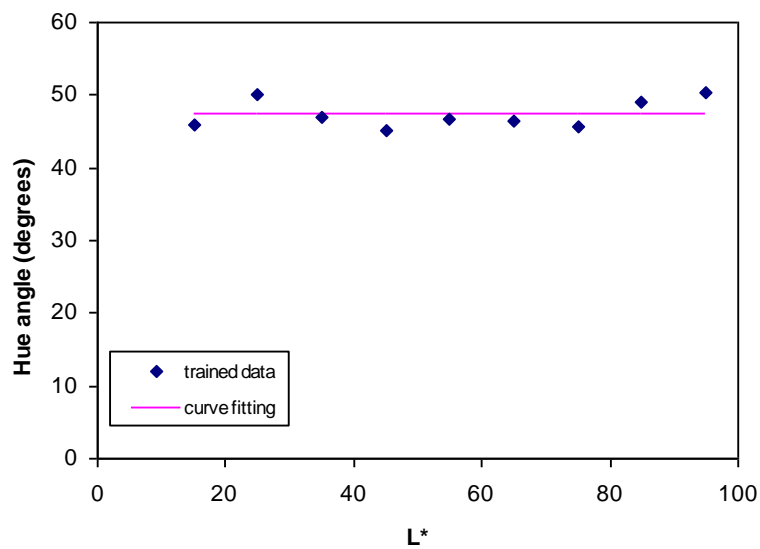
Fig. 3.6.1.2-3 Hue angles (degrees) of the skin centres

Hue angles of ellipse centres are plotted in Fig. 3.6.1.2-3. Since they are close to a constant, a line was fitted with a constant hue angle of 47.35^{o} averaged from all hue angles.

3.6.1.2.2 Orientation and Sizes of Ellipses

The orientations (θ) of the trained major axis (negative means clock-wisely rotation) are plotted in Fig. 3.6.1.2-4. The angle of the last bin for the highlight region does not follow the global trend. Since the result may be affected by lighting

and white balance, this last point was ignored from curve fitting. The orientations of the major axes were fitted with a straight line by an equation:

$$\theta = 49.00 - 0.23 \cdot L*.$$
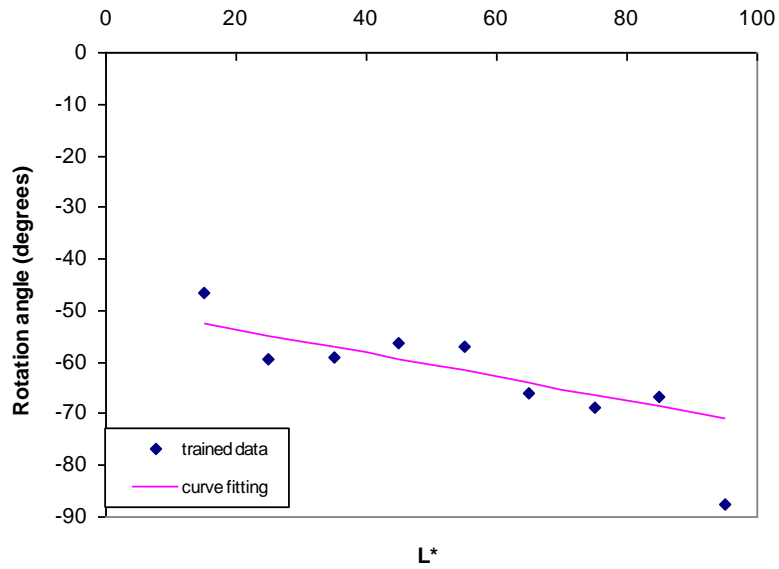
Fig. 3.6.1.2-4 Orientations of the major axes (negative means clock-wise)

The length of the trained semi-major axis in each L* level and its fitting curve are plotted in Fig. 3.6.1.2-5. $\Phi(X)$ was set to 1 ($\rho = 1$) as the skin boundary. The semi-major axes were fitted with a polynomial equation:

$$A = 4.0 \left(\frac{L*}{100} \right)^3 - 127.0 \left(\frac{L*}{100} \right)^2 + 133.3 \left(\frac{L*}{100} \right) - 5.0.$$
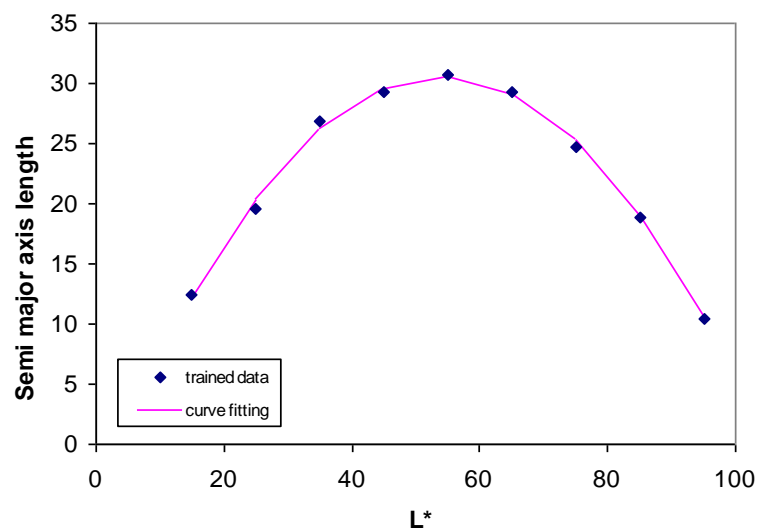
Fig. 3.6.1.2-5 Semi-major axes of skin ellipses
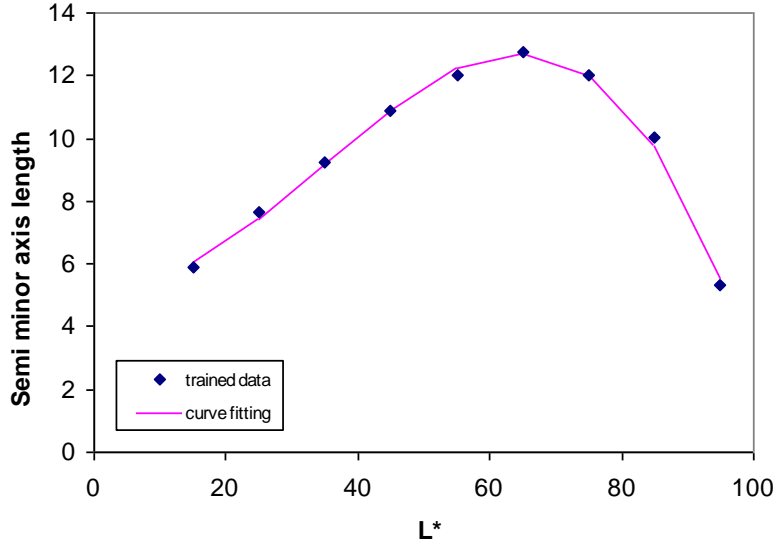
Fig. 3.6.1.2-6 Semi-minor axes of skin ellipses

The length of the trained semi-minor axis in each L* level and its fitting curve are plotted in Fig. 3.6.1.2-6. The points were fitted with a polynomial equation:

$$B = 65.5\left(\frac{L*}{100}\right)^3 + 67.7\left(\frac{L*}{100}\right)^2 - 5.3\left(\frac{L*}{100}\right) + 5.5 .$$

As shown in Figures 3.6.1.2-3 and 3.6.1.2-4, the hue angles of the centres and the hue angles of the orientations of the principal axis were fitted with smooth curves, because the physical behaviour should be smooth. More attentions were paid for fitting the mid-tone region. The curves were smoothly extended to both ends. It is suspected that the shadow region is more noisy and the highlight region are affected more by the lighting condition and the white balance, therefore the curve fitting was not attempted to fit both ends if the curve has to be bended abruptly.

3.6.1.3 An Alternative Formulation of the Ellipse Model

Based on Eq. (3.5-6), skin colours are bounded within the region of:

$$u_0(x - x_0)^2 + u_1(x - x_0)(y - y_0) + u_2(y - y_0)^2 \leq \rho \qquad (3.6-1)$$

In this study, ρ was set to 1 to train u_0, u_1, and u_2 so that ellipses covered 90% of skin colours in the database. ρ may then be reduced or increased to adjust the skin region. The trained values of u_0, u_1, and u_2 are plotted in Fig. 3.6.1.3-1. In general, each data point set is smooth in the mid-tone area and is not smooth in shadow and highlight. Again, all curves were to fit mid-tone areas accurately and to extend to both ends smoothly, and the abrupt behaviours in both ends were ignored. u_0, u_1, and u_2 were fitted with following equations:

$$u_0 = 0.005 + 0.006\left(\frac{L^* - 60}{30}\right)^2$$

$$u_1 = 0.0218\left(\frac{L^*}{100}\right)^3 - 0.0678\left(\frac{L^*}{100}\right)^2 + 0.0684\left(\frac{L^*}{100}\right) - 0.0258$$

$$u_2 = 0.0205\left(\frac{L^*}{100}\right)^3 - 0.0055\left(\frac{L^*}{100}\right)^2 - 0.0184\left(\frac{L^*}{100}\right) + 0.0108$$
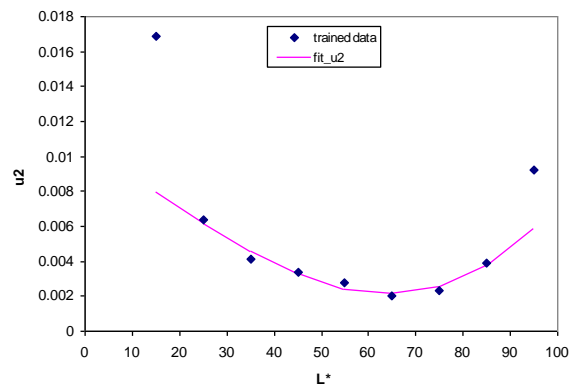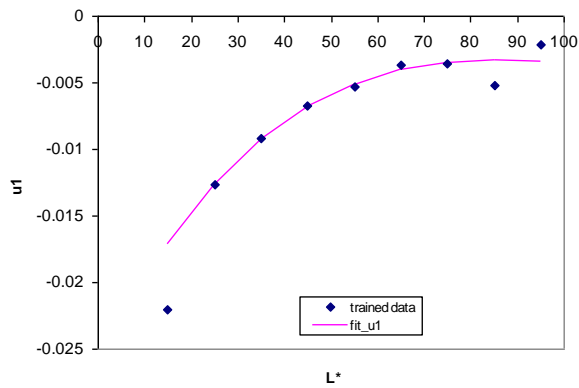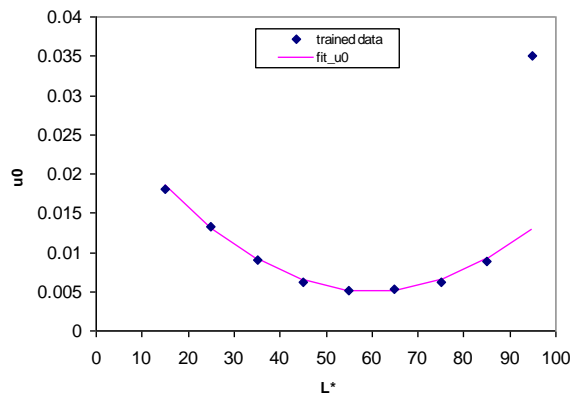
Fig. 3.6.1.3-1 u_0, u_1, and u_2 of skin colour ellipses

3.6.2 Ellipsoid Skin Colour Model

3.6.2.1 Training Ellipsoid Skin Colour Model in CIELAB Colour Space

Instead of modelling lightness-dependent ellipses, modelling an ellipsoid to fit the skin colour boundary considerably simplifies the modelling and training process. Fig. 3.6.2.1-1 shows a trained ellipsoid that covers 90% of the skin colours (black dots) in CIELAB colour space (Section 3.6.3 will discuss how to choose a proper coverage rate to achieve desired skin colour detection accuracy). It should be noted that skin colour that are not within the ellipsoid mostly have very low occurrences. The ellipsoid centre is (59, 19, 20); the principal axis parameters [A, A/B, A/C] are [38, 1.4, 2.5], where A, B, and C are semi-principal axes; and the unit vectors of three principal axes relative to the centre are (0.97, -0.14, -0.19), (0.24, 0.44, 0.87), and (0.04, 0.89, -0.46). See Appendix C for more details of the training result.
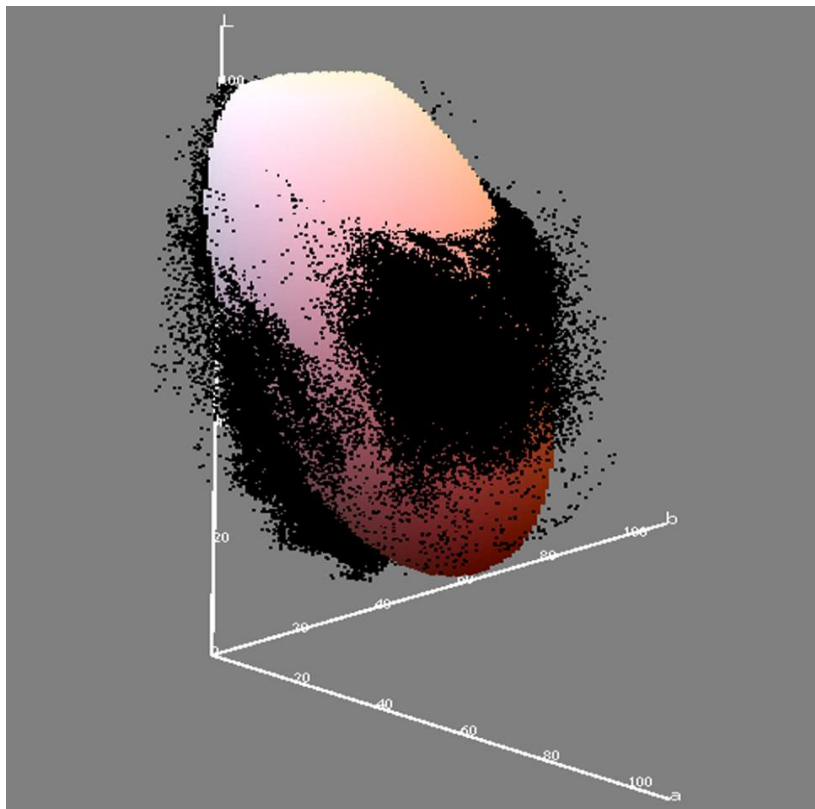
Fig. 3.6.2.1-1 An ellipsoid to cover 90% of skin colours

Constant hue-slices of the ellipsoid covering 90% of the skin colours are shown in Fig. 3.6.2.1-2. There is no ellipse at L*=15. The L* from 25 to 95 at the interval of 10 are drawn, to be compared with the ellipses modelled with the lightness-dependent ellipses shown in Fig. 3.6.1-2. The largest ellipse is at L* = 65 in both models (L*=65 in Fig. 3.5.2-2 is comparable with L* bucket of [60, 70] in Fig. 3.6.1-2). Sizes of ellipses reduce gradually as L* increases or decreases in both

models. Their orientations are very similar, and their eccentricities are similar as well.
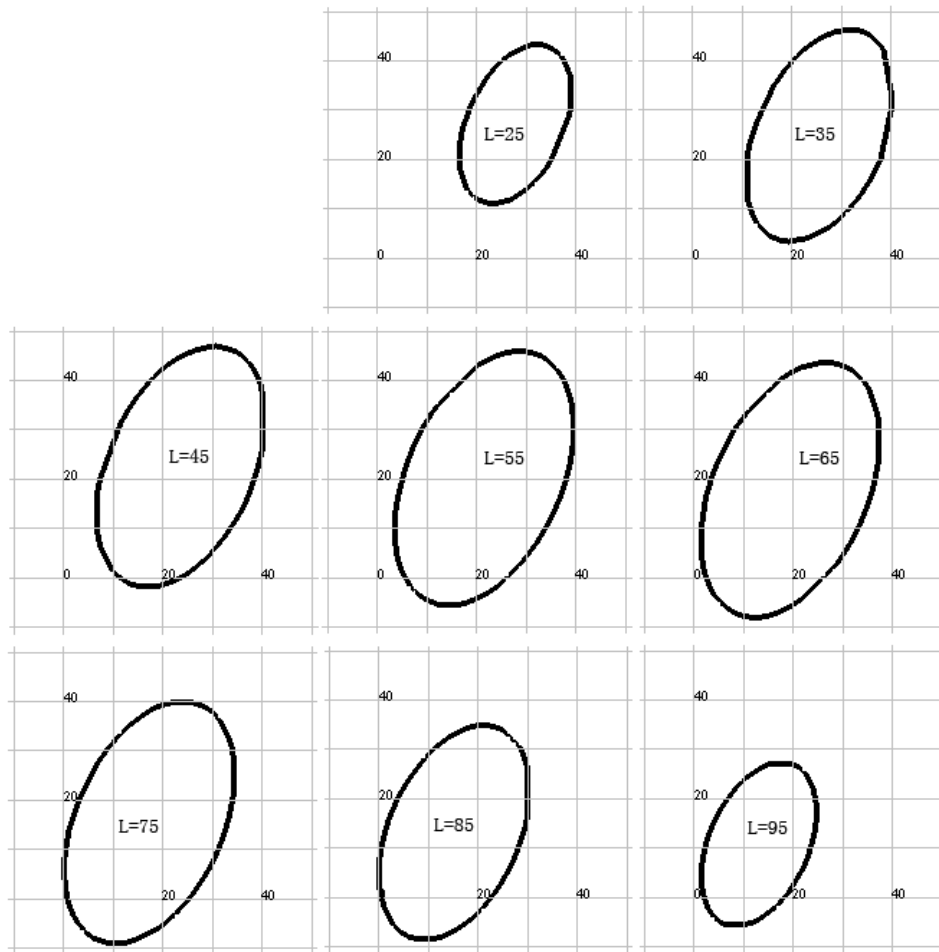
Fig. 3.6.2.1-2 Constant-lightness slices of the ellipsoid covering 90% of skin colours

3.6.2.2 Training Ellipsoid Skin Colour Model in CIECAM02-UCS

The uniform colour space modified from CIE CAM02 colour model is used to model the skin colour boundary in this section. The CIE XYZ values computed from sRGB images are transformed to the CAM02-UCS for elliptical modelling. The scene luminance is set to 500lux, and the surround viewing condition is set to average. The parameters for 90% coverage rate are:

Skin centre: (62, 13, 12);

Principal axes [A, A/B, A/C]: (38, 2.7, 3.7);

The unit vectors of three principal axes relative to the centre: (1.00, -0.07, -0.06), (-0.09, -0.56, -0.82), and (-0.02, -0.83, 0.56);

u_i (i = 0, 1, 2, 3, 4, 5): (0.00074, 0.00081, 0.00824, 0.00045, -0.00392, 0.00672), with $\Phi(X) = 1$. See Appendix D for the detailed training result.

In ellipsoid modelling, the longest axis, A, is almost parallel with the lightness axis in both CIELAB colour space and CAM02-UCS. This reveals that the longest axis primarily models the lightness dependency. The other two axes, B and C, model chroma and hue dependency. The 'eccentricity', B/C, equals 0.56 for the ellipsoid in CIELAB colour space, while $B/C = 0.73$ in CIECAM02-UCS. The B/C closer to unity in CAM02-UCS implies that the distribution of skin colours in CAM02-UCS is slightly more uniform than in CIELAB colour space.

3.6.3 Comparing Skin Colour Detection Accuracy among Three Models

Fig. 3.6.3-1 shows an example of skin colour detection using different skin colour models. Detected skin colours are marked with pink. The results look similar. It is very difficult to find the differences in skin colour detection accuracies visually.
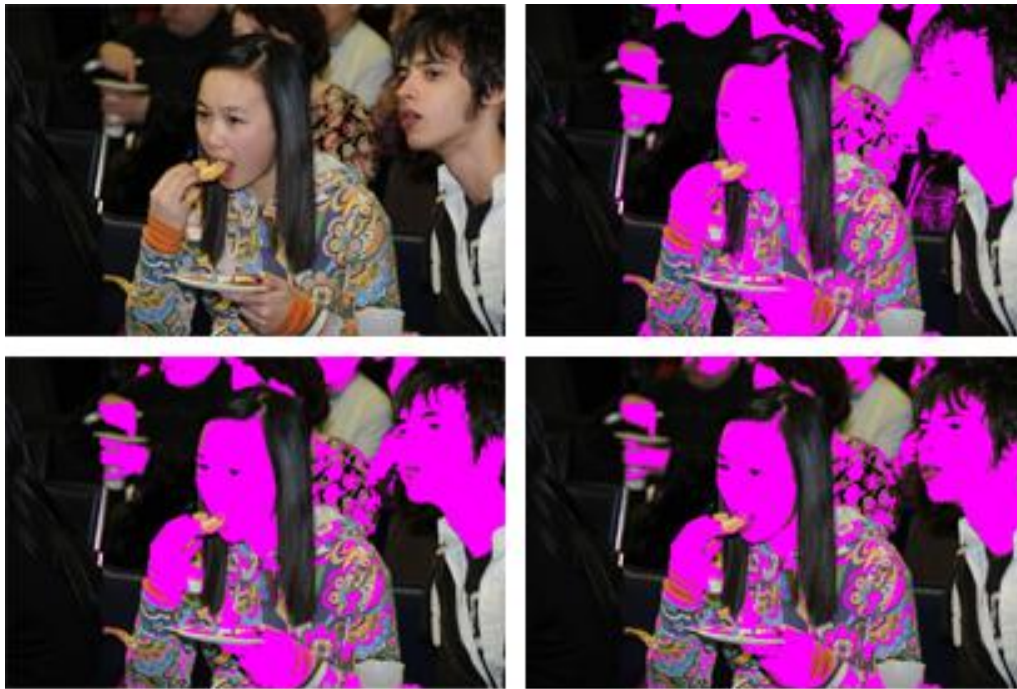
Fig. 3.6.3-1 Skin colour detection using different models: original (upper-left), skin colour detection using an ellipse model (upper-right), a lightness-dependent ellipse model (lower-left), and an ellipsoid model (lower-right)

The skin colour detection accuracy of a skin model is typically evaluated using True Positive detection rates (TP) and False Positive detection rates (FP). TP is the ratio of the number of skin pixels detected as skin pixels over the total skin pixels. FP is the ratio of the number of non-skin pixels detected as skin pixels over the total non-skin pixels. Increasing TP typically forces to increase FP as well. In other words, to increase the likelihood that a true skin pixel is detected as a skin pixel, a non-skin pixel is more likely to be falsely detected as a skin pixel. Optimizing a skin detector is to achieve a TP as high as possible for a given FP. The relationship

between TP and FP is plotted with a curve, the Receiver Operating Characteristics (ROC) curve. The curve is very useful for determining a proper skin detection threshold with the trade-off between TP and FP.

To verify detection rates on an image, all skin pixels of the image must be labelled. Since the Halloween image database used for skin colour modelling do not have all skin pixels labelled, it cannot be used to compute skin detection rates. A different image database that consists of 106 images was constructed to analyse the skin colour detection accuracy of the three elliptical models. Fig. 3.6.3.2 shows a few examples and their corresponding manual labelled skin masks. These images cover different skin types and different capturing conditions. The skin pixels of each image were labelled manually using Photoshop. Each skin colour model was applied to original images to detect skin colours, and the corresponding labelled images were applied to verify whether the skin detection for each pixel is correct. TP and FP were computed using all tested images.

Fig. 3.6.3-2 Selected images for analysing skin colour detection accuracy

By changing ρ of a skin model, a set of FP versus TP was obtained. Fig. 3.6.3-3 shows the ROC curves of the three elliptical models. It depicts that increasing TP is at the cost of increasing FP. The figure shows that Single-Ellipse Model (lightness-independent model) has the lowest detection accuracy in general, and Multi-Ellipse Model (lightness-dependent skin model) has slightly higher detection accuracy than Ellipsoid Model. Because a fixed ellipse is applied to cover skin colours in different lightness levels in Single-Ellipse Model, in order to reach the same TP as the other two models do, it must cover larger portion of dark colours and highlight colours that are not skin colours and therefore its FP is higher. As FP reaches to a very high value, the TP differences among three models diminish. It demonstrates that if high FP is acceptable, optimizing a skin colour models is not critical; instead, choosing a skin colour model with high computation efficiency and low hardware cost may be more important.
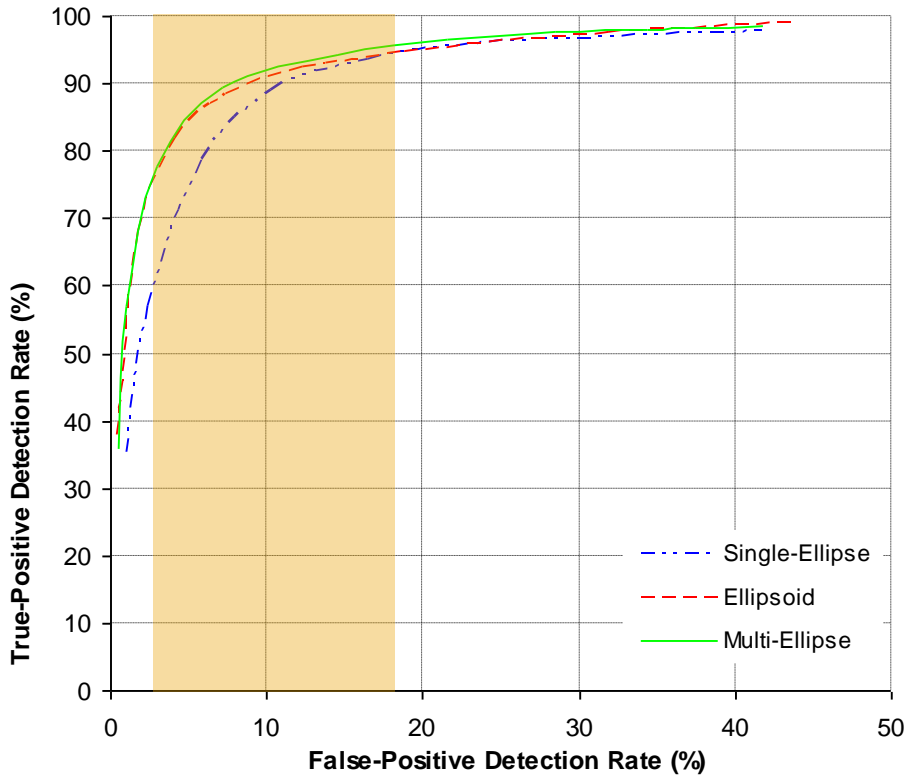
Fig. 3.6.3-3 ROC curves of three skin elliptical models

Tuning a skin detection algorithm to have a very low FP, and therefore a very low TP is practically useless. On the other hand, tuning a skin detection algorithm to have a very high TP, and therefore a very high FP is practically useless, too. A practical range is marked in yellow in Fig. 3.6.3-3. In this area, the single-ellipse model is most inaccurate and the multi-ellipse model is most accurate in skin colour detection.

Since Multi-Ellipse Model is trained in each lightness level, it should theoretically achieve higher detection accuracy than Ellipsoid Model. It is surprising that the detection accuracy of Ellipsoid Model is so close to that of the Multi-Ellipse Model, as shown in Fig. 3.6.3-3. Because the majority of test images have mid-tone skin colours, the total number of dark and light skin pixels is much smaller than the number of mid-tone skin pixels, and therefore the contribution of the detection accuracy of dark and light skin pixels may be negligible. If both models were well optimized for mid-tone skin colours, the differences of detection accuracies in light-tone and dark-tone may have little influence on the overall detection accuracy. Ellipsoid Model fits skin clouds well for mid-tone but fits not so well for light-tone and dark-tone, while Multi-Ellipse should well fit skin colour clouds for every lightness level. To verify the hypothesis, seven dark skin images from the 106 images were chosen to compute detection rates of the three models.

Their ROC curves are plotted in Fig. 3.6.3-4. The result that the difference of the detection rates between Ellipsoid Model and Multi-Ellipse Model is larger in this case than that using all images was expected. Because Multi-Ellipse Model was trained on each lightness bucket, its detection accuracy is the highest. Since the skin colour boundary parameter of Single-Ellipse Model, ρ, is adjusted to fit dark skin colours of test images, its detection accuracy is close to that of Multi-Ellipse Model.
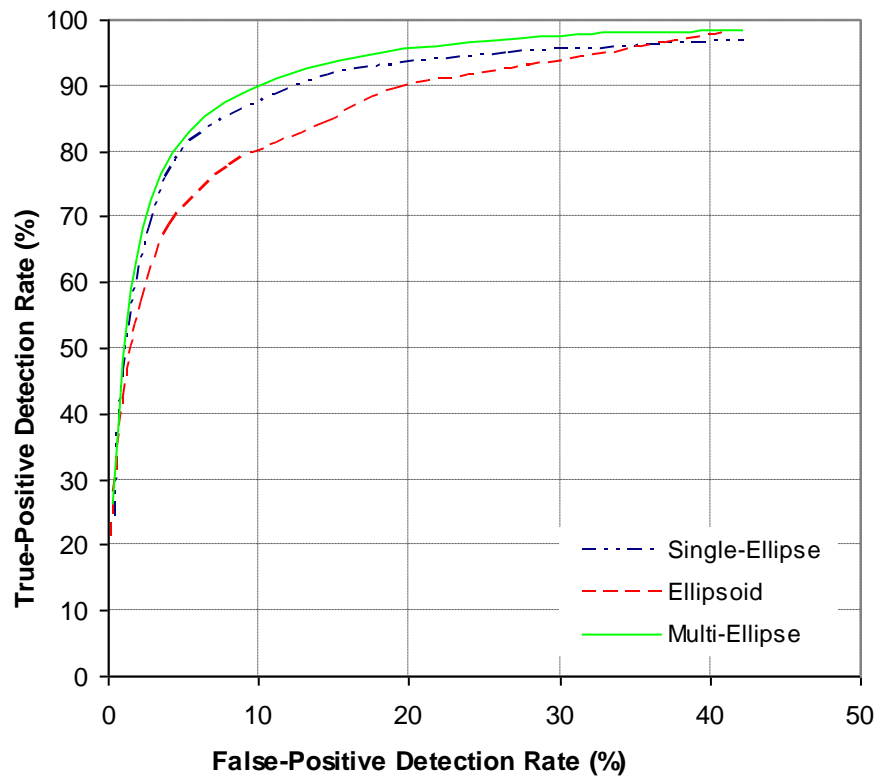
Fig. 3.6.3-4 ROC curves of three elliptical skin models tested on dark skin images

3.6.4 A Few Factors that Affect Training Results

Knowing how different factors influence training results of the elliptical modelling will be helpful for training models accurately and evaluating models confidently. Three important factors that will be evaluated in this section are skin types, image database, and colour space.

3.6.4.1 Skin Colour Modelling of Different Skin Types

The RPS database includes three sub-sets: a Caucasian set composed of 302 Caucasian images, an Oriental set composed of 285 Oriental images, and an African set composed of 28 African images. Each set was used to train a lightness-independent skin model and an ellipsoid model for each skin type. A comparison of the three ellipses is shown in Fig. 3.6.4.1-1. Although the Caucasian skin colour

region is shifted slightly toward less chromatic and less yellowish colour region, the Caucasian skin colour region and the Oriental skin colour region are very similar. The African skin colour region has a higher mean chroma, a larger chroma variation, and a smaller hue variation. Its hue range is within those of the other two.
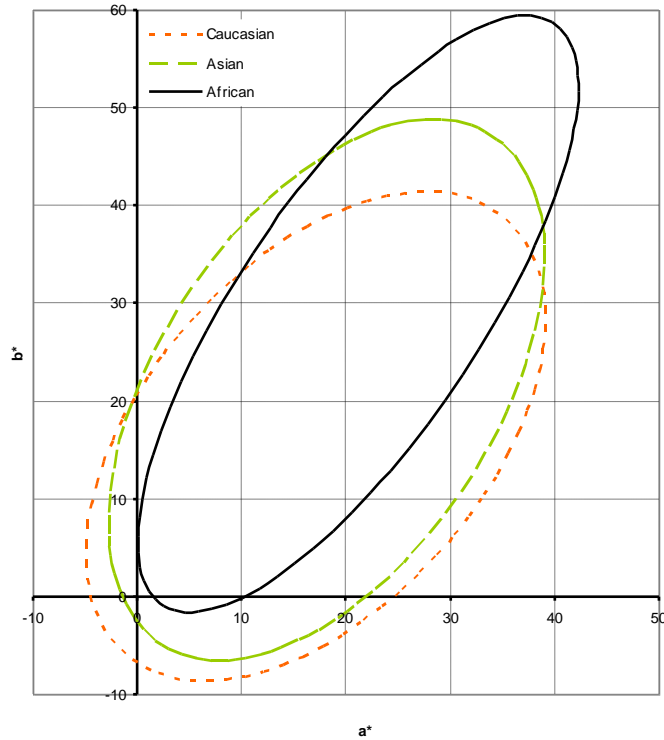
Fig. 3.6.4.1-1 Caucasian, Oriental, and African skin ellipses in CIELAB a*-b* coordinates

The centre coordinates, together with the semi-major axis (A), the 'eccentricity' (A/B), and the orientation of the major axis (θ) (negative θ means counter-clockwise rotation) of three ellipses are listed in Tables 3.6.4.1-1 and 3.6.4.1-2. 95% skin coverage rate was used for all three skin types.

Table 3.6.4.1-1 A comparison of ellipse coefficients of three different skin types

	Skin centre	A	A/B	θ
Caucasian	(17, 16)	29	1.7	-52°
Asian	(18, 21)	31	1.9	-60°
African	(21, 29)	35	3.0	-58°

Table 3.6.4.1-2 Covariance coefficients u_i (i = 1, 2, and 3)

	u_0	u_1	u_2
Caucasian	0.00268462	-0.00227808	0.00207791
Asian	0.00302517	-0.00225233	0.00172195
African	0.005373	-0.00567292	0.00257024
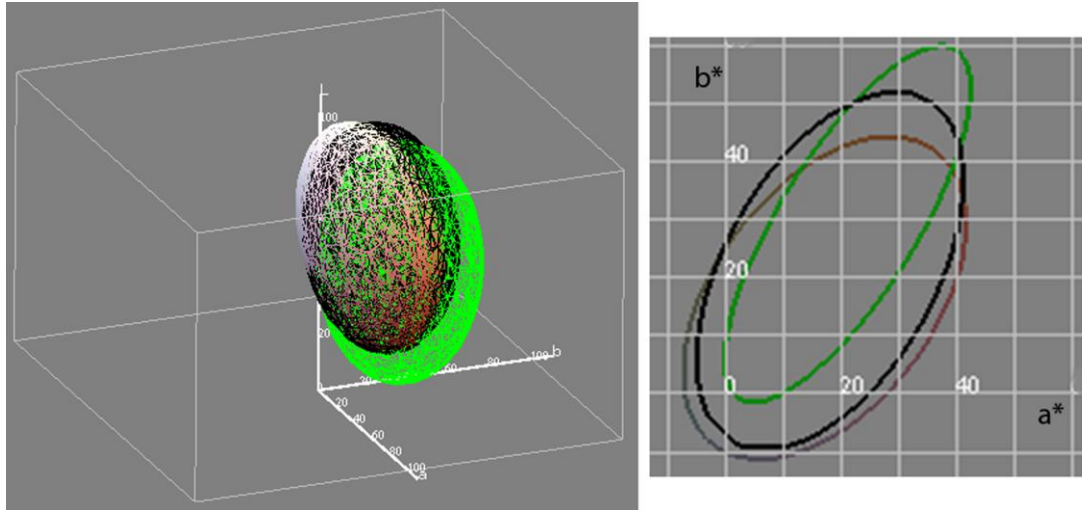
Fig. 3.6.4.1-2 Caucasian (colour), Oriental (black), and African (green) skin colour ellipsoids in CIELAB colour space (left) and their projection in a*-b* coordinates (right)

An ellipsoid was trained for each skin type to cover 95% skin colours. Fig. 3.6.4.1-2 shows a side by side comparison of Caucasian, Oriental, and African skin colour ellipsoids in CIELAB colour space and their projection on a*-b* coordinates. The lightness ranges of Caucasian and Oriental skin colours are about the same, while the African skin colour region is slightly darker than the other two. Regardless the lightness coordinate, the result is consistent with the 2-D ellipse modelling. The Oriental skin colour region is slightly more yellowish and slightly more chromatic than the Caucasian skin colours, and the African skin colour region is more chromatic than the other two skin colour types.

The coefficients of Caucasian ellipsoid:

Centre: (61, 17, 16)

Principal axis parameters [A, A/B, A/C]: [43, 1.4, 2.3]

Unit vectors of three principal axes relative to the centre:

(0.93, -0.24, -0.28)

(-0.37, -0.55, -0.75)

(-0.03, -0.80, 0.60)

$$\text{Matrix } \Lambda: \begin{bmatrix} 1724.7 & -218.5 & -235.8 \\ -218.5 & 627.0 & 343.7 \\ -235.8 & 343.7 & 810.1 \end{bmatrix}$$

u_i (i = 0, 1, 2, 3, 4, 5) for $\Phi(X)$ = 1: (0.00061, 0.00030, 0.00212, 0.00023, -0.00171, 0.00163)

The coefficients of Asian ellipsoid:

Centre: (60, 18, 21)

Principal axis parameters [A, A/B, A/C]: [42, 1.2, 2.3]

Unit vectors of three principal axes relative to the centre:

(0.98, -0.17, -0.11)

(0.18, 0.48, 0.86)

(0.09, 0.86, -0.50)

$$\text{Matrix } \Lambda: \begin{bmatrix} 1753.2 & -169.5 & -27.4 \\ -169.5 & 549.8 & 359.6 \\ -27.4 & 359.6 & 965.9 \end{bmatrix}$$

u_i (i = 0, 1, 2, 3, 4, 5) for $\Phi(X)$ = 1: (0.00059, 0.00045, 0.00249, -0.00013, -0.00184, 0.00138)

The coefficients of African ellipsoid:

Centre: (50, 21, 29)

Principal axis parameters [A, A/B, A/C]: [45, 1.2, 3.7]

Unit vectors of three principal axes relative to the centre:

(1.00, 0.03, 0.08)

(-0.09, 0.54, 0.84)

(0.03, 0.84, -0.55)

$$\text{Matrix } \Lambda: \begin{bmatrix} 2021.8 & -2.4 & 69.3 \\ -2.4 & 478.1 & 527.6 \\ 69.3 & 527.6 & 999.4 \end{bmatrix}$$

u_i (i = 0, 1, 2, 3, 4, 5) for $\Phi(X)$ = 1: (0.00050, 0.00019, 0.00503, -0.00017, -0.00532, 0.00241)

3.6.4.2 Training with Different Image Databases

To study how training results of modelling parameters influenced by different image databases, the lightness-independent ellipse trained earlier using the Halloween database was compared with the result trained using the RPS database. In Fig. 3.6.4.2-1, the Halloween ellipse and the RPS ellipse were trained using the same configuration parameters. The centres of two ellipses are almost the same (the circular orange dot is the centre of the RPS ellipse and the square green dot is the centre of the Halloween ellipse); the eccentricities of two ellipses are very close; and the orientations of two ellipses are about the same. However, the ellipse trained using the RPS database is larger. This is the result that the other person labelled skin pixels more aggressively. By controlling the threshold value, ρ, the size of an ellipse can be increased or decreased proportionally. With $\rho = 1.25$, the Halloween ellipse is expanded to Adjusted-Halloween ellipse which is very close to the RPS ellipse. The result demonstrates that the results trained using these two different databases are very consistent, and the training result is independent of skin colour labelling by different persons.
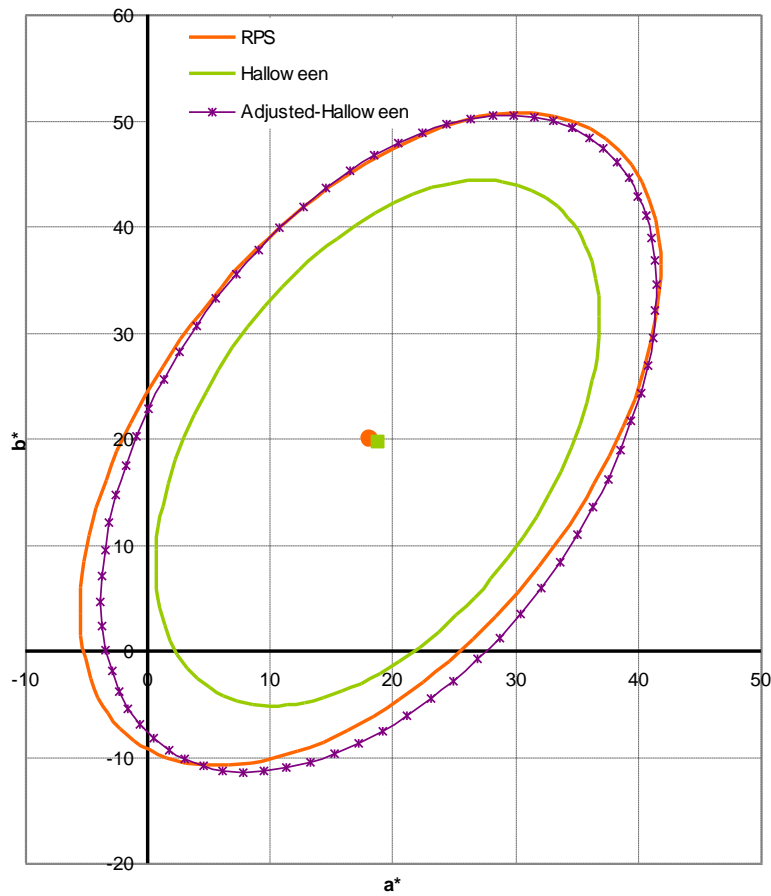
Fig. 3.6.4.2-1 Skin colour ellipses trained using two different databases

3.6.4.3 Skin Colour Modelling under Different Colour Spaces

Various colour spaces (e.g. RGB, r-g, YC_bC_r, HSV/HIS/HSL, YUV, YIQ, L*u*v*, L*a*b*, etc.) have been used to define skin colour gamut for skin colour detection, face detection, or skin colour enhancement. Zarit et al. investigated five colour spaces (L*a*b*, Fleck HS, HSV, r-g, and YC_rC_b) for skin detection. Their result shows that the goodness of a skin model depends on the colour space used. Albio et al. theoretically proved that "separability of the skin and no skin is independent of the colour space chosen". This disagrees with practical implementations. Shin et al. evaluated skin detection using RGB colour space and other eight colour spaces: normalised RGB, CIE XYZ, CIE L*a*b*, HIS, SCT, YC_rC_b, YIQ, and YUV, and concluded that the RGB colour space provided the best separability between skin and non-skin. This result may only confirm that Shin's skin detection method works best in RGB colour space.

In summary, an RGB colour space may be more suitable for histogram based models, for an RGB LUT to store the trained skin colours can be used directly to process RGB pixels without additional colour transformation. Using a luminance-chrominance colour space for skin colour detection reduces the interaction between luminance and chrominance, therefore simplifies the process. Ignoring the dependency on luminance (or lightness), skin colour detection using chrominance (e.g. rg, C_bC_r, a*b*, or u*v*) further simplifies the process and improves the efficiency. However, the detection rate may be compromised.

The present study is aimed for the preferred colour enhancement of digital images. Although CIELAB colour space, a profile connection colour space in ICC colour management, was chosen for the workflow, a more uniform colour space, CAM02 uniform colour space (UCS) has been in our consideration. Therefore, the skin colour modelling in CIELAB and CAM02-UCS were studied.

Since CAM02-UCS is more uniform than CIELAB colour space, the skin colour boundary of an elliptical model in CAM02-UCS may be closer to circular than in CIELAB colour space. To verify whether this is true, skin ellipsoids trained in CIELAB and CAM02-UCS were compared. As discussed in Section 3.6.2, the ellipsoid modelling result shows that the longest axis is almost parallel with the lightness axis in both CIELAB colour space and CAM02-UCS. This implies that the longest axis primarily models the lightness dependency. The other two axes, B and C, primarily model chrominance dependency. The ratio of these two axes, B/C, can be viewed as the eccentricity of an ellipse that an ellipsoid projected on the chromaticity axes. $B/C = 1$ means that the ellipse is a circle. B/C is 0.56 for the ellipsoid in CIELAB colour space and is 0.73 for the ellipsoid in CAM02-UCS. The

B/*C* closer to unity in CAM02-UCS evinces that the distribution of skin colours in CAM02-UCS is slightly more uniform than in CIELAB colour space.

Skin colour detection accuracies in CIELAB and CAM02-UCS were compared as well. The ROC curves of the ellipsoid modelling in CIELAB and CAM02-USC were generated using the database described earlier in Section 3.6.3 to study skin detection accuracy. The results plotted in Fig. 3.6.4.3-1 illustrates that the skin detection accuracy in CIECAM02-UCS is higher than that in CIELAB colour space. Improved uniformity of skin colours in CAM02-UCS may be the reason that the skin detection accuracy is more accurate in this colour space.
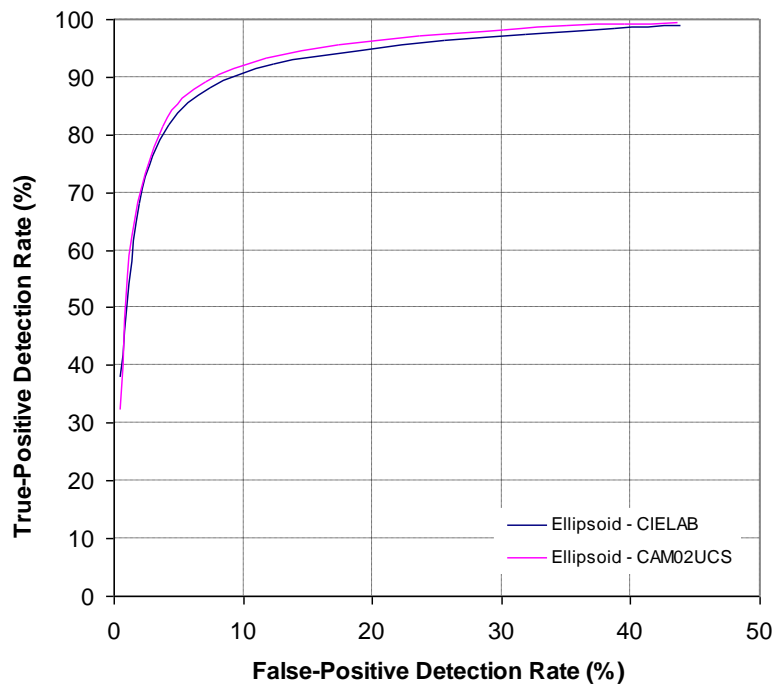
Fig. 3.6.4.3-1 ROC curves of the ellipsoid modelling in CIELAB and CAM02-UCS colour spaces

3.6.5 Conclusion of Elliptical Modelling of Skin Colours of Digital Photographic Images

Skin colour distributions were estimated using three elliptical models. Modelling skin colours with a single ellipse is simple in training, and is efficient in computation. To cover high chroma skin colours in the mid-tone region, a large enough ellipse must be determined, although smaller ellipses better fit light skin colours and dark skin colours. To improve the skin colour detection accuracy, a lightness-dependent ellipse model was developed to adjust skin colour ellipses that fit skin colours in different lightness. However, formulating lightness-dependent ellipses is complex, and computing skin colour boundary is less efficient. A third

model, an ellipsoid skin colour model, is a compromise among modelling complexity, computation efficiency, and detection accuracy. Unlike the single-ellipse model, it adapts skin gamut boundary to different lightness. Although the gamut adaptation to different lightness is not as accurate as that in the lightness-dependent ellipse model, the ellipsoid modelling is simpler to train and more efficient in computation.

The consistent results of skin colour ellipses trained with two different databases verify that the method to construct databases is reliable for skin colour modelling. A separate training of Caucasian, Oriental, and African skin colours reveals that the Caucasian skin colour gamut and the Oriental skin colour gamut are very similar; the Oriental skin colours are slightly more yellowish and slightly more chromatic than the Caucasian skin colours; the lightness ranges of the Caucasian and Oriental skin colours are about the same. Comparing to the Caucasian and Oriental skin regions, the African skin colour region is slightly darker, its centre is more chromatic, its chroma variation is higher, and its hue range is within those of the other two skin regions. The result of the skin colour ellipsoids trained in CIELAB and CAM02-UCS colour spaces reveals that CAM02-UCS is slightly more uniform in the skin colour area. With ellipsoid modelling, the skin colour detection accuracy in CAM02-UCS is slightly higher than that in CIELAB colour space.

3.7 Training Results of Skin Colour Modelling of Colorimetric Skin Colours

The RIT and Oulu spectral data sets of skin colours were used to model skin colorimetric colour boundary.

RIT Data Set: The lighting system included two lighting heads (Scanlite Digital 1000, Elinchrom) with halogen Photo Optic lamps (FEF/1000W, 120V). A Photo Research Spectroradiometer, SpectraScan 704, was used for spectral measurement. The measurement system was calibrated using a high quality white reference, a barium sulphate coated paper which was spectrally flat and uniform. The distance from PR-704 to the subject was about 1.6m. 11 female and 23 male subjects with ages ranging from 18 to 40 participated in the experiment. The subjects included five culture backgrounds, 11 Pacific-Asian subjects, 8 Caucasian subjects, 7 Black subjects, 6 subcontinental Asian subjects, and 2 Hispanic subjects.

Oulu Data Set: A hand-held, contact spectrophotometer Minolta CM-2002 was used to measure skin spectral reflectance. For each person, there were measurements of diffusely reflected light (the surface or specular component excluded) on the skin at the wavelength range of 400nm to 700nm by 10nm steps.

For a group of 20 persons, the skin was also measured with a specular component included as an option which takes into account specularly reflected light at the same wavelength range. The measurement positions on the face were the forehead, left cheek, and right cheek, and each result was obtained as an average of three measurements. The illuminant SPDs were obtained from their definitions (confirmed by spectroradiometric measurement).

There were total of 697 measurements (340 from RIT and the rest from Oulu), covering Caucasian, Hispanic, and Asian skin colours. Both databases can be downloaded from http://mcsl.rit.edu/. The spectral data were converted to CIEXYZ in D65 illuminant. The colours in CIEXYZ colour space were adapted to D50 with the Bradford chromatic adaptation transformation. The XYZ data were then converted to CIELAB colour space for modelling in CIELAB colour space, or converted to CAM02-UCS colour space for modelling in the uniform colour space. The reason to adapt colours to D50 is to be consistent with the colour transformation of digital images using ICC colour management workflow.

To model the skin colour boundary, the RIT and Oulu skin colour cluster is drawn in CIELAB colour space for visual check (see Figs. 3.7-1 and 3.7-2). Since both data sets occupy about the same region, no separate analysis was tried. Instead, both data sets were merged to a single set for skin colour modelling. The skin colour cluster takes up much smaller space than that of the image database, because of strict measurement conditions and no illuminant mismatch exists. The figure shows that skin chroma maximizes at about 55 L* units, and gradually reduces as lightness increases or decreases.
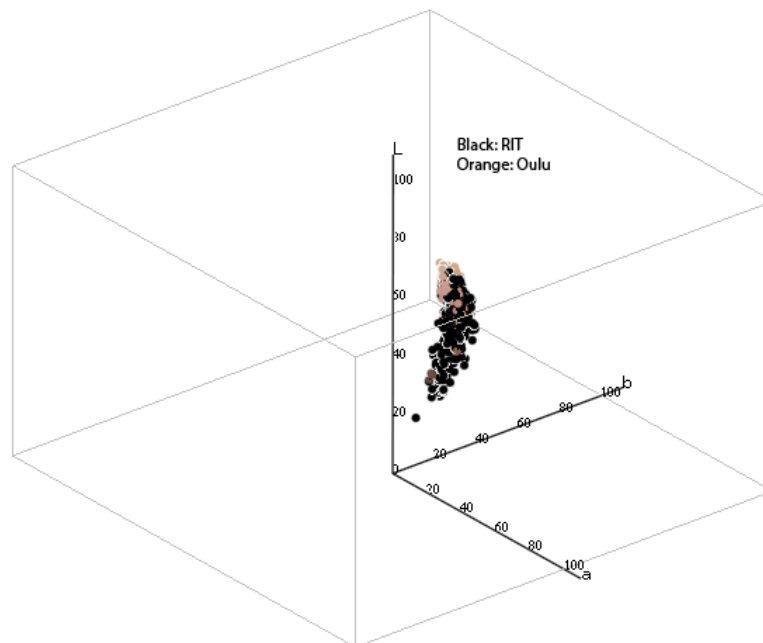
Fig. 3.7-1 The RIT and Oulu skin colour data in L*a*b* colour space
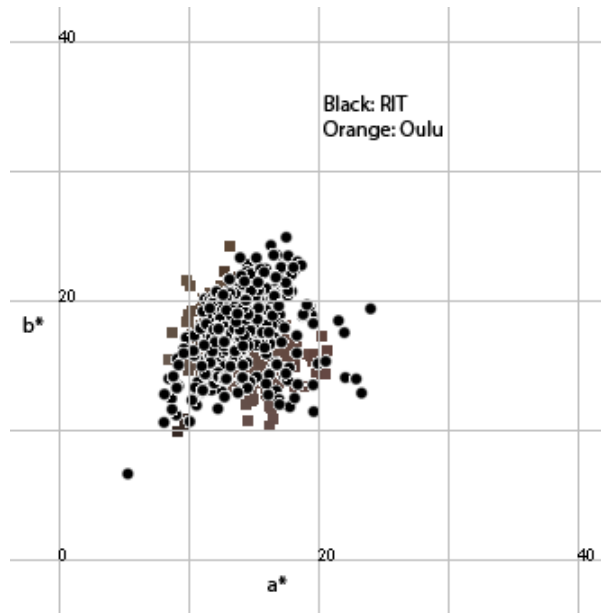
Fig. 3.7-2 The RIT and Oulu skin colour data in a*-b* coordinates

3.7.1 Ellipse Modelling in CIE a*b* Colour Space

Modelling an ellipse in CIELAB a*-b* coordinates (adapted to D50 illuminant) with 95% coverage rate, the colour centre is (14.0, 17.1), together with the ellipse parameters [A, A/B, θ] of [7.1, 1.1, -63°] (negative-degree means counter-clockwise rotation). See Appendix E for the detailed training result. In Fig. 3.7.1-1, the black circles are from the RIT skin colour data set, and the cyan crosses are from the Oulu skin colour data set.
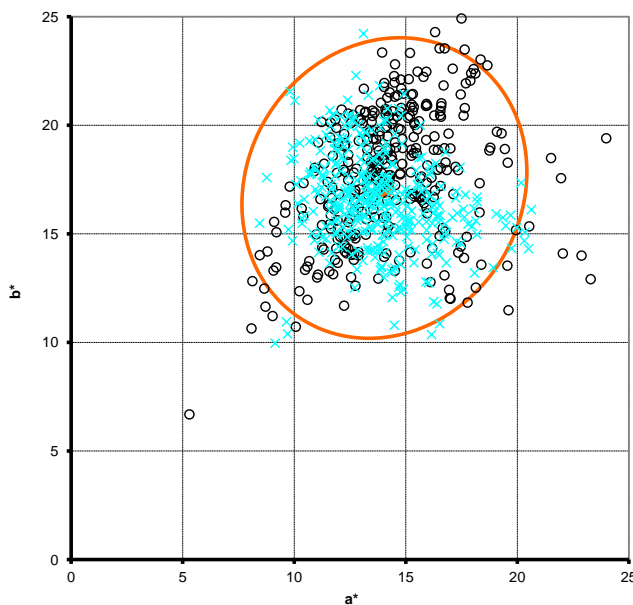
Fig. 3.7.1-1 An ellipse to cover 95% of colorimetric skin colours in CIE a*b* coordinates ('o' – RIT data, 'x' – Oulu data)

3.7.2 Ellipse Modelling in CAM02-UCS

The CIE XYZ values computed using D65 illuminant were converted to the CAM02-UCS colour space. The ambient illuminant was set to 1000 lux (318.3 cd/m^2), and the average surround viewing condition was applied.

The ellipse with 95% skin colour coverage rates is shown in Fig. 3.7.2-1. Again, the black dots are from RIT skin colour data set, and the cyan crosses are from Oulu skin colour data set. The colour centre is (9.5, 5.1), together with the ellipse parameters [A, A/B, θ] of [5.4, 1.2, 72°] (positive-degree means clockwise rotation). See Appendix F for the detailed training result.
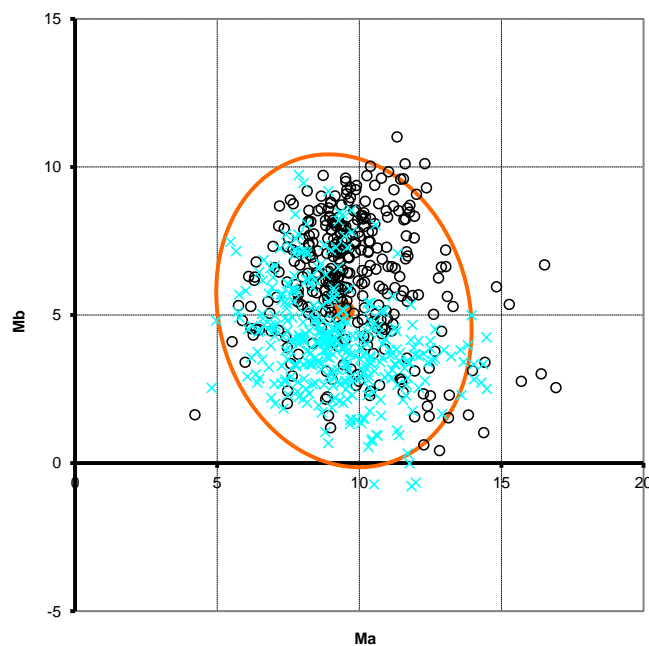
Fig. 3.7.2-1 An ellipse to cover 95% colorimetric skin colour in CAM02-UCS ('o' − RIT data, 'x' − Oulu data)

3.7.3 Ellipsoid Modelling in CIELAB Colour Space

Fig. 3.7.3-1 shows the ellipsoid modelling in CIE L*a*b* colour space (D50) with 100% (skin colours), 99% (green), and 95% (pink) skin colour coverage rates. Skin colours for modelling are shown together for comparison. The ellipsoid with 99% coverage rate covers samples very well. Except for a dark skin colour that is far away from the ellipsoid (this point might be a colour measured incorrectly), all other skin colours are either within the ellipsoid or are close to the boundary. To encompass the darkest colour sample, an ellipsoid must be expanded significantly (see the ellipsoid with 100% coverage rate). The ellipsoid with 95% coverage rate misses to cover most of dark skin colours.
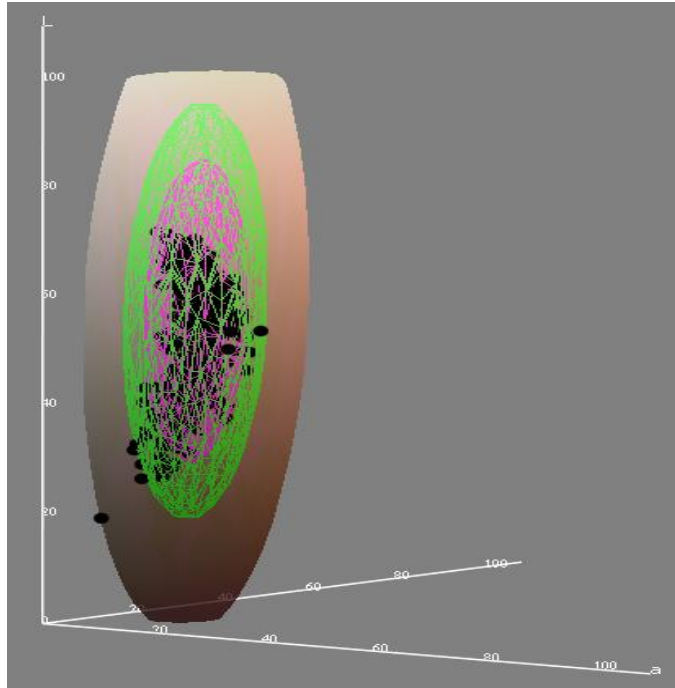
Fig. 3.7.3-1 Skin colour ellipsoids with 100% (skin colours), 99% (green), and 95% (pink) coverage rates in CIELAB colour space

The parameters for 99% coverage rate are:

Colour centre: (57, 14, 17);

Principal axis coefficients [A, A/B, A/C]: (38.7, 3.52, 4.27);

The unit vectors of three principal axes relative to the centre: (1.00, 0.05, -0.01), (0.02, -0.43, -0.90), and (0.04, -0.90, 0.43);

$$\text{Matrix } \Lambda: \begin{bmatrix} 1499.3 & 62.1 & -3.4 \\ 62.1 & 89.8 & 10.6 \\ -3.4 & 10.6 & 105.5 \end{bmatrix};$$

u_i (i = 0, 1, 2, 3, 4, 5): (0.00069, -0.00097, 0.011612, 0.000141, -0.002356, 0.009602), with $\Phi(X) = 1$.

3.7.4 Ellipsoid Modelling in CAM02-UCS

The setting parameters for CAM02-UCS are the same as those in Section 3.6.2. Ellipsoids with 100% (skin colours), 99% (green), and 95% (pink) skin colour coverage rates are shown Fig. 3.7.4-1. The black dots are the skin sample colours for modelling. Again, it shows that an ellipsoid must be enlarged significantly to cover the darkest sample colour. For the ellipsoid with 99% coverage rate, every sample skin colour is either encompassed by the ellipsoid or is very close to the boundary of the ellipsoid. The ellipsoid with 95% coverage rate misses to encompass many dark skin colours.
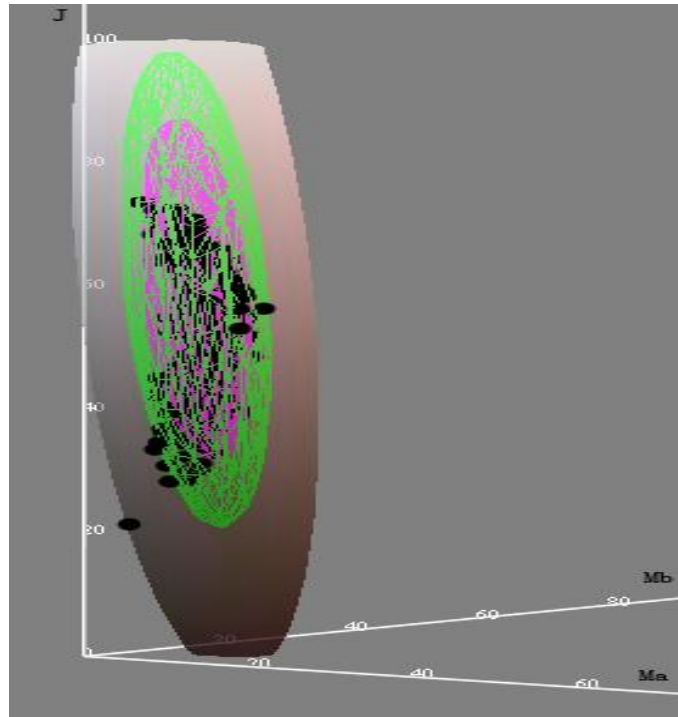
Fig. 3.7.4-1 Skin ellipsoids with 100% (skin colours), 99% (green), and 95% (pink) coverage rates in CAM02-UCS colour space

The parameters for 99% coverage rate are:

Colour centre: (60.1, 9.5, 5.1);

Principal axis coefficients [A, A/B, A/C]: (39.9, 4.64, 5.85);

The unit vectors of three principal axes relative to the centre: (-0.99, -0.01, 0.11), (-0.09, 0.67, -0.73), (0.07, 0.74, 0.67). See Appendix G for detailed training result.

3.7.5 Summary of the Elliptical Modelling of Colorimetric Skin Colours

The RIT and Oulu skin colour data sets were used to model skin ellipses in CIELAB colour space and CAM02-UCS. Ellipses modelled in both colour spaces are close to circles, for both are uniform colour spaces. In CIEXYZ colour space, the skin colours cluster is a thin and long strip, implying a fitting ellipse would be thin and long, which is not ideal for colour adjustment.

An ellipsoid may be used to model skin colour boundary in 3-D colour space. An ellipsoid encompassing 99% of colour samples covers the skin cloud reasonably well. The fact that the principal axis is very close to parallel to the lightness axis and is very long reveals that the axis mainly models the large lightness variation of different skin colours. The other two axes mostly determine chromatic extents. The 99% coverage rate was used to compute the ratio of the lengths of the two shorter axes to analyse the uniformity of the chroma axes. The ratio in CAM02-UCS is

slightly closer to unity than that in CIELAB colour space, but the difference between the two is very small.

3.8 Summary of Skin Colour Modelling

Different image databases were created from a collection of rendered (output-referred) images, and were used for skin colour modelling of digital photographic images. During the colour rendering from the scene-referred state to the output-referred (display-referred) state, the contrast and chroma are typical boosted. Combining with other factors, such as under-exposure or over-exposure, and illuminant detection inaccuracy, the skin colour gamut is increased considerably compared with the colorimetric gamut of skin colours.

While the colorimetric skin colour gamut may be used for skin/face detection and illuminant detection for scene-referred images, the rendered skin colour gamut generated from output-referred digital images may be used for skin/face detection and preferred skin colour reproduction of general digital photographic images.

Three elliptical skin colour models: Single-Ellipse Model (Lightness-Independent Ellipse Model), Multiple-Ellipse Model (Lightness-Dependent Ellipse Model), and Ellipsoid Model, were developed to model skin colour regions of rendered digital images as well as skin colorimetric data. A method to train elliptical models was presented. Skin colour databases were created to train these three elliptical models. Their detection accuracies were analysed. The Lightness-Independent Ellipse Model is easy to train, efficiency in computation, yet the detection accuracy is lower than the other two models. The Lightness-Dependent Ellipse Model has the highest detection accuracy; however, the training is most complicated. Compared with the two ellipse models, Ellipsoid Model is a good comprise among modelling complexity, detection accuracy, and computation efficiency.

Another method of modelling a colour region is to construct a convex hull for the region and fit the convex hull with formulae. The method can be used to model any specific object colour gamut.

Chapter 4
Preferred Skin Colours

Various researches support the idea that there is a preferred skin colour centre for human eyes. In preferred colour reproduction, moving skin colours toward the preferred centre should improve the colour preference. Finding the preferred skin colour centre is a basic step for preferred skin colour reproduction. In this chapter, the elliptical skin colour model developed in the prior chapter was applied to study skin colour preference. A series of psychophysical experiments were conducted to analyse skin colour preference, and to optimise algorithms and parameters for skin colour enhancement.

4.1 Introduction

People, particularly facial patterns, are often the primary visual subjects in a colour image. Reproducing them with highest possible image quality is crucial in photographic colour reproduction. Since people typically rely on their preference on skin colours to judge the colour reproduction quality of face objects, it is important to know preferred skin colours for preference colour reproduction.

Bartleson investigated the preferred colour reproduction of skin colours and found that the actual colour and the memory colour were significantly different in chroma, and the preferred flesh tone appeared to be yellower and more chromatic than the colours of real flesh tone. Bartleson and Bray further investigated the preferred colour reproduction of flesh tone, blue-sky, and green-grass, and concluded that the preferred colour for reproducing Caucasian complexions was to have the same chromaticness as the mean memory colour of the flesh tone. Sanders studied the colour preference of natural objects, and found that the preferred Caucasian facial colour was more saturated than actual facial colours. Hunt et al. studied the preferred colour reproduction in colour photography, and concluded that for reflection prints the preferred Caucasian skin colour had about the same purities as the real skin colour but was a little yellower. Sanger et al. used portrait photos of Mongoloid, Caucasoid, and Negroid to study preferred skin colours, and found that chroma of preferred skin colours increases steadily in the order of Caucasoid, Mongoloid, and Negroid, preferred hue angles among three groups are about the same, with dominant wavelength at about 590nm. Yano and Hashimoto studied the preference of Japanese complexion, and found that the preferred complexion of

Japanese women was shifted to a slightly higher chroma and was more reddish in hue than the actual complexion of Japanese women; the direction of hue shift is different from that of the preferred Caucasian women; and the preferred skin colour of Caucasian women is more colourful than that of the Japanese woman.

Park et al. studied preferred skin colour reproduction on display. The skin colours were determined using a bivariate Gaussian function. The centre of the skin colour boundary was used as the preferred skin colour centre. Skin colours were moved toward a small colour region around preferred skin colour centres for preference enhancement. Kuang et al. conducted psychophysical experiments to study the influence of different factors on skin colour preference for photographic colour reproduction. They found that background lightness has little influence on skin colour preference; the preference variances on Oriental and Caucasian skin colours are smaller than those on Indian and African American; and no significant culture difference among different ethnic observers. Their finding that capturing illuminants have significant influence on skin colour preference may be the result of inaccurate white balance in the cameras they used. Fernandez and Fairchild studied the observer and cultural variability for preferred colour reproductions of pictorial images. Their experiments yielded that inter-observer variability was approximately twice the magnitude of intra-observer variability; and images containing people (faces) were routinely less variable than images without people (faces). Although the preference variability due to observers' cultural background was found to be statistically significant, it was not visually significant. The preference variability due to image contents and the preference variability among observers were more significant than the variability due to cultural background.

Bodrogi used photo-realistic images containing sky, plant, and Caucasian skin colours, as well as standalone colour patches taken from the corresponding photo-realistic images to study memory colour shift on a calibrated CRT monitor. Memory colour shift in photo-realistic images was found larger than that in colour patches, and later (long-term) memory colours had higher chroma than the instant memory colour in both photo images and colour patches. For skin, observers' long-term memory colours tended to be yellower than original colours.

It can be concluded from different studies that preferred skin colours are different from actual skin colours. However, preferred skin colour centres from various studies are somewhat different. In order to have a solid understanding of skin colour preference for reliable skin colour enhancement of photographic images, psychophysical experiments were conducted to revisit and to verify preferred skin colours, to determine preferred skin colour regions, and to study inter-observer variation and tolerance.

4.2 Experiment I: Skin Colour Preference of Mixed Culture Backgrounds

This psychophysical experiment was to study the colour preference of African, Caucasian, and Oriental skin tones judged by a pool of observers with mixed culture backgrounds (African, Caucasian, Asian, and Hispanics). The experiment was divided into two phases as presented in following sub-sections.

4.2.1 Experiment I-1

To simplify the experiment, the lightness-independent skin ellipse model developed in Chapter 3 was applied to detect skin colours. An image database composed of approximately 2500 digital images was used to train the skin model. The images were captured using various digital cameras under different conditions. The subjects covered different skin-tones, including Caucasian, Asian, Hispanics, African, and Indian. This image dataset is named 'skin image database', and the selected skin colours from the image dataset is name 'skin colour database' throughout this paper.

Psychophysical experiments were conducted to determine preferred skin colour regions for preference colour enhancement. The procedure were: 1) the skin colour gamut is uniformly sampled to obtain an N-point skin colour set; 2) skin colours of each test image is morphed toward each of these N skin colour points; and 3) observers evaluate the preference of the N versions of each image displayed on LCD displays. A paired comparison method was used for the experiment. The number of judgements on each image is m = N(N–1)/2. If skin sample points are large (a large N), m may be too large for practical evaluation. As a compromise, 9 sample points are chosen. The total number of judgements on each image by an observer is 9x8/2 = 36. To ensure the quality of observations, each observer was to judge images for no more than 30 minutes in a single session. With this constraint, an observer was able to judge 4 images within about half an hour (4x36 = 144 pairs of comparisons). Twelve images were judged by each observer. The experiment was divided into 3 sessions. Each observer completed a session each day and therefore all observations were completed in three days.

A set of nine pre-determined colour centres uniformly sampled within the skin colour ellipse in CIE a*b* diagram was used to morph skin colours of test images without changing lightness. Fig. 4.2.1-1(a) shows the nine pre-determined colour centres uniformly distributed on the skin colour ellipse that was trained using all skin types. The dot in the centre is the statistical skin colour centre. The skin model coefficients can be found in Chapter 3. The centre point #4 is overlapped with the skin elliptical centre. Because of a software bug, an sRGB display ICC profile

instead of the actual monitor display colour characterisation was applied to the colour transformation, the nine pre-determined colour centres were actually shifted to positions shown in Fig. 4.2.1-1(b).

(a)   (b)
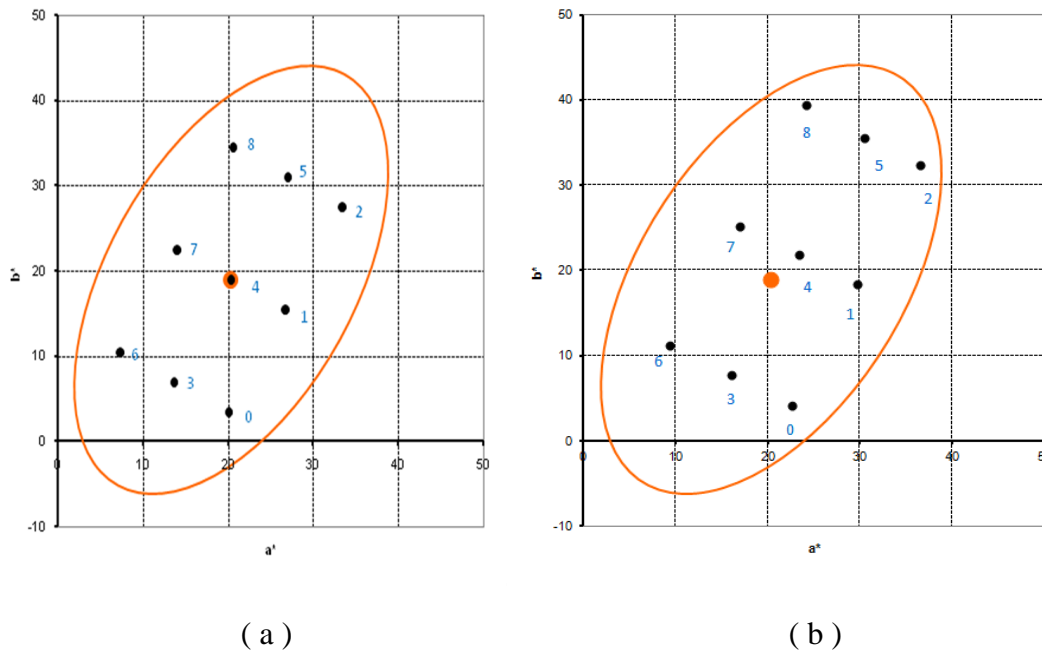
Fig. 4.2.1-1 Nine predetermined skin colour centres in CIELAB a*-b* diagram

A test image was morph toward each pre-determined colour centre to produce a new image in which skin colours were adjusted. With nine skin colour centres, nine versions of adjusted images were produced to judge skin colour preference.

Twelve sRGB images for the experiment were carefully selected to cover different skin types (see Fig. 4.2.1-2). General criteria for selecting images were: the colour balance of an image should not be too much off from ideal; the background behind a person's face should not be highly chromatic; the global tone should not be too much off from ideal; and the image quality should be good (no visible noise).

The skin colours of each image were processed in a way that skin colours were morphed toward a skin colour centre. As colours changed from the statistical skin colour centre to the skin colour boundary, the adjustment gradually faded off. Each image was first transformed from its source RGB colour space to CIELAB using it source ICC profile (ICC website, Nielsen and Stokes 1998, Zeng 2002). To create ICC profiles for colour transformation, a linear Bradford chromatic adaptation matrix (Luo and Hunt 1998) was applied to adapt colours from the white point of the RGB colour space to D50 . The skin colour ellipse model was applied to compute Mahalanobis distance, $\Phi(X)$.

Fig. 4.2.1-2 Test images used in Experiment I-1
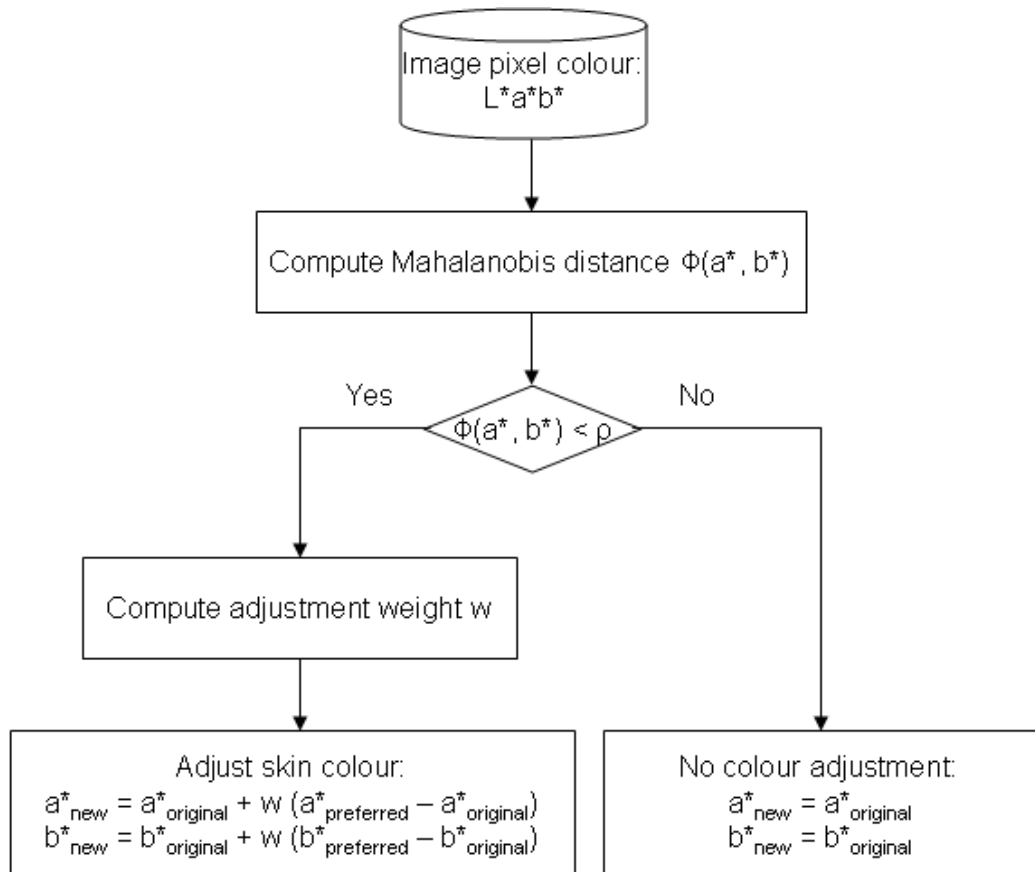
Fig. 4.2.1-3 A block diagram illustrating skin colour adjustment on test images

$Φ(X) = ρ$ defines the skin colour boundary. If $Φ(X)$ is greater than $ρ$, the colour X is considered a non-skin colour, and no colour adjustment is applied. Otherwise, a weight is computed from the Mahalanobis distance to morph the skin colour toward each of the nine skin colour centres. Fig. 4.2.1-3 shows a block

diagram for adjusting skin colours of images used for the experiment. Lightness is not adjusted, and a*b* are adjusted if the colour is a skin colours. Pseudo codes to compute the weight are:

if ($\Phi(a, b) < \rho$){

    r = $\Phi(a, b) / \rho$;

    if (r < 0.5) r = 0;

    else r = (r - 0.5)/0.5;

*....w = (1 - r)*0.5;*

}

As shown in the pseudo code, a colour at the statistical skin colour centre is adjusted the most, and colours on or outside the skin colour gamut are not adjusted. With nine predetermined skin colour centres, nine versions of images are created from each image. Fig. 4.2.1-4 shows an example.
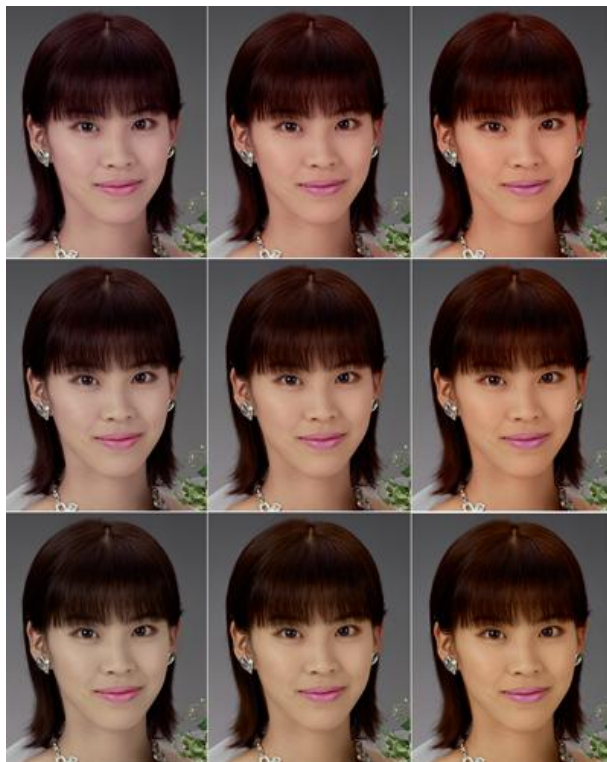
Fig. 4.2.1-4 An image morphed toward nine colour centres

If teeth of a person in an image have yellowish tint, they may become more yellowish after the skin colour adjustment. It is obvious that highlight colours are adjusted too much. Because the artefact was found in a very late stage of the preparation for the psychophysical experiment, instead of tuning skin colour adjustment algorithm, images were carefully selected so that this type of artefact

was not seen in images. The skin colour adjustment algorithm was not modified to fix the artefact until a subsequent experiment.

Because paired-comparison is slow for its large amount of comparisons to evaluate an image, and there are only nine coarse colour centres to manipulate images practically, other experimental methods were designed and tested to speed up the psychophysical experiment and to allow denser sampling points to manipulate images.

In an initial study, a tool was developed to display a test image at a time on a monitor screen for evaluation. The image can be modified and morphed toward each of nine pre-set skin colour centres using three sliders (see Fig. 4.2.1-5). As an observer adjusts a slider position from 0 to 8, skin colours of the image are changed accordingly. An observer stops on slider positions in which the image is mostly preferred. There are three sliders to manipulate. The Coarse slider morphs skin colours toward nine colour centres uniformly sampled on the skin colour region (A, B, ..., I in Fig. 4.2.1-6). After a preferred skin colour position is found by manipulating the Coarse slider, another set of eight skin colour centres around the coarse preferred skin colour centre is generated (there are total of nine preferred skin colour centres including the coarse preferred skin colour centre) (see a, b, ..., i in Fig. 4.2.1-6). The sampling density is doubled in this step (i.e. the distance between two neighbour skin colour centres is half of the previous one). In the third step, the observer manipulates the Fine slider to find a most preferred skin colour position. After a fine preferred skin colour centre is found, a last set of eight skin colour centres around the fine preferred skin colour centre is generated (there are total of nine preferred skin colour centres including the fine preferred skin colour centre). The sampling density is doubled again at this time, The observer manipulate the Finer slider to find a most preferred skin colour position (0, 1, ..., 8 in Fig. 4.2.1-6). Finally, the most preferred colour centre is saved in a file. Fig. 4.2.1-6 shows an example: nine coarse skin colour centres (A, B, ..., I) are first generated to process images controlled by the Coarse slider; after #C is selected, nine finer skin colour centres (a, b, ..., i) are then generated to process image controlled by the Fine slider; and after #i is selected, nine finest skin colour centres (1, 2, ..., 8) are generated to process image controlled by the Finer slider.

Because a single image was displayed at a time with this experimental setup, observers must rely on their memory of preference levels of nine images to determine a most preferred one, which is very difficult. An initial psychophysical experiment conducted by this approach did not yield converged result.

Fig. 4.2.1-5 A psychophysical experimental tool to find a preferred skin colour centre
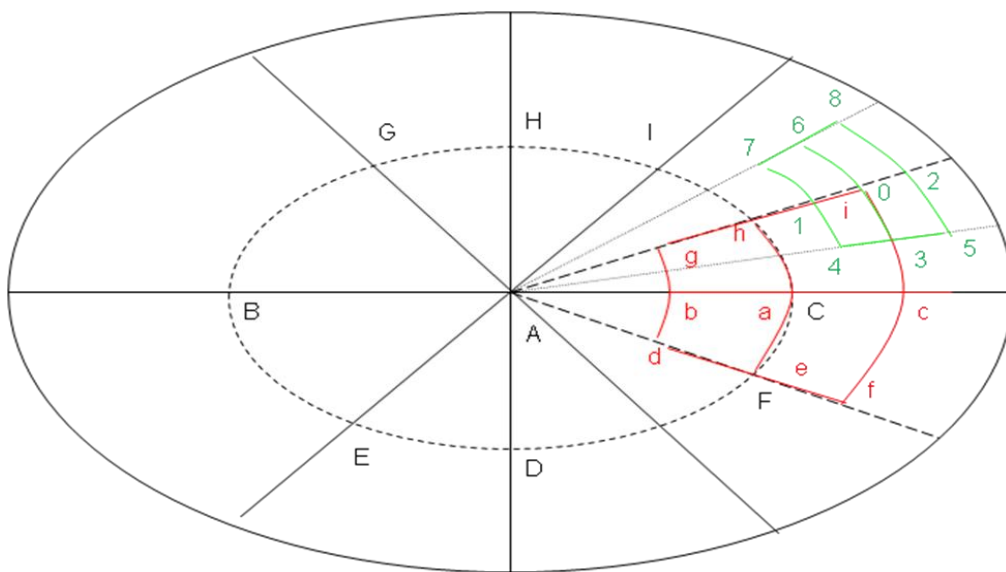
Fig. 4.2.1-6 A diagram illustrating the distribution of nine skin colour centres generated in each of three phases

The above experimental design was modified so that observers did not need to remember preference of nine versions of a test image. Instead of displaying an image at a time, nine versions of images are displayed simultaneously on a monitor screen (see Fig. Fig. 4.2.1-7). After an observer clicks on an image that is most preferred to him or her, the corresponding skin colour centre is applied to generate a denser set of nine skin colour centres that are applied to update these nine images. The observer selects a most preferred image again and the nine versions of images are updated with further denser skin colour centres. After the process is repeated three times (equivalent to adjust three sliders shown in Fig. 4.2.1-6), the preferred skin colour centre corresponding to the most preferred version of image is saved to a file. The result from a preliminary psychophysical experiment shows that the repeatability of observer judgment is poor. Reasons may be that 1) images must be scaled to very a small dimension to fit on a 21-inch display for observer judgment; and 2) judging nine images at once may be a difficult task for many observers or observers may rush to pick an image that is pleasing but not most preferred.
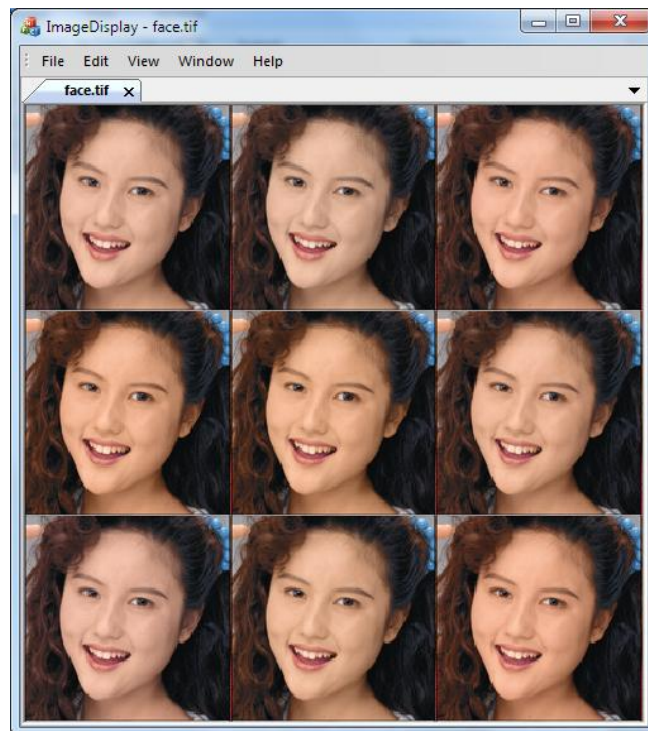
Fig. 4.2.1-7 Another psychophysical experimental tool to find a preferred skin colour centre

For these failures in preliminary psychophysical experiments, the paired-comparison method was finally adopted for this study.

Five workstations were used to conduct the experiment simultaneously, each with an HP L2335 active matrix TFT 23-inch LCD display to display images. The

colour characteristics of the displays will be described in Section 4.2.1.1. The room lighting was adjusted to simulate a typical dim surround condition.

Nineteen observers participated in this phase of the experiment. All of them came from a pool of HP employees at the site in Vancouver, Washington, US. They were diverse in gender and culture backgrounds (Caucasian dominated), and ages were between 25 and 50. All of them satisfactorily completed the colour vision discrimination test and observer orientation training. They were experienced at evaluating image quality because of involvement in colour and image quality evaluations that were conducted regularly.

All test images were cropped to a uniform size of 8-inch width by 10-inch height. As a pair of images was displayed on a display each time, the remaining area of the display was filled with uniform medium gray (see Fig. 4.2.1-8). Each observer was instructed to sit at distances that was most comfortable for viewing, followed by the presentation of an image pair on display at a time, and was asked to indicate which rendition of the two was preferred for skin colours. After the response was recorded, the next image pair was loaded and the observer proceeds until all samples were evaluated. All possible pair combinations of the nine treatments (36 in total) were presented to each observer via a script that randomized the order and the placement (left/right) of the treatments. With 12 images, each observer compared 432 pairs. There are 8208=36x12x19 total judgments from all observers.

Fig. 4.2.1-8 A snapshot of a display screen for the experiment

4.2.1.1 Display Colour Characterization

Since five workstations are used to conduct the experiment simultaneously, it is very important to have all five LCD displays perform consistently. An X-Rite Eye-One Pro spectrophotometer was used to characterise each display. Each display was adjusted to a target D65 white point, and the RGB tone curves were adjusted to have a gamma of 2.2. Then an ICC profile was generated for each display's colour

transformation.   Figures 4.2.1.1-1 and 4.2.1.1-2 show the gamut comparison between a display monitor used for the experiment and sRGB in CIELAB colour space. The display has substantially more saturated red and green primaries than the corresponding sRGB primaries, and the blue primary of the display is about the same as the sRGB blue primary. For a set of skin tone RGB colours directly displayed on an sRGB display and on an actual display, it is obvious that the actual display produces more chromatic skin colours.

To study the consistency of all five monitors, a set of 5x5x5 RGB data uniformly sampled the entire RGB colour space was created, and converted to CIELAB using each of the five ICC profiles. The mean of each colour from the five CIELAB data sets was computed. The differences of each of the 5x5x5 = 125 colours between each data set and the mean data set were computed. The mean difference, maximum difference, and standard deviation of the differences in CIEDE2000 (ΔE^*_{00}) were calculated. Table 4.2.1.1-1 shows mean differences, maximum differences, and standard deviations of the differences in ΔE^*_{00}. Monitor #4 has the largest deviation from the mean, mostly in dark colours. Overall, the colour consistency among five monitors is reasonably good.
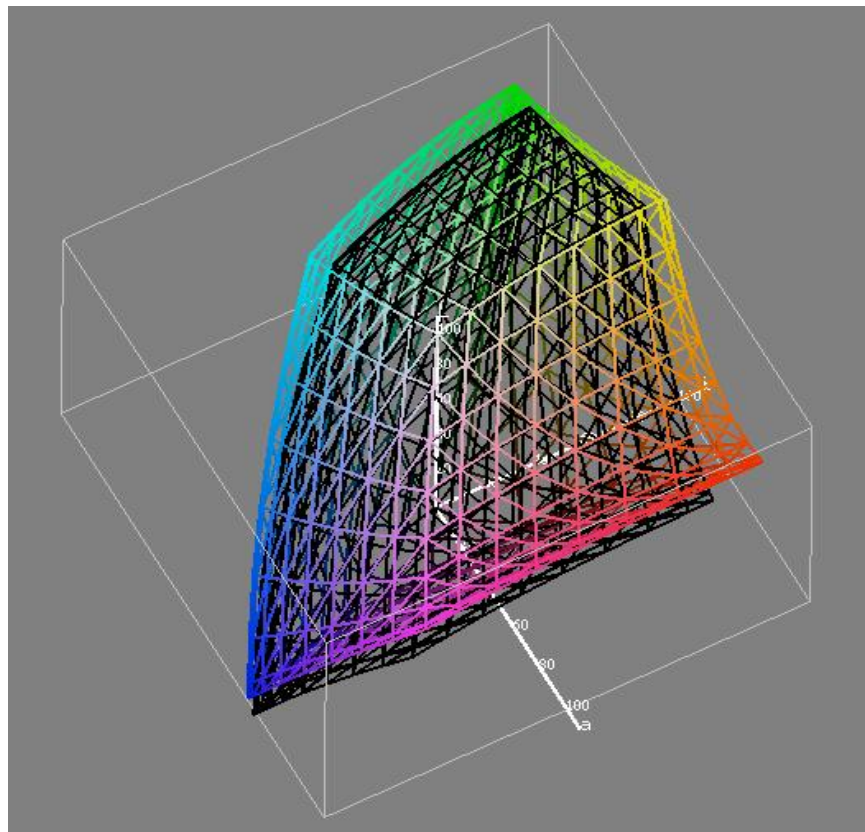
Fig. 4.2.1.1-1 sRGB gamut (black) and a display gamut (colour) in CIELAB colour space
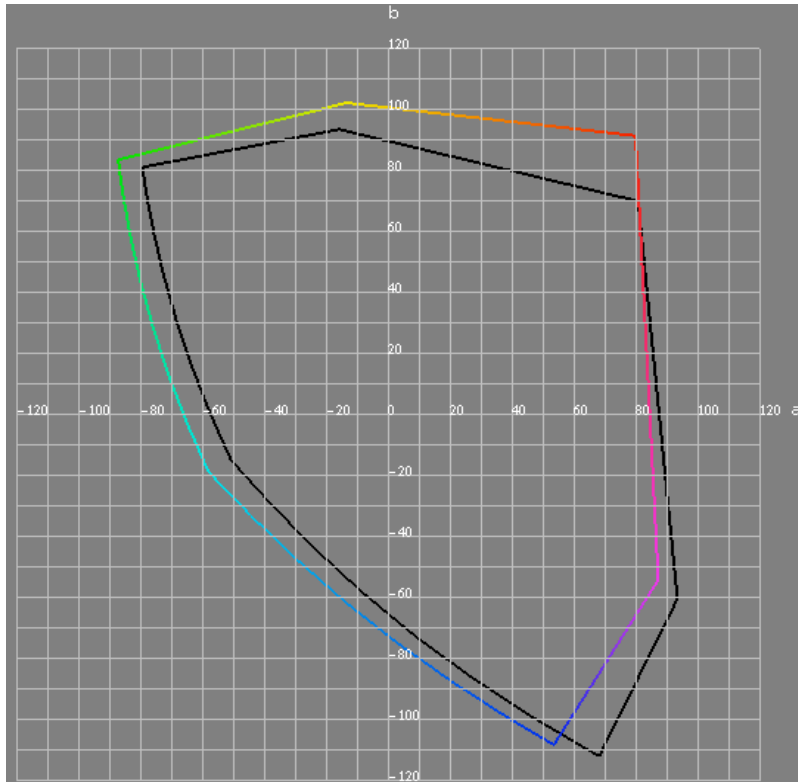
Fig. 4.2.1.1-2 sRGB gamut (black) and a display gamut (colour) in CIE a*b*
  coordinates

Table 4.2.1.1-1 CIE ΔE^*_{00} between each monitor and the mean from all monitors

	MEAN	*MAX*	*STDEV*
Monitor #1	0.2	0.7	0.1
Monitor #2	0.3	1.2	0.2
Monitor #3	0.2	0.7	0.1
Monitor #4	0.5	2.6	0.5
Monitor #5	0.2	0.7	0.2

4.2.1.2 Colour Distribution of Test Images

The 12 test images were carefully selected and visually judged to avoid biases
in skin colour distributions. Quantitative analysis were performed to analyse skin
colour distributions of the set of images and to compare them with the statistical
distribution of skin colours. The purpose was to confirm that the skin colour
distribution of the set of image was reasonably balanced.

The skin colours of each image were masked manually. A histogram of skin
colours of the 12 images was then generated. Two steps were performed to reduce
noise in histogram: 1) images were de-noised prior to skin colour masking; and 2) a

small percentage (5% in this experiment) of least occurred skin colours in each labelled skin image were removed. Step 2 was to guarantee that incorrectly masked non-skin colours were removed. The skin colour histogram was applied to train an ellipsoid that covered 90% of masked skin colours. Fig. 4.2.1.2-1 shows the skin colour ellipsoids in CIELAB colour space, where the skin colour ellipse of the 12 images is illustrated in orange, and the ellipsoid of the skin colour database is drawn in black. 3-D visualization of the ellipsoids demonstrates that the orange ellipsoid is approximately in the centre of the skin colour database, which means no obvious overall skin colour bias in the skin colour distribution of test images. Fig. 4.2.1.2-2 shows three constant-lightness planes of the ellipsoids. Orange ellipses are skin colour ellipses of 12 images and black ellipses are ellipses of the skin colour database in constant-lightness planes. Fig. 4.2.1.2-2 shows skin colours of 12 test images are approximately distributed around the centre of the skin colour database, although the dark skin tone ellipse of test images (the right figure) is slightly shifted off the centre of the overall skin colour distribution. In overall, the skin colour distribution of these 12 images has very little bias against the centre of the skin colour database. This is important because if skin colours of an image are too much off from average skin colours or preferred skin colours, the skin colour adjustment function may not be able to move them to preferred skin colour centres.
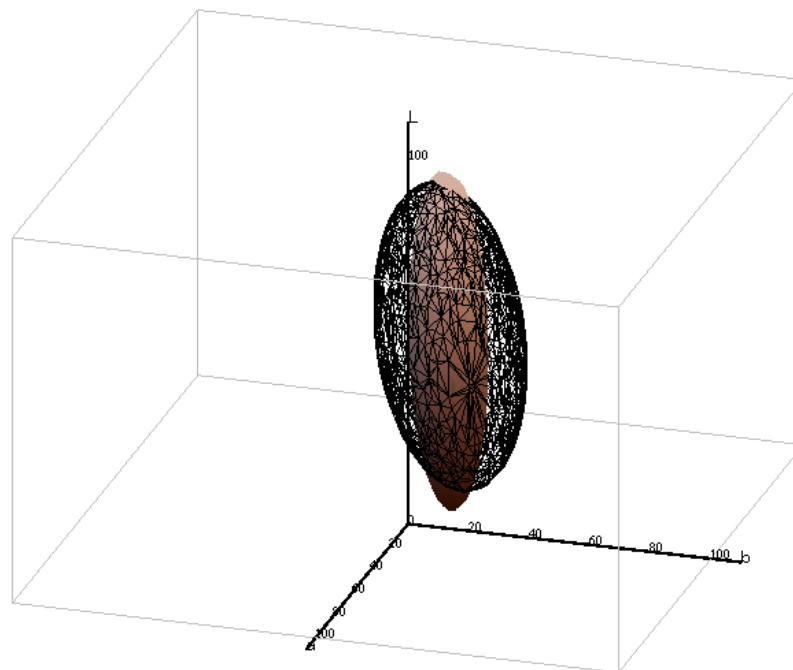
Fig. 4.2.1.2-1 The skin colour ellipsoid of the 12 images (orange) and the skin colour ellipsoid of the image database (black) in CIELAB colour space
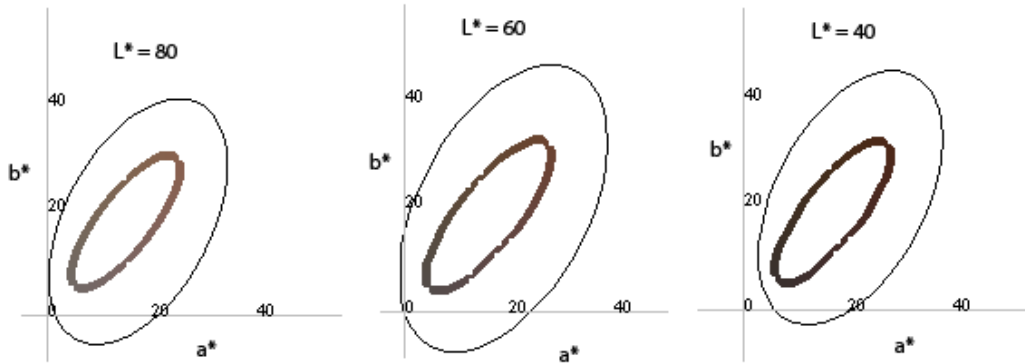
Fig. 4.2.1.2-2 Constant-lightness slices of the skin colour ellipsoid of the 12 images (orange) and the skin colour ellipsoid of the image database (black)

4.2.1.3 Preferred Skin Colour Centre

The Thurston's Law of Comparison Case 5 was applied to analyse the result (Bartleson and Grum 1984). The z-scores of each image at skin centres 0 to 8 obtained from all judgements are plotted in Fig. 4.2.1.3-1. A higher z-score means stronger 'prefer' (or less 'dislike'). Error bars represent the 95% confidence interval (Montag 2006). The figure shows that skin centres #0 and #2 are least preferred to most images, and #4 and #7 are most preferred to most images.
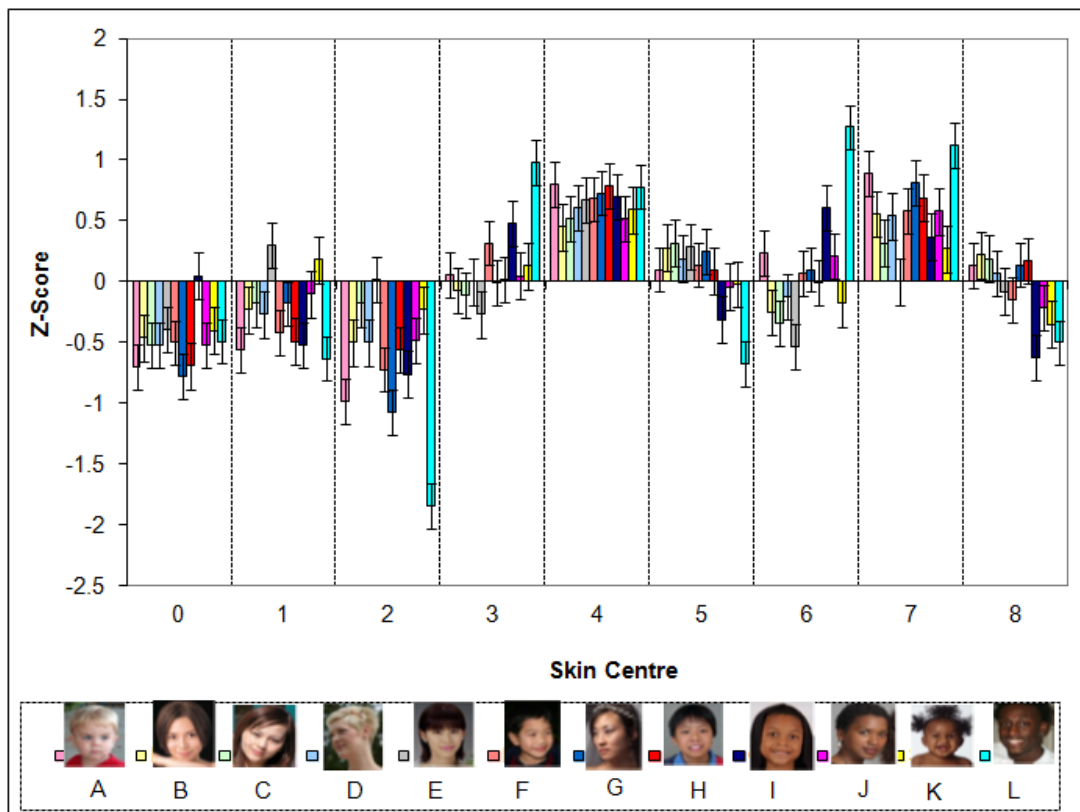
Fig. 4.2.1.3-1 z-score of each individual image at each skin colour centre

Characterising skin colour centres using a representative display ICC profile (an ICC profile that approximately represents the average of all five displays) and using the average z-scores of skin centres #4 and #7 as weights, an approximate preferred skin colour centre a* b* = (20.4, 23.4) is obtained.

A preferred skin colour centre of a test image can be computed from each image using the a*b* of nine colour centres and their corresponding z-scores as weights:

$$a* = \frac{\sum_{i=0}^{8} a_i^* \cdot Z_i}{\sum_{i=0}^{8} Z_i},$$

$$b* = \frac{\sum_{i=0}^{8} b_i^* \cdot Z_i}{\sum_{i=0}^{8} Z_i}$$

where (a_i^*, b_i^*) is the mean skin colour of the i-th version of the image, Z_i is the Z-score of the i-th version of an image.

Although the method to adjust skin colours of test images morphs skin colours toward each of the nine predetermined skin colour centres, it does not morph overall skin colours or the mean skin colour exactly to each predetermined skin colour centre. Furthermore, although statistical analysis of test images confirms that the overall skin colour distribution of test images have no obvious bias compared to the overall skin colour distribution of the skin colour database generated with large amount of images for skin colour modelling, skin chromaticity distributions of different test images are not exactly the same. Since observers rate a image by judging overall skin colours of the image to, instead of computing preferred skin colours using nine preferred skin colour centres, preferred skin colours should be computed using skin colours of nine versions of each test image and their corresponding z-scores.

To compute preferred skin colours using skin colour distributions of each image, a skin mask was made for each of 12 images. Fig. 4.2.1.3-2 shows an example. Using a mask to index each pixel of each of the nine versions of an image, all skin pixels were found. To remove noisy pixels and colours that were less likely to be skin colours, a small percentage of pixels in the lower end of the histogram were removed. This percentage was set as 10% to remove noise pixels, specular reflectance colours, and objects such as hair that might be included in skin mask. A mean skin colour was computed for each version of adjusted images. Assuming images with negative scores are not acceptable, positive z-scores were used as

weights to draw elliptical contours and to compute weighted average colours as preferred skin colours (Bartleson and Bray 1962).

By averaging skin colours in each image to compute a preferred skin colour, it assumes that all skin colours are visually equally important in colour preference judgment. This might not be true. Some critical spots in faces may play more importantly than rest of spots in determining skin colour preference. For this reason, a slightly different method that takes only critical spots (typically forehead and cheeks are critical spots) to compute preferred skin colours was tested as well. Fig. 4.2.1.3-3 shows an example. Three circle areas were selected critical regions of this image. The nose area was ignored because of specular reflectance. Ears and regions that have shades were ignored as well. A mean colour of critical regions was computed on each of nine versions of a test image.
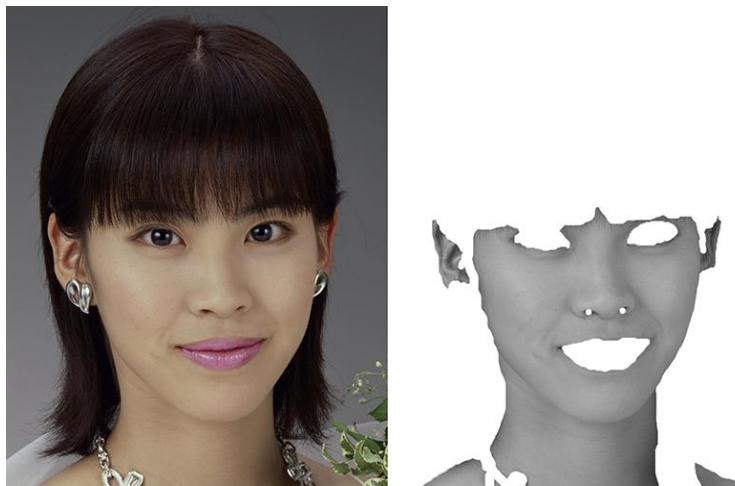
Fig. 4.2.1.3-2 A test image and its skin mask

Fig. 4.2.1.3-3 Critical regions in a test image

A final preferred skin colour was computed as weighted average of the nine mean colours using their corresponding z-scores as weights. The results of preferred

skin colour computed by the method using the skin colour distribution of all face skin colours and by the method using the skin colour distribution of critical spots were compared. The preferred skin colours computed by these two methods have ΔE^*_{ab} of 1.0 by averaging preferred skin colours computed on all nine images.

Since preferred skin colours computed using the colour distribution of all skin colours are very close to those computed from critical spots and the method using critical spots may subject to personal bias in determining critical spots, the method using the colour distribution of all skin colours was accepted to compute preferred skin colours in this thesis.

After a preferred skin colour from each of 19 observers on each image was computed, an ellipse was generated from the 19 preferred skin colours of each image. Fig. 4.2.1.3-4 shows the preferred skin colour ellipses of 12 test images in CIELAB a*-b* coordinates (L* is ignored). The pink dot in the centre is the centre of the skin colour database. Each small ellipse, which covers about 50% of the sum of scaled positive z-scores, represents a preferred skin colour region judged by observers on one image. The centre of an ellipse was considered the preferred skin colour centre of the corresponding image. The diamond dot is the preferred skin colour centre averaged from preferred skin centres of all images. The distribution of preferred skin colour centres has smaller difference in hue than in chroma, which implies that the tolerance of preferred skin colours is smaller in hue than in chroma.
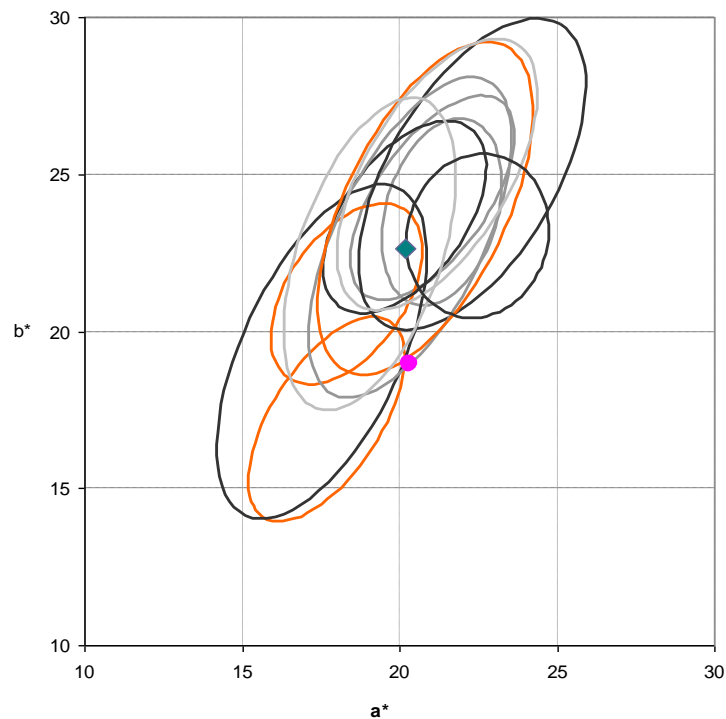
Fig. 4.2.1.3-4 Preferred skin colour ellipses of 12 test images in Experiment I-1

To understand the underlying trends of different skin colours, the skin colours were categorised into light, medium, and dark skin-tones. They were categorised mainly based on the average L* of skin colours. L* at 58 and 48 were considered the boundaries of light/medium and medium/dark skin tones, respectively. However, since the visual perception of the "whiteness" of face tones were not completely determined by lightness, average L* of skin colours of an image at or close to a boundary were visually evaluated to determine a skin tone group that the image belonged to. The first five images (A, B, C, D, E) were categorised as light skin-tone images (Caucasian dominated), the next three images (F, G, H) were categorised as medium skin-tone images (Oriental), and the remaining four images (I, J, K, L) were categorised as dark skin-tone images (African dominated).

The preferred skin colour ellipses of three groups are illustrated in Fig. 4.2.1.3-3, where ellipses of light, medium, and dark skin-tone images are drawn in orange, gray, and black, respectively. Except that the distribution for medium skin-tone images has smaller variations than other two groups, there are no clear disparities among three groups. Table 4.2.1.3-1 lists the average preferred skin colour centres of three groups. It shows that preferred skin colours among three groups are about the same in chrominance.

Table 4.2.1.3-1 Preferred skin colour centres of three skin-tone groups

	a^*	b^*	C^*_{ab}	h_{ab}
Light-tone	19.8	23.2	30.5	49.5^o
Mid-tone	21.3	25.0	32.8	49.5^o
Dark-tone	21.0	24.0	31.9	48.8^o

Table 4.2.1.3-2: Preferred skin colour centres of three ethnic groups

	a^*	b^*	C^*_{ab}	h_{ab}
Caucasian	19.3	22.1	29.3	48.8^o
Oriental	20.7	24.4	31.9	49.7^o
African	20.5	23.3	31.0	48.7^o

To analyse the skin colour preference among different culture backgrounds, the images were categorised into Caucasian, Oriental, and African groups. Because it was difficult to determine ethnic groups for three images, (B, G, and I in Fig.

4.2.1-2), these three were not used for analysis. Three images were selected for each group: A, C, and D for Caucasian; E, F, and H for Oriental; and J, K, and L for African. The result is shown in Table 4.2.1.3-2.

4.2.1.4 Inter-Observer Variation

There are 19 observer preferred skin colour centres represented with a*b* (ignoring L*) on each image. Each observer's preferred skin colour centre against the mean skin colour centre on each image were computed. They represent the observer variations, (Δa^*, Δb^*), on each image. Dots in Fig. 4.2.1.4-1 are these (Δa^*, Δb^*) points. Each point is a preferred skin colour centre of an observer judgement on an image. The 19 points on each image represent inter-observer variances on skin colour preference for this image. An ellipse to cover 85% of 19 sets of (Δa^*, Δb^*) from all observer judgements on each image was generated. It was found that typically, two or three observer data points in a set were noisy and should be excluded from the ellipse fitting. For such reason, an 85% coverage rate for an ellipse was determined to cover 16 points, i.e., three outlier points was discarded. All ellipses show very long major-axis and very short minor-axis, and have about the same orientation. Translating each ellipse centre to its original a*b*, one will see that the orientation of each ellipse lies within a small hue range, implying preferred skin colours lying within a limited hue range; and their chroma variations are more tolerable.

If each ellipse in Fig. 4.2.1.4-1 is translated to absolute a*b* coordinates, the orientation of each ellipse reveals an interesting hue preference: if a chroma higher than the mean chroma is preferred, the preferred hue angle tends to be slightly higher than the average preferred hue angle (the hue preference is slightly more yellowish); if a chroma lower than the mean chroma is preferred, the preferred hue angle tends to be slightly lower than the average preferred hue angle (the hue preference is slightly redder).

There are total of 228 (19 by 12) observer preferred skin colour centres. Fig. 4.2.1.4-2 illustrates the colour preference ellipse (orange ellipse) from Experiment I-1 to cover 85% of these preferred skin colours projected to CIELAB a*-b* coordinates (the ellipse from Experiment I-2 is plotted for comparison and will be discussed in Section 4.2.2). The shape and orientation of the ellipse illustrate that observer variations are larger in chroma than in hue, i.e., the hue tolerance is smaller than chroma tolerance among observers
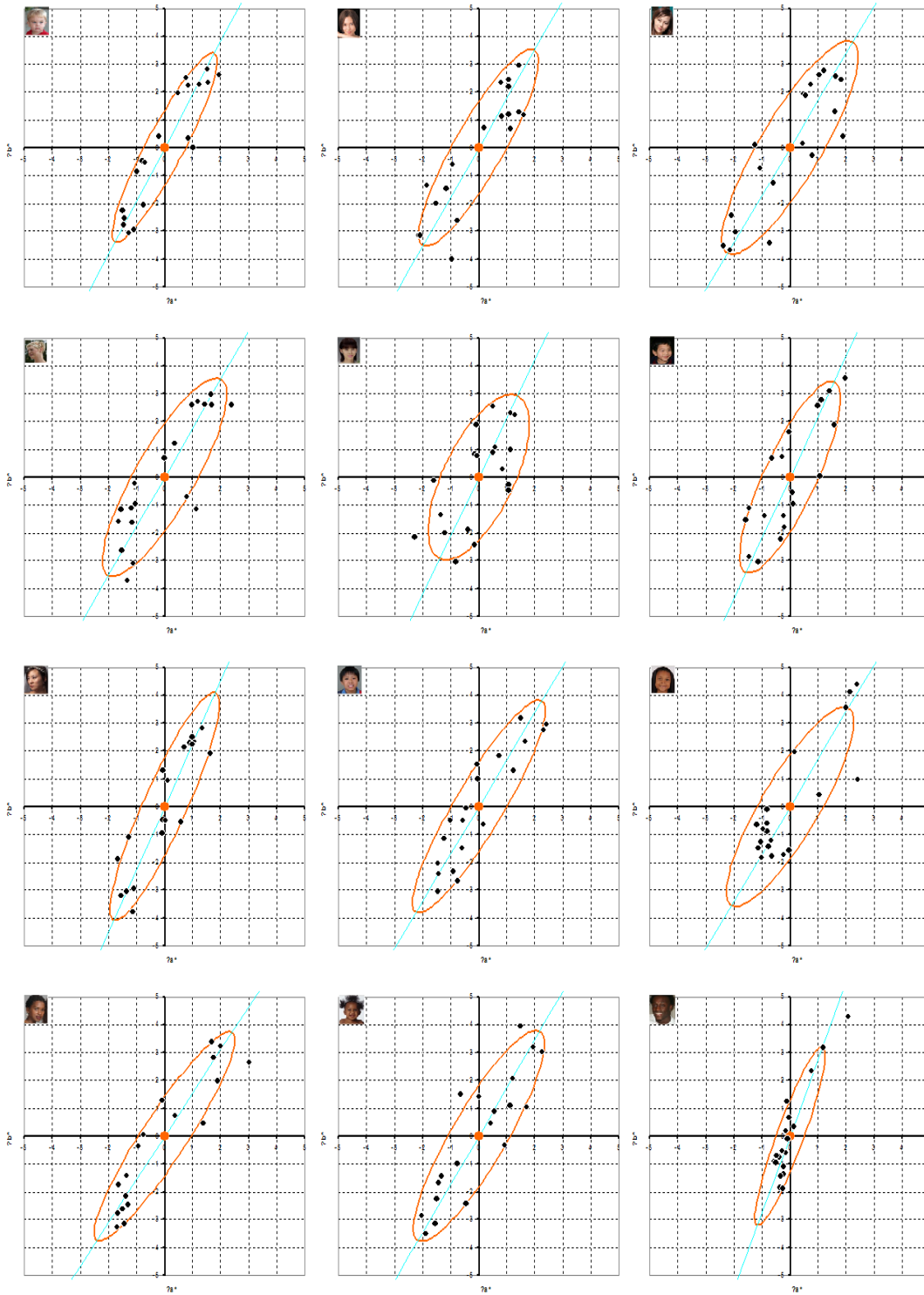
Fig. 4.2.1.4-1 Variations of observer judgements on each image in CIELAB a*-b* diagram
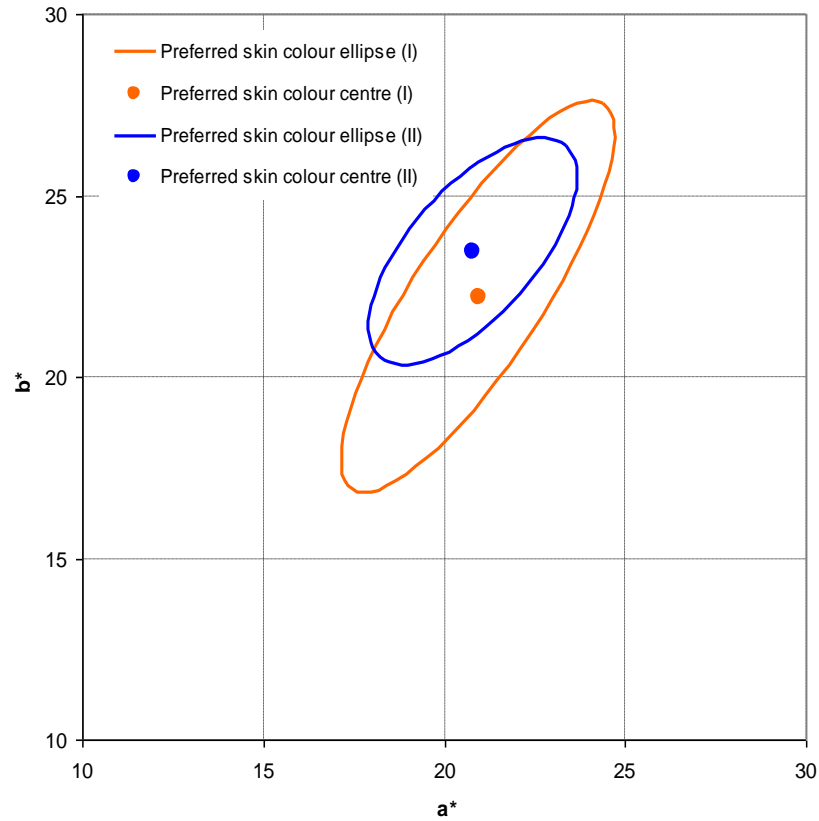
Fig. 4.2.1.4-2 Preferred skin colour ellipses from all observers on all images in CIELAB a*-b* diagram

4.2.1.5 Inter-Image Variation

The preferred skin colour centre of each image is plotted in Fig. 4.2.1.5-1. There are no significant differences among three skin colour groups. All of these skin colour centres spread around a large area, but in a narrow hue range with a mean hue angle of about 49° (the straight line in Fig. 4.2.1.5-1). It implies that preferred skin colours lie within a small hue range and have a larger discrepancy or tolerance in chroma. To reproduce skin colours pleasingly, it is important to morph them toward their ideal hue centre. It is not very clear why the results of the image *A* (the orange dot in the bottom) and image *K* (the black dot far away from the fitted line) are more different from others. It was found that higher chromatic versions of the adjusted images of the image *A* look flat and unnatural.

Table 4.2.1.5-1 lists each of these 12 preferred colour centres. A mean preferred skin colour centre is averaged from all individual preferred skin colour centres (a preferred skin colour centre computed by this approach is slightly different from that generated as the centre of a colour distribution ellipse). ΔE^*_{ab} of the preferred skin colour of each image to the mean preferred skin colour is distributed in a range of 0.4 and 6.0, with a mean ΔE^*_{ab} of 2.3. Very light and very

dark skin colour images tend to have larger ΔE^*_{ab}, and medium skin colour images seem to have smaller ΔE^*_{ab}. The large spread of ΔE^*_{ab} seems to indicate that image-dependent skin colour enhancement may be an optimal solution.
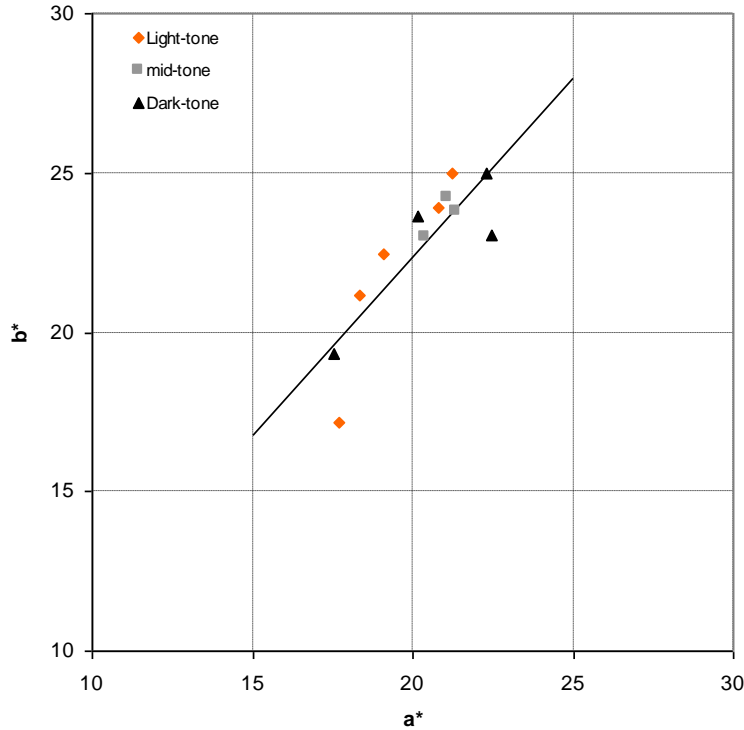
Fig. 4.2.1.5-1 Preferred skin colour centres of individual images in CIELAB a*-b* diagram

Table 4.2.1.5-1 Preferred skin colour centres of individual images

Image	A	B	C	D	E	F	G	H	I	J	K	L	Average
a*	18.1	18.7	21.2	21.6	19.5	20.7	21.4	21.8	22.7	20.6	22.9	17.9	20.6
b*	18.5	22.5	25.2	26.3	23.7	24.3	25.5	25.1	26.3	24.9	24.3	20.6	23.9
C^*_{ab}	25.9	29.3	33.0	34.0	30.7	31.9	33.4	33.2	34.7	32.3	33.4	27.4	31.6
h_{ab}	45.6	50.2	49.9	50.6	50.7	49.5	50.0	49.1	49.2	50.5	46.8	49.0	49.2
ΔE_{a*b*}	6.0	2.4	1.4	2.5	1.2	0.4	1.8	1.6	3.2	1.0	2.3	4.2	2.3

4.2.2 Experiment I-2

The experiment I-1 was considered to be an initial study of the evaluation. The results reveal a strong preference at an 'ideal' skin colour centre. As a subsequent experiment, Experiment I-2, was to refine the preferred skin colour region in a finer resolution around the preferred skin colour centre found in Experiment I-1. The intention was to produce a more accurate preferred skin colour centre.

In this experiment, a denser sampling of nine skin colour centres surrounding the preferred skin centre found in Experiment I-1 were generated to evaluate the skin colour preference in a smaller region. In Fig. 4.2.2-1, the cross points (marked 'x') noted with A, B, …, I are the nine pre-determined skin centres for this experiment; and the black dots noted with 1, 2, …, 8 are the nine colour centres used in Experiment I-1 (display colour characterisation was not taken into account in the plot). Point #E is the preferred colour centre found in Experiment I-1. The skin colour sampling in Experiment I-2 is about twice as dense as that in Experiment I-1.

The skin ellipse model was the same as that in Experiment I-1. Since the skin colour adjustment was found to be too strong on some images (e.g. teeth with yellowish tint become more yellowish), the strength of the colour morphing was reduced to relief some artefacts found in Experiment I-1. If a colour is a skin colour, i.e., $\Phi(a, b) < \rho$, the weight for skin colour adjustment is computed by W = 0.5 (1 - $\Phi(a, b) / \rho$).
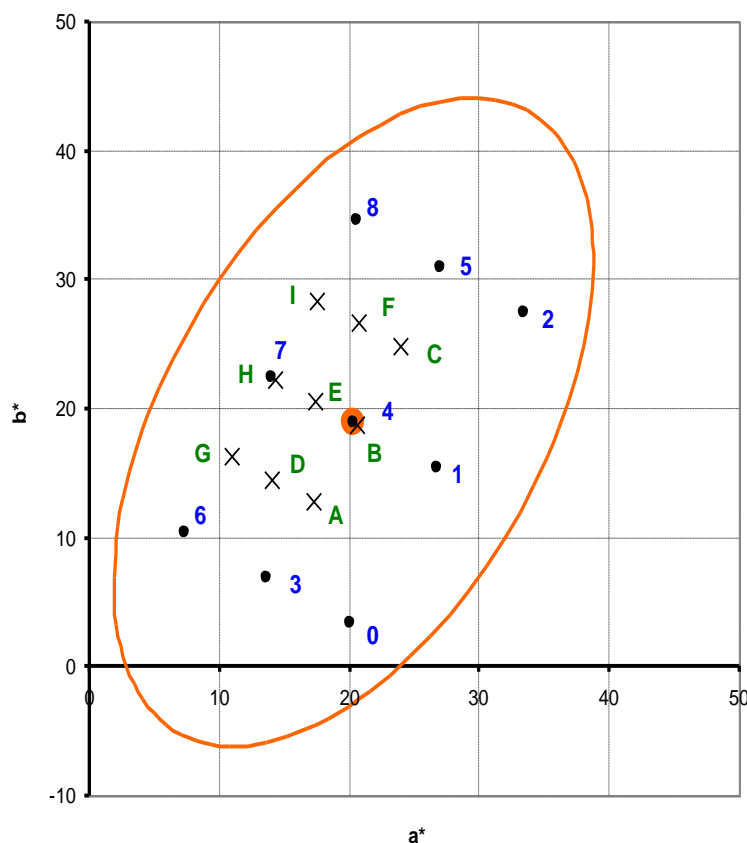
Fig. 4.2.2-1 Skin colour centres for the experiment in CIELAB a*b* diagram

Monitor displays, and experimental set-up and procedures were the same as in Experiment I-1. To avoid potential bias toward certain images, a complete different set of 12 images were carefully selected to cover various skin types (see Fig. 4.2.2-

2). Quantitative analysis of the statistical colour distributions of the set of 12 images and comparing them with the skin image database verified that the overall statistical distribution of the skin colours of the 12-image set was reasonably balanced. 20 observers from the same HP observer pools participated in this phase of experiment. Five of them participated in Experiment I-1 as well. Again, observers were Caucasian dominated. There were 8640 total judgments from 20 observers on 12 images by 9 observer centres (8640 =36x12x20).

Fig. 4.2.2-2 Test images used in Experiment I-2

4.2.2.1 Preferred Skin Colour Centre

Fig. 4.2.2.1-1 shows z-scores of individual images. Error bars correspond to the 95% confidence interval. Overall, there is a relative stronger preference for skin colour locations #E, #F, #H and #I than for other skin centres. However, the preference is not as selective as in Experiment I-1 due to less discrepancy among nine colour centres. Among these 12 images, the preference of Image *e* (see the green bar in the figure) is very different from others. This image is strongly preferred in locations that have lower chroma (#A, #D, and #G), and is strongly unfavoured in locations that have higher chroma (#C, #F, and #I). Skin colours of this image are very chromatic. It was suspected that this was an image scanned from a negative film.

Again, assuming images with negative scores are not acceptable, the positive z-scores and mean skin colours of their corresponding versions of each image were used to construct elliptical contours for preferred skin colours and to compute z-

score weighted average preferred skin colours for each image. An overall preferred skin colour was averaged from all preferred skin colours.
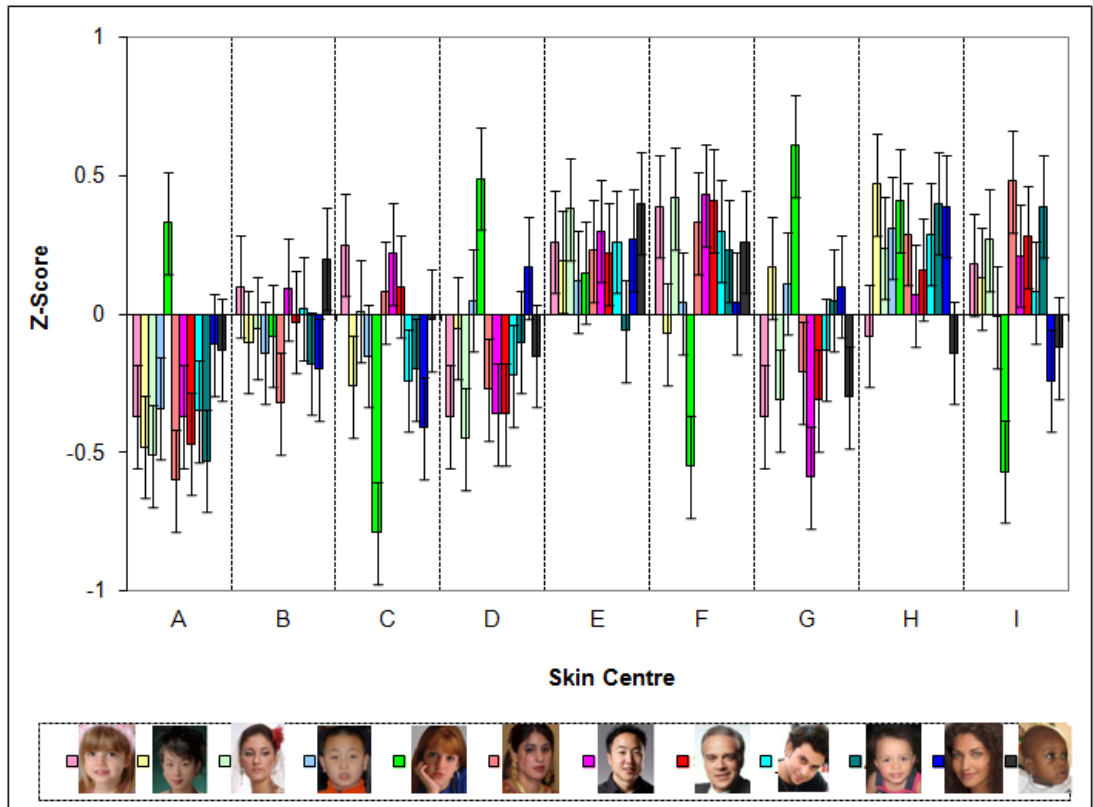
Fig. 4.2.2.1-1 Preference scores of individual images (Experiment I-2)
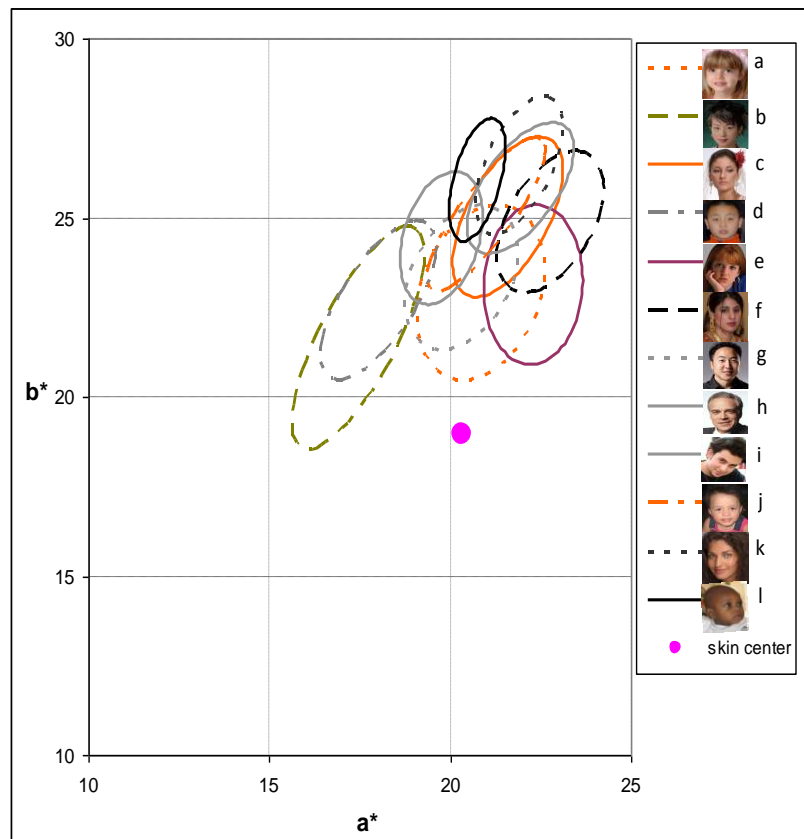
Fig. 4.2.2.1-2 Preferred skin colour ellipses of 12 test images (Experiment I-2)

Fig. 4.2.2.1-2 shows the preferred skin colour ellipses of 12 test images in CIELAB a*-b* coordinates (ignoring L*). The pink dot in the centre is the statistical skin colour centre. Again, each small ellipse, which covers about 50% of the sum of scaled positive z-scores, represents a preferred skin colour region judged by observers on an image. Each ellipse centre represents the preferred skin colour centre of its corresponding image. The orientation of the ellipse of Image *e*, with a major axis in vertical direction, is very different from other. The hue preference of this image is lower than overall trend as well. Preference of Image *b* has smaller chroma than others.

4.2.2.2 Inter-Observer Variation

The ellipse of the distribution of the preferred skin colour centre offset (Δa*, Δb*) from each observer on each image was generated and plotted in Fig. 4.2.2.2-1. This represents observer variation projected to a*-b* coordinates (ignoring L*). With smaller colour differences among nine versions of images, their sizes are smaller than those in Experiment I-1. Similar to Experiment I-1, variation in hue is smaller than variation in chroma.

All (Δa*, Δb*) of the 20 observers' preferred skin colour centres on 12 images were applied to generate an ellipse that covers 85% of the data points (see orange ellipses in Fig. 4.2.2.2-2). This is the observer variation projected into a*-b* coordinates. The ellipse from Experiment I-1 is plotted in black for comparison. The orientations and eccentricities in two ellipses are about the same. The size of the ellipse in Experiment I-1 is about twice of that in Experiment I-2, which corresponds to that the colour differences among nine versions of each image in Experiment I-1 are about twice to those in Experiment I-2. With smaller variation in test images, observers' judgment for skin colour preference was more consistent.

A preferred skin colour ellipse to cover 85% of individual preferred skin colours in Experiment I-2 is plotted in Fig. 4.2.1.4-2 (the blue ellipse). The preferred skin centre was changed to a slightly different position, and preferred skin colour ellipses from two phases are mostly overlapped. The results demonstrate that the experiments are reliable and repeatable. Although colour differences among nine versions of each test image in Experiment I-2 are about half of those in Experiment I-1, the preferred skin colour ellipse that represents the observer variation in Experiment I-2 is only slightly smaller than that in Experiment I-1.
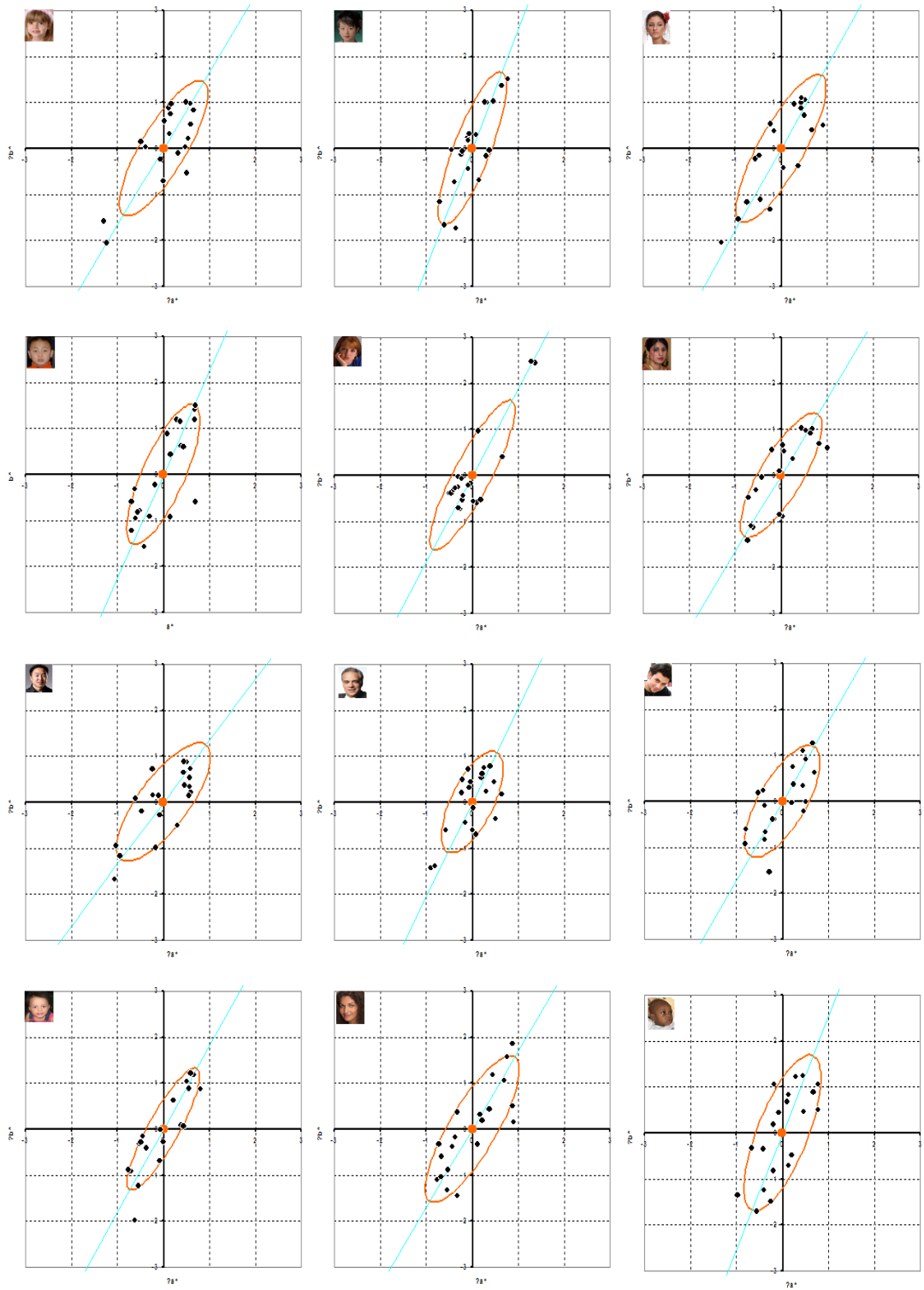
Fig. 4.2.2.2-1 Variations of observer judgments on each image in CIELAB a*-b* diagram (Experiment I-2)
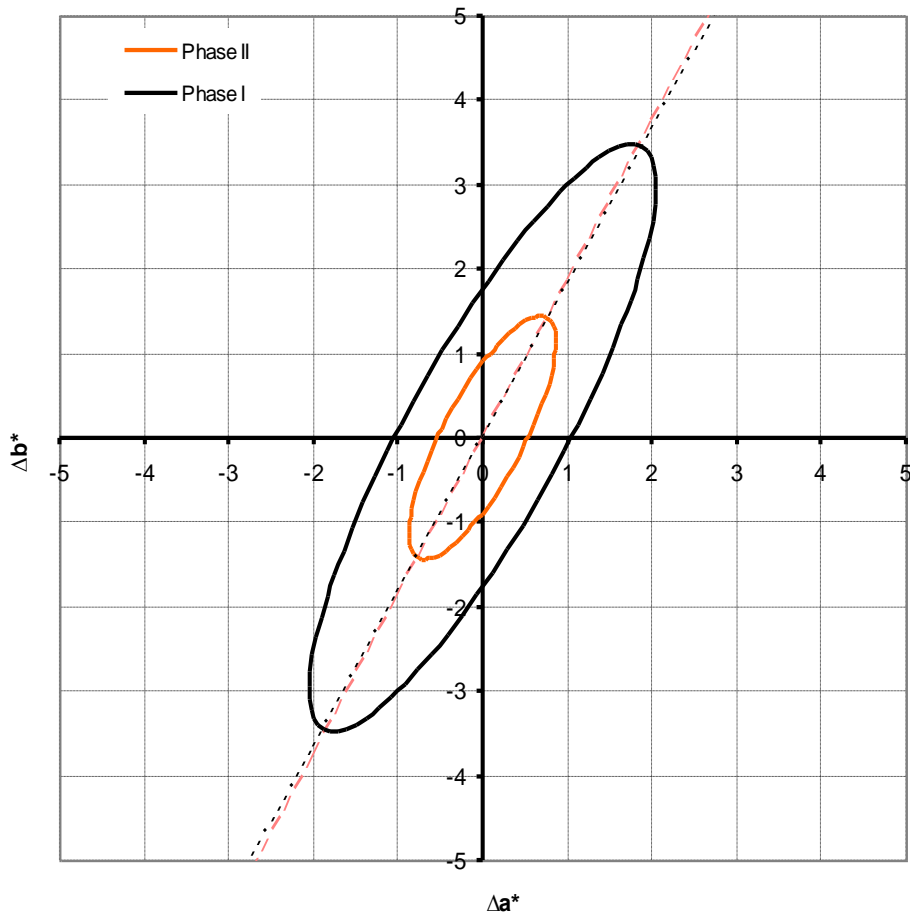
Fig. 4.2.2.2-2 Variations of all observer judgements on all images in CIELAB a*-b* diagram

4.2.2.3 Inter-Image Variation

Table 4.2.2.3-1 lists the preferred skin colour centre of each image computed using positive z-scores as weights. The colour difference (ΔE^*_{ab}) of each preferred skin colour centre against the average preferred skin colour centre were computed and listed in the last row. The inter-image variation is about the same as that in Experiment I-1.

Table 4.2.2.3-1 Preferred skin colour centres of individual images

Image	a	b	c	d	e	f	g	h	i	j	k	l	Average
a*	21.2	17.9	22.0	18.4	22.7	23.2	20.7	20.2	22.3	21.4	22.3	21.2	21.1
b*	24.2	22.9	26.3	24.0	24.4	26.2	24.6	25.7	27.1	26.4	27.8	27.4	25.6
C*$_{ab}$	32.2	29.1	34.3	30.2	33.3	35.0	32.2	32.7	35.1	34.0	35.6	34.6	33.2
h$_{ab}$	48.7	52.1	50.1	52.5	47.1	48.5	49.9	51.9	50.5	51.0	51.2	52.3	50.5
ΔE_{a*b*}	1.4	4.2	1.1	3.1	2.0	2.1	1.0	1.0	2.0	0.9	2.5	1.8	1.9

4.2.3 Discussion

4.2.3.1 Recalibration of Preferred Skin Colour Centre

Since the colour transformation using the display ICC profile of monitor #3 is most close to that by averaging the colour transformation using all five profiles, the display ICC profile of monitor #3 was used to convert display RGB to CIELAB for computing skin colour centres. The display ICC profile is modelled with a matrix plus R, G, and B tone curves for colour transformation. To improve the colour accuracy, the RGB colour of a final preferred skin colour centre (a*b*) obtained in Experiment I-2 with different lightness along with the monitor white point (R=G=B=255) and the monitor black point (R=G=B=0) were displayed on all five displays, and their colorimetric values were measured using an X-Rite Eye-One Pro spectrophotometer. The a*b* values of the preferred skin colour were averaged from the white point adapted colours of the measurement data. The differences between a measured skin colour value and the same colour computed using a display ICC profile are about (0.4, 1.3) in a* and b*, respectively. Hence, a*b* of about (0.4, 1.3) should be added to the results of preferred skin colours.

Preferred skin colours in all tables above have taken this set of calibration values into account. However, the calibration values are not added to any plots above.

4.2.3.2 Preferred Skin Colours from Experiments I-1 and I-2

The overall preferred skin colour (mixed preferred skin colour) may be computed by averaging preferred skin colours of 12 images. Another method is to generate a preferred skin colour ellipse using preferred skin colours judged by all observers and determine the ellipse centre as the overall preferred skin colour centre. Tables 4.2.3.2-1 and 4.2.3.2-2 list the results from Experiments I-1 and I-2. a*b* have been added by (0.4, 1.3) to calibrate the colour inaccuracy computed using a display ICC profile. Because some extreme observations were discarded while an ellipse is trained, an ellipse centre should be more representative for preferred skin colour centre than a mean colour.

Table 4.2.3.2-1 Mixed preferred skin colours computed with two different approaches (Experiment I-1)

Method	a^*	b^*	C^*_{ab}	h_{ab}
Mean	21.2	24.3	32.2	48.9^o
Ellipse centre	21.3	23.5	31.7	47.8^o

Table 4.2.3.2-2 Mixed preferred skin colours computed with two different
approaches (Experiment I-2)

Method	a^*	b^*	C^*_{ab}	h_{ab}
Mean	21.1	25.6	33.2	50.5^o
Ellipse centre	21.2	24.7	32.6	49.4^o

It has been mentioned in Section 4.2.2.1 that the colour preferences of Image *b* and Image *e* are different from the overall trend. To investigate this problem, nine versions of adjusted images of each test image were analysed to see if in some test images, the deviation of nine versions of adjusted images were not sufficient for distributing their skin colours around a most preferred skin colour centre.

For each test image, the mean skin colours of nine adjusted images were computed, and the average of these mean colours was computed. ΔE^*_{ab} of each of nine mean colours to the average of nine mean colours represents ΔE^*_{ab} of the skin colours of the corresponding adjusted image to the average skin colours of the all nine adjusted images. An average ΔE^*_{ab} from ΔE^*_{ab} of 12 images was computed. In Experiment I-1, average ΔE_{ab} of 12 images are in the range of 5.6 to 6.8, while the range is from 2.4 to 3.0 in Experiment I-2. If the mean skin colour of an image is more than 3.0 ΔE^*_{ab} away from its most preferred skin colour, the skin colour adjustment function may not be able to produce nine versions of adjusted images whose mean skin colours are distributed around a most preferred skin colour centre. Fig. 4.2.3.2-1 illustrates another evident that the range of adjustment is potentially not sufficient. The plot shows Z-scores averaged from all 12 images for each skin colour centre in Experiment I-2. The most preferred regions are E and H. These two regions have about the same Z-score. A more preferred colour centre could be somewhere further away from H if nine predetermined colour centres were in a larger region. Since the result from Experiment I-2 is very close to Experiment I-1, if the range to adjust skin colours in Experiment I-2 is not sufficient for some images, it is probably very small.

Although the denser sampling density of skin colours in Experiment I-2 should improve the accuracy mathematically for computing preferred skin colours through interpolation (weighted averaging) in a small area, the potential insufficient range of the skin colour distribution of nine adjusted images on some test images makes the result less reliable and may degrade the colour accuracy as well. Consequently, the result from Experiment I-1 is believed to be more reliable and potentially more accurate.

Although an ellipse centre is probably more representative for preferred skin colour centre than a mean colour, preferred colour centres obtained from these two

approaches are about the same (see Table 4.2.3.2-2). The result of the preferred mixed skin colour is about (21, 24) for (a*, b*) with a hue angle of 49°.
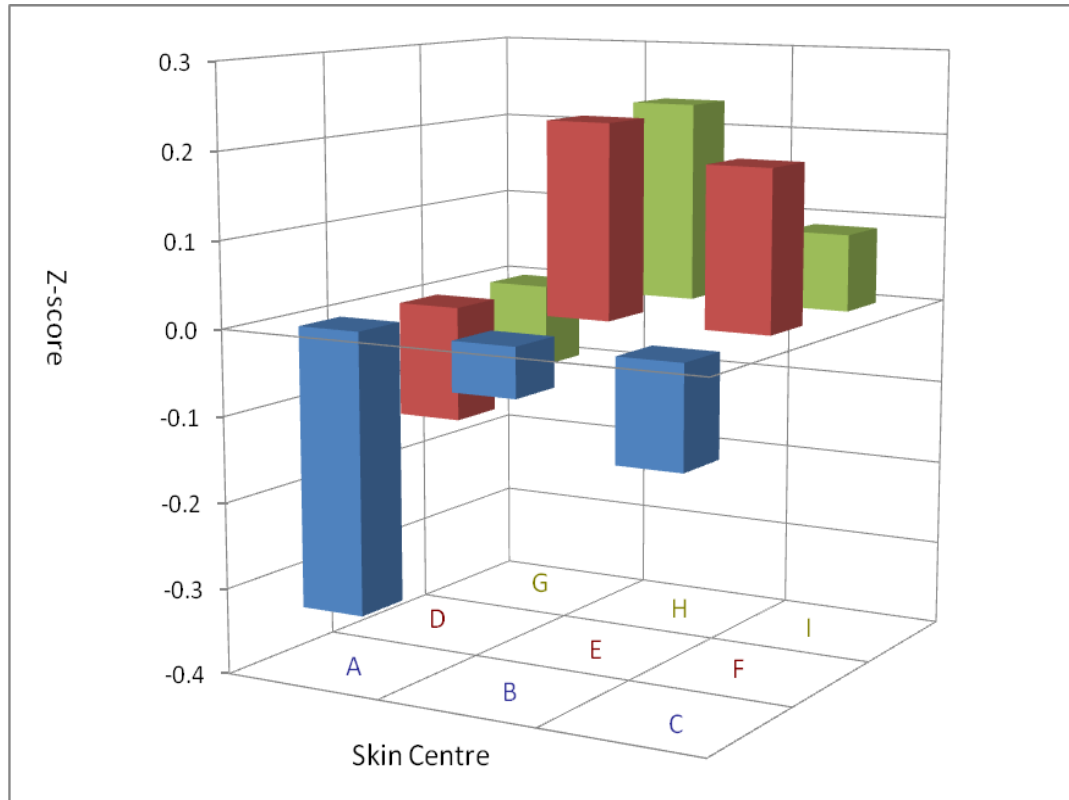
Fig. 4.2.3.2-1 Mean Z-score in each skin colour centre (Experiment I-2)

4.2.3.3 Comparing the Present Studies to Others

To compare preferred skin colours with real skin colours, the RIT and Oulu spectral data sets of skin colours were analysed (RIT Munsell Website, Sun and Fairchild 2002, Martinkauppi 2002). CIE XYZ values of each skin colour were computed using D65 illuminant, and then adapted to D50 using the linear Bradford chromatic transformation (same as that used to create display ICC profiles) and finally converted to CIELAB values. The skin colours of three categories are plotted: African (black 'x'), Asian (pink 'x'), and Caucasian (orange 'x') (see Fig. 4.2.3.3-1). The preferred skin colour centres found from the present study are circled with a small black ellipse. The largest ellipse is the skin colour boundary. Except for the result obtained by Sanger in which Japanese prefer less chromatic skin colours on the three ethnic groups (Caucasian, Japanese, and African), preferred skin colours are clearly more chromatic than real skin colours from all other studies. This confirms that the memory skin colour is more colourful than real skin colours. The hue angle of the preferred Caucasian skin colour is slightly more yellowish than that of the real Caucasian skin colour. The preferred Oriental and African skin colours are slightly more reddish than real Oriental and African skin

colours, respectively. Since a single group of observers judges images of all skin types, the preferred skin colours of Caucasian, Oriental, and African from the present study represent cross-culture preference. This may be the reason that three preferred skin colour centres have very small discrepancies.
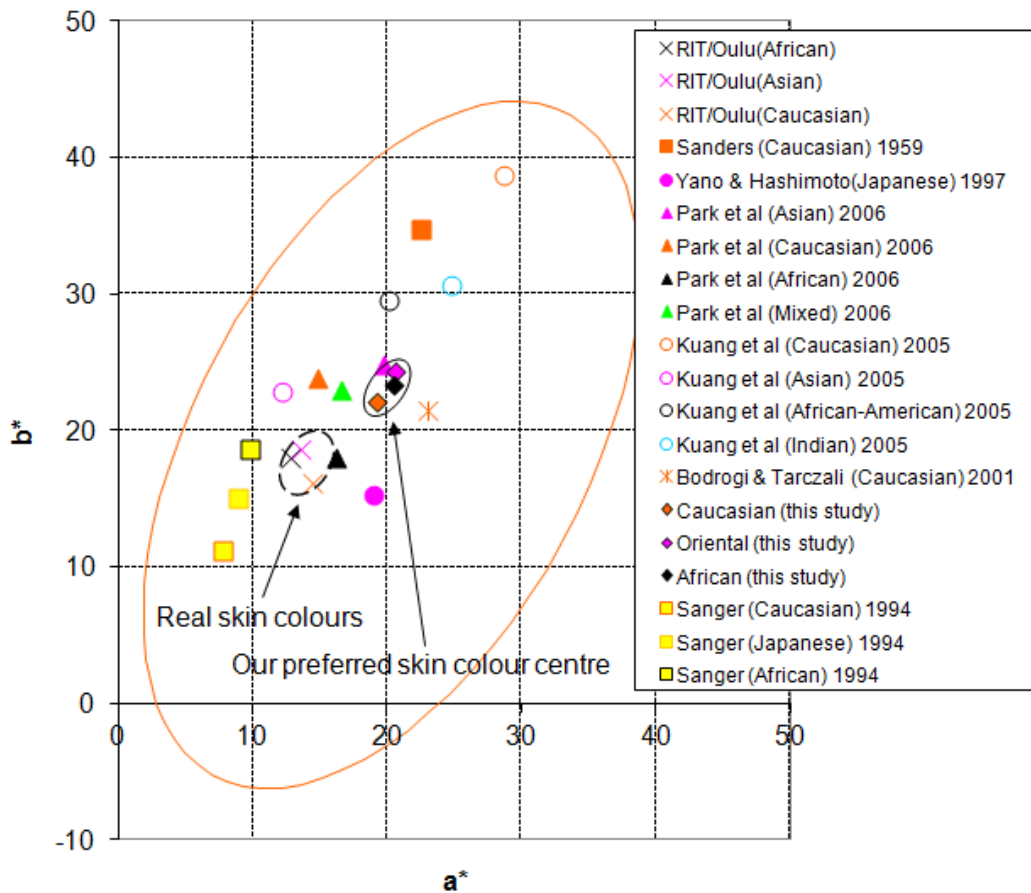
Fig. 4.2.3.3-1 Skin colour centres in CIELAB a*-b* coordinates (adapted to D50) from different sources

The remark from Hunt et. al. that preferred Caucasian skin colours were slightly more yellowish than the real skin colours agrees with results from many other studies. However, Hunt's finding that the chroma of preferred Caucasian is about the same as that of the real skin colour is different from the results of the present study and most of other reports.

Sanders' result of the preferred Caucasian face colour centre under C illuminant is $(x, y) = (0.441, 0.379)$. Converting the colour with different Y values to CIELAB under D50, the hue angle is about 57°. Since the mean L* of Caucasian and Asian skin colours computed from the skin image database is about 60, it was applied to compute Sander's preferred Caucasian skin colour. The result is a*b* = (22.6, 34.7) (the orange square in Fig. 4.2.3.3-1). The preferred hue angle is almost

10° higher than the real Caucasian skin colour, and is about 8° higher than that of the preferred Caucasian skin-tone of the present study. The colour is more chromatic than that from the present study.

Sanger's result of preferred Caucasian, Japanese, and African skin tones judged by Japanese in D65 are (x, y) = (0.355, 0.351), (0.367, 0.360), (0.387, 0.373), respectively. Assume L* to be 60 for Caucasian and Japanese and 50 for African, their a*b* adapted to D50 are (7.8, 11.2), (8.9, 15.1), and (9.8, 18.6), respectively. All preferred skin colours are less chromatic than actual skin colours.

The average preferred Japanese complexion found by Yano and Hashimoto is (u', v') = (0.2425, 0.4895) in D65 illuminant, or (x, y) = (0.3881, 0.3482). Assuming L* = 60, the preferred skin colour is a*b* = (18.9, 15.4) (the pink solid circular dot in Fig. 4.2.3.3-1). Its chroma is lower than the result of the present study. Its hue angle is about 39°, which is lower than the present result as well.

Kuang et. al. studied colour preferences of different skin-tones under different conditions for photographic colour reproduction. The preferred skin colour centres of Caucasian, Asian, African-American, and Indian found by them were marked with small circles in Fig. 4.2.3.3-1. The chroma of the preferred Caucasian skin colour is unreasonably higher than the results from other researches; but the hue angle (53°) is only slightly higher than that of the present results. The preferred Asian skin colour is slightly more colourful than that of real skin colours; however, the hue angle (62°) seems to be very high.

Park et. al. defined a memory skin colour ellipse and adjusted skin colours within the large skin colour ellipse toward a smaller skin memory colour ellipse to improve skin colour preference. The skin colour centre was used as the memory skin colour centre (the preferred skin colour centre) in their skin colour enhancement. This is different from our approach in which the centre of skin colour ellipse and the preferred skin colour ellipse are different. Their skin colour centres for East Asian, Caucasian, African, and Mixed skin colours represented in YC_bC_r colour space were converted to RGB and then to CIEXYZ using sRGB specification, adapted to D50, and finally transformed to CIELAB for comparison. The results are (51.4, 19.8, 24.8), (64.7, 14.8, 23.9), (40.5, 16.3, 18.0), and (56.8, 16.6, 23.0), respectively (see triangles in Fig. 4.2.3.3-1). Their hue angles are 52°, 59°, 48°, and 54°, respectively. The skin colour centre for East Asian is similar to the present finding for mixed skin colours, the preferred Caucasian skin colour centre is more yellowish than the present finding, and the preferred African skin colour centre is much less chromatic than the present finding.

Bodrogi and Tarczali found that skin colours shifting towards its memory prototypical colour centre occurred not only in photo contents but also in standalone colour patches, although the memory colour shift in standalone patches was weaker. This suggests that preferred skin colour adjustment may be applied to non-skin skin colours as well, but with less adjustment. With complete adaptation of their bluish reference white to D50, their memory skin colour centre is plotted as an orange star in Fig. 4.2.3.3-1. The memory skin colour is more reddish compared to those from other studies. One reason is that their memory colour study is different from the study of preferred colours, and to compare their data to others a complete adaptation from the bluish white to D50 was assumed.

The preferred skin colours plotted in Fig. 4.2.3.3-1 are spread in a small hue range, with a mean hue angle of 52° and a standard deviation of 7°. The mean hue of preferred skin colours is about the same as that of real skin colours, while chroma of preferred skin colours are significantly higher than those of real skin colours. The variation in chroma is larger than the variation in hue, which is similar to that of the inter-observer variations of the present study.

A serial of psychophysical experiments were further conducted and will be presented in next few sections. These experiments confirm the repeatability of our experimental method and verify the reliability of our experimental results.

4.2.3.4 Tolerances in CAM02-UCS

Preferred skin colour ellipses confine within a small hue range and a relatively large chroma range. In other words, there is smaller tolerance in hue than in chroma. To study whether this is related to the colour space uniformity of the skin colour region in CIELAB colour space and whether the uniformity is improved in CAM02-UCS, the observer data from Experiment I-1 were plotted in CAM02-UCS for comparison (see Fig. 4.2.3.4-1). It can be seen from Figures 4.2.2.2-1 and 4.2.3.4-1 that the ellipses in CAM02-UCS are closer to circle than ellipses in CIELAB colour space. However, no matter what colour space is used, hue tolerance is tighter than chroma tolerance.

An ellipse to cover 85% of all observer preferred skin colour centres on all images is generated and compared with that generated in CIELAB colour space. The ratio of the major axis over the minor axis, *A/B*, in CIELAB and CAM02-UCS from all observers on all images are 4.2 and 3.0, respectively. The result that *A/B* in CAM02-UCS is closer to unity indicates that CAM02-UCS is slightly more uniform in representing skin colours.
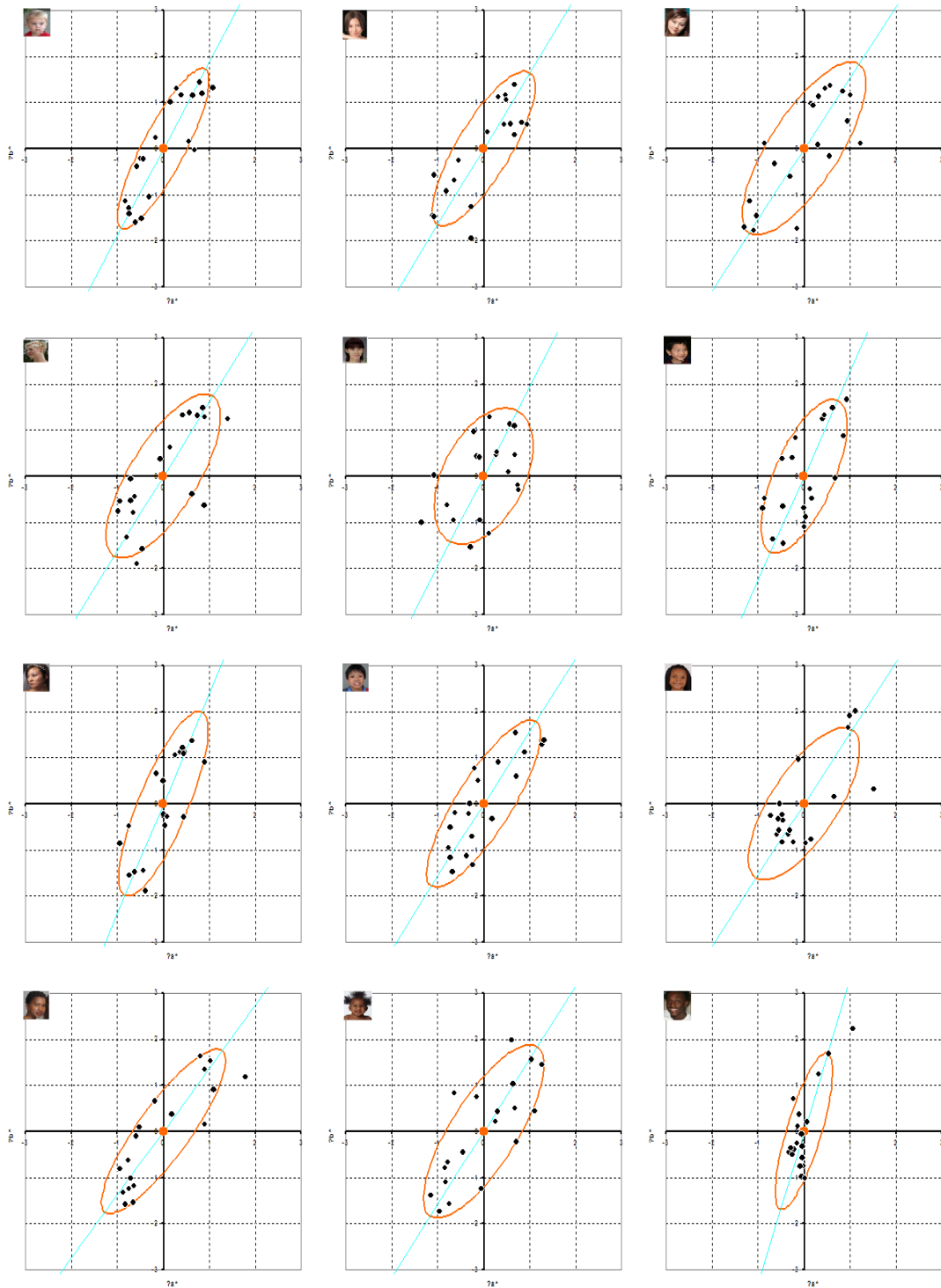
Fig. 4.2.3.4-1 Variation of observer judgments (Experiment I-1) on each image in CAM02-UCS chroma coordinates

4.2.4 Summary

Psychophysical experiments were conducted to evaluate skin colour preference and tolerance. The findings from the psychophysical experiments are summarized below: 1) preferred skin colours are more chromatic than real skin colours; 2)

observer variances in skin colour preference are larger in chroma than in hue, i.e. hue tolerance is tighter than chroma tolerance; 3) the preferred skin colour centre for mixed skin colours is about (21, 24) for (a*, b*) with a hue angle of 49° in D50 illuminant; 4) the preferred Caucasian skin colour is slightly more yellowish than average real Caucasian skin colour, and preferred Oriental and African skin colours are slightly more reddish than their real skin colours; and 5) CAM02-UCS is slightly more uniform than CIELAB in the skin colour region.

4.3 Experiment II: Chinese Skin Colour Preference Judged by Chinese

The objective of this experiment was to find the preferred Chinese skin colour judged by Chinese and to exam the reliability of the experimental method by analysing the results of this experiment and Experiment I.

The experimental procedure in Experiment I was utilized. Since the colour range for skin colour adjustment in Experiment I-2 may be slight too small, a larger range of nine skin colour centres were selected to adjust skin colours. Four Chinese portrait images (see Fig. 4.3-1) were judged by 19 Chinese observers through paired comparison. Images were displayed on a 24-inch Eizo ColorEdge CG241W TFL active matrix LCD monitor which has a native resolution of 1920x1200, a 12-bit LUT for each of R/G/B channels, and a wide gamut covering about 96% of Adobe RGB gamut. The monitor was calibrated to achieve gamma value of 2.2, luminance of 120cd/m^2, and a white point of D65 using ColourNavigator CE software and Eye-One Pro.

Man   Woman   Boy   Girl

Fig. 4.3-1 Images to judge Chinese skin colour preference

The preferred skin colour centre found in the prior experiment was selected as the initial preferred skin centre for the experiment. A set of nine preferred a*b* centres was used to produce nine versions of images for pair comparison. Table 4.3-1 shows the set of a*b* centres. In Fig. 4.3-2, the cross points ('x') noted with *A, B, …, I* are the nine pre-determined skin centres for this experiment; and the black circle dots noted with 1, 2, …, 8 are the nine colour centres used in Experiment I-1

of the prior experiment. Point #E is the preferred colour centre found in the prior experiment. The predetermined skin colour centres for this experiment is slightly coarser than those in Experiment I-2. The skin colour ellipse model is the same as that in Experiment I-2. The method of skin colour morphing is exactly the same as that of Experiment I-2 as well.

Table 4.3-1 Nine preferred skin colour centres

	A	B	C	D	E	F	G	H	I
a*	20.9	25.9	30.9	16.1	21.1	26.1	11.3	16.3	21.3
b*	12.7	21.8	30.8	15.3	24.4	33.5	18.0	27.0	36.1
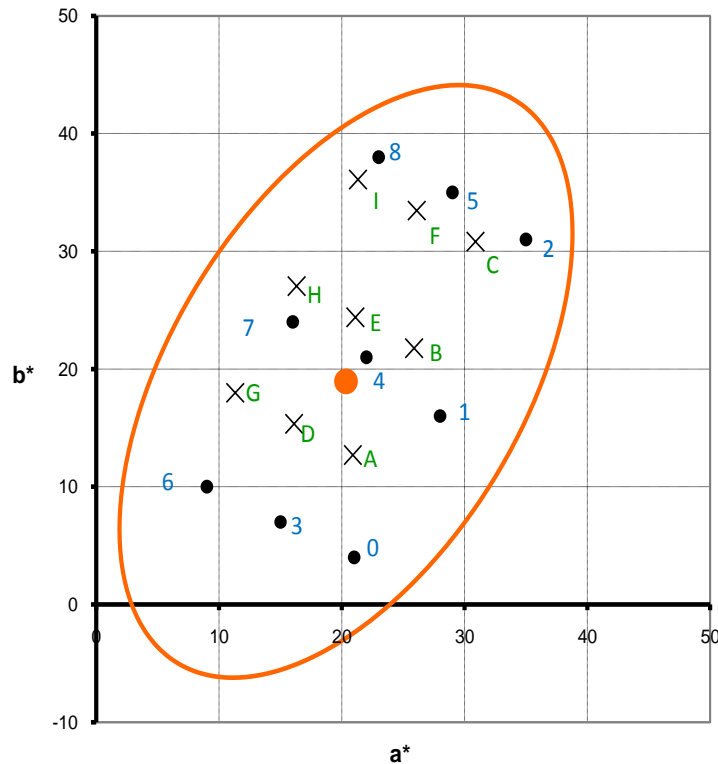
Fig. 4.3-2 Nine predetermined skin colour centres to test Chinese skin colour preference

4.3.1 Experimental Result and Discussion

Among the nine versions of images processed from each of four images, skin colours are different and non-skin colours are the same. There are 36 pairs to judge on each test image. Each pair of images was displayed on the monitor screen side by side. Observers were asked to select a more preferred one between two images based on their judgment on overall colour preference.

Again, the Thurston's Law of Comparison Case 5 was used to analyse the result. The z-scores of each image at skin centres *A* to *I* obtained from all observers are shown in Table 3.4.1-1. The first column is the image name. The 2nd to 9th columns are the z-cores at skin centre *A*, *B*, …, *I*, respectively. The last column is the 95% confidence interval. The last row lists the average z-scores of all images. A higher z-score means stronger preference. Fig. 4.3.1-1 shows the z-scores of each image. The error bars correspond to the 95% confidence interval. Overall, there is a relatively stronger preference at skin colour centres *A*, *B*, *C*, *E* and *F*; and a very strong dislike at the centre *G*. The overall preferences of all four images are very similar.
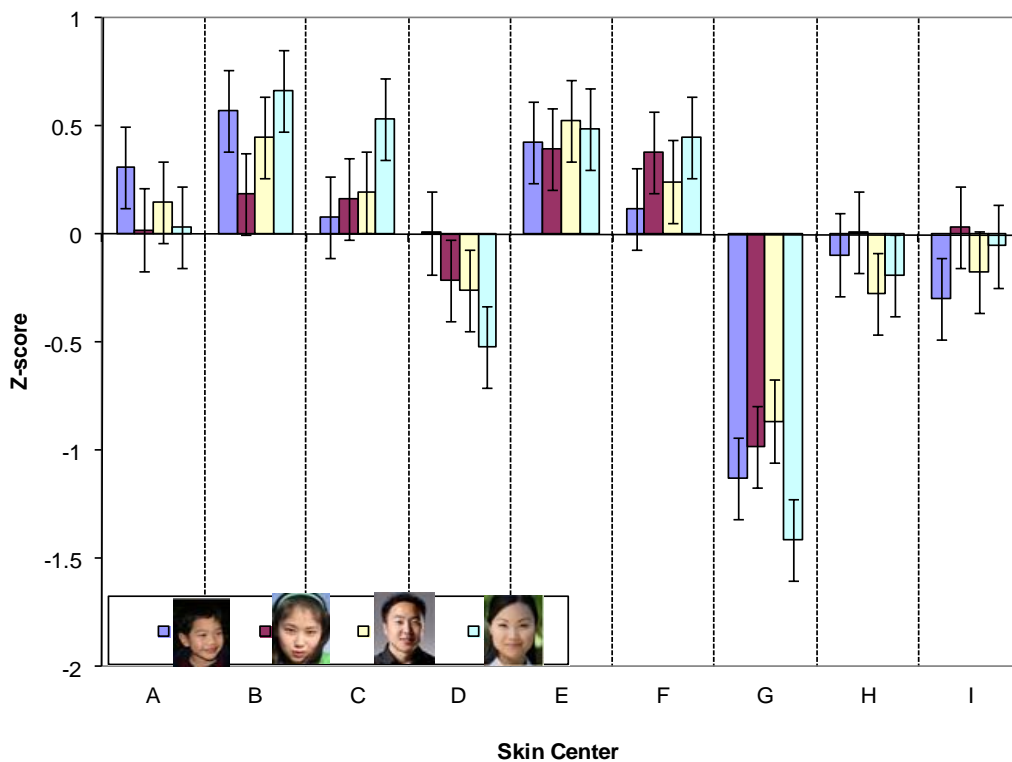
Fig. 4.3.1-1 Preference scores of individual images

Table 4.3.1-1 Z-scores of each image obtained from all observers

	A	B	C	D	E	F	G	H	I	95% confidence
Boy	0.31	0.57	0.08	0.01	0.43	0.12	-1.13	-0.09	-0.30	0.32
Girl	0.02	0.19	0.16	-0.21	0.40	0.38	-0.98	0.01	0.03	0.32
Man	0.15	0.45	0.20	-0.26	0.53	0.25	-0.86	-0.27	-0.17	0.32
Woman	0.04	0.67	0.53	-0.52	0.49	0.45	-1.41	-0.19	-0.05	0.32
Average	0.13	0.47	0.24	-0.25	0.46	0.30	-1.10	-0.14	-0.12	0.32

The average Z-scores were computed from all images and shown in Fig. 4.3.1-2. The skin centre *G* is strongly disliked, and skin centres *B*, *E*, and *F* are strongly

preferred. Fig. 4.3.1-3 shows that observer's most preferred pick of skin centre is not on boundaries. It implies that the region for the preset of nine skin colours is large enough for judgment.
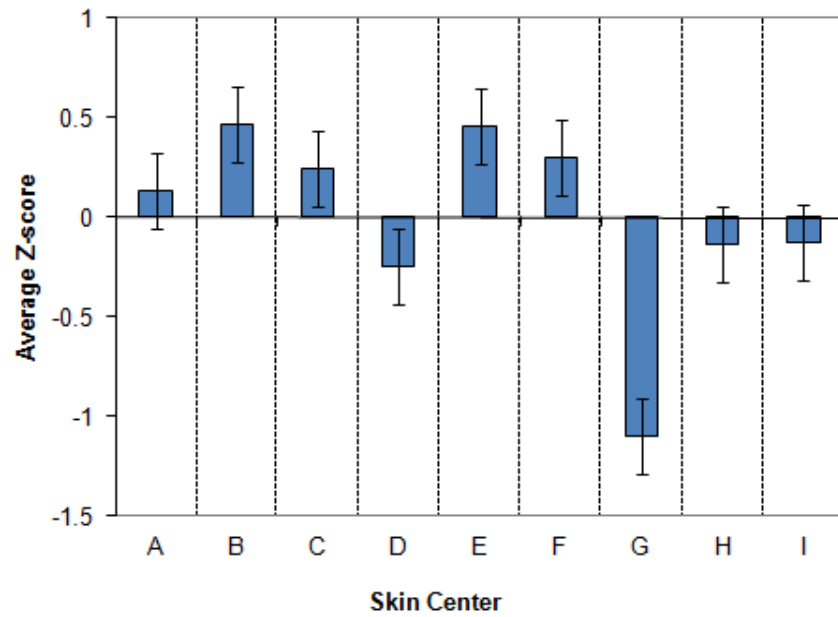
Fig. 4.3.1-2 Overall preference scores from all images
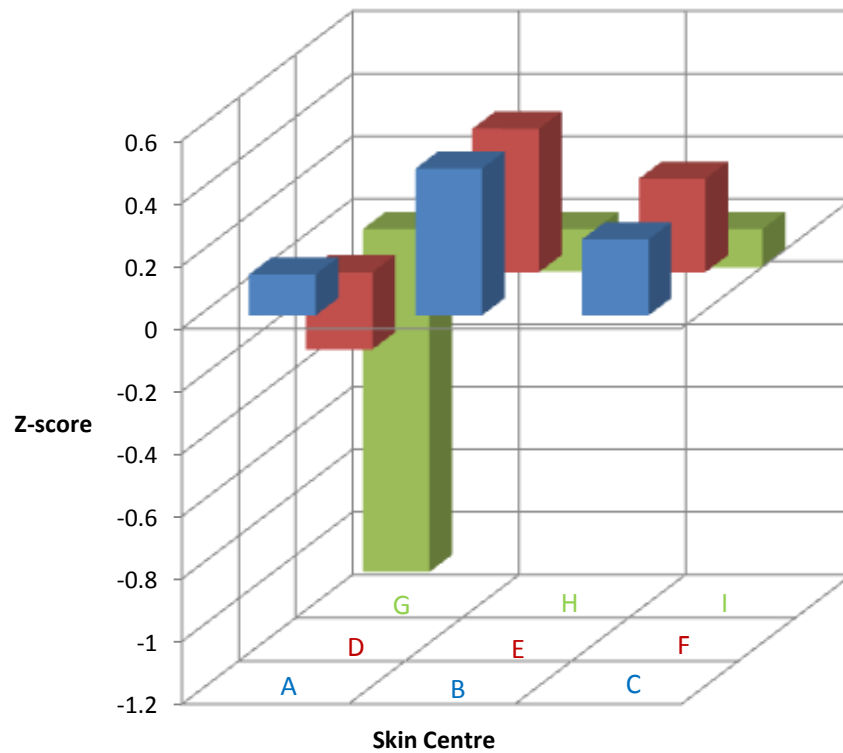
Fig. 4.3.1-3 Overall preference scores from all images

4.3.2 Determine a Preferred Skin Colour Centre

Since observers rated images based on the skin colour appearance of test images, the preference of skin colours should directly correlate to skin colours of test images. Consequently, skin colour distribution of each test image was applied to compute preferred skin colours. Similar to Experiment I, a skin mask was made from each original image, and a mean skin colour was computed for each version of adjusted images. Again, images with negative z-scores were considered unacceptable, positive z-scores and their corresponding versions of images were used to train preferred skin colour ellipses and to compute a z-score weighted average colour as a final preferred skin colour. The result is shown in Table 4.3.2-1. The final average preferred skin colour centre is a*b* = (19.9, 23.0). This is slightly different from (20.7, 24.4), the preferred Oriental skin colour centre judged by observers with mixed culture backgrounds in Experiment I.

Table 4.3.2-1 Preferred skin colour centres of all four images

	Boy	*Girl*	*Man*	*Woman*	*Mean*
a*	21.0	19.8	20.8	17.9	19.9
b*	22.9	24.5	22.6	22.2	23.0
C*	31.1	31.5	30.7	28.5	30.4
h_{ab}	47.6°	51.0°	47.5°	51.1°	49.3°
ΔE^*_{ab}	1.1	1.4	1.0	2.2	1.4

4.3.3 Summary

This psychophysical experiment was designed to study the skin colour preference of Asian skin tone judged by Chinese. The preferred skin colour centre was found to be a*b* = (19.9, 23.0) in D50 computed using a method of weighted average of mean skin colours of nine versions of each test image and their corresponding z-scores. This is slightly different from (20.7, 24.4), which is the preferred Oriental skin colour centre judged by observers with mixed culture backgrounds in Experiment I-1. Although the hue angles of the two are very close, the result from the current experiment is slightly less chromatic. The result suggests that Chinese prefers slightly less chromatic Oriental skin colours.

4.4 Experiment III: Skin Colour Preferences of Africans, Caucasians, and Orientals

Skin colour preferences for different ethnic skin tones judged by observer groups with mixed ethnic backgrounds have been studied in Experiment I, and the

Chinese skin colour preference judged by Chinese has been studied in Experiment II. However, these two experiments did not answer all questions about skin colour preferences of single-culture backgrounds and cross-culture backgrounds. This study was to investigate the skin tone preferences of following two aspects: skin tone preference by ethnicity (an ethnic group's skin tone preference of its own ethnic group), and skin tone preference across ethnicities (an ethnic group's skin tone preference of other ethnic groups). The result was to be used for optimising skin colour reproduction of colour imaging products for different geographical regions.

4.4.1 Experimental

Images were displayed on LCD monitors under the dim surround condition in the previous studies. In this study, an HP P1100 21-inch CRT monitor was used to display images in a completely dark room. An African image, a Caucasian image, and an Oriental image were chosen for judgment (see Fig. 4.4.1-1). Similar to Experiments I and II, CIE a*b* of skin colours of each image was adjusted to produce nine versions of images for paired comparison. 18 Caucasians (British dominated), 16 Africans from Africa and UK, and 21 Oriental observers (19 Chinese and 2 Korean) judged all three images. All observers were between 19 and 45 years old, and they all passed through Ishihara's Tests for Colour-Blindness.

African   Caucasian   Oriental

Fig. 4.4.1-1 Images to judge skin colour preferences

The parried-comparison method was chosen for the experiment to determine a preferred skin colour centre. Nine versions of adjusted images were produced for each image. The total number of judgements on each image by an observer is 9x8/2 = 36. As a pair of images was displayed on the display each time, the remaining area of the display was filled with uniform medium gray. Each observer was instructed to sit at a distance that was most comfortable for viewing, followed by the presentation of an image pair on display at a time, and was asked to indicate which rendition of the two was preferred for skin colours. After the response was recorded, the next image pair was loaded and the observer proceeds until all samples were evaluated. All 36 pair combinations of the nine treatments were presented to

each observer via a script that randomized the order and the placement (left/right) of the treatments.

4.4.1.1 Skin Colour Adjustment for Psychophysical Experiment

Skin colours of each image were detected using a skin colour model and were morphed toward nine different directions to produce nine versions of images. Psychophysical experiments were conducted to determine preferred skin colour regions for preferred skin colour enhancement. A pair of images from the nine images was displayed on the monitor screen each time for paired comparison.
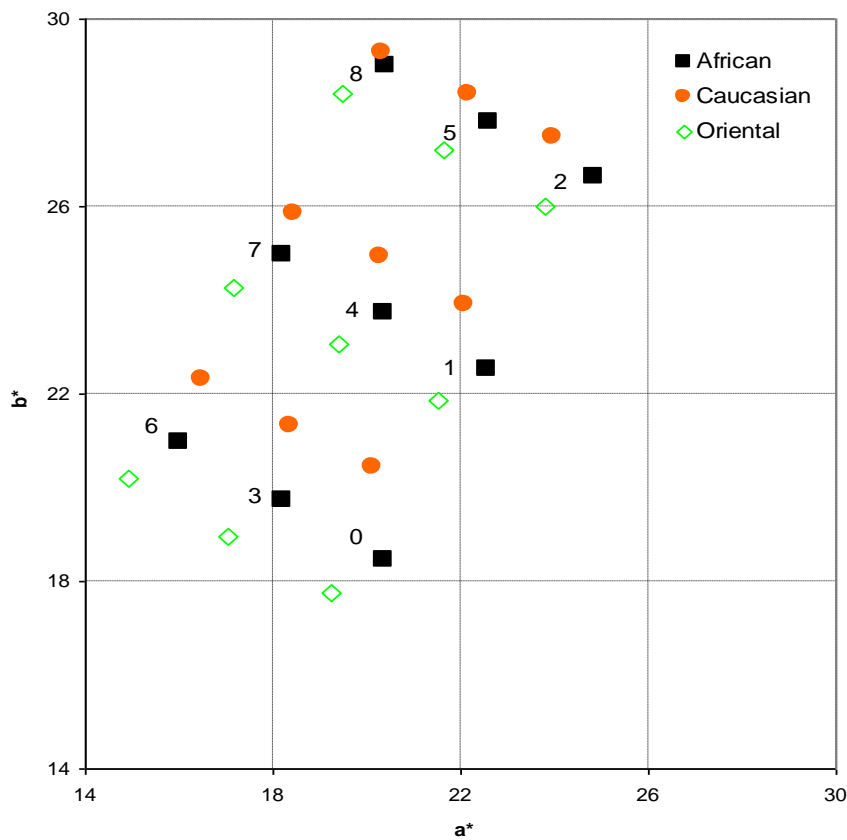
Fig. 4.4.1.1-1 Mean skin colours of nine versions of images processed from three original images

A skin mask was created from each original image to determine skin colours that were used to compute a mean skin colour to represent the skin colour of a test image (referred to Sections 4.2). A mean skin colour of each image version was computed by averaging colours of skin pixels. Fig. 4.4.1.1-1 shows the mean skin colours of nine versions of images processed from every test image. A successful design is to have each set of nine mean skin colours distributed around observers' preferred skin colour centres. A simple approach to meet this requirement is to have these nine images distribute around a large skin colour region. However, since a

final preferred skin colour centre is to be interpolated from all or some of these nine colours using Z-scores or frequencies as weights, the accuracy from interpolation will degrade if these nine colours spread around a large region. Therefore, the best design is to have these nine skin colour centres spread around a region just enough to cover observers' preferred skin colours. However, since preferred skin colours were not known yet, parameters to determine how to spread these nine skin colour centres were guessed based on the knowledge from prior experiments.

This experimental method has been used in Experiment I and Experiment II. In Experiment I-1, nine skin colour centres were distributed around a statistical skin colour centre and were spread on a large region. An approximate preferred skin colour was derived. In Experiment I-2, nine skin colour centres were distributed around this approximate preferred skin colour centre and were spread on a smaller region. It was later found that a parameter to control the range of spreading was not large enough in Experiment I-2. In this experiment, the parameter to control the range of spreading was set to be a value half way between the values in these two phases. However, because a different monitor that has a smaller colour gamut was used to display images and the computation of spreading was in the device RGB colour space, the spreading of nine skin colour centres were not as large as expected.

4.4.1.2 Display Colour Characterisation

An X-Rite Eye-One Pro sensor was used to measure the monitor display for colour characterisation. Because the display's white point was close to D65 and the gamma value of each primary was close to 2.2, the original video LUT was not adjusted. An ICC profile was generated for the display colour transformation. The ICC profile was formulated with a model using a 3x3 matrix and a set of R, G, and B tone curves for the transformation between CIEXYZ and display RGB.

A comparison of the display colour gamut and sRGB gamut is shown in Fig. 4.4.1.2-1. The gamut shapes in the skin tone region, in which we are interested, are very close with each other. A top-down view of sampling points in entire gamut is shown in Fig. 4.4.1.2-2 where dots are sRGB sampling points, and the length of each line represents the colour difference between an sRGB colour and a corresponding P1100 CRT display colour with the same driving RGB digital counts. It shows that colour differences between the display and sRGB are very small in the skin tone region.

The display was also characterised with measurement using a Konica Minolta CS-1000A/ST spectroradiometer. Fig. 4.4.1.2-3 shows gamut differences using two colour characterisation sets. Fig. 4.4.1.2-4 shows colour differences of 7x7x7 uniformly sampled RGB colours transformed using two colour characterisation sets.

Colours in green, blue, and magenta regions characterised with measurements using two different instruments are very different. Fortunately, colours in the skin colour region are very close with each other.
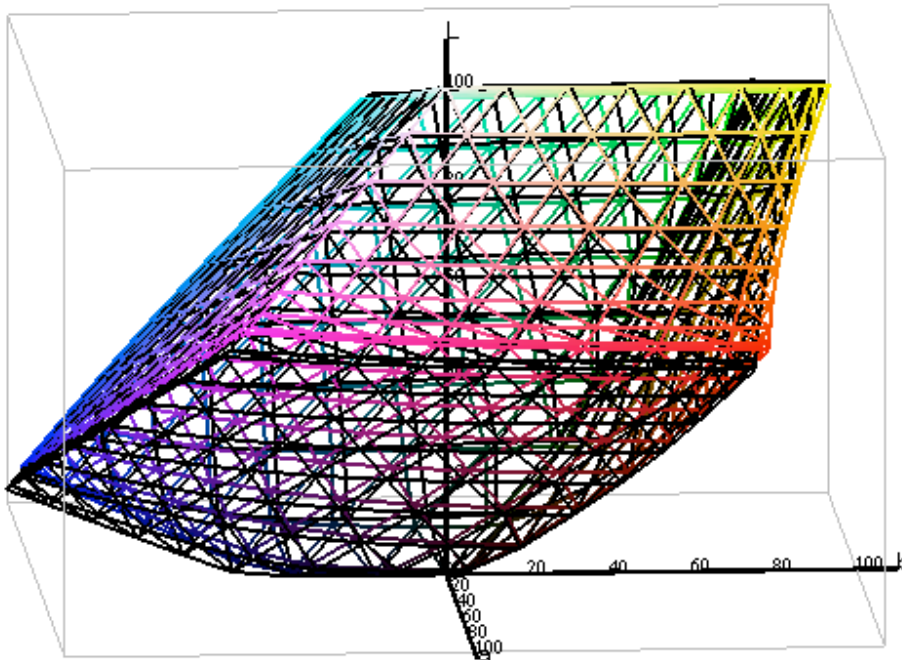
Fig. 4.4.1.2-1 Gamut comparison between the display (colour) and sRGB (black)
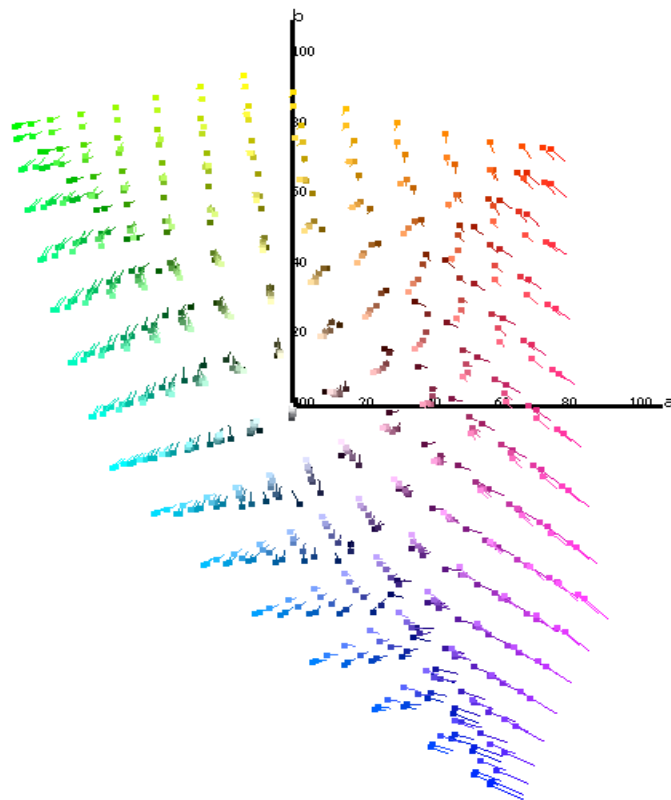
Fig. 4.4.1.2-2 Colour differences between the display and sRGB on 7x7x7 RGB uniform sampling grids
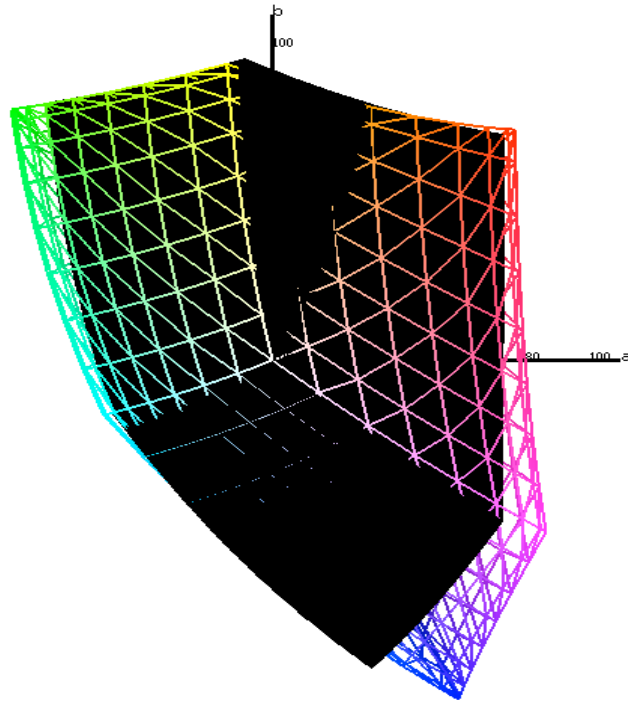
Fig. 4.4.1.2-3 The results of the display colour gamut characterised using X-Rite Eye-One Pro (colour) and Konica Minolta CS-1000A/ST (black)
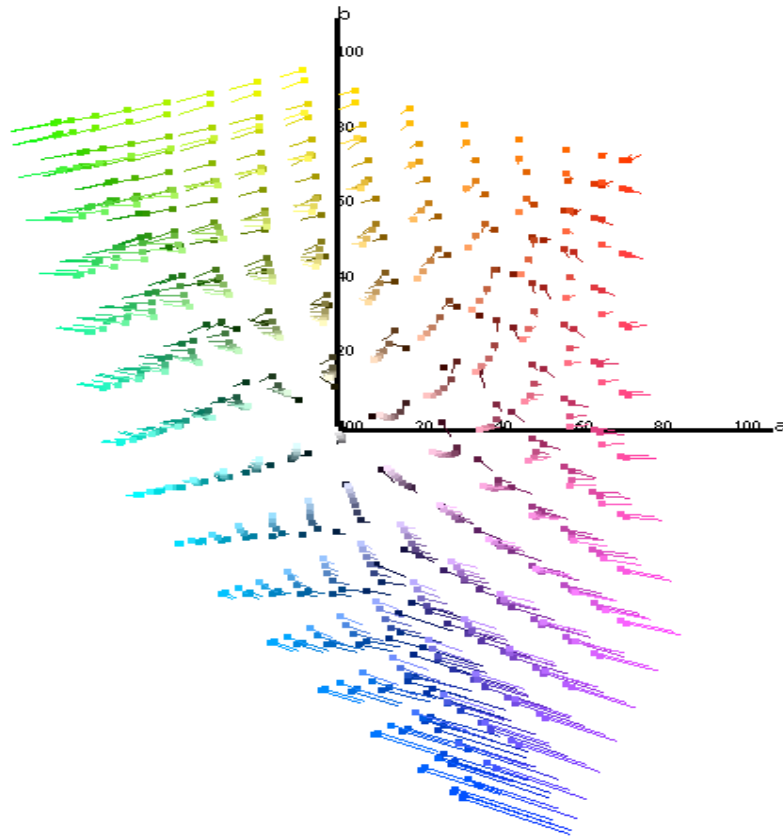
Fig. 4.4.1.2-4 Colour differences of the display characterised using X-Rite Eye-One (line end) and Konica Minolta CS-1000A/ST (dot)

To numerically study the colour consistency in the skin colour region measured using two instruments, skin colours among a 17x17x17 uniformly sampled sRGB colours detected using a skin colour model were analysed. 159 skin colours were obtained. These colours in RGB colour space were converted to CIEXYZ using both colour characterisation sets, adapted to D50, and finally converted to CIELAB. The colour differences are listed in Table 4.4.1.2-1. The colour differences of skin colour patches of Munsell Colour Checker, patches #0 and #1, were listed in Table 4.4.1.2-2. Both data sets show that ΔC^*_{ab} contributes to most of the colour difference between two instruments.

Table 4.4.1.2-1 Inter-instrument colour difference of 159 skin colours

Mean ΔE^*_{ab}	Max ΔE^*_{ab}	Mean ΔL^*	Mean ΔC^*_{ab}	Mean ΔH^*_{ab}	Mean ΔE_{00}	Max ΔE^*_{00}
1.7	4.3	0.2	1.6	0.8	1.0	2.5

Table 4.4.1.2-2 Inter-instrument colour difference of two skin colours in Munsell Colour Checker

ΔE^*_{ab}	ΔL^*	ΔC^*_{ab}	ΔH^*_{ab}
1.5	0.4	1.4	0.5
1.1	0.4	1.0	0.8

In this study, an ICC profile generated using data measured with an Eye-One was used for colour transformation. The colour transformation model in the ICC profile contains a set of R, G, and B 1-D lookup tables for RGB linearization and a 3x3 matrix for the colour transformation between RGB and CIEXYZ.

To numerically investigate the colour accuracy of the colour transformation in the skin tone region, a skin colour, $L^*a^*b^* = (60, 21, 24)$ in D50 illuminant, in the preferred skin colour region was converted to RGB of the display using the display ICC profile; and then a uniform colour patch with this RGB colour was displayed on the screen and measured using the Eye-One spectrophotometer. A white patch (RGB=255, 255, 255) was measured as well, which was to convert absolute colours to colours relative to the white point of the display. The measured skin colour in CIEXYZ colour space was fully adapted to D50 using the linear Bradford chromatic adaptation matrix and converted to CIELAB. The result was (60.8, 21.9, 23.9). The ΔE^*_{ab} between the direct measurement and from the colour transformation using the ICC profile is 1.2.

The same RGB colour patch and the white patch were also measured using the CS-1000A/ST spectroradiometer. The skin colour was adapted to D50, and

converted to CIELAB, which became (60.5, 21.6, 23.8). The ΔE^*_{ab} between the direct measurement and from the colour transformation using the ICC profile is 0.8.

The above analysis shows that the colour transformation using the ICC profile is about 1 ΔE^*_{ab} in the skin colour region. The major chromaaticity error is in a*. The a*b* computed using the ICC profile should add about (0.9, -0.1) to correlate with the measurement using Eye-One, or add about (0.7, -0.2) to correlate with the measurement using CS-1000A/ST. The ΔE^*_{ab} for the skin colour measured using two instruments is 0.4, which is very small.

4.4.1.3 Skin Colour Preference by Ethnicity

The Z-scores of the African image judged by Africans, the Caucasian image judged by Caucasian, and the Oriental image judged by Oriental are shown in Fig. 4.4.1.3-1. The 95% confidence error bar is drawn as well.
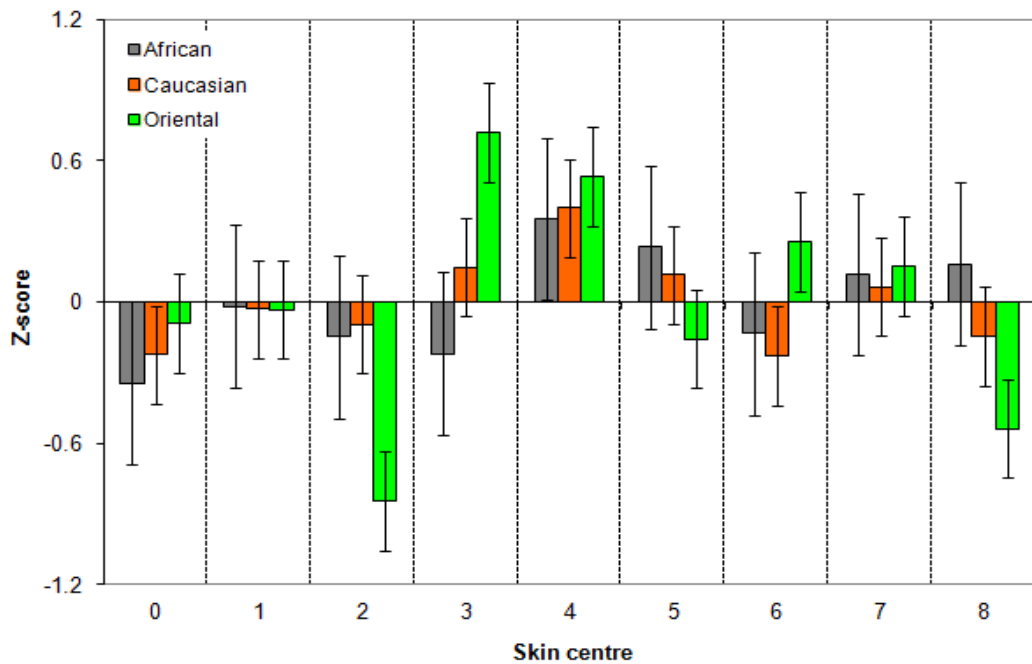
Fig. 4.4.1.3-1 Z-scores of the African, Caucasian, and Oriental images judged by African, Caucasian, and Oriental observers, respectively

The maximum Z-score among Z-scores in the African image judged by African is in #4 which is not on the boundary (see Fig. 4.4.1.3-2 to visualise relative locations of these nine skin colours). It means that these nine skin colour centres encompass a preferred skin colour, i.e., the range of skin colour sampling is large enough for observers to choose their preferences. Similar result was found in the Caucasian image judged by Caucasian observers (see Fig. 4.4.1.3-3).

The peak Z-score among Z-scores of the Oriental image judged by Oriental observers is at #3, which is on the low chroma boundary of the nine sampled mean skin colours (see Fig. 4.4.1.3-4). Although the peak value is close to that of the centre point #4, it is possible that a more pleasant colour centre is slightly out of range, toward a less chromatic direction.
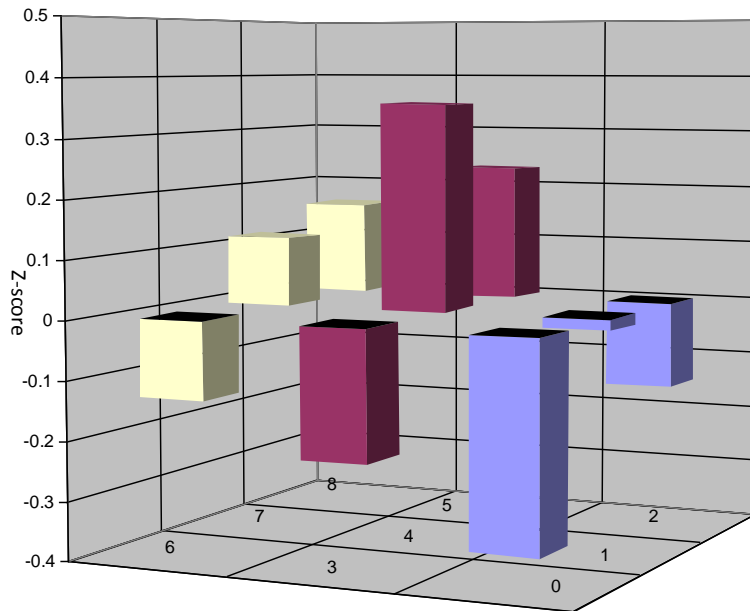
Fig. 4.4.1.3-2 Z-scores on nine skin colour centres in the African image judged by African observers
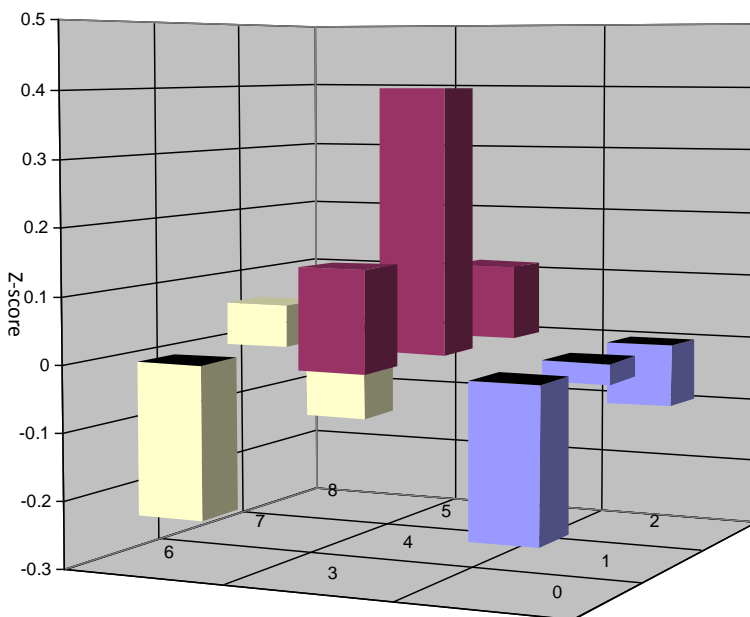
Fig. 4.4.1.3-3 Z-scores on nine skin colour centres in the Caucasian image judged by Caucasian observers
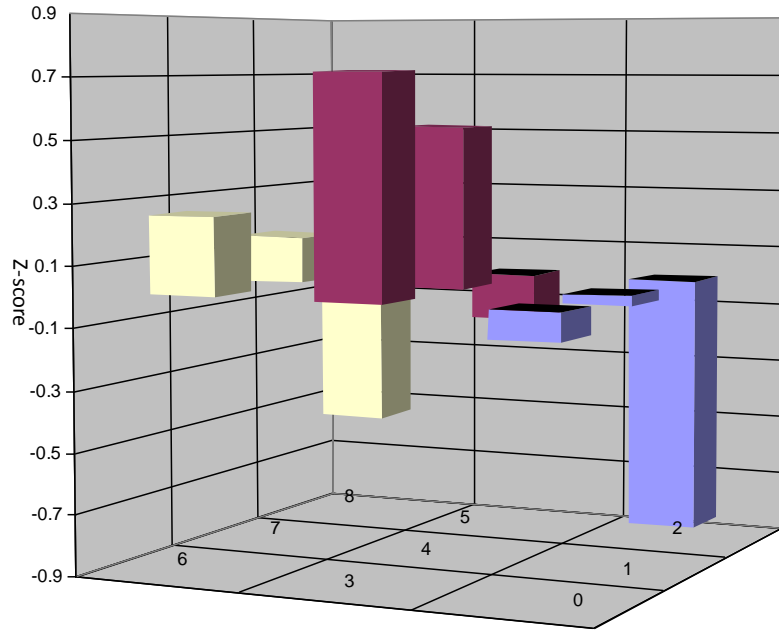
Fig. 4.4.1.3-4 Z-scores on nine skin colour centres in the Oriental image judged by Oriental observers
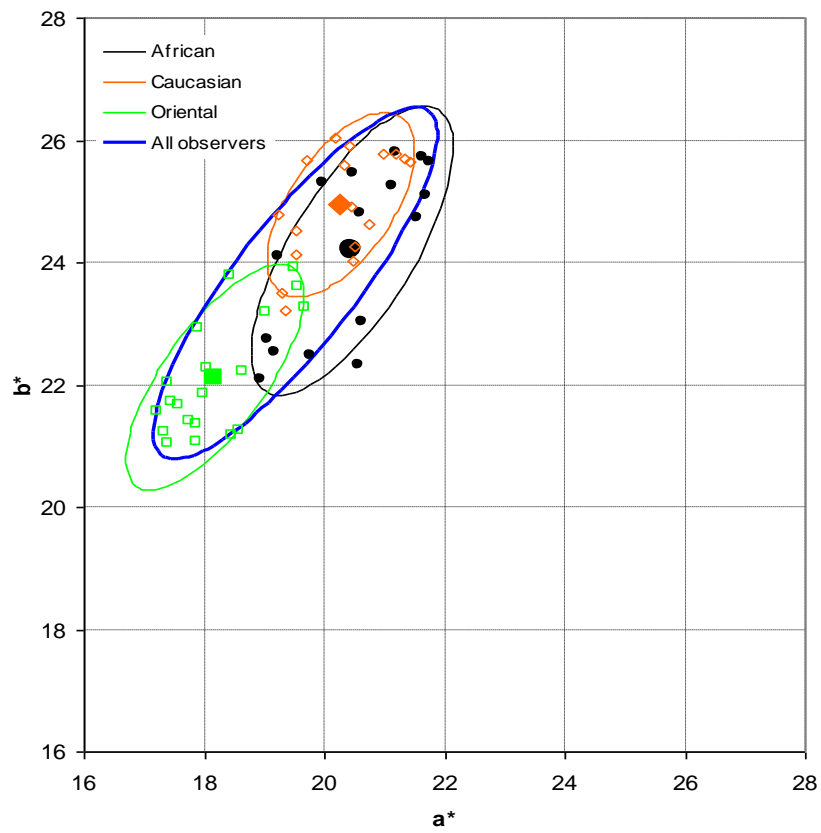
Fig. 4.4.1.3-5 Preferred skin colours of African, Caucasian, and Oriental judged by African, Caucasian, and Oriental observers, respectively

The preferred skin colours on each image judged by its corresponding ethnic group are illustrated in Fig. 4.4.1.3-5. Each small black dot is a preferred skin colour judged by an African observer; the black ellipse is the preferred skin colour region of African observers; and the large black dot is the centre of the ellipse. The results from the Caucasian image judged by Caucasian observers and the Oriental image judged by Oriental observers are plotted in the same figure for comparison. The figure shows that preferred skin colour distributions between African and Caucasian are very close. Oriental prefers less chromatic skin colours than other two groups. African preferred skin colour ellipse is larger than the other two, which implies the skin colour preference from African is less consistent among different observers. Because the most preferred Oriental skin colour may be slightly out of range toward a less chromatic direction, the real preferred skin colour centre may be slightly less chromatic than the centre of the ellipse.

The blue ellipse in Fig. 4.4.1.3-5 is the overall preferred skin colour ellipse from all three ethnic groups. Although it distributes around a large chroma area, it occupies a smaller hue range. The location and orientation of preferred skin colour ellipses confirm that the distributions of preferred skin colours are more consistent in hue than in chroma.

As discussed in Section 4.4.1.2, another step of colour transformation was applied to compensate the residue colour error in using the ICC profile. The a*b* transformed using the ICC profile should add (0.9, -0.1) so that they approximately agree with the measurement using Eye-One. Taking this colour characterisation factor into account, the preferred skin colour centres (a*b* adapted to D50) are adjusted and listed in Table 4.4.1.3-1 and plotted in Fig. 4.4.1.3-6. Orientals prefer slightly less chromatic skin colours than Africans and Caucasians, and Caucasians may prefer slightly more yellowish skin colours than Africans and Orientals.

Above results are the preferred skin colours judged by observers with the same ethnical background. Comparing the preferred Oriental skin colour centre of this study (a*b* = 19.9, 22.8) with the result of Chinese skin color preference from Experiment II (a*b* = 19.9, 23), two experimental results are very consistent.

Table 4.4.1.3-1 Preferred skin colour centres by ethnicity

	$a*$	$b*$	$C*_{ab}$	h_{ab}
African	21.4	24.1	32.2	48.4°
Caucasian	21.2	24.8	32.6	49.5°
Oriental	19.9	22.8	30.3	48.9°
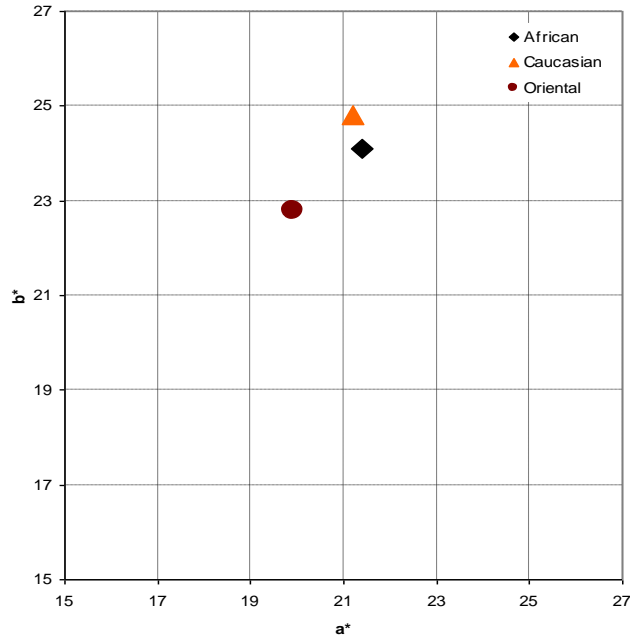
Fig. 4.4.1.3-6 Preferred skin colour centres of the African skin tone judged by Africans, the Caucasian skin tone judged by Caucasians, and the Oriental skin tone judged by Orientals

The statistical significance of the differences of the skin tone preference among three culture backgrounds were analysed with ANOVA. The ttest2 function in MATLAB (http://www.mathworks.com/) was applied to comput p-values in the 5% significance level. The result is shown in Table 4.4.1.3-2 (training data can be found in Appendix K. A p-value of greater than 0.05 means that two groups are not significant different at 5% significant level.

Table 4.4.1.3-2 t-test results between two culture backgrounds

	p-value (a*)	*p-value (b*)*
Caucasian, African	0.536	0.068
Caucasian, Oriental	< 0.0001	< 0.0001
African, Oriental	< 0.0001	< 0.0001

The p-values between the Caucasian group and the Oriental group are almost zero for both a* and b*. This indicates that there is statistical significance at 5% significance level in the difference of skin tone preferences between Caucasians and Orientals.

The p-values between the African group and the Oriental group are almost zero for both a* and b*, too. This indicates that there is statistical significance at

5% significance level in the difference of skin tone preferences between African and Orientals.

The p-values between the Caucasian group and the African group are 0.536 and 0.068 for a* and b*, respectively. Both p-values are higher than 0.05. This indicates that there is no statistical significance in the preference difference of a* and b* of skin tones between Caucasians and Africans at 5% significance level. With this result, it is not certain whether the Caucasian group and the African group are significantly different by considering a*b* together.

Multi-dimensional ANOVA (MANOVA) analysis was conducted to analyse the difference between the Caucasian group and the African group using SAS software. The result shows that the two groups are indeed significantly different at 5% significant level. The result of MANOVA analysis can be found in Appendix K. As illustrated in Fig. 4.4.1.5-3 and with the result of MANOVA analysis, it suggests that Caucasians prefer slightly more yellowish skin tones than Africans (or Africans prefer slightly more reddish skin tones than Caucasians).

In summary, statistical analysis of skin colour preference among African, Caucasian and Oriental culture backgrounds reveals that all three preferred skin colour cenrtes are significantly different from each other in 5% significant level. The previous result of Chinese skin colour preference from Experiment II agrees well with the current Oriental data, which means high repeatability in our experiments.

4.4.1.4 Cross-Culture Skin Colour Preference

The study of skin colour preference of each of African, Caucasian, and Oriental skin tones judged by each of the three ethnic groups is discussed below.

<u>African Skin Colour Preference Judged by Different Ethnic Groups</u>

Z-scores from the African image judged by Africans, Caucasians, and Orientals separately are drawn in Fig. 4.4.1.4-1. Note a*-b* coordinates of the skin centres are the mean skin colours of the nine versions of the image shown in Fig. 4.4.1.1-1. Skin centres #0, #3, and #6 are in the low chroma side; #2, #5, and #8 are in the high chroma side; and #1, #4, and #7 are in the middle. Z-scores from Orientals are lower in #2, #5, and #8, which means that Orientals prefer less chromatic African skin colours than Africans and Caucasians. Caucasians prefer #2, #5, and #8 more than Africans and Orientals, which means Caucasians prefer more chromatic African skin colours than Africans and Orientals.

Caucasians strongly prefer skin colour centres #2 and #5. Since these two colour centres are in the boundary, the most preferred African skin colour from

Caucasians may be out of the colour region encompassed by the nine skin colour centres. Hence, computing a preferred African skin colour judged by Caucasians using this set of Z-scores may be unreliable. Thus, we do not attempt to analyse preferred skin colours from all three ethnical groups quantitatively.
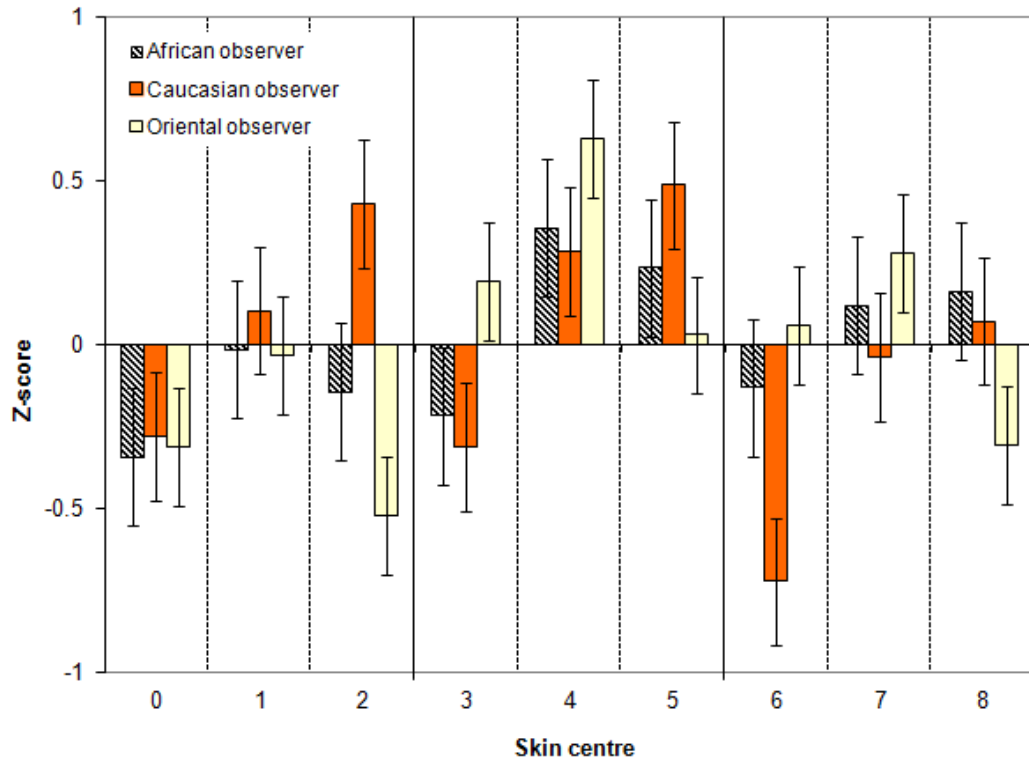
Fig. 4.4.1.4-1 Z-scores of the African image judged by three ethnic groups separately

Caucasian Skin Colour Preference Judged by Different Ethnic Groups

Z-scores from the Caucasian image judged by Africans, Caucasians, and Orientals separately are drawn in Fig. 4.4.1.4-2. Z-scores from Africans are lower in #0, #3, and #6, and are higher in #2, #5, and #8. Oppositely, Z-scores from Orientals are in overall higher in #0, #3, and #6, and lower in #2, #5, and #8. The results suggest that the chroma preference on Caucasian skin colours from highest to lowest is Africans, Caucasians, and Orientals.

Since the highest preferred skin colour centre from Africans is #8 which is in the high chroma corner, the most preferred Caucasian skin colour judged by Africans may be out of the colour gamut encompassed by the nine skin colour centres. Hence, computing a preferred Caucasian skin colour judged by Africans using this set of Z-scores is probably not reliable. As a result, we are not able to compute preferred skin colours judged by all three ethnic groups.
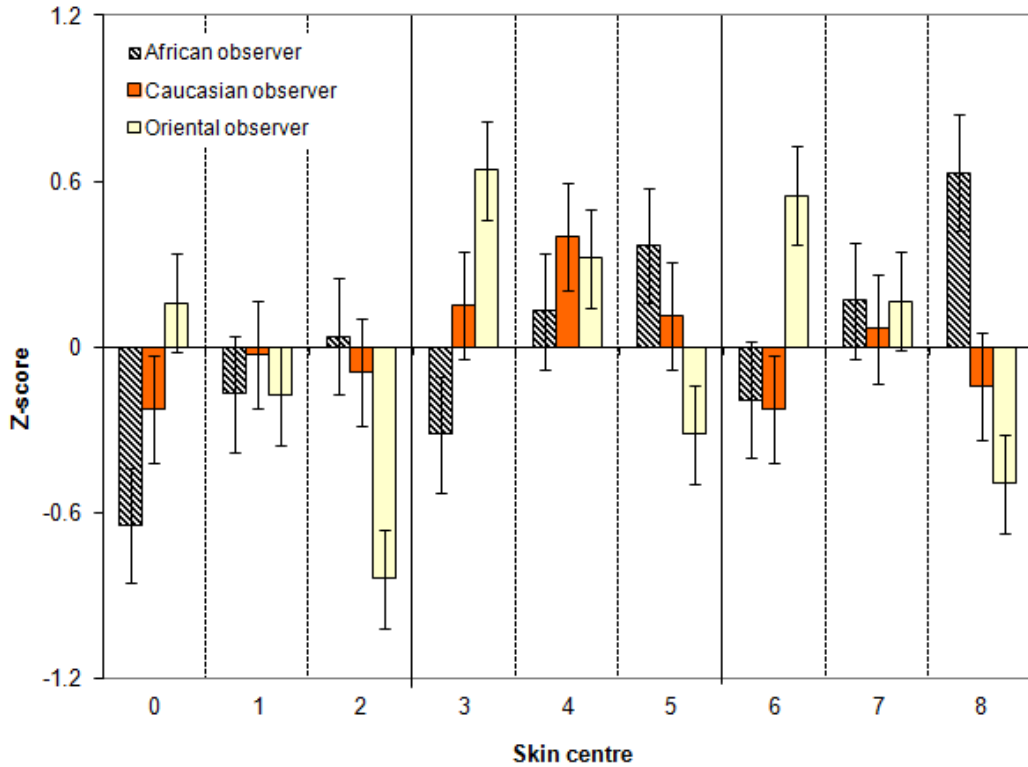
Fig. 4.4.1.4-2 Z-scores of the Caucasian image judged by three ethnic groups separately

<u>Oriental Skin Colour Preference Judged by Different Ethnic Groups</u>

Z-scores from the judgments on the Oriental image by Africans, Caucasians, and Orientals are plotted in Fig. 4.4.1.4-3. In general, Z-scores from Africans are lower in #0, #3, and #6, and are higher in #2, #5, and #8 than Z-scores from Orientals. Oppositely, Z-scores from Orientals are lower in #2, #5, and #8 than Z-scores from Africans and Caucasians. The results suggest that the order of chroma preference on Oriental skin colours from high chroma to low chroma is Africans, Caucasians, and Orientals.

The highest preferred skin colour centres from Africans is #5 and #8, which are in the boundary. This means that the most preferred Oriental skin colour from Africans could be out of the colour region encompassed by the nine skin colour centres. Hence, computing a preferred Oriental skin colour judged by Africans using this set of Z-scores is probably not reliable. For this reason, we do not compute preferred skin colours from all three ethnical groups for comparison.
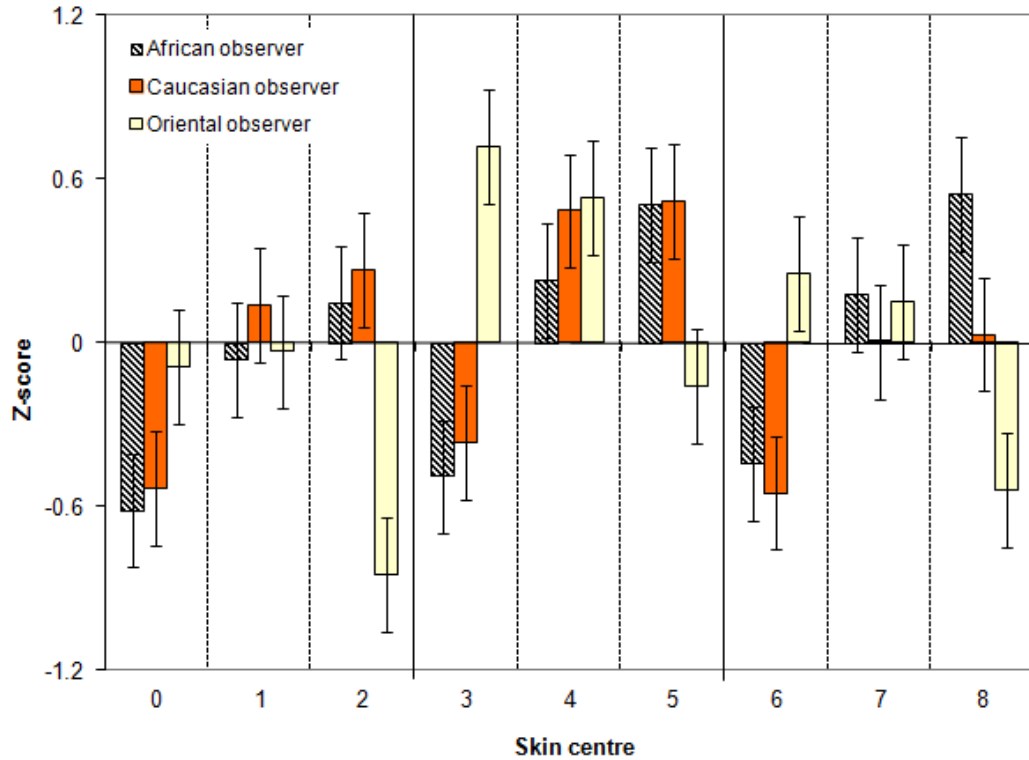
Fig. 4.4.1.4-3 Z-scores of the Oriental image judged by three ethnic groups separately

4.4.2 Summary

African, Caucasian, and Oriental images were judged by African, Caucasian, and Oriental observers in this psychophysical experiment to study skin colour preferences of these three ethnic groups. The results of skin colour preferences of by ethnicity are: the preferred hue angle in CIELAB adapted to D50 white point is about 49° in all three groups; Orientals prefer slightly less chromatic skin colours than Africans and Caucasians; the inter-observer variation of the skin colour preference of Africans is larger than those of Caucasians and Orientals; and Caucasians may prefer slightly more yellowish skin tones than Africans. In cross-culture preference, Orientals prefer slightly less chromatic skin colours than Caucasians and Africans, and Africans prefer more chromatic Caucasian and Oriental skin colours than Caucasians and Orientals.

4.5 Comparing Results among three Experiments

Preferred skin colour centres obtained from Experiment I is listed in Table 4.5-1 to compare with the result from this experiment listed in Table 4.4.2.2-1. In Experiment I, five LCD displays were used to display images in dim surround

viewing condition, while in the current experiment images were displayed on a CRT monitor in a dark surround viewing condition. A single observer group with mixed culture backgrounds (Caucasian dominated, plus Hispanic, African, and Asian) judged all images in Experiment I. Because nine predetermined skin colour centres were computed using different parameters among different experiments, a set of nine versions of images generated from an original image are different among different experiments, even if a same original image is used. Preferred African skin colours are very close between Experiments I and III. A factor that the preferred Caucasian skin tone from Experiment I is less chromatic may be that one of the test images is a high-key image, its original chroma is low, its chroma may be limited by the gamut of the device when adjusted, and the 3-D depth effect on the face is low when increasing chroma. The result that chroma of the preferred Oriental skin tone is not lower than that in preferred Caucasian and African skin tones in Experiment I may be that the same group of observers judged all three groups of images.

In Experiment II, four Oriental images were displayed on a large-gamut LCD monitor in a typical office viewing condition (average surround lighting condition) and judged by 19 Chinese observers. In Experiment III, images were displayed on a CRT monitor in a complete dark room and judged by a different group of observers. A preferred skin colour centre was found to be a*b* = (19.9, 23.0) in D50, with C^*_{ab} = 30.4 and h_{ab} = 49.3^o in Experiment II. This result is very close to the preferred Oriental skin colour found in Experiment III. This suggests that the skin colour preference is not affected by these two different viewing conditions.

Table 4.5-1 Preferred skin colour centres from Experiment I-1

	a*	b*	C^*_{ab}	h_{ab}
African	20.5	23.3	31.0	48.7^o
Caucasian	19.3	22.1	29.3	48.8^o
Oriental	20.7	24.4	31.9	49.7^o

4.6 Conclusions

The results of psychophysical experiments confirm that preferred skin colours are more chromatic than real skin colours. Observer variances in skin colour preference are larger in chroma than in hue, i.e. hue tolerance is tighter than chroma tolerance.

In Experiment I, the preferred skin colour centre for mixed skin colours is found to be about (21, 24) in CIE a*b* adapted to the D50 white point and its hue angle is 49°. A comparison of preferred skin colour ellipses between colour spaces reveals that CAM02-UCS is slightly more uniform than CIELAB in the skin colour region.

In Experiment II, the preferred Chinese skin tone judged by Chinese was found to be about (19.9, 23.0) in CIE a*b* adapted to the D50 white point and its hue angle is 49°. This is slightly different from (20.7, 24.4), the preferred Oriental skin colour centre judged by observers with different culture backgrounds in Experiment I. Although the hue angles of the two are very close, the result from Experiment II is slightly less chromatic. Since Oriental images were judged by observers with Caucasian-dominated culture backgrounds in Experiment I and Oriental images were judged by Chinese in Experiment II, the result suggests that Chinese prefers less chromatic Oriental skin colours.

Preferred African, Caucasian, and Oriental skin colours judged by their corresponding ethnic observers found in Experiment III are: the preferred hue angle in CIELAB adapted to the D50 white point is about 49° in all three groups; statistical analysis of skin colour preference among African, Caucasian and Oriental culture backgrounds reveals that all three preferred skin colour cenrtes are significantly different from each other in 5% significant level; Orientals prefer slightly less chromatic skin colours than Africans and Caucasians; the inter-observer variation of the skin colour preference of Africans is larger than those of Caucasians and Orientals; Caucasians may prefer slightly more yellowish skin colours than Africans; and the result of Chinese skin colour preference from Experiment II agrees well with the Oriental data in Experiment III, which means high repeatability in our experiments. In cross-culture preference, Orientals prefer slightly less chromatic skin colours than Caucasians and Africans, and Africans prefer more chromatic Caucasian and Oriental skin colours than Caucasians and Orientals.

Although different display types (regular LCD display, Adobe RGB LCD display, and CRT display) were used to display images and different groups of observers participated in the psychophysical experiments, the results are consistent. Verifications using hardcopy were conducted in Chapter 6, which further confirms that preferred skin colours obtained in this study are very reliable.

Chapter 5
Developing Preferred Skin Colour Enhancement Algorithms

Skin tones are the most important colours among the memory colour category. Reproducing them pleasingly is a critical factor in photographic colour reproduction. Moving skin colours toward their preferred skin colour centre improves the skin colour preference on photographic colour reproduction. Building on the solid foundations of skin colour modelling described in Chapter 3 and preferred skin colour experiments described in Chapter 4, new approaches to enhance skin colours for preferred colour reproduction of photographic images were developed and will be presented in this chapter. The differences of our approaches over other approaches will be discussed.

5.1 A Method to Enhance Skin Colours for Preferred Colour Reproduction

In this method, an ellipsoid skin colour model is applied to compute skin colour probabilities for skin colour detection and to determine weights for skin colour adjustment. Preferred skin colour centres determined through psychophysical experiments are applied for skin colour adjustment. Preferred skin colour centres for dark, medium, and light skin colours are applied to adjust skin colours differently. Skin colours are morphed toward their preferred colour centres. Highlight colours are processed specially to avoid contrast loss. A 3-D interpolation method is applied to fix a potential contouring problem and to increase the computation efficiency. Psychophysical experiments are conducted to validate the effectiveness of the skin colour enhancement.

5.1.1 Algorithm

5.1.1.1 Basic Algorithm

The ellipsoid skin colour model is used for skin colour detection for its efficiency in computation and its accuracy in skin colour detection. Mahalanobis distance of a point (x, y, z) to the ellipsoid centre $(x0, y0, z0)$ is computed using equations described in Section 3.4. $\Phi(x, y, z) < \rho$ defines the boundary of the ellipsoid.

Fig. 5.1.1.1-1 is a sketch diagram for skin colour adjustment. The large ellipsoid (drawn in 2-D space for simplification) represents the skin colour region, Point *A* is the centre of the region, and Point *B* is the Preferred Skin Colour Centre (PSCC). Skin colours (the yellow region) are morphed toward the preferred skin colour region (the orange region) for skin colour enhancement.
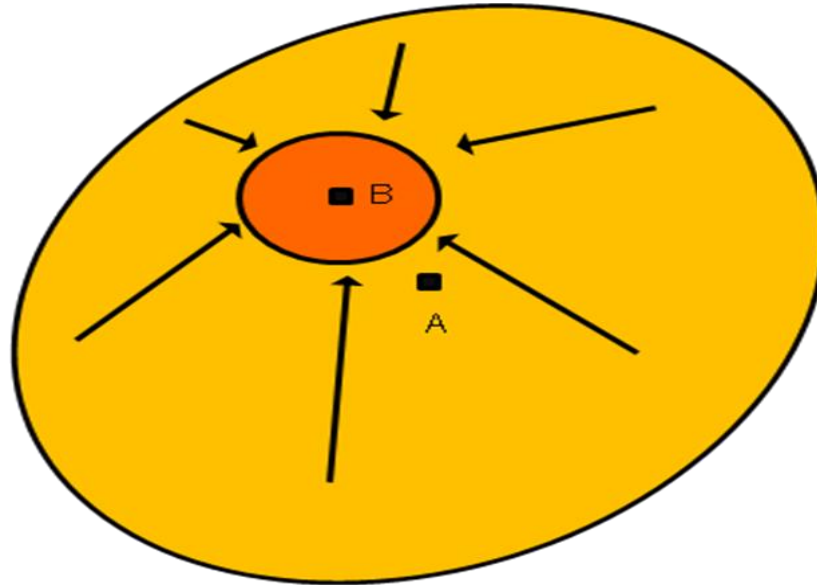
Fig. 5.1.1.1-1 A sketch diagram for skin colour adjustment

Fig. 5.1.1.1-2 depicts a workflow to process a colour image. *P* is an input colour and *P'* is its corresponding output colour. The source colour of each pixel is converted to CIELAB (or another luminance-chrominance space, such as CEICAM02 JAB, CAM02-UCS, or YC_bC_r). Mahalanobis distance, $\Phi(L, a, b)$, is computed. If $\Phi > \rho$, the colour is not a skin colour and no colour adjustment is performed on the pixel. Otherwise, the colour is a skin colour, and a weight, *w*, to adjust the skin colour is computed as a function of the Mahalanobis distance. The weight is applied to adjust a*b*.

At the ellipsoid centre, $\Phi(L, a, b) = 0$, *w* is maximized; on the ellipsoid boundary, $\Phi(L, a, b) = \rho$, *w* is zero. A weight for colour adjustment is computed as

$$w = 1 - \Phi(L, a, b) / \rho. \tag{5.1.1-1}$$

Other linear or nonlinear formulae may be applied to compute a weight. A basic idea is that the smaller Φ, the larger *w*. Based on the desired strength for colour enhancement, *w* may be modulated with a strength factor, w_0, i.e.,

$$w = w_0(1 - \Phi(L, a, b) / \rho), \tag{5.1.1-2}$$

where w_0 is a factor to adjust the strength of colour adjustment. Without adjusting L*, a*b* are adjusted by equations:

$$a_{new} = a + w \cdot (a_{center} - a)$$
$$b_{new} = b + w \cdot (b_{center} - b)$$

(5.1.1-3)

where (a_{center}, b_{center}) are PSCC; (a, b) are the original a*b* of a skin colour, and (a_{new}, b_{new}) are the enhanced a*b* of the original skin colour.
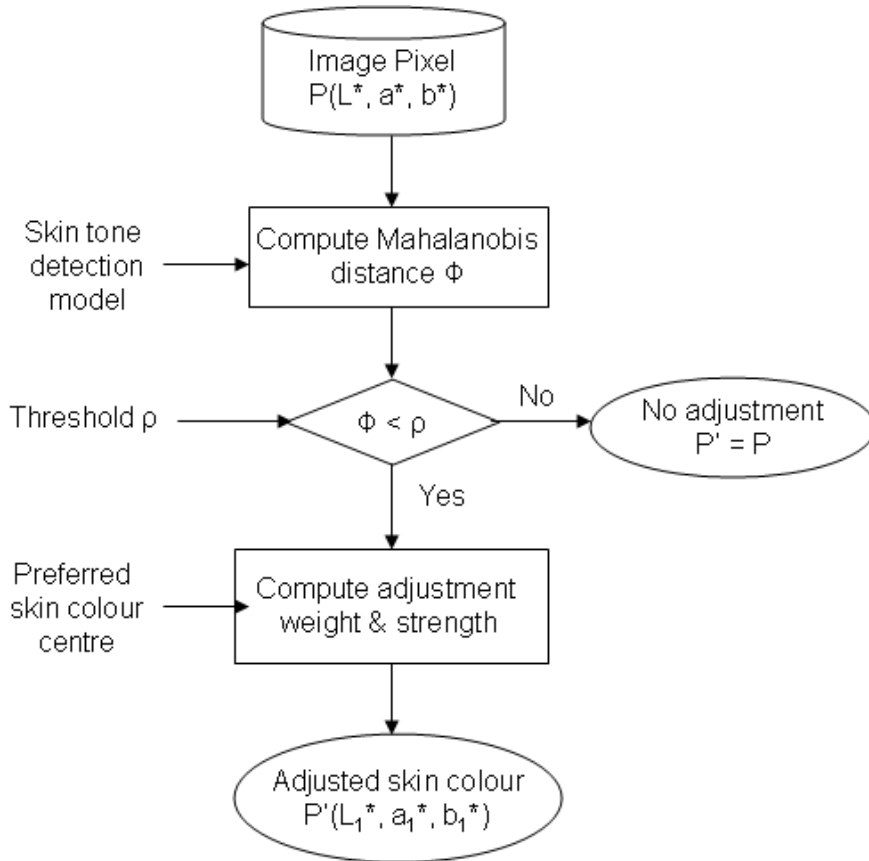
Fig. 5.1.1.1-2 A flow chart for skin colour adjustment

5.1.1.2 Lightness-Dependent Preferred Skin Colour Enhancement

It was found that PSCC should be slightly different for different lightness. To enable different PSCCs for different lightness, three PSCCs (preferred skin colours of light, medium, and dark skin colours) were used as parameters in the algorithm. In Fig. 5.1.1.2-1, the largest blue ellipsoid illustrates the skin colour boundary; each of the three PSCCs is at the centre of a constant-lightness ellipse (dark orange ellipses); and the red vertical dash curve represents PSCCs at different lightness levels interpolated from three PSCCs. With this property, the preferred skin colour centre, (a_{center}, b_{center}), becomes a function of lightness. In each lightness level, skin colours are morphed toward the preferred skin colour centre of its lightness level (in the figure, a colour on the pink area is moved towards a point on the PSCC curve).

In our implementation, a preferred skin colour LUT of 1001 items for L* from 0 to 100 at 0.1 interval was pre-computed for fast processing.
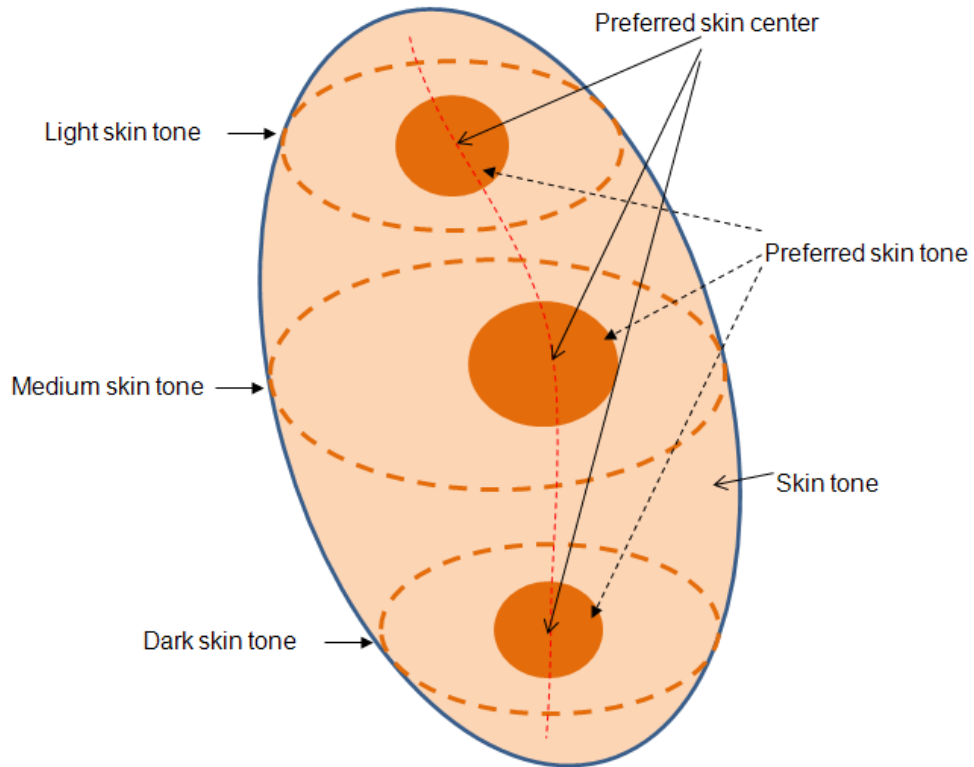
Fig. 5.1.1.2-1 A sketch diagram for skin colour adjustment using three PSCCs

5.1.1.3 Skin Colour Adjustment in the Highlight Colour Region

By testing the algorithm on various images, it was found that the contrast in the highlight skin colour region may decrease after skin colour adjustment. This is due to the fact that low chroma skin colours in the highlight region are moved toward more chromatic colours. If the adjusted colours are out of the device gamut (or the encoding gamut of the colour space), they are then clipped to the gamut boundary. The effect is a slightly lost in near-neutral highlight colours and results in a slight reduction of visual contrast. A simple approach to fix the problem for conservative skin colour enhancement is to reduce the adjustment of colours with high L*. The weight, w, in Eq. (5.1.1-3) is multiplied with a factor, w_L, for lightness-dependent adjustment as shown in Eq. (5.1.1-4):

$$a_{new} = a + w \cdot w_L \cdot (a_{center} - a)$$
$$b_{new} = b + w \cdot w_L \cdot (b_{center} - b)$$

(5.1.1-4)

w_L is 1 for L* that is smaller than or equal to a threshold, L_0 (L_0 is set to 65 in our experiment), it gradually decreases as L* increases, and it becomes 0 at L*=100.

If skin colours in highlight are not in the preferred condition, reducing the skin colour adjustment using Eq. (5.1.1-4) has a negative effect that morphing skin

colours toward the preferred skin colour centre may not be effective. In order to adjust highlight skin colours effectively without affecting the contrast, another algorithm was developed. With this new approach, chroma is not adjusted but hue is adjusted for highlight skin colours. After applying Eq. (5.1.1-3) to compute a new skin colour, an adjusted hue angle (noted as h_a) and an adjusted chroma (noted as C_a), are computed from the adjusted colour. Chroma of the original colour, C_0, is computed as well. Since the aim is to move hue toward the hue of the PCSS and not to change chroma for highlight skin colours, C_0 and h_a are used to compute a corresponding adjusted skin colour. In order to have a smooth transition from medium to highlight skin tones, chroma must be adapted from what it is adjusted in mid-tone slowly to no-adjustment in chroma (hue adjustment only). This is done with following equation:

$$C = C_0 + w_L \cdot (C_1 - C_0) \qquad (5.1.1\text{-}5)$$

Chroma, C, and the adjusted hue angle, h_a, are used to compute a final skin colour (a_{new}, b_{new}):

$$a_{new} = C \cdot \cos(h_a)$$
$$b_{new} = C \cdot \sin(h_a) \qquad (5.1.1\text{-}6)$$

This method produces more favourable highlight skin colours than that with the first approach.

5.1.1.4 Processing Images Using a Pre-Generated LUT

With the algorithms described above to adjust skin colours, a colour at A (the centre of the large ellipse in Fig. 5.1.1.1-1) is moved to the position B (the preferred skin colour centre) if strength, w_0, is set to 1. This is illustrated in Fig. 5.1.1.4-1, where A is mapped to A' after the colour adjustment. A and B in this figure corresponds to A and B in Fig. 5.1.1.1-1, respectively. A colour, C, between A and B is moved to C' based on the above algorithm because the adjustment weight is less than 1. Before skin colour adjustment, C is closer to B than A. After the adjustment, A is closer to B than C (in fact, A and B become the same colour if $w_0=1$). The colour transition between colour A and colour C is inversed after the adjustment. The problem occurs only in the region close to the line segment AB. The simple adjustment method has to be modified to fix this problem. Instead of applying more complex and less efficient formulae to fix the problem, a more effective approach is to utilize a pre-built LUT to adjust colours.

In the image processing framework, all input images are converted to a common RGB colour space, such as sRGB or Adobe RGB colour space. A 17x17x17 3-D RGB LUT may be generated for colour transformation. If the input

RGB colour space and the output RGB colour space are identical, it is an identity LUT. To adjust skin colours, the input colour in each node of the LUT is converted to CIELAB (or another luminance-chrominance colour space, such as CAM02-UCS), and Mahalanobis distance is computed to determine whether the colour is within the skin colour region. If the colour is within the skin colour region, the skin colour adjustment is applied to adjust the colour. The CIELAB values are then converted to the output RGB colour space to update the colour values of the node in the LUT.
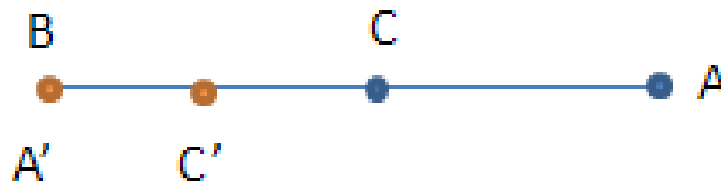
Fig. 5.1.1.4-1 A sketch diagram to depict the transition inversion in skin colour adjustment

If a source colour space is sRGB-like colour space, or a colour space with a larger gamut (e.g. Adobe RGB), the distance (i.e., the chroma difference, $(\Delta a^{*2}+\Delta a^{*2})^{0.5}$) between two neighbour nodes of a 17x17x17 LUT within the skin colour region in CIELAB colour space is about 8 or larger than 8. This can be analysed by converting sRGB of each node into CIELAB, and computing chroma difference between two neighbour nodes in the skin colour region. The chroma distance between the statistical skin colour centre (*A*) and the preferred skin colour centre (*B*) is unlikely to be larger than 8. Fig. 5.1.1.4-2 shows likely locations of line *AB* in a LUT. A 2-D diagram is drawn for simplification (we may assume that the horizontal axis is R axis, the vertical axis is G axis, and the B axis is not drawn). Cross points between a black horizontal line and a black vertical line are the nodes in a LUT. In a 3-D LUT, a node is the intersection of three lines. The orange line is the line segment connected by the statistical skin colour centre (*A*) and the preferred skin colour centre (*B*). In different colour spaces, the positions of *AB* in a LUT are different. It may be within a cube connected by neighbour nodes (see *A1-B1*); it may be located in two cubes (*A2-B2* or *A3-B3*); and in a most unlikely case, it may be on a plan or on a line of the LUT nodes (*A4-B4*). Due to the large distance between two neighbour nodes in a 17x17x17 RGB LUT, *A* (or a point close to *A*) and *B* (or a point close to *B*) can only exist on two neighbour nodes, i.e. it is impossible to have them exist around two nodes that are not neighbour nodes and to have a colour, *C*, between *A* and *B* exists on a node in-between. Therefore, the colour inversion existed in point by point processing will not occur in colour transformation using a 17x17x17 LUT. However, it should be realized that the

colour inversion could occur if a larger LUT, such as a 33x33x33 LUT, is used for interpolation.
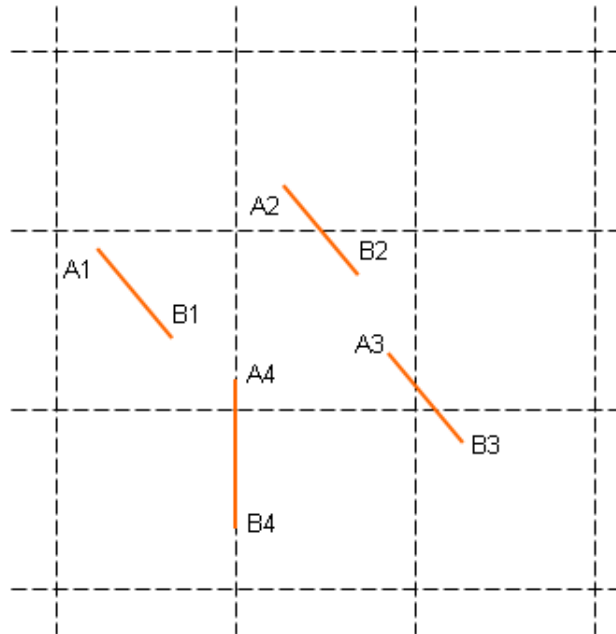
Fig. 5.1.1.4-2 Likely locations of a line segment connected by the statistical skin colour centre (*A*) and a preferred skin colour centre (*B*) in a LUT

Besides fixing the colour inversion or colour contouring problem, using a LUT to process images greatly increases the efficiency for colour adjustment. Other colour enhancements may be merged with the LUT to further increase the computation efficiency.

5.1.1.5 System Tuning

Testing the skin colour enhancement of different skin tones judged by observers with different ethnic backgrounds, we found that the preferred skin colour adjustments among different ethnic backgrounds were similar in the mid-tone area, the preferred skin adjustments between Asian and Caucasian skin tones are similar in the dark skin colour region, but the preferred skin adjustment between African and Caucasian/Asian skin tones are very different in the dark skin colour region. To automatically enhance skin colours of photographic images in a system in which skin tones of different ethnic types cannot be detected automatically, a conservative approach is to reduce the adjustment strength for dark skin tones. Since too much adjustment in highlight may reduce overall contrast and therefore reducing the face depth effect, one method to fix the problem is to reduce the adjustment in highlight. The skin colour ellipsoid may be adjusted to reduce adjustment in both highlight and shadow regions of skin colours. Fig. 5.1.1.5-1 shows a reduced ellipsoid to lower skin colour adjustment in highlight and shadow. The skin ellipsoid colour model is tuned in the final system tuning step.
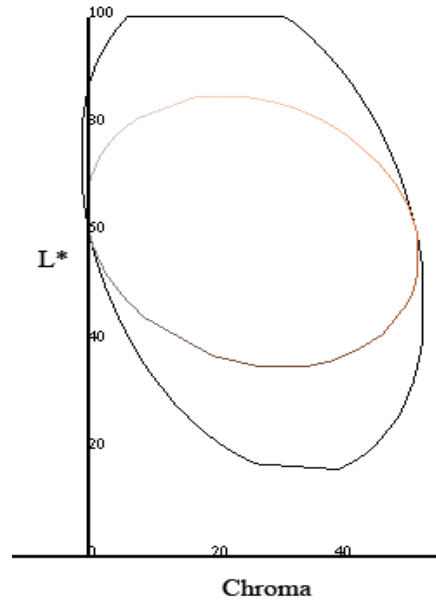
Fig. 5.1.1.5-1 A trained skin colour ellipsoid (black) and its modified ellipsoid to reduce highlight and shadow skin colour adjustment

Neutral colours are usually defined as colours with zero chroma (or R=G=B in an RGB colour space). If neutral colours are not to be adjusted, it can be fixed in the final 3-D LUT by snapping the transformation of neutral nodes to identity mapping. To optimise skin colour adjustment for different geographical regions worldwide, a parameter set for each geographical region may be optimised. Fig. 5.1.1.5-2 shows a prototype interface for personalised skin colour adjustment. *Region* may include General, Africa, North America, Europe, Australia, Asia, India, etc. *Strength* is to modify the weight for skin colour adjustment. *Saturation* is to make the preferred skin colours more or less chromatic. *Hue* is to adjust the preferred skin colour slightly toward the pinkish or yellowish direction. The default *Saturation* and *Hue* are initialized using the preferred skin colour centre and then adjusted during the system tuning step.
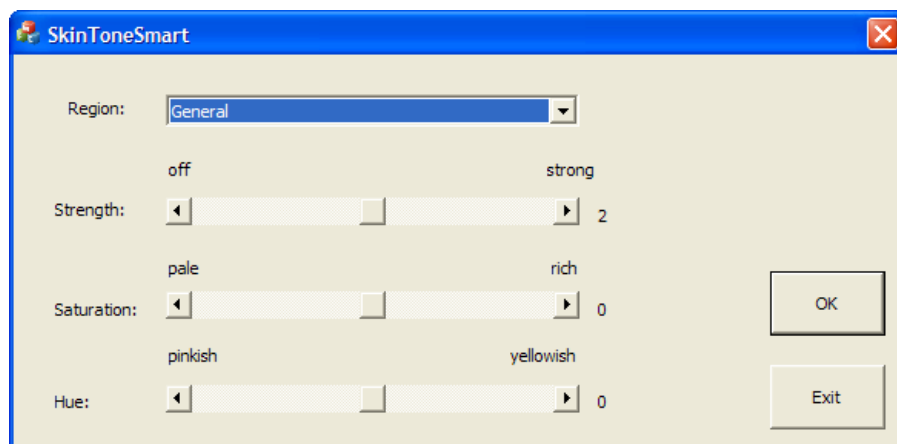
Fig. 5.1.1.5-2 A prototype user interface for preferred skin colour personalisation
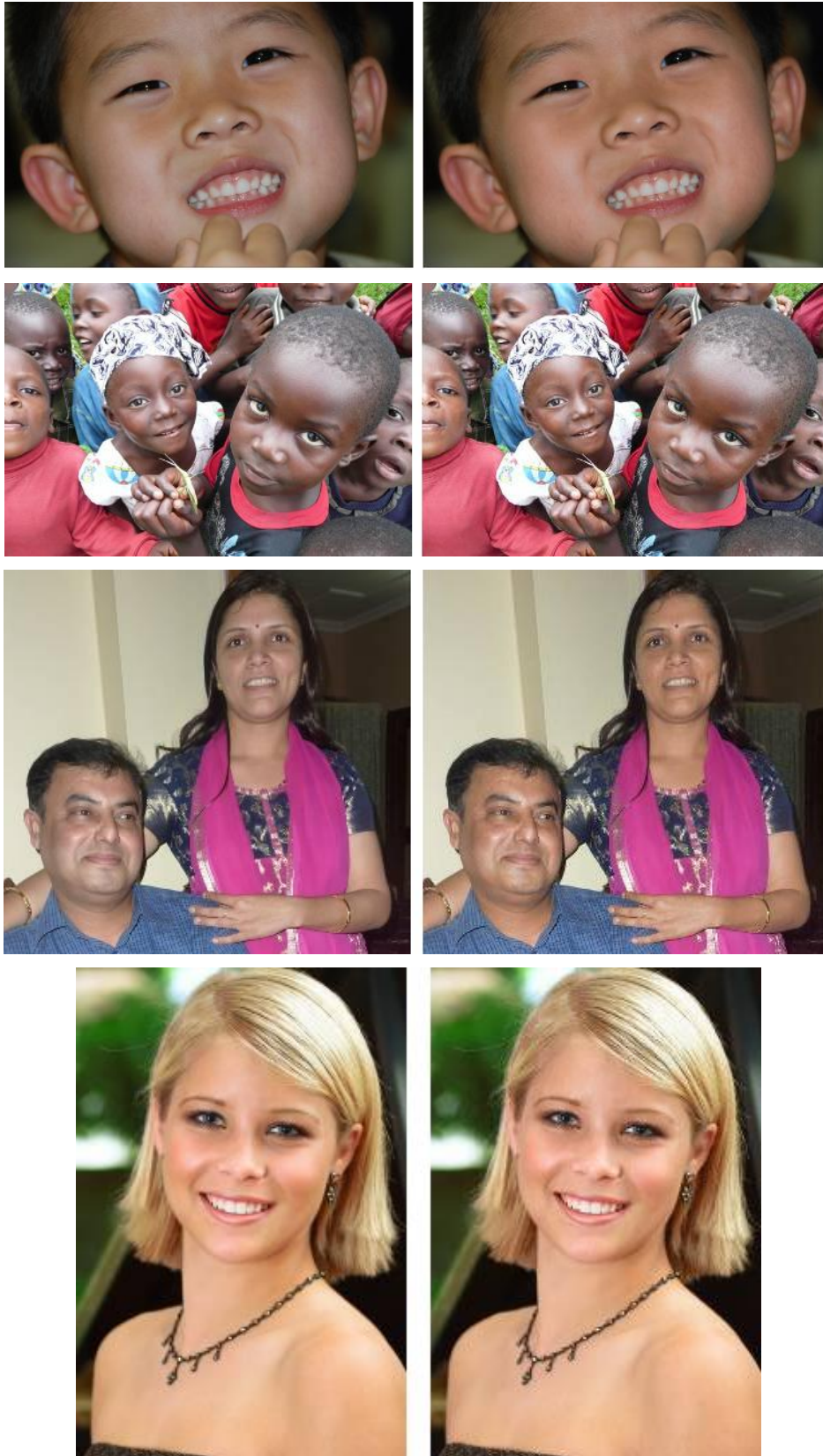
Fig. 5.1.1.5-3 Original images (left) and their corresponding enhanced images using
default parameters (depending on the colour management setup of the
document viewer or printer, image colours may be displayed or printed
inaccurately)

Fig. 5.1.1.5-3 show four example images on the left and their corresponding enhanced images using default setting parameters. If skin tones of an image are in the preferred state, the enhanced image is almost the same as the original image (the last image pair is an example). Fig. 5.1.1.5-4 shows the effect of adjusting chroma of the preferred skin colour centre. Fig. 5.1.1.5-5 shows the effect of adjusting hue of the preferred skin colour centre.

Fig. 5.1.1.5-4 Adjusting chroma of the preferred skin colour: default skin colour enhancement (middle), decreasing chroma of the preferred skin colour centre (left), increasing chroma of the preferred skin colour centre (right)

Fig. 5.1.1.5-5 Adjusting hue of preferred skin colours: default skin colour enhancement (middle), the preferred skin colour centre to be slightly more pinkish (left), the preferred skin colour centre to be slightly more yellowish (right)

5.1.2 Discussion

Compared to other skin colour enhancement methods, this method has following advantages:

1) Compared to methods using an ellipse skin colour detection model, this method utilises an ellipsoid skin colour detection model to increase the accuracy for the skin colour detection. A systematic method was developed to train skin colour models for mixed skin tones or separate ethnic skin tones.

2) Preferred skin colours are determined in light, medium, and dark skin tones. Lightness-dependent preferred skin colours are interpolated from these three points. Since preferred skin colours are adapted to lightness, preferred skin colour enhancement is optimized for difference lightness levels.

3) In the system tuning step, the highlight skin colour region is processed differently to avoid losing contrast, the skin colour model and three preferred skin colour centres are adjusted to optimise for a specific imaging system.

4) Region selection, strength adjustment, and personal preference in preferred skin colour centres (hue and chroma) can be built into the algorithm for colour customisation.

4) Implementation using 3-D LUT and interpolation increases computation efficiency.

5.2 Face Detection Assistant Skin Colour Enhancement

There are a few limitations in the skin colour enhancement algorithm described in the prior section. Because of the way the elliptical skin colour model was trained, it is most suitable for detecting skin colours distributed around a statistically averaged skin colour centre. If skin colour distribution of an image is too much biased toward a certain direction, skin colours may be close to or out of the edge of the skin colour boundary determined by the elliptical skin colour model, therefore skin colours will be adjusted insufficiently or will not be adjusted. In such a case, skin colours should be adjusted strongly for effective skin colour enhancement. In order to resolve this problem, additional information from face detections are used to analyse original skin tones and to construct an image-dependent skin colour distribution model, and the image-dependent skin colour model is applied to adjust the ellipsoid model for skin colour detection and to determine how to shift skin colours toward a preferred skin colour centre.

First, a face detection method is applied to detect faces in an image (Viola and Jones 2004). Because of potential false face detections, another step is applied to verify each detected face using a skin colour model. The order of these two operations may be exchanged or merged into a single step, depending on how the face detection algorithm is implemented. The skin colour detection model for this

step has a relatively high tolerance for false skin colour detection rate, and a subsequent step using face boxes information is applied to modify the skin colour model for accurate skin colour detection on the image. Because an accurate skin detection model is not required in the first step, the ellipse skin colour model that is more efficient but less accurate than the ellipsoid model or the lightness-dependent ellipse model is applied. Each pixel in a rectangle face box is transformed into a colour in a uniform colour space, such as CIELAB. The skin colour model is applied to classify each pixel in a face box as a skin pixel or a non-skin pixel. If the ratio of skin pixels over all pixels within a face box is lower than a pre-determined percentage , this face is classified as a false detected face and is removed from the face list (about 1/4 to 1/2 of pixels in the face box must be skin colours in our experiment). In Fig. 5.2-1, the original and its enhanced images are shown on left and right, respectively. All rectangle boxes on the right images are original detected faces and the yellow rectangle box is a face box removed through skin colour detection.

Fig. 5.2-1 An original image (left) and the face detection and skin colour enhancement results (right). Depending on the colour management setup of the document viewer, image colours may be displayed inaccurately.

The procedure for skin colour enhancement is described below:

Step 0: coefficients of the skin colour detection ellipse in CIELAB D50 are initialized using the result trained from a larger number of images (in the order of thousands). The coefficients used in this study are listed below:

skin centre: (18.74, 19.64); and

$(u0, u1, u2, \rho)$: (0.0039, -0.0027, 0.0021, 1).

Step 1: a face detection method is applied to detect faces.

Step 2: any face boxes with skin colours very far away from normal skin colures are removed. The skin colour detection model is applied to detect skin colours in each face box, and a mean skin colour is computed from detected skin

colours in each face box. The histogram of skin colours in each face box is generated, and skin colours in the top 25% occurrence rates are retained and other skin colours in the bottom 75% occurrence rates are discarded. Mean a*b* of skin colours are computed from all remaining skin colours. The mean skin colour is compared with the statistical skin colour centre, and if their colour difference is larger than a pre-determined threshold, this face box is removed from skin colour analysis. In this study, if the chroma difference is larger than 20 or the hue angle difference is larger than 30° between the face mean colour and the statistical skin colour centre, the face box is removed.

Step 3: a global mean skin colour is computed from the remaining face boxes. This is averaged from the mean skin colour of each remaining face box weighted with its skin pixel counts. The mean a*b* are compared with a preferred skin colour. If the distance between the two in a*-b* coordinates is less than a pre-determined threshold, the overall skin tone of the image is considered to be within the preferred colour range, therefore no skin colour adjustment is performed and the skin colour adjustment ends here. Otherwise, skin colour adjustment in the whole image is performed.

Step 4: a skin colour ellipse that is specific for the skin colour adjustment of the image is constructed. It starts from a static skin colour ellipse as described in Step 0. The centre of the skin colour ellipse is then replaced with the mean skin colour of the image computed in the prior step. Because the skin colour ellipse is to represent the skin colour distribution of this image, the size of the ellipse (the major and minor axes) is reduced (ρ was reduced to 0.7 in our experiment). This skin colour ellipse is applied to detect skin colours of the whole image. In this step, a simpler circular boundary model with the mean skin colour of the image as the centre and a properly determined radius may be used as the skin colour detection model, or a Gaussian model may be used.

Step 5: skin colours of the image are adjusted in this last step. Instead of limiting to process skin colours within face boxes, all skin colours (skin colour of any objects) in the whole image are adjusted. If the Mahalanobis distance of a pixel is smaller than a threshold, the pixel is a skin colour, and the Mahalanobis distance is used to compute a weight that is applied to determine how much to shift the colour toward the preferred skin colour centre. Following equations are used to compute a new skin colour, (a_{new}, b_{new}), from an original skin colour, (a, b):

$$a_{new} = a + w \cdot (a_{center} - a)$$
$$b_{new} = b + w \cdot (b_{center} - b)$$

(5.2-1)

where *w* is a weight computed from Mahalanobis distance, and (a_{center}, b_{center}) is the preferred skin colour centre.

Since large colour adjustment on skin colours may have an effect that skin colours are not harmonized with the overall colour balance of the image, the morphing from a mean skin colour to a preferred skin colour centre is restricted if the difference between the two is larger than a threshold. Rules of the adjustment are determined experimentally. In this study, the chroma difference was computed, and only half of the chroma difference was applied to colour adjustment, and the maximum chroma adjustment was limited to 10. A hue angle difference between the mean skin colour and the preferred skin colour centre was computed and the maximum hue angle adjustment was limited to 20°. In other words, if the hue angle difference was larger than 20, the hue angle adjustment was clipped to 20°.

To further optimize the preferred skin colour reproduction for skin tones, the preferred skin colour centre, (a_{new}, b_{new}), in Eq. (5.2-1) may be optimised as a function of lightness (Zeng and Luo 2011).

Similar to the previous algorithm, three additional parameters were provided for personalisation of the skin colour enhancement. These three parameters are strength, chroma, and hue. *Strength* is to adjust how much a skin colour is moved toward a preferred skin colour centre. *Chroma* is to adjust the chroma of the preferred skin colour, i.e., to make the preferred skin colour paler or more chromatic. *Hue* is to shift the hue of the preferred skin colour toward yellowish or pinkish.

Fig. 5.2-2 An original image (left) and the result of the face detection and skin colour enhancement (right). Depending on how an application interprets colours of the images, colours may be displayed or printed inaccurately.

In Fig. 5.2-1, the skin tones on the left image are too yellowish. The right image shows the result of skin colour enhancement. Fig. 5.2-2 shows another example. The facial tones on the original image (left) are too pale. The skin colour enhancement adjusts skin colours on faces, bodies, and skin colours of golden-

colour trees and ground as well. This implies that the skin colour enhancement modifies the overall colour balance of the whole image as well, i.e., it adjusts the white balance of the image and therefore it has an additional benefit of fixing the inaccurate illuminant detection problem.

Because the ellipse skin colour detection model used in Step 0 detects a larger region of colours than that used in the first skin colour enhancement method, this skin colour enhancement method is able to adjust wider range of skin colours that deviate more seriously from normal skin colours. Because the ellipse used in Steps 3 and 4 is adapted to a specific image, this method adjusts skin colours more effectively than the previous approach.

This algorithm works well in a uniform luminance-chrominance colour space, such as CIELAB a*b* coordinates or CIECAM02 chrominance coordinates. Replacing the working colour space with YC_bC_r increases the computation efficiency for processing RGB images and videos. However, chroma coordinates (C_bC_r) of preferred skin colours are changed considerably among different luma values, Y. C_bC_r of preferred skin colours and skin colour ellipses should be adapted to different luma for skin colour enhancement.

To increase the computation efficiency for processing a large image, after all skin colour enhancement parameters for processing the image is obtained, the skin colour enhancement method can be applied to process a 3-D LUT and then the image is adjusted through 3-D interpolation using the LUT. For example, to process an sRGB image, a 17x17x17 LUT may be generated. sRGB colours of 17x17x17 = 4903 nodes are converted to CIELAB or CAM02-UCS; each node colour is treated as the colour of an image pixel and is adjusted accordingly; and the colour is then converted to the destination colour space.

A few cases that depict the improvement of the approach over the first approach are discussed below.

Case 1 - skin tones are highly chromatic: Fig. 5.2-3 illustrates the skin colour region of an elliptical skin colour model as the black solid ellipse and the skin colours of an image in the dash ellipse region. With the prior method, skin colours that are out of the solid-black elliptical region will not be adjusted; and the adjustment strength of each colour within the elliptical region is proportional to the Mahalanobis distance in the large black elliptical region. A colour in location *A* has the highest adjustment strength and colours around *B* that are near the boundary of the black ellipse are adjusted very weakly. With the new approach, an ellipse skin colour model is adjusted to centre at the mean of the skin colours of the face boxes of image (the red ellipse in the figure). Skin colours to be adjusted are judged using this red ellipse;

and the strength of the adjustment is proportional to the Mahalanobis distance in the red ellipse. A colour in location *B* has the highest adjustment strength, and a colour on the boundary of the red ellipse is not adjusted. Because the skin colour ellipse (the red ellipse) is adapted to colours of the skin pixels of the image, the size of the ellipse may be reduced. It is clear that the new method is more effective for skin colour adjustment.
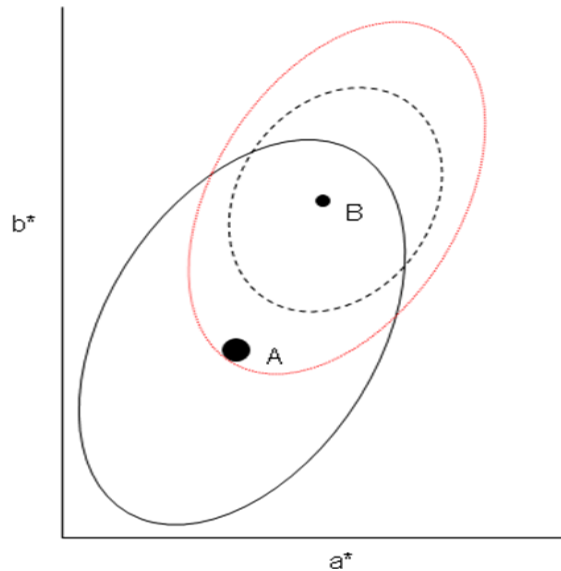
Fig. 5.2-3 A sketch diagram showing effective adjustment of highly chromatic skin colours

Case 2 - Skin hues are shifted off the regular skin colour region: Fig. 5.2-4 shows the elliptical skin colour region of an elliptical skin colour model in a large black ellipse and the skin colour region of an image in a small dash ellipse. The skin tones of the image are distributed around the red ellipse (skin colours are shifted to the yellowish direction). Again, the strength of the skin colour adjustment is proportional to the Mahalanobis distance computed using the skin colour model. With the prior method, a colour in location *A* has the highest adjustment strength and a colour on the boundary of the black elliptical region or out of the ellipse has zero strength (no adjustment). Thus, the yellowish skin colours that are out of the black skin colour ellipse are not adjusted. With the new method, an ellipse skin colour model is adjusted to centre at the mean skin colour of the face boxes of the image (the red ellipse in the figure). Skin colours to be adjusted are detected using this red ellipse; and the strength of adjustment is proportional to the Mahalanobis distance in the red ellipse. A colour in location *B* has the highest adjustment strength, and a colour on the boundary of the red ellipse is not adjusted. Because the skin colour ellipse (the red ellipse) is adapted to colours of the skin pixels of the image, the size of the ellipse may be reduced. In this case, it is very likely that the white balance of the image is not properly determined and the entire image is shifted

to the yellowish direction. Because the method of skin colour enhancement adjusts all colours within the red ellipse, all yellowish colours in the image are adjusted. Thus, an additional benefit through the skin colour enhancement is that it removes the yellow cast. The relative location of *B* and *A* can actually be used to assist illuminant detection and white balance.
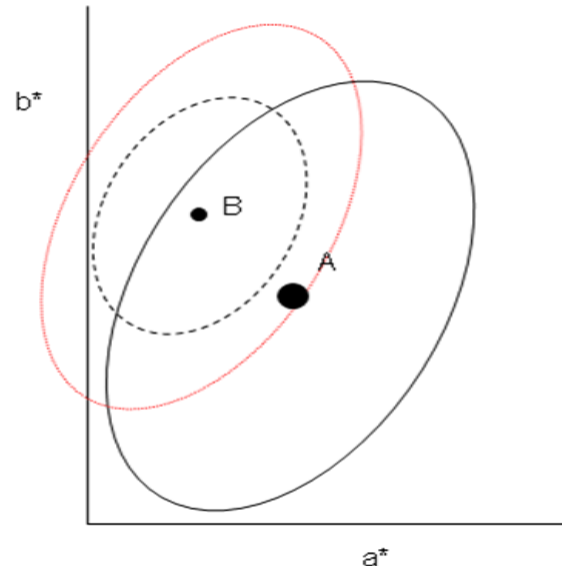
Fig. 5.2-4 A sketch diagram showing the effective adjustment of yellowish skin tones

Case 3 - Bright and dark skin colours: Fig. 5.2-5 shows the elliptical skin colour region of an elliptical skin colour model in a large black ellipse and the skin colour region of an image in a small dash ellipse. Very bright and very dark skin colours in a digital photographic image tend to have lower chroma. If a skin colour model is not adapted to highlight and shadow regions, the skin elliptical model tend to have a higher mean chroma than the actual skin chroma. With the prior method, high chroma skin colours close to the centre, A, of the skin colour model is adjusted the most. And very low chroma skin colours that are close to the boundary of the black ellipse or out of the ellipse are adjusted very weakly or are not adjusted. With the new method, an ellipse skin colour model is adjusted to centre at the mean skin colour of the face boxes of the image (the red ellipse in the figure). Skin colours to be adjusted are detected using this red ellipse; and the strength of the adjustment is computed based on the relative distance to the centre B instead to the point A. It is clear that the new method adjusts skin colours more properly and more effectively. In this case, the skin colour ellipse may be reduced because colour gamut in highlight or shadow is smaller than that in normal skin tones. Again, the red skin colour ellipse may be reduced because it is to model skin colours of an image.

In summary, a benefit of using face detection information is that the skin colours of faces are known, and therefore a skin colour model adapted to face tones of the image can be constructed and used for skin colour adjustment.
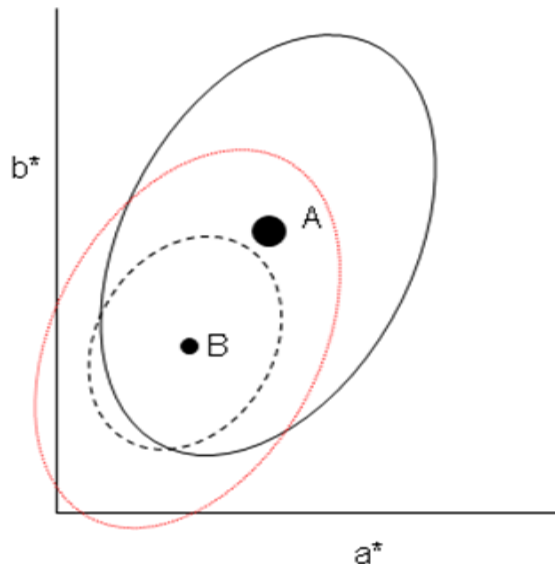
Fig. 5.2-5 A sketch diagram showing effective and proper adjustment of skin colours

5.3 Skin Colour Morphing by Triangular Re-shaping

In both skin colour enhancement methods described in Sections 5.1 and 5.2, once a weight is computed for a skin colour and a target preferred colour is determined, Eqs. (5.1.1-1) to (5.1.1-3) are applied to adjust the skin colour. An original skin colour at the preferred skin colour centre is not adjusted because its adjustment weight, w, is equal to zero. If a colour at the original skin colour centre is moved to the target preferred skin colour centre, these two different original colours will be mapped to the same colour. A simple method to fix the problem is to reduce the adjustment rate. Another issue of this colour adjustment method is that contouring may happen after the adjustment. This problem is fixed with a 3-D interpolation method as described in Section 5.1.1.4.

In this section, a new colour adjustment method that may be used to replace the method described in Eqs. (5.1.1-1) to (5.1.1-3) is proposed. In Fig. 5.1.1.1-1, the ellipse and the centre A correspond to the skin colour ellipse and the skin colour centre as shown. Fig. 5.3-1 shows a skin colour ellipse that is divided into many triangles. Each triangle connects two neighbour points on the skin colour ellipse boundary and the central point A. More triangles are used, more accurate the ellipse can be represented. In order to morph the statistical skin colour centre A to a preferred skin colour centre B, A is moved to out of the central position (see Fig.

5.3-2). All triangles are reshaped accordingly, but the skin colour boundary points are not changed, i.e., *C0'* and *C1'* in Fig. 5.3-2 are the same as *C0* and *C1* in Fig. 5.3-1, respectively.
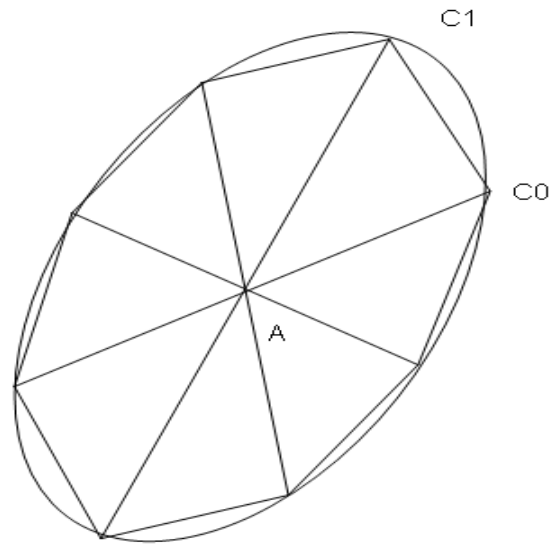
Fig. 5.3-1 A skin colour ellipse divided into many triangles (A is the statistical skin colour centre)
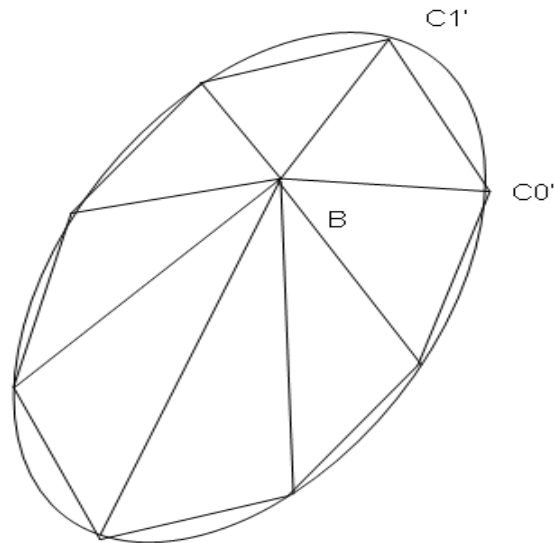
Fig. 5.3-2 A skin colour ellipse divided into many triangles (B is the preferred skin colour centre)

To adjust a skin colour, a triangle that contains the colour is found, and then a triangle-based interpolation is performed. Let's assume a skin colour, *P*, is within the triangle *A-C0-C1*, as shown in Fig. 5.3-3, and the mean skin colour *A* is mapped to the preferred skin colour *B* while *C0* and *C1* stay unchanged. A method to preserve area ratio of three sub-triangles may be used to compute a new mapping colour *P'*. Areas of triangles *A-P-C0*, *A-P-C1*, and *P-C0-C1* are noted $S_{A\text{-}P\text{-}C0}$, $S_{A\text{-}P\text{-}}$

$_{C1}$, and $S_{P\text{-}C0\text{-}C1}$ respectively. They are computed using three known colours, A, $C0$, and $C1$, and the original skin colour P. A new colour, P', adjusted from the original colour, P, is computed by the following equation:

$$P' = \left(C0 \cdot S_{A-P-C1} + C1 \cdot S_{A-P-C0} + B \cdot S_{P-C0-C1}\right) / \left(S_{A-P-C1} + S_{A-P-C0} + S_{P-C0-C1}\right)$$
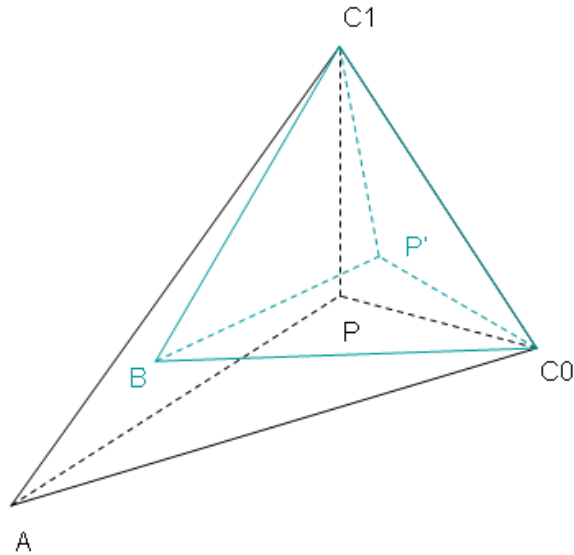
Fig. 5.3-3 A triangle that contains an original skin colour, P, to be adjusted and mapped to P'.

One important property of this new method is that the statistical colour centre of the original skin colours A is mapped to a target preferred skin colour, B, and all other colours are morphed smoothly. No contouring is produced with this approach.

If lightness is modified together with chrominance, the morphing method must be expanded to a 3-D space. The original central colour A in each of sampled lightness level is mapped to a corresponding preferred colour B in which lightness may be different. A set of sampling points to represent the boundary of the skin colour gamut defined with a lightness-dependent ellipse model, an ellipsoid model, or any other models are constructed. The boundary sampling points and the interior points (A's in the original skin colour domain or B's in the reproduced skin colour domain) are used to construct a set of tetrahedral. Tetrahedral interpolation is applied to map each original skin colour to a corresponding output skin colour for preferred skin colour reproduction.

5.4 Lightness Adjustment for Skin Colour Enhancement

In all above skin colour adjustment algorithms, lightness is not modified. It is clear that lightness of facial tones closes to the white point or closes to the black point is too extreme and is very likely not preferred, and should be adjusted to

improve the skin colour preference. On the other hand, the mean lightness of facial tones in an image may be in the preferred region, however, faces may look flat due to low contrast in facial tones. In both cases, adjusting lightness of skin tones will improve the overall image quality.

Adjusting lightness of skin colours was tested in a previous study. Mean and standardization of lightness of skin tone were computed. The contrast of skin tones was increase if the standardization was low. A clear benefit is that the depth effect of faces is increased, thus it improves the 3-dimensional effect of people characters. However, if the image is noisy, skin tones becomes noiser after the lightness adjustment. For this reason, lightness is usually untouched.

If an image is noisy, probabilities of colours to be skin colours will be noisy. Although adjusting chromaticity of skin colours may increase colour noise, the visual noise is not amplified because colour noise is not sensitive to human eyes. Since noise in lightness/luminance channel is very sensitive to human eyes, the amplification of lightness noise due to lightness adjustment will be significant if the original image is noisy. To resolve this problem, an original image may be segmented into a pair of a low-frequency image and a high-frequency image and the lightness adjustment is performed only on the low-frequency image.

Skin tones are very dark in under-exposure images and are very light in over-exposure images. The mean lightness of face tones may be used to readjust the tone curve of the image. This will not only improve the preference of skin tones, but also improve the overall global tone characteristics.

5.5 Conclusions

Different preferred skin colour enhancement algorithms were developed for skin colour enhancement. The first method applies a statistical skin colour model to detect skin colours, and morphs skin colours toward a preferred skin colour centre. Psychophysical experiments validated that the method of preferred skin colour enhancement effectively identified skin colours without face recognition, improved the skin colour preference, and did not objectionably affect preferred skin colours in original images.

If skin colours are too much off from the regular skin colour distribution, applying above skin colour enhancement method may not enhance skin colours effectively. A face detection aided skin colour enhancement method was developed to resolve the limitation. With face box information, skin colour detection is more accurate, and a wider range of skin tones can be enhanced. With the skin colour model adapted to the individual image using face information, skin colours that are

far away from the preferred skin colour centre can be morphed toward a preferred skin colour centre more effectively.

To increase the computation efficiency, both algorithms may be implemented by pre-generating a 3-D LUT and applying 3-D interpolation to process image pixels.

Chapter 6
Verifying Preferred Skin Colour Enhancement

Psychophysical experiments described in Chapter 4 were designed to prove that preferred skin colours existed in a very small colour region within the skin colour region and to find preferred skin colour centres that would be used for skin colour enhancement. Different from the earlier experiments, the objective of the psychophysical experiments introduced in this chapter was to verify the skin colour enhancement algorithms developed in the prior chapter. Since all earlier psychophysical experiments have been conducted using CRT or LCD displays, the new experiments were conducted in hardcopies. It was anticipated that this could be useful for analysing whether skin colour preferences between display and hardcopies were different.

6.1 Verifying Preferred Skin Colour Centres for Hardcopy Colour Reproduction

Since viewing conditions and adapted white points in hardcopies are different from those in displays, it is not clear whether preferred skin colour centres between display and hardcopy are the same. For such reason, a set of skin colour centres around the preferred skin colour region found through softcopy were carefully selected for the experiment to verify and to optimize the preferred skin colour centre for hardcopies. It was expected that the preferred skin colour centre on print should be close to that on display. Different from the experiments in Chapter 4, each original image was compared with skin colour adjusted images to verify whether skin colour enhanced images were more preferred to the original image.

Test images were printed on 4x6 -inch HP Advanced Photo Paper using an HP Photosmart Premium printer was used to print with the best print mode. A 10x10x10 printer RGB target was printed and measured using a Gretag Spectroscan in the spectral mode for printer colour characterisation. The relative spectral radiance curve of a D50 simulated light booth was applied to compute CIE XYZ values of each patch. A printer ICC profile was created for the colour transformation from PCS (profile connection space) to the printer colour space. The linear Bradford chromatic adaptation was applied to adapt the media white of the

target paper to the D50 white point in ICC PCS. A minimum-ΔE mapping was applied for gamut mapping, in which colours within the printer gamut were not adjusted and other colours were clipped to the printer gamut surface with a minimum colour difference metric. The colour difference was computed using the equation, $\Delta E = \sqrt{(w_L \Delta L^*)^2 + (w_c \Delta C^*)^2 + (w_H \Delta H^*)^2}$, where w_H was set to 1.5 and the other two weights were set to unity to produce a more accurate hue mapping.

The gamut mapping is performed in a uniform colour space. Since CIELAB colour space is lack of constant hue appearance in blue hue angles, gamut mapping in CIELAB without special treatment will introduce hue shift for blue colours (Zeng 2000, 2001). Since a special adjustment is required for the gamut mapping in the blue region if gamut mapping is performed in CIELAB colour space, a straight-forward approach is to perform gamut mapping in CIECAM02 colour space. However, many non real world colours in ICC PCS cannot be converted to CIECAM02 colour coordinates (Tastl et. al. 2005, Brill and Süsstrunk 2008). Although Gill (2008) modified CIECAM02 equations to resolve this problem, results of the colour transformation for colours out of the spectrum locus do not behave properly. As a result, the gamut mapping to create ICC profiles for investigating colour preference for the mapping from display to hardcopy was performed in CIE CAM97s, which is most close to CIE CAM02. The PCS black point was adapted to the printer black point using a simple black point compensation method in CIE XYZ colour space.

Five carefully selected skin colour centres shown in Table 6.1-1 and Fig. 6.1-1 were tested. (21.1, 24.4) is the PSCC found for mixed skin colours judged dominantly by Caucasian using LCD displays. Because the photo printer had a very larger gamut, it was speculated that observers might prefer more chromatic skin colour. With some reference information from another ongoing psychophysical experiment and with some pre-testing, three more chromatic skin colours and one less chromatic skin colours were chosen for testing, and their hue angles are close with each other.

Table 6.1-1 Five skin colour centres for testing

	A	B	C	D	E
a*	19	21.1	23	25	24
b*	23	24.4	23	25	27

Light, medium, and dark skin colour centres were set to be the same, i.e., a single skin colour centre was used for skin colour adjustment. As skin colours of

each image were morphed toward each of five skin colour centres, five versions of images were created. These versions of images and the original image were used to test the colour preference by a rank-order method.
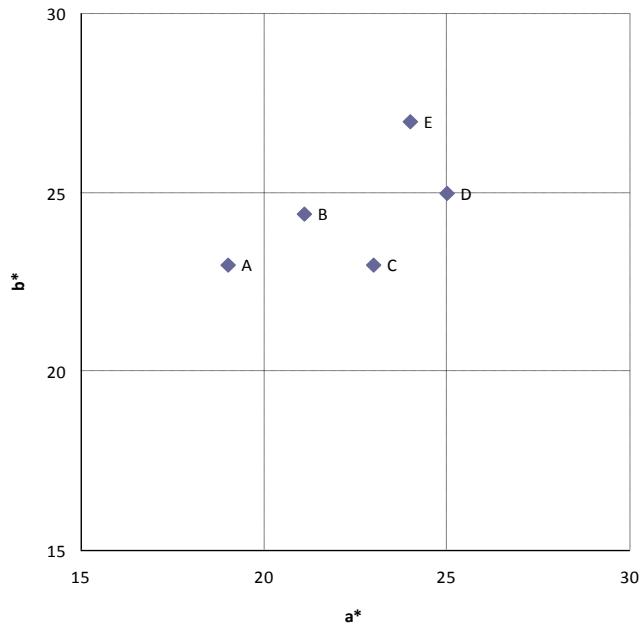
Fig. 6.1-1 Five skin colour centres for testing

The experiment was divided into two parts: a group of Chinese observers to judge Oriental face images; and a group of Caucasian observers to judge Caucasian images. Since the result would be used for consumer retail photo printing, most of observers chosen to participate the experiment were not professionals in colour imaging and were not experienced in colour image quality judgment. However, all of them had normal colour vision (wearing glasses if necessary). It was expected that the final result would be noisier than those obtained from softcopy studies.

6.1.1 Verifying Chinese Preferred Skin Colour Centre for Hardcopy Colour Reproduction

Four images as shown in Fig. 6.1.1-1 were used for testing. 19 Chinese observers participated in the experiment. 15 of them were male and others were female. Their ages were between 25 and 50. Observers evaluated print hardcopies displayed in a lighting booth. None of them was professional in colour imaging. They were guided to sort six versions of images based on their colour preference. The preferences from most disliked to most preferred were given scores from 1 to 6, respectively.

The total scores are converted to percentages and finally to z-scores. Z-scores are then shifted so that all of them are positive. The results, including the 95% confidence interval, are plotted in Fig. 6.1.1-2. Table 6.1.1-1 lists the z-scores. Two

images, Asian_light and Maxwell, having small discrepancies among the original version and all other colour adjusted versions. The reason is that skin colours of these two images are close to optimal, the adjustments are subtle, and therefore the visual results before and after adjustment are about the same. The results from these two images show that the skin colour adjustment does not degrade the quality of images in which skin colours are optimal.

For the other two images, the original version is least preferred; the adjustment toward the skin colour centre (19, 23) improves slightly; and the adjustment toward other four skin colour centres has a trend to improve the preference. The skin colour centres, (23, 23) and (25, 25), are slightly more pleasing than others, and the next preferred skin colour centres are (21.1, 24.4) and (24, 27).

Asian_light   South_Asian   Maxwell   Teresa

Fig. 6.1.1-1 Images to test Oriental skin colour preference on hardcopy
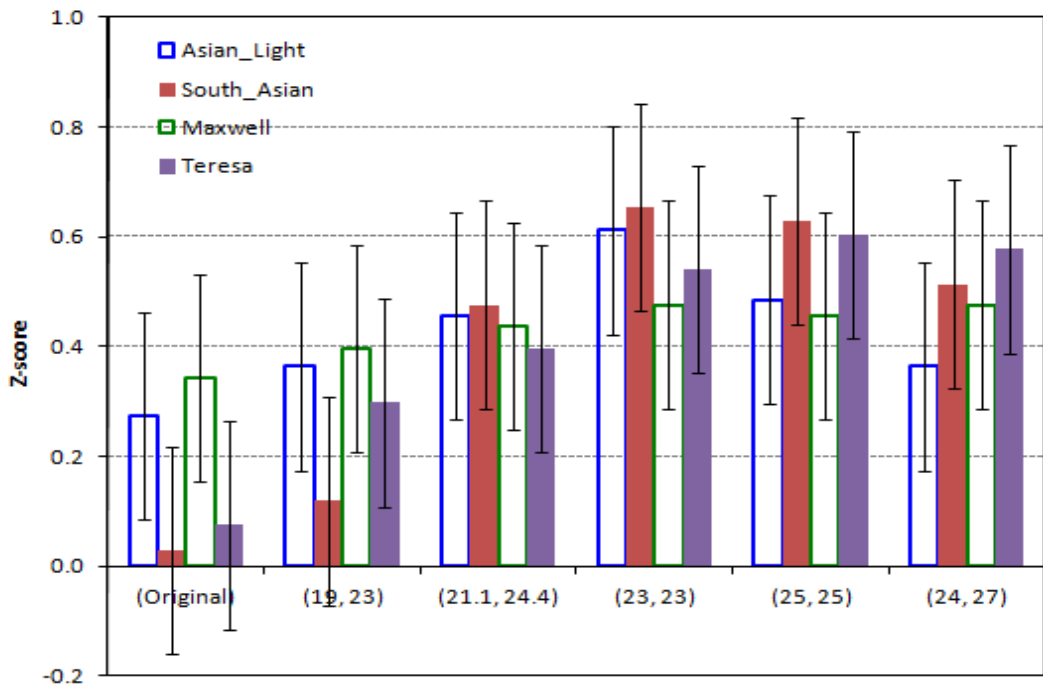
Fig. 6.1.1-2 Z-score of Chinese colour preference on hardcopies

Table 6.1.1-1 Z-scores of Chinese colour preference on hardcopies

	(Original)	*(19, 23)*	*(21.1, 24.4)*	*(23, 23)*	*(25, 25)*	*(24, 27)*
Asian_Light	0.3	0.4	0.5	0.6	0.5	0.4
South_Asian	0.0	0.1	0.5	0.7	0.6	0.5
Maxwell	0.3	0.4	0.4	0.5	0.5	0.5
Teresa	0.1	0.3	0.4	0.5	0.6	0.6

The overall performances of the four preferred skin colour centres are very close. This suggests that the preferred skin colour centre is a region instead of a point. A preferred skin colour centre for hardcopy seems to be slightly more chromatic than that in display. One possible reason is that observers prefer more chromatic skin colours in hardcopy than in monitor display.

6.1.2 Verifying Caucasian Preferred Skin Colour Centre for Hardcopy Colour Reproduction

The same experimental procedures were repeated to verify preferred Caucasian skin colour centres. Four images shown in Fig.6.1.2-1 were judged by 19 Caucasian observers. 10 of them were male and others were female. Their ages were between 20 and 50. All of them were not professionals in colour imaging.

Baby   Halloween   PianoGirl   Eating

Fig. 6.1.2-1 Images to test Caucasian skin colour preference on hardcopy

The z-scores and their 95% confidence intervals are plotted in Fig. 6.1.2-2. The z-scores are listed in Table 6.1.2-1 as well. Because the skin tone of PianoGirl is close to optimal, the skin colour adjustment neither improves the preference nor degrades the preference. Except for PianoGirl, the skin colour adjustment improves the preference on other three images. Among five skin colour centres, (19, 23) is least preferred and other four have similar preference. The preference differences among (21.1, 24.4), (23, 23), (25, 25), and (24, 27) are not significant. The result shows that the average preferred skin colour locates in a small colour area. A factor

for the wide distribution of preferred skin colour centres may be that all observers in this experiment were non-experience in judging colour image quality and therefore were not sensitive in small colour difference.
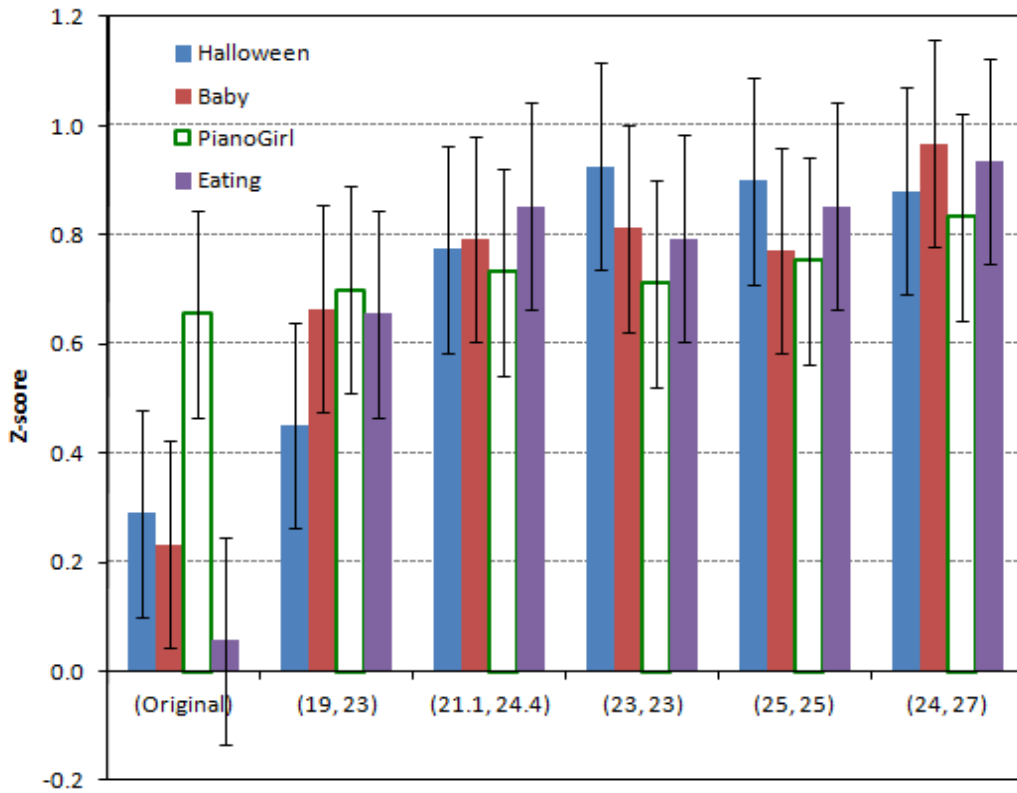
Fig. 6.1.2-2 Z-scores of Caucasian colour preference on hardcopies

Table 6.1.2-1 Z-scores Caucasian colour preference on hardcopies

	(Original)	*(19, 23)*	*(21.1, 24.4)*	*(23, 23)*	*(25, 25)*	*(24, 27)*
Halloween	0.3	0.5	0.8	0.9	0.9	0.9
Baby	0.2	0.7	0.8	0.8	0.8	1.0
PianaGirl	0.7	0.7	0.7	0.7	0.8	0.8
Eating	0.1	0.7	0.9	0.8	0.9	0.9

6.2 Validating the Skin Colour Enhancement Algorithm

A psychophysical experiment was conducted by a third party to evaluate the preferred skin colour enhancement on hardcopy. The purpose was to validate the effectiveness of the first skin colour enhancement algorithm, the skin colour enhancement without face detection that was implemented in a system for consumer

photo printing. All test images were printed using an HP commercial retail photo printer.

50 Caucasian images and 50 Oriental images were selected for testing. Most of them were captured using consumer digital cameras. Face colours of most images are close to optimal or have slight colour casts. 28 Caucasian observers and 25 Asian observers judged Caucasian images and Oriental images, respectively. All observers had normal colour vision. Observers directly compared between each pair of the original image and its corresponding processed image for overall preference and answered whether the quality of each of them was acceptable or not.

The psychophysical experiment was to verify following properties:

- Skin tones in an image can be effectively identified without facial recognition

- Skin tones can be adjusted automatically towards a preferred colour centre to improve skin colour acceptance

- Optimal skin tones remains unchanged while non-optimal skin tones are adjusted to improve acceptance

- Non-skin tone colours are not objectionably affected

- No objectionable artifacts are introduced
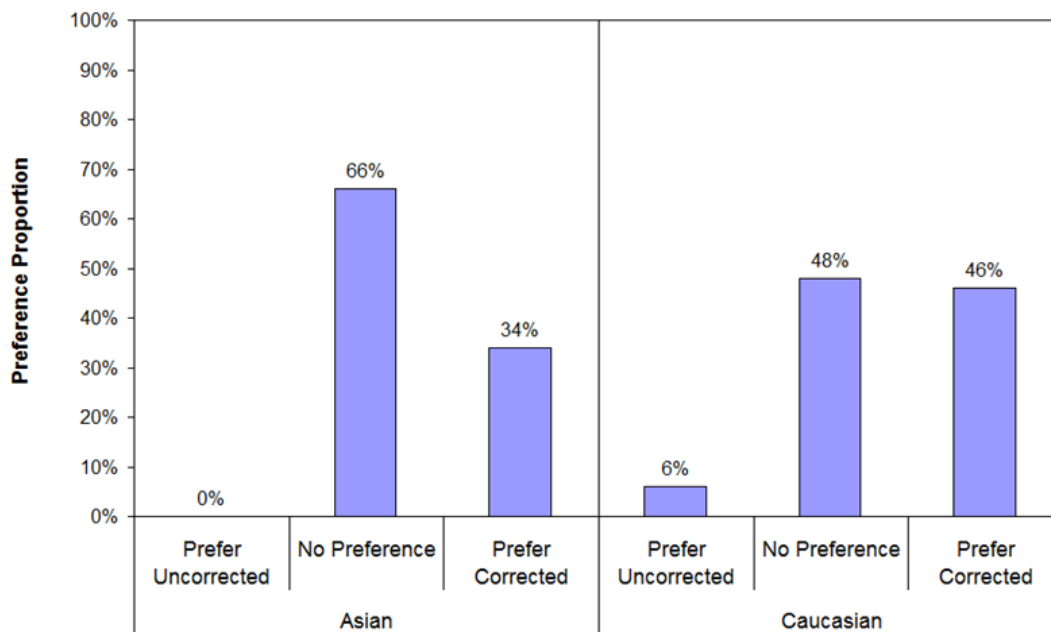
Fig. 6.2-1 Psychophysical experimental result

Experimental results (see Fig. 6.2-1), observations, and comments are summarized below:

- 46% have significant improvement while 6% have negative impact for Caucasian images;

- Overall slightly too reddish corrections for Caucasian skin tones from observer comments (preferred skin centre needs to be optimized);

- 34% have significant improvement while no negative impact for Oriental images;

- No objectionable artifacts introduced;

- Virtually no visible changes to non-skin tone images;

- Although the skin colour adjustment modifies all skin colours including those non-skin objects, there is no objections that skin colours of non-skin objects are adjusted; and

- Expecting further improvement after fine tuning the algorithm, refining preferred skin colour centres, optimizing adjustment knobs, and increasing correction strength.

The skin colour detection method using the ellipsoid modelling without face recognition modifies all colours that are skin colours, including skin colours of non-skin objects. Small adjustment of skin colours of non-skin objects is generally not objectionable to observers. Although adding face detection will solve the problem that skin colours of non-skin objects are modified, other body skin colours may be excluded from enhancement as well.

In this experiment, skin colour centres and other parameters have not been optimized yet. With final optimization of the algorithm, skin colour centres, and other parameters, the result should be improved.

6.3 Summary

The results from the first part of psychophysical experiments reveal that the preferred skin colour centre exists on a small colour region; if skin tones of an image are within the preferred skin colour region, morphing skin colours towards the preferred skin colour centre does not further improve skin colour preference; and observers seems to prefer slightly more chromatic skin colours in hardcopy than in display (i.e. a preferred skin colour centre for hardcopy may be slightly more chromatic than that in display).

Results of the other psychophysical experiment validate that even without applying skin colour detection, the proposed skin colour enhancement methods effectively improve skin colour acceptance rates; and although the skin colour enhancement without face detection modifies skin colours of non-skin objects, no objections were found.

Chapter 7
Green Foliage and Blue Sky Colours

Reproducing memory colours pleasing is essential for preferred colour reproduction of photographic images. Skin tone, green foliage, and blue sky are the main categories of memory colours. Preferred reproduction of these three prototypical colours is very important. The study of skin colour detection and enhancement has been presented in previous chapters. A brief study of green foliage and blue sky are presented in this chapter

7.1 Modelling Green Foliage Colours for Green Foliage Detection and Colour Reproduction

Detecting foliage colours based on a hue angle range and a chroma range has been widely used for the colour enhancement of foliage colours (referred to Section 2.4.5). Although it is very simple, the detection accuracy may be compromised. In this study, a new approach to model green foliage colours was developed to improve the accuracy for detecting green foliage. The colour preference in printing foliage images was studied as well.

7.1.1 Green Foliage Colour Cluster

To study the shape of the colour gamut of green foliage, about 400 sRGB green foliage images were collected. Approximately 80% of images were captured by the author using different digital cameras, including a few Canon and Nikon professional DSLR cameras and several consumer cameras. Most of images were captured outdoor in different seasons. No scenes were captured repeatedly. The CMT described in Section 3.2 was used to mask green foliage pixels for histogram analysis. A slight difference of this version of the tool from the version used before is that the seed colour is displayed on the bottom left (see Fig. 7.1.1-1). The pixels labelled as foliage colours are masked with magenta on the centre window. The mask values of the image are drawn as a gray-scale image shown on the right window.
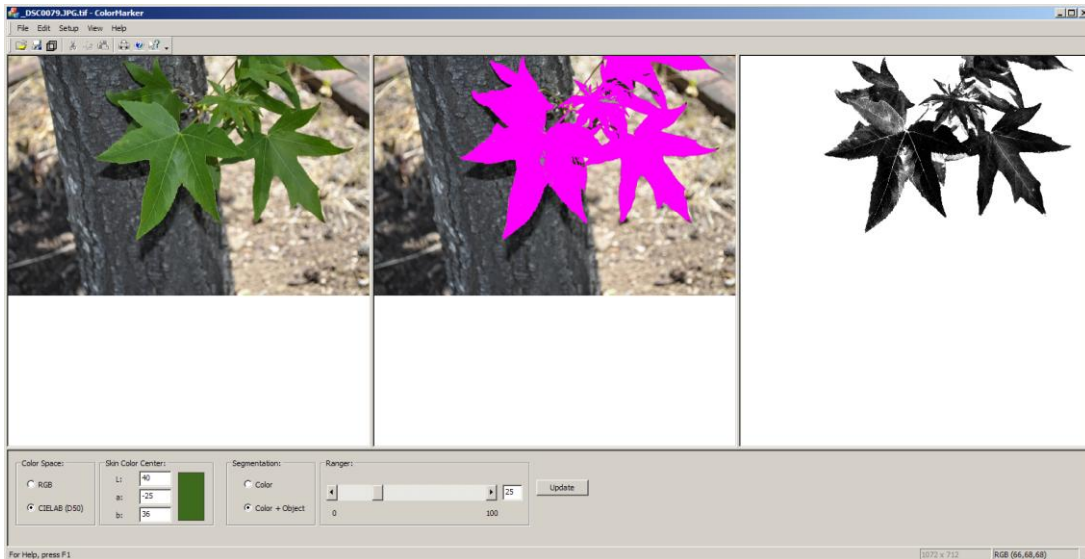
Fig. 7.1.1-1 The colour masking tool to create green foliage colour database

The foliage colours of all images were selected mostly by the author. Because a another step was followed to remove lower occurrence pixels when counting pixel occurrences of each image and a huge amount of foliage pixels (in the order of billions) were collected from the 400 collected images, the bias from user selection should be insignificant.

The method to construct a colour histogram LUT described in Section 3.2 was applied to construct a 256x256x256 RGB LUT to count the foliage colour occurrences. 5% least frequent pixels were removed from each image. After a LUT was generated from all images, 1% of the least occurred colours were removed from the LUT. The method to process LUT described in Section 3.2 was applied to generate foliage colour histogram in CIELAB colour space (adapted to D50). The foliage colours are plotted in Fig. 7.1.1-2, along with the sRGB gamut. Because sRGB gamut is not large enough to encode green colours, high chromatic green foliage colours are clipped to the sRGB gamut surface. Another commonly used RGB colour space, Adobe RGB 1998 colour space, encodes a much larger colour gamut (Adobe RGB Colour Image Encoding, 2005). Fig. 7.1.1-3 shows a comparison of sRGB colour space and Adobe RGB colour space in CIELAB a* b* coordinates. Adobe RGB has a much larger colour gamut around the green region. Consequently, it was decided to capture foliage images using Adobe RGB colour space.

800 Adobe RGB images were captured to study green foliage colours. These images were captured using Nikon D5000 and Canon 40D SLR professional digital cameras during spring, summer, and fall seasons in north-west United States. The procedure to process sRGB images was repeated to create an Adobe RGB histogram LUT.
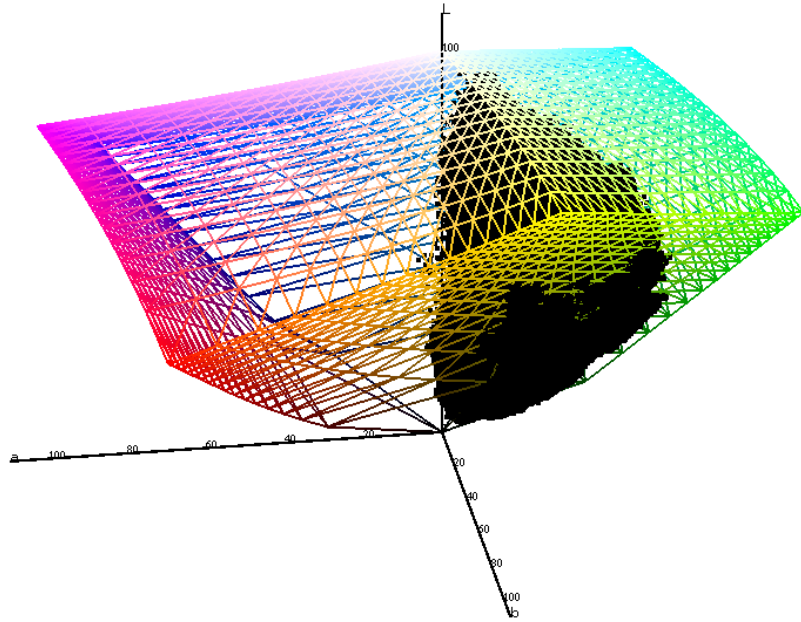
Fig. 7.1.1-2 Foliage colour cluster (black) and sRGB gamut (colour wireframe) in CIELAB colour space
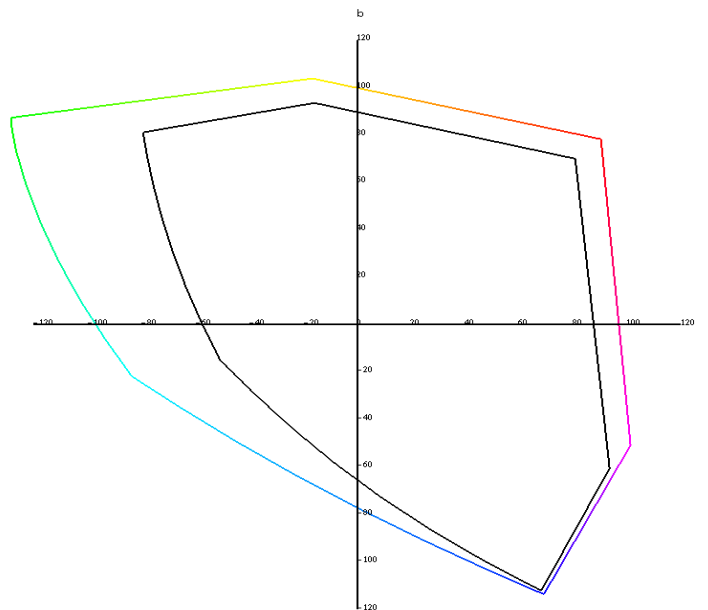
Fig. 7.1.1-3 A comparison of sRGB colour space and Adobe RGB colour space in CIELAB a* b* coordinates

Fig. 7.1.1-4 shows the green foliage colour cluster of Adobe RGB images along with the Adobe RGB gamut. Compared to Fig. 6.1.1-2, the area of the foliage colour cluster intercepting on gamut surface is smaller, which implies chances of foliage colours clipping due to gamut limitation are smaller.
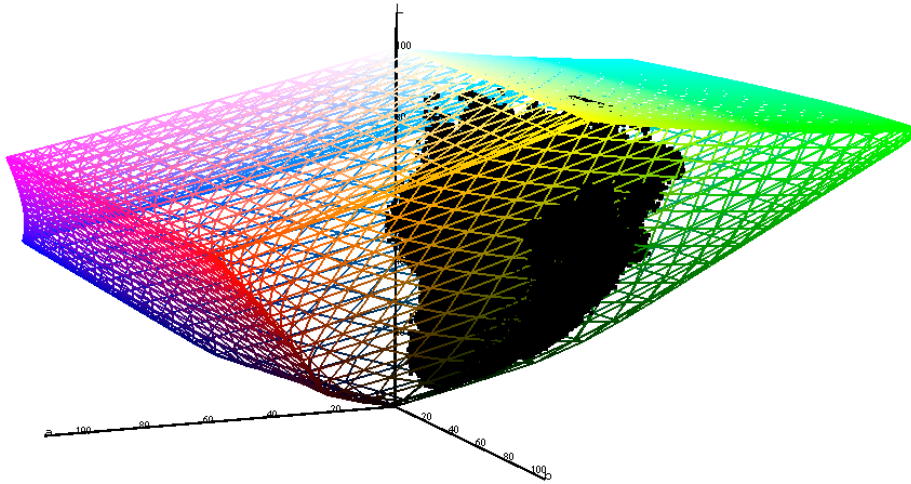
Fig. 7.1.1-4 Foliage colour cluster (black) and Adobe RGB gamut (colour wireframe) in CIELAB colour space

7.1.2 Foliage Colour Modelling

Since the elliptical model has been successfully applied for skin colour modelling, it was tested for foliage colour modelling. Fig. 7.1.2-1 shows an ellipsoid to encompass the foliage colour cluster. In the right plot, the b* positive direction points out of paper toward the reader. The ellipsoid covers many high chroma green colours that are not foliage greens collected from our image set (see the boundary regions in the left plot). This seems to be fine, because 1) there are very few Adobe RGB colours in that area therefore there will be no false detection for colour in this region for Adobe RGB images; and 2) there may be some high chroma green colours existed in the high chroma region and are clipped to the gamut surface of the Adobe RGB colour space so a model stretching a little bit toward the high chroma region may help cancelling out the limitation of the colour space encoding. Overall, the ellipsoid practically fits foliage colours.

Fig. 7.1.2-2 shows the projection of the green foliage colours and the trained ellipsoid on CIELAB a*-b* plan. The large and small hexagons are Adobe RGB gamut and sRGB gamut, respectively. A method that has been widely used for green colour detection for enhancing green foliage colours is to consider that green foliage colours are confined within a range of hue angles. If a colour is within this hue range, it is a green foliage colour. Fig. 7.1.2-2 shows that a trained ellipsoid covers the green foliage colours very well, and using a hue range to set a boundary for green foliage colours is subject to high inaccuracy. The foliage colours span an approximate hue range of $[100^o$ to $190^o]$ and their chroma values are up to about 80. The lower-end hue angle in the yellow-green side can be determined fairly well using a constant hue threshold (see a red straight-line). However, in the green-blue

region, using a constant hue threshold to judge whether a colour is foliage green is inaccurate and will subject to larger errors (see another red straight-line).
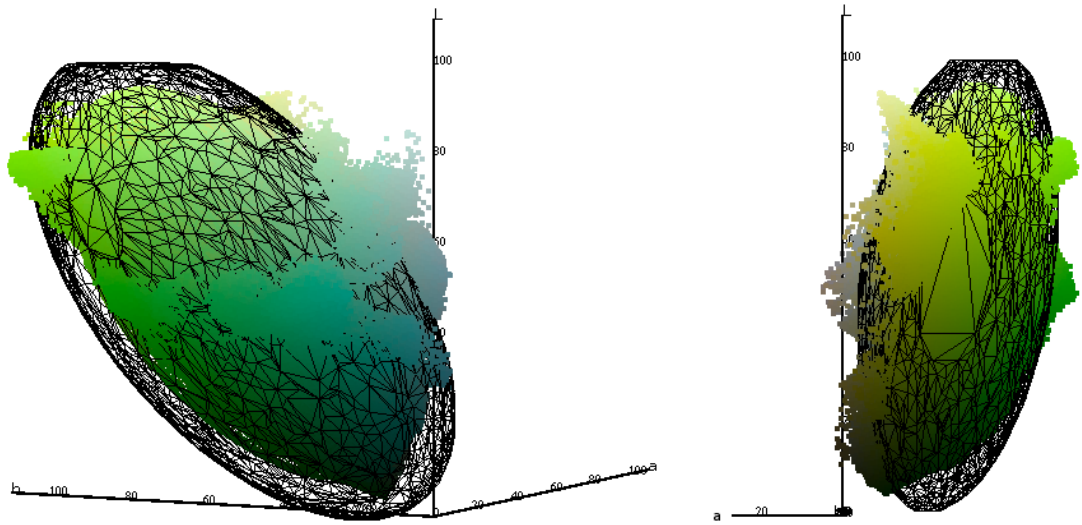
Fig. 7.1.2-1 Foliage colour cluster and an ellipsoid to encompass the region in CIELAB colour space
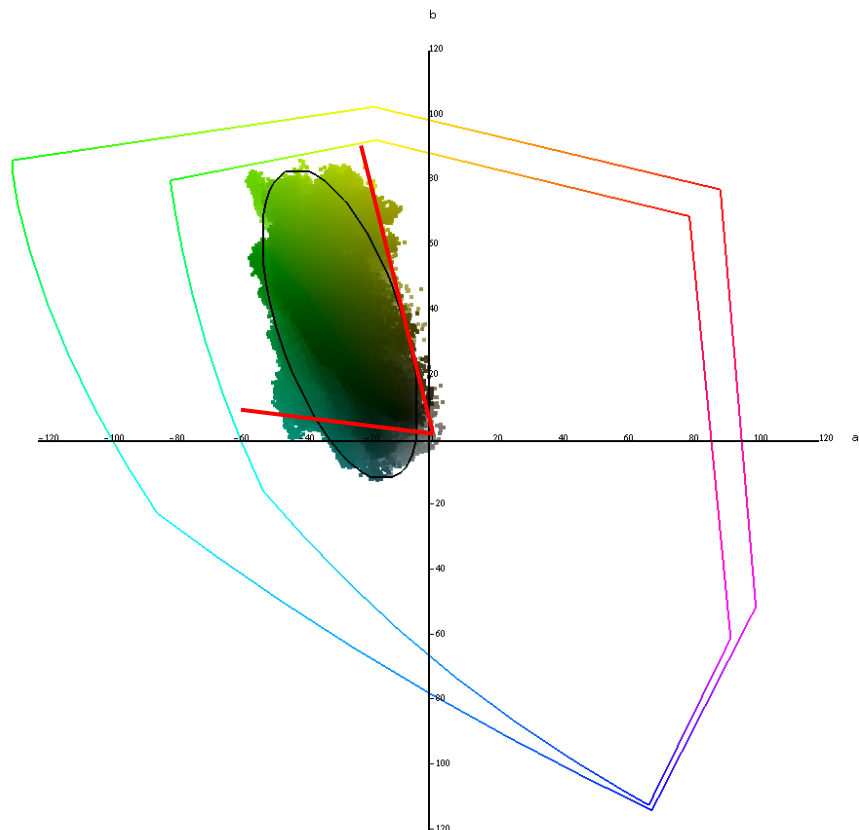
Fig. 7.1.2-2 Foliage colour cluster and the trained ellipsoid projected on CIELAB a*-b* plan

7.1.3 Results of the Foliage Colour Modelling

The elliptical boundary model used for skin colour modelling is applied for foliage colour modelling as well.

The training result of an ellipse to cover 97% of foliage colours (a colour with n occurrences is counted as n colours) is shown in Fig. 7.1.3-1. The centre is (-24.7, 34.2), and ($A, A/B, \theta$) are (32.9, 2.0, 74.1^o), where $A, A/B$, and θ are the semi-major axis, ratio of major and minor axes, and the orientation of the major axis from the horizontal axis.

The same data set was used to train an ellipse to cover 97% of foliage colours in CAM02-UCS as well. The result is shown in Fig. 7.1.3-2. The ellipse centre is (-16.3, 19.5), and ($A, A/B, \theta$) is (14.7, 1.6, 76.9^o). The ellipse in CAM02-UCS is slightly closer to circle (A/B is closer to unity). This may imply that CAM02-UCS is slightly more uniform in representing green foliage colours. More detailed training data can be found in Appendix L.

An ellipsoid to cover 97% of foliage colours in CIELAB colour space (a colour with n occurrence is counted as n colours) is shown in Fig. 7.1.3-3. The ellipsoid centre is (48.0, -24.7, 34.2); the principal axis parameters [$A, A/B, A/C$] are [36.7, 1.2, 2.0], where A, B, and C are three semi-major axes; and the unit vectors of three principal axes relative to the centre are (-0.31, 0.27, -0.91), (0.95, 0.07, -0.30), and (0.02, 0.96, 0.29). u_i (i = 0, 1, 2, 3, 4, 5) coefficients are (0.000755838, 0.00032089, 0.00280571, -0.0010427, 0.000955474, 0.00123239), with $\rho = 1$.

The same data set was used to train an ellipsoid to cover 97% of foliage colours in CAM02-UCS as well. The ellipsoid centre is (49.7, -16.3, 19.5), and [$A, A/B, A/C$] is [36.7, 1.8, 2.7]. Unit vectors of three principal axes relative to the centre are (0.97, 0.25, -0.07), (0.14, -0.28, 0.95), and (-0.05, 0.96, 0.29). u_i coefficients are (0.000629658, -2.40587e-005, 0.00829304, -0.00167367, 0.00225355, 0.00487879). More details of the training results can be found in Appendix M.

Fig. 7.1.3-4 shows the projection of green foliage ellipsoids with four coverage rates (99%, 97%, 95%, and 90%) on CIELAB a*-b* plane. From 90% to 95% coverage rates, a modelled ellipse grows very little, while from 95% to 99% coverage rates, a modelled ellipse grows a lot. This is the result of the histogram distribution where green foliage colours occur more frequently in the centre region than in the exterior region.
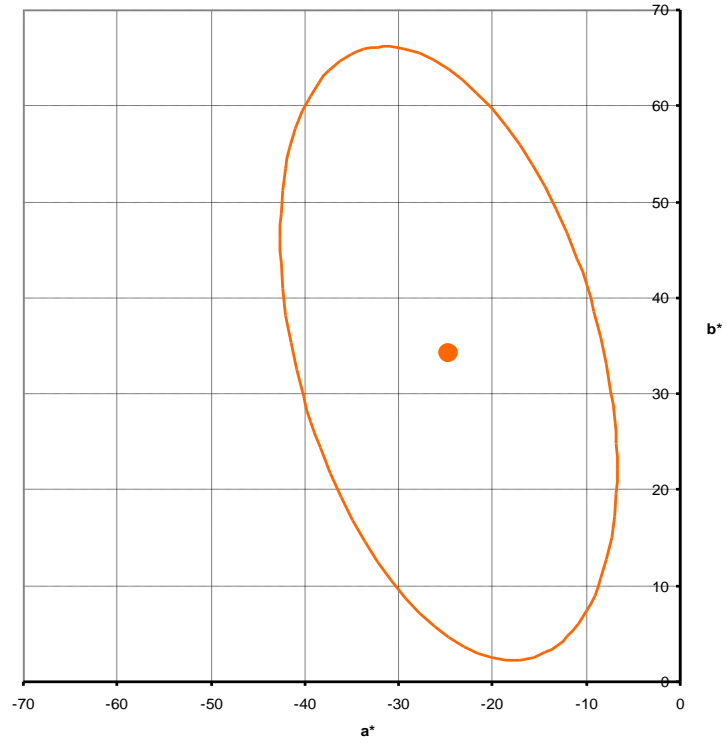
Fig. 7.1.3-1 An ellipse to cover 97% of foliage colours in CIELAB a*-b* coordinates
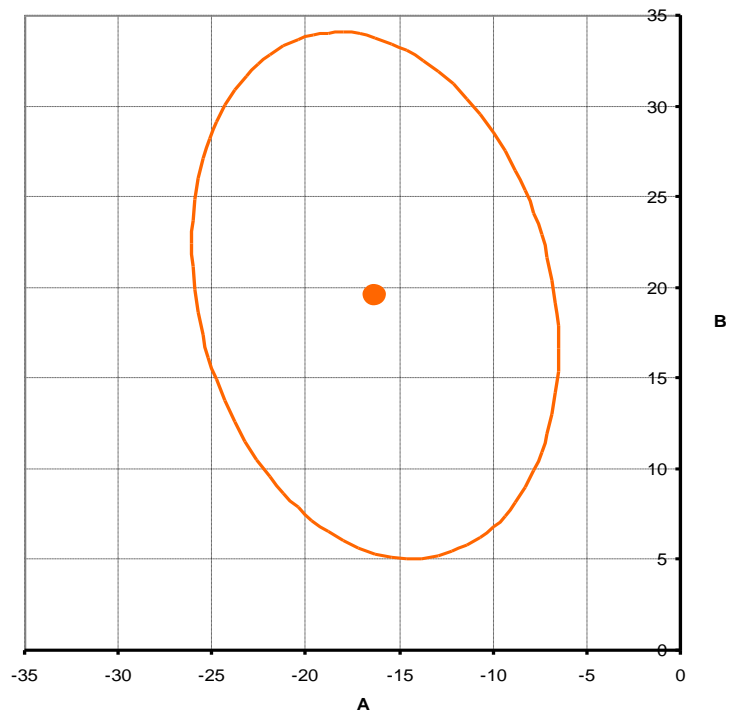
Fig. 7.1.3-2 An ellipse to cover 97% of foliage colours in CAM02-UCS chroma coordinates
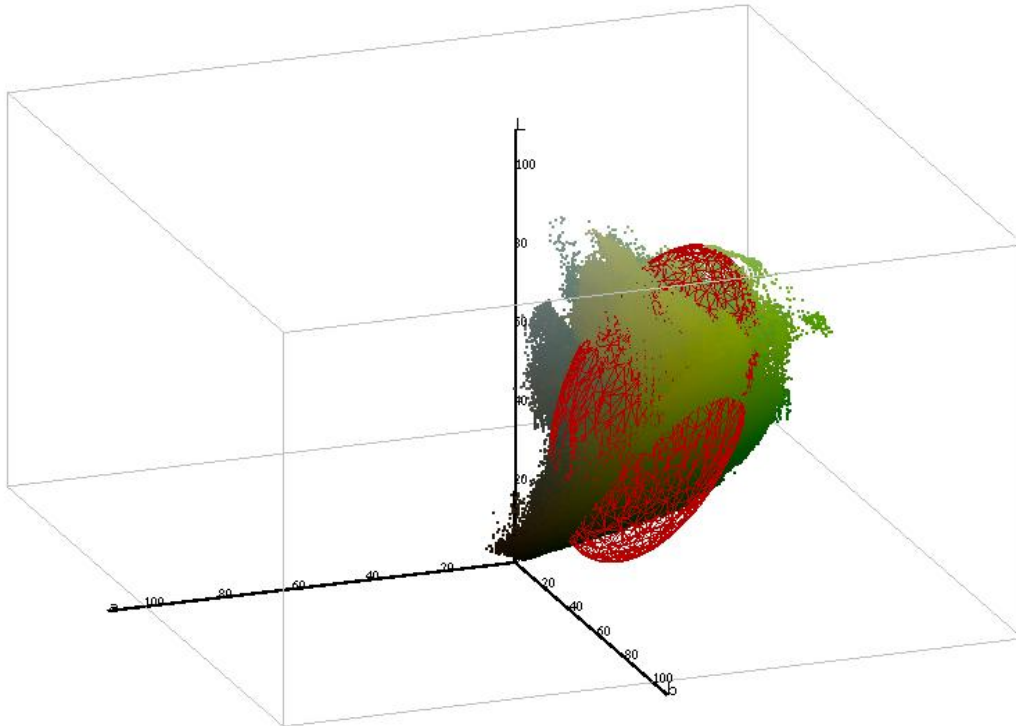
Fig. 7.1.3-3 An ellipsoid to cover 97% of foliage colours in CIELAB colour space
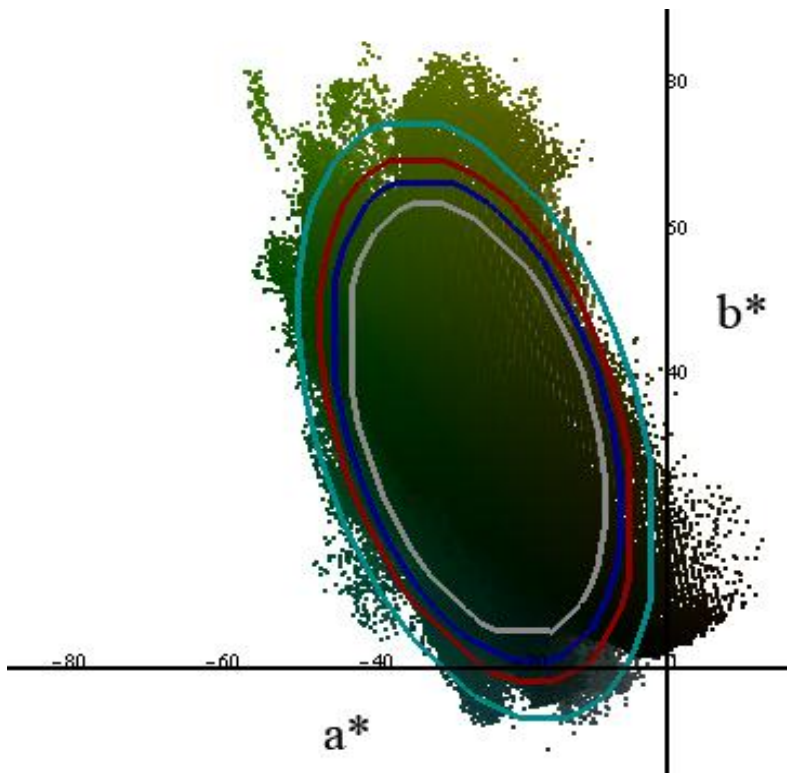
Fig. 7.1.3-4 Four green foliage ellipsoids projected on CIELAB a*-b* plane: the green foliage colours masked from the foliage database are shown in emulated colours; cyan, red, blue, and white ellipses correspond to the modelling with 99%, 97%, 95%, and 90% coverage rates, respectively.

Fig 7.1.3-5 shows the comparison of foliage detection using an ellipse model and an ellipsoid model in CIELAB colour space, both with a 95% coverage rate. Detected colours are marked in pink. The ellipse model detects more light green colours, because with an ellipse model, a fixed ellipse is applied to all lightness levels. Although the gamut of highlight green foliage colours is smaller than that in the mid-lightness level, the size of the ellipse is not reduce, thus more colours are detected in the lighter region than that using an ellipsoid model.

Fig. 7.1.3-5 A comparison of green foliage detections by an ellipse model and by an ellipsoid model: original (left), detection using an ellipsoid model with 95% coverage rate (centre), and detection using an ellipse model with 95% coverage rate (right).

Fig. 7.1.3-6 shows the impact of modelling coverage rates on foliage detection. Increasing modelling coverage rate increases the foliage detection rate, however, the chance of false detection increases as well.

Fig. 7.1.3-6 Ellipsoid modelling with different coverage rates: original (upper-left), 95% coverage rate (upper-right), 97% coverage rate (lower-left), and 99% coverage rate (lower-right)

If a modelling coverage rate is very high, colours near the region of green foliage colours will be detected as green foliage colours. On the other hand, if a coverage rate is very low, green foliage colours in the outer layer of the elliptical model will not be detected. Different coverage rates were tested on many different images to empirically determine a coverage rate for general green foliage detection. After testing on many images, an ellipsoid model with 97% coverage rate was found to be a good trade-off between correct detection and false detection.

7.1.4 Comparison of Real Foliage Colours and Foliage Colours of Digital Photographic Images
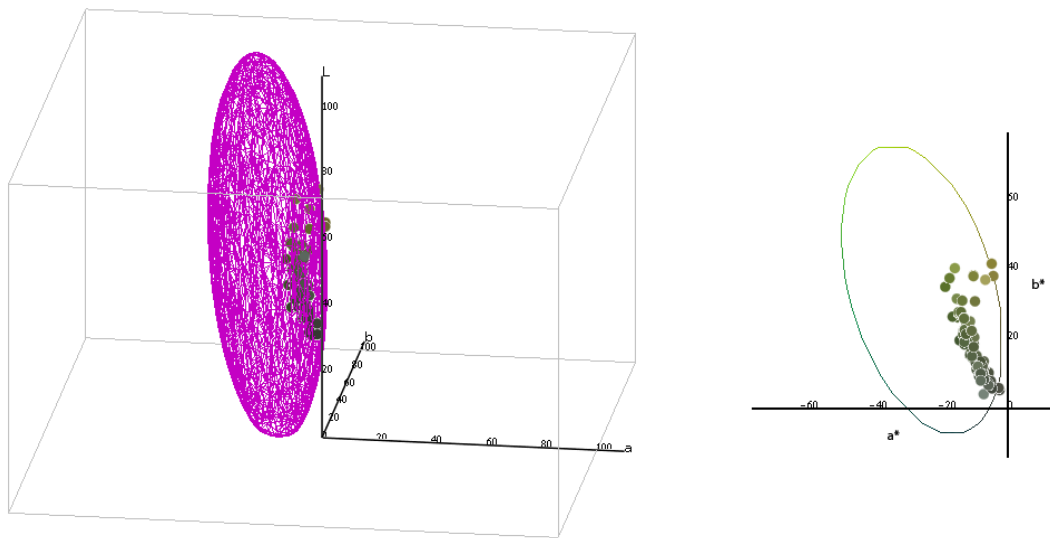
Fig. 7.1.4-1 SOCS Foliage colours (dots) and the foliage colour ellipsoid of digital photographic images in CIELAB colour space

Foliage colours from the Standard Object Colour Spectra database for colour reproduction evaluation (SOCS) [ISO/TR16066 Technical Report: Graphic technology - Standard object colour spectra database for colour reproduction evaluation (SOCS), 2003] were converted to colorimetric colours using D65 illuminant. Because all CIELAB data transformed from digital images were adapted to D50 using the linear Bradford chromatic adaptation transformation, the colorimetric data in D65 were adapted to D50 in the same manner. They are plotted as dots in CIELAB colour space in Fig. 7.1.4-1 (two colours in SOCS that are clearly not green foliage colours were excluded). The left figure shows the 3-D plot and the right figure shows its projection on the a*-b* plane. The ellipsoid model with 99% coverage rate is plotted for comparison. All colours are within the ellipsoid or are very close to the boundary of the ellipsoid. However, the SOCS colours are all in the yellowish side of the ellipsoid and their mean chroma is lower than the mean chroma of the foliage green colours of digital images. This suggests that foliage memory colours are shifted to the blue direction with higher chroma.

The hue shift is to make plant colours appear healthier and increasing chroma is to further improve preference. In other words, preferred green foliage colours are more chromatic and less yellowish than real green foliage colours.

An obvious difference between the skin colour preference and the green foliage colour preference is that the preferred skin colours are in a small region around a centre while preferred green foliage colours does not have a centre. There could be a preferred foliage hue centre, but it is clear that there is no preferred foliage chroma centre. When skin colour chroma is higher than the chroma of the preferred skin colour, the chroma should be lower down. However, the chroma of foliage colours should normally not be reduced in colour enhancement.

7.1.5 Summary

The green foliage colours distribute around a region in which a portion of the gamut cannot be encoded by sRGB colour space, i.e., sRGB colour space is not large enough to encode all green foliage colours. The Adobe RGB colour space was then used to encode foliage images for this study. Visually checking the colour cluster of the green foliage samples masked from a large set of foliage images, it was found that the colour cluster could practically be fitted with an elliptical model, which was simple and easy to train. The elliptical model was therefore applied to model green foliage colours. Ellipses and ellipsoids were trained to model green foliage. The ellipsoid model with different coverage rates were tested on various images. An ellipsoid that covers 97% of the training data set was found to be a good trade-off between correct detection and false detection for green foliage detection.

Comparing the green foliage colours of photographic images with real green foliage colours reveals that the preferred green foliage colours are less yellowish and more chromatic than the real green foliage colours.

7.2 Modelling Blue Sky Colours for Blue Sky Colour Enhancement

As discussed in Chapter 2, the blue sky detection may be colour based, feature based, or the combination of both. In this study, the elliptical colour modelling that had been applied to detect skin tones and green foliage colours was applied to detect blue sky colours for sky colour enhancement.

7.2.1 Blue Sky Colour Cluster

400 sRGB blue sky images were collected to study blue sky colour detection. About half of the images were captured by the author using several different digital cameras, including professional digital cameras and consumer digital cameras. The

other half were collected from different sources, in which some were captured by co-workers when they travelled around the world and others were downloaded from World Wide Web. Again, CMT was used to label blue sky colour cluster for histogram analysis, CIELAB colour space and "colour + object" were used for region growing and segmentation, and very high-resolution images were re-sampled to an ideal size to avoid that high resolution images were over-weighted.

Similar to the skin colour modelling and the green foliage colour modelling, the frequencies of masked pixels were used to fill a 256x256x256 RGB LUT for colour modelling. To remove noisy pixels and pixels that were inaccurately labelled as sky pixels, 5% least frequent pixels were removed from each image. After a LUT is generated from all images, 1% of least occurred colours were removed from the LUT.

The method to process LUT described in Section 3.2 was applied to generate sky colour histogram in CIELAB colour space (adapted to D50). The sky colours are plotted in Fig. 7.2.1-1 in black dots, along with the sRGB gamut.
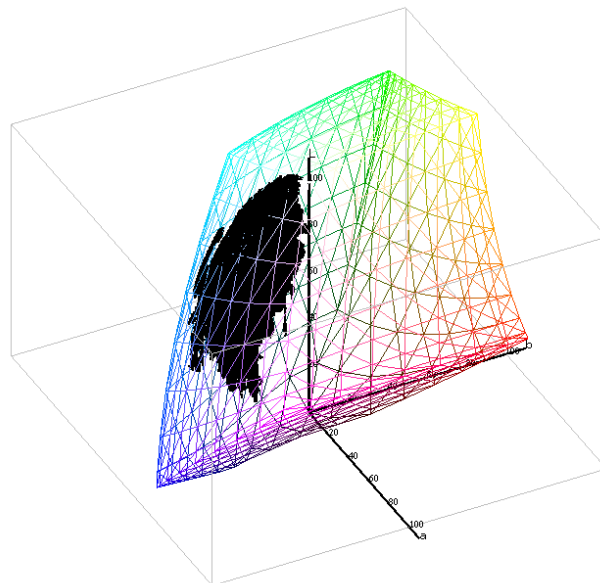
Fig. 7.2.1-1 Sky colour cluster (black) and sRGB gamut (colour wireframe) in CIELAB colour space

7.2.2 Results of the Blue Sky Colour Modelling

The training result of an ellipse in CIELAB colour space to cover 95% of blue sky colours (a colour with n occurrences is counted as 1 colour because occurrence/histogram may be biased with a relatively small amount of images) is shown in Fig. 7.2.2-1. The centre is (-5.6, -28.5), and (*A, A/B, θ*) is (29.3, 2.4, 79.1°), where *A, A/B*, and *θ* are the semi-major axis, ratio of major and minor axes, and the orientation of the major axis from the horizontal axis.

The same data set was used to train an ellipse to cover 95% of foliage colours in CAM02-UCS as well. The result is shown Fig. 7.2.2-2. The centre is (-10.1, -20.3), and (*A, A/B, θ*) is (16.1, 2.0, -84.3°). The ellipse in CAM02-UCS is slightly closer to circle (*A/B* is closer to unity). This implies that CAM02-UCS may be slightly more uniform than CIELAB in representing blue sky colours. More details of the training results can be found in Appendix N.

The ellipse modelling ignores the lightness dependency. To take lightness into account, the ellipsoid modelling was applied. The training result of the ellipsoid modelling in CIELAB colour space is plotted in Fig. 7.2.2-3 in which the ellipsoid covers 95% of blue sky colours. The ellipsoid coefficients are: the ellipsoid centre - (62.8, -5.6, -28.5), the principal axis parameters [*A, A/B, A/C*] - [30.8, 1.4, 2.3], and the unit vectors of three principal axes relative to the centre - (0.97, -0.11, -0.23), (0.15, -0.53, 0.83), and (-0.03, -0.84, -0.53). u_i (*i* = 0, 1, 2, 3, 4, 5) coefficients are (0.000934281, 0.00154247, 0.00624211, -0.000745766, 0.00116825, 0.00131317), with $\rho = 1$.

The same data were used to train an ellipsoid to cover 97% of foliage colours in CAM02-UCS as well. The ellipsoid centre is (65.0, -10.1, -20.3), and [*A, A/B, A/C*] is [33.0, 2.2, 3.8]. Unit vectors of three principal axes relative to the centre are (-0.99, 0.13, -0.02), (0.05, 0.45, 0.89), and (-0.05, -0.89, 0.45). u_i coefficients are (0.000935748, 0.00165794, 0.013329, -0.00209243, -0.00372016, 0.00457517). See Appendix O for more details.

Fig 7.2.2-4 shows a comparison of sky colour detection using an ellipse model and an ellipsoid model in CIELAB colour space, both with 95% coverage rate. Detected colours are marked in pink. Because the ellipse model ignores lightness, it detects dark blue water colours as blue sky colours.

Fig. 7.2.2-5 shows blue sky colour detection using the ellipsoid model in CIELAB colour space with three different coverage rates (detected sky colours are marked with pink). Increasing the coverage rate increases the sky detection rate, however, the chance of false detection increases as well.

If a modelling coverage rate is very high, other colours close to sky blue colours will be detected as sky colours. On the other hand, if a coverage rate is very low, sky blue colours in the outer layer of the elliptical model will not be detected. Different coverage rates were tested on many different images to empirically determine a coverage rate for general blue sky colour detection. An ellipsoid model with a coverage rate in the range of 90% to 95% may be a good trade-off between correct detection and false detection.
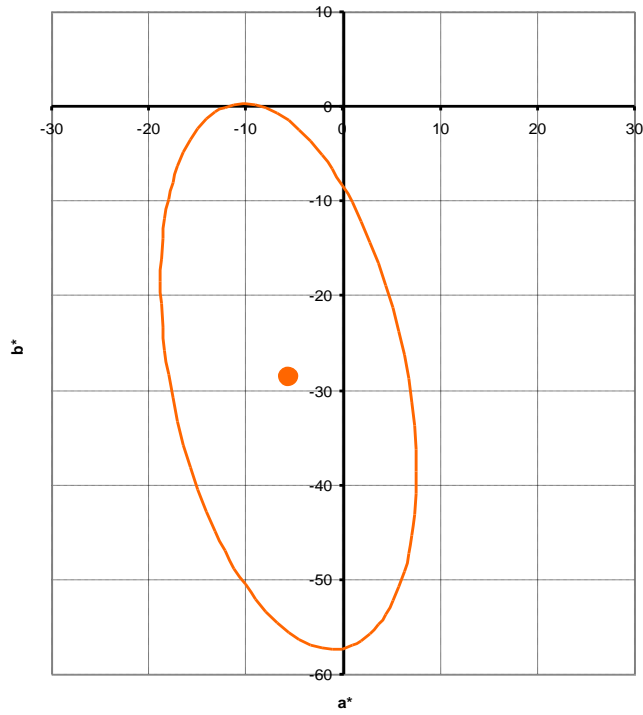
Fig. 7.2.2-1 An ellipse to cover 95% of blue sky colours in CIELAB a*-b* coordinates
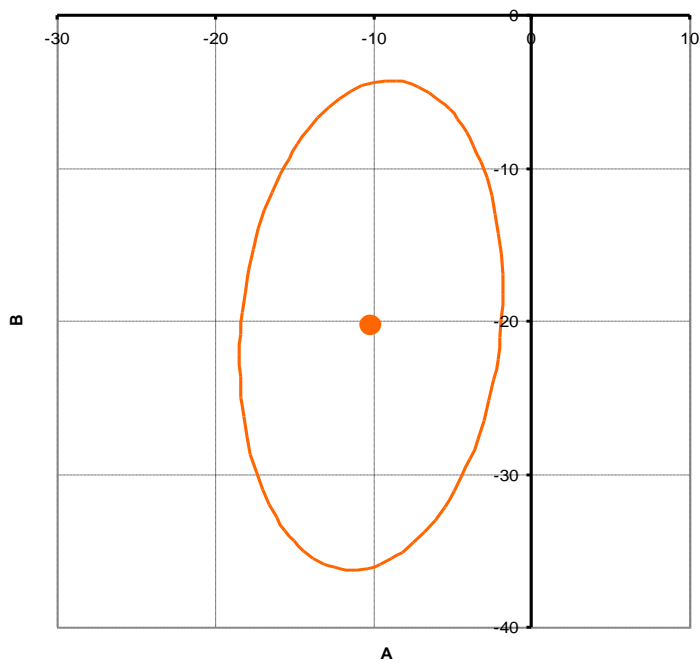
Fig. 7.2.2-2 An ellipse to cover 95% of blue sky colours in CAM02-UCS chroma coordinates
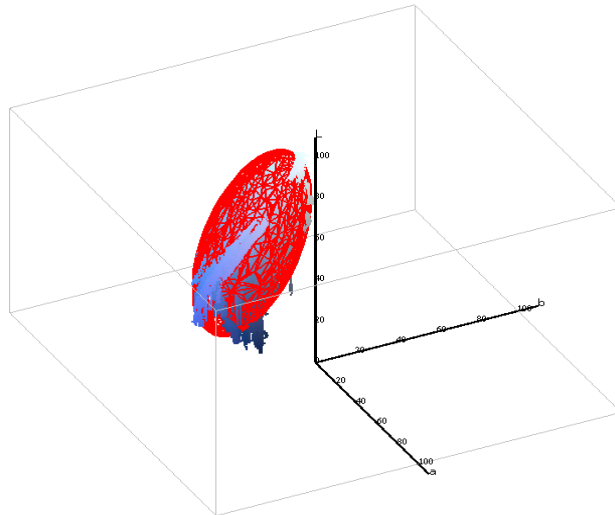
Fig. 7.2.2-3 Sky colour cluster (black) and an ellipsoid (red) to model the sky colour cluster in CIELAB colour space

Fig. 7.2.2-4 A comparison of blue sky detection by an ellipse model and by an ellipsoid model: original (left), detection using an ellipsoid model with 95% coverage rate (centre), and detection using an ellipse model with 95% coverage rate (right).

Fig. 7.2.2-5 Ellipsoid modelling with different coverage rates: original (upper-left), 90% coverage rate (upper-right), 95% coverage rate (lower-left), and 97% coverage rate (lower-right)

7.2.3 Investigating Hue Linearity of Colour Spaces Using Blue Sky Colours

Fig. 7.2.3-1 shows the blue sky cluster of our image database in CIE a*-b* coordinates. Blue skin colours span in a hue range of about [220°, 300°] (CIELAB adapted to D50 illuminant).
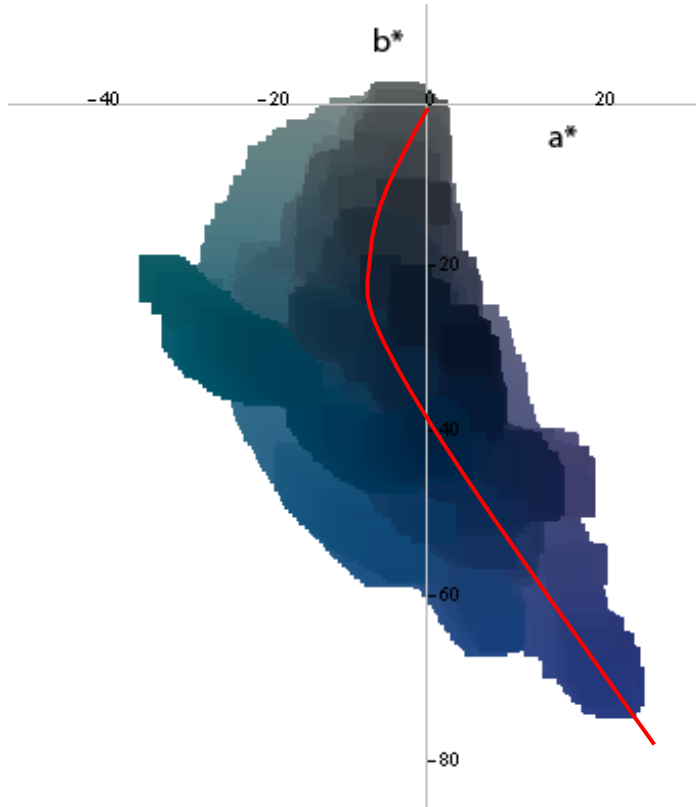
Fig. 7.2.3-1 Blue sky colour cluster of our image database in CIELAB a*b* coordinates

Blue sky colours around 240° hue angle are often seen in low chroma cloudy or polluted sky and very cyan sky. Figures 7.2.3-2 and 7.2.3-3 are two sample images. Blue sky colours around 280° hue angle are slightly purple (see Fig. 7.2.3-4). Blue sky colours with hue angles lower than 240° are greenish, and blue sky colours with hue angles higher than about 280° may be purplish. Preferred hue angles of blue sky colours are roughly in the range of 260° to 270° (see Figures 7.2.3-5 and 7.2.3-6).

In the blue-purple region, the hue perceptions of colours with constant-hue angles are very different, depending on their lightness and chroma. This in fact illustrates a big problem of CIELAB, i.e. the same hue appearance of blue in different chroma levels are not in a constant hue. In other words, there is a large range of hue angles representing the same blue hue appearance. This was also found by many researchers such as Hung and Berns (Huang and Berns 1995, Luo et. al.

1991, Luo et. al. 2001). It can be concluded that for low chroma blue sky colours, the CIELAB greenish hue angle will be more preferred. For higher chroma colours, a more purplish (or reddish) hue angle is more preferred. In other words, hue angles for low chroma blues should be lower than hue angles for high chrom blues. This is entirely due to a lack of hue consistency in CIELAB colour space.

Fig. 7.2.3-2 Foggy sky (hue angle at about 240$^{\text{o}}$)

Fig. 7.2.3-3 Blue sky (hue angle at about 240$^{\text{o}}$)
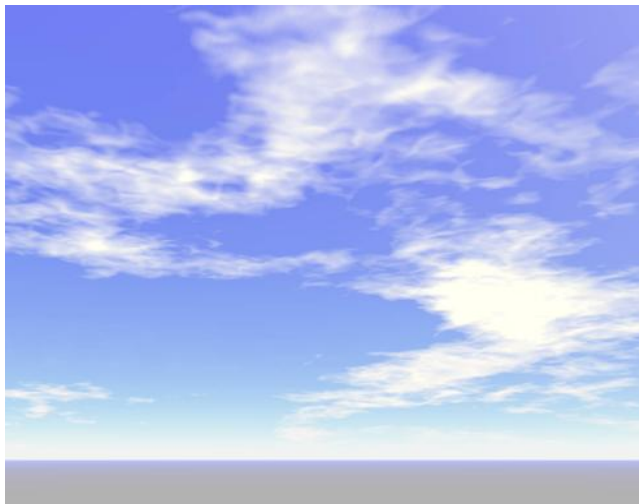
Fig. 7.2.3-4 Purple-blue sky (hue angle at about 280°)

Fig. 7.2.3-5 Blue sky with hue angles roughly at 260°

Fig. 7.2.3-6 Blue sky with hue angles roughly in 270°

Fig. 7.2.3-7 shows the same blue sky colour cluster drawn in CAM02-UCS. The hue angle is close to linear, which depicts the hue constancy of CAM02-UCS in the blue region. The blue sky data set was drawn in CAM97s JAB for comparison as well (see Fig. 7.2.3-8). The blue hue angle centre in CAM97s is not as straight as that in CAM02-UCS but is greatly improved over CIELAB.
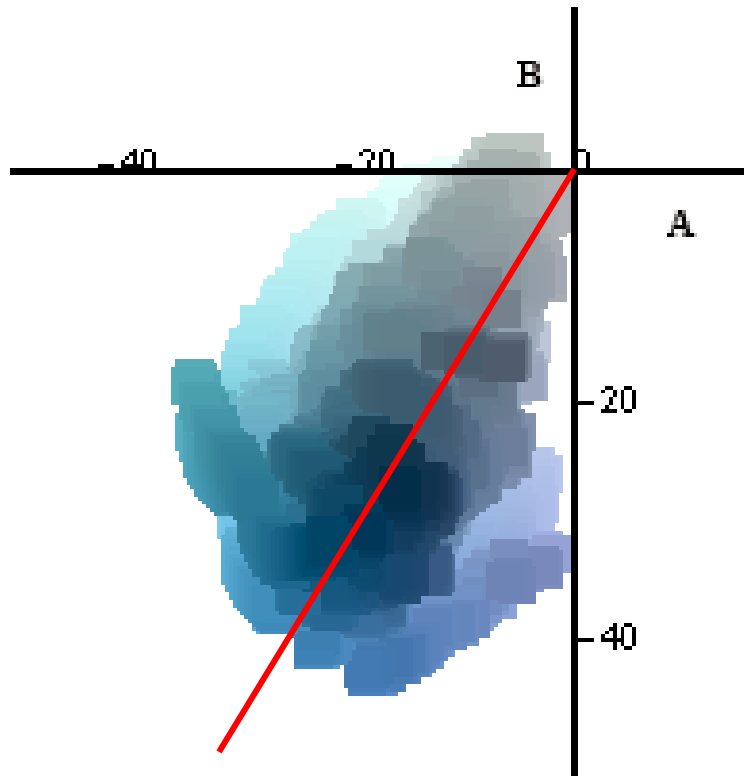
Fig. 7.2.3-7 Blue sky colour cluster of our image database in CAM02-UCS chroma coordinates
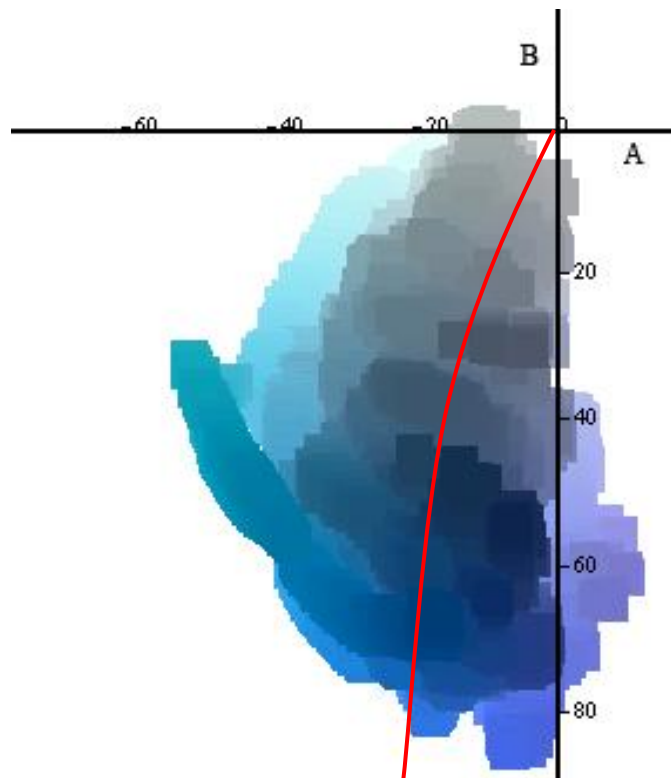
Fig. 7.2.3-8 Blue sky colour cluster of our image database in CIE CAM97 AB chroma coordinates

7.2.4 Summary

An elliptical model that had been successfully applied to model skin colours and foliage green colours was applied to model blue sky colours. The modelling coefficients of a 2-D ellipse model and a 3-D ellipsoid were trained using about 400 sRGB images. An ellipsoid model with coverage rates in the range of 90% to 95% was found to be a good trade-off between correct detection and false detection.

The hue centre of blue sky colours of digital photographic images with the white point adapted to D50 was found to be about 230° to 240° in CIECAM02 colour space. While the hue centre of the blue sky colour cluster in CIELAB colour space is a curve bended toward the purple direction, it is close to a constant in CIECAM02 colour space. This confirms that as chroma changes, the blue hue angle is not a constant in CIELAB colour space while it is approximately constant in CIECAM02 colour space. The blue hue constancy in CIECAM97s colour space is not as good as in CIECAM02 but it is greatly improved over CIELAB colour space.

7.3 Comparing Three Prototypical Colours

Elliptical models have been used to model skin colours, green foliage colours, and blue sky colours of digital photographic images. A comparison of them side by side in CIELAB a*-b* coordinates is shown in Fig. 7.3-1. The colour ellipses of skin colours, green foliage colours, and blue sky colours are replicated from Fig. 3.5.1-1, Fig. 7.1.3-1, and Fig. 7.2.2-1, respectively. Each coverage rate to determine the size of each ellipse, which was trained using each training data set, was chosen to achieve a good trade off between correct detection and false detection as discussed before. With these coverage rates, three colour regions are not overlapped. Because of the hue angle problem of CIELAB colour space in the blue region, blue sky colours span a larger range of hue angles than skin colours and green foliage colours.

The training results of these three groups of object colours in CAM02-UCS with the same criteria are drawn in Fig. 7.3-2. All three ellipses in CAM02-UCS are slightly closer to circle than their corresponding ellipses in CIELAB colour space. This demonstrates that CAM02-UCS is slightly more uniform in representing colours for these three objects. Comparing to that in CAM02-UCS, the orientation of the blue ellipse in CIELAB colour space tilting toward purple is the result of nonlinearity of the colour space in the blue region. In CAM02-UCS, the orientation and shape of each ellipse show that the span in hue range is smaller than that in chroma. This is agreed with the fact that people can tolerate more in chroma than in hue in reproducing memory colours. The separation among three ellipses in

CAM02-UCS are wider than that in CIELAB colour space, which means a better separation among these three colour regions in CAM02-UCS. This is useful for object segmentation of these objects.
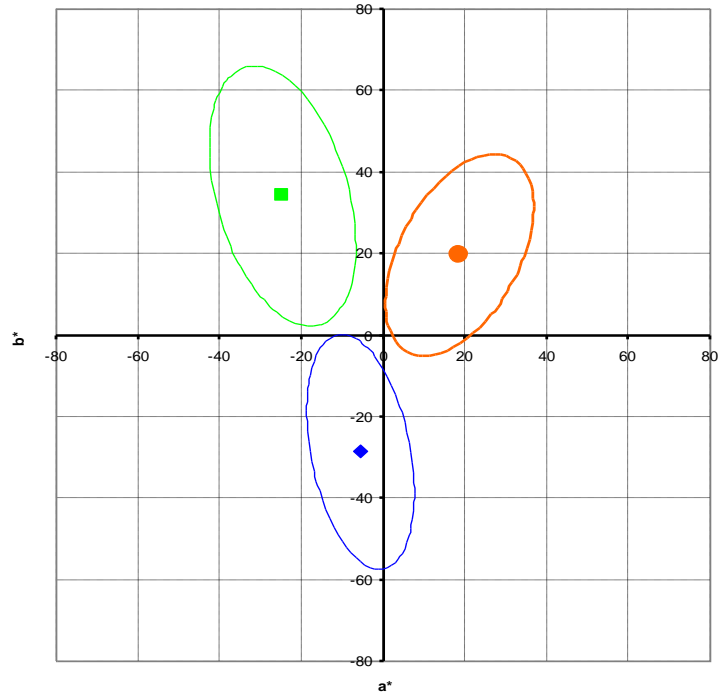
Fig. 7.3-1 Modelling colour ellipses of skin, green foliage, and blue sky colours in CIELAB a*-b* coordinates
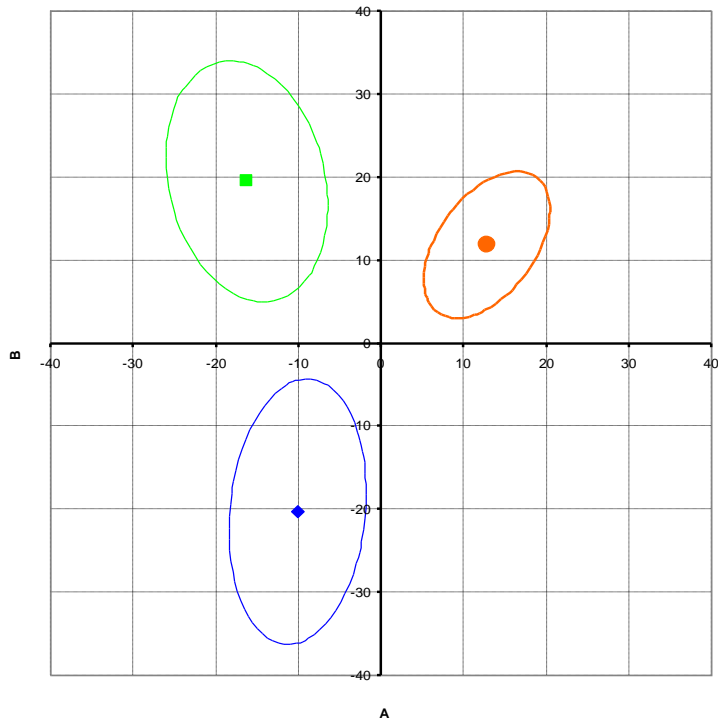
Fig. 7.3-2 Modelling colour ellipses of skin, green foliage, and blue sky colours in CAM02-UCS chroma coordinates
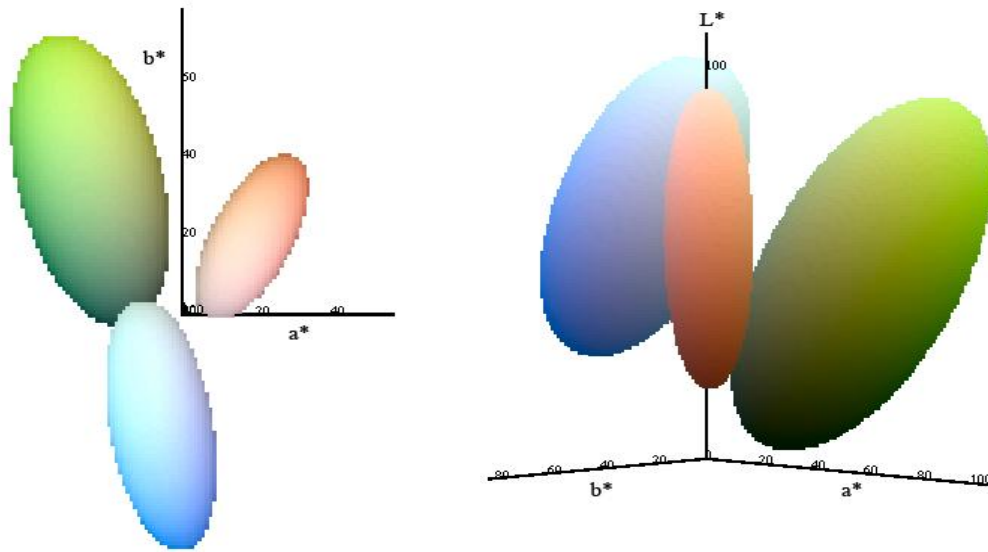
Fig. 7.3-3 Modelling colour ellipsoids of skin, green foliage, and blue sky colours in CIELAB colour space
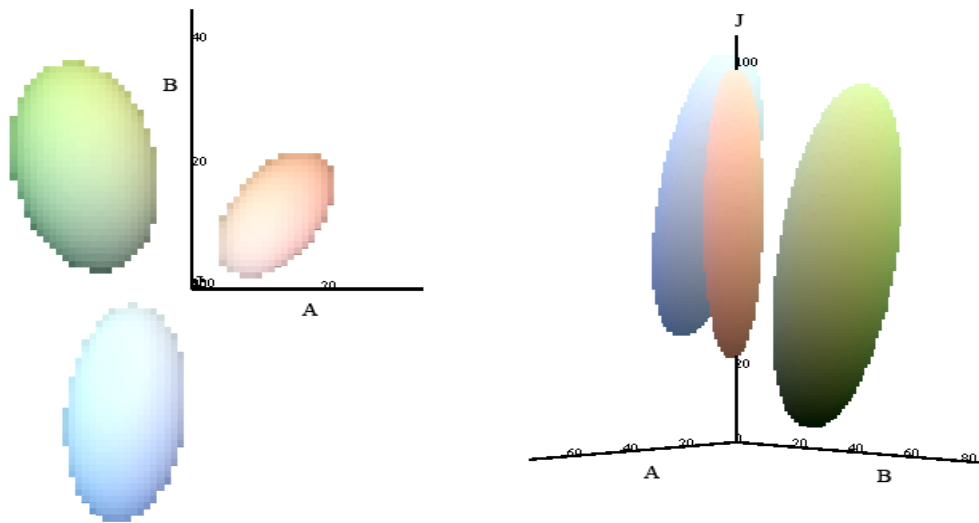
Fig. 7.3-4 Modelling colour ellipses of skin, green foliage, and blue sky colours in CAM02-UCS

The modelled ellipsoids of skin colours, green foliage colours, and blue sky colours in CIELAB colour space and CAM02-UCS (adapted to D50) are plotted in Figs. 7.3-3 and 7.3-4 for comparison. The left plot is the top-down view, and the right plot shows the differences along lightness axis. There are no overlaps among three ellipsoids. The longest principle axis mainly models the lightness variation and the two other axes model the chroma variation. Similar to the observation in the ellipse modelling, the shape in chroma axes in CAM02-UCS is closer to circle than that in CIELAB and the separation of three regions in CAM02-UCS are wider than

that in CIELAB. The hue range for blue sky colours in CAM02-UCS is smaller than that in CIELAB, which means better hue constancy in CAM02-UCS. Furthermore, the CAM02-UCS ellipsoids in the lightness dimension are more vertical (ellipsoids in CAM02-UCS have very smaller rotations in different L*, while ellipsoids in CIELAB rotate to different directions). This means that in CAM02-UCS, the three principal axes have better separation between lightness and chroma. This property is very useful for image processing in chrominance space ignoring lightness. If the lightness channel has to be dropped in image processing, CAM02-UCS should perform better than CIELAB.

7.4 Conclusions

The method of the elliptical skin colour modelling was applied to model the colour distributions of green foliage colours and blue sky colours. In terms of green foliages, heavy clipping of green foliage colours was found in sRGB images, i.e., sRGB colour space is not large enough to encode all green foliage colours. Digital images captured using the Adobe RGB colour space was then used for this study. Ellipses and ellipsoids were trained to model green foliage in CIELAB colour space. Testing with various images, an ellipsoid that covers 97% of the training data set was found to be a good trade-off between correct detection and false detection for green foliage detection. In printing foliage photographic images on photo inkjet printers (or other large gamut printers), expanding chroma slightly and shifting hue slightly toward the blue direction improves colour preference on foliage colours.

The elliptical model was applied to train ellipses and ellipsoids that represent the colour distribution of blue sky colours in CIELAB colour space. It was found that detecting blue sky colours using an ellipse model was less accurate than using an ellipsoid model, because the lightness was ignored. An ellipsoid model with a coverage rate in a range between 90% and 95% was found to be a good trade-off between correct detection and false detection.

When studying blue sky colours, a lack of hue constancy (blue sky colours having a similar hue does not appear in constant hue angle) in CIELAB colour space was again revealed. A comparison of the blue sky colour cluster in CIELAB and CAM02-UCS reveals that CAM02-UCS has better hue constancy. CAM02-UCS should be more appropriate for gamut mapping and colour adjustment.

Comparing the ellipses and ellipsoids trained on skin colours, green foliage colours, and blue sky colours in these two colour spaces, following observations were found: 1) CAM02-UCS is slightly more uniform than CIELAB; 2) elliptical modelling in CAM02-UCS has better separation among three colour regions, which

is useful for the classification of these three objects; 3) in the ellipsoid modelling, the three principal axes in CAM02-UCS have better separation between lightness and chroma , and therefore CAM02-UCS is more appropriate for modelling and detecting of these object colours if lightness is to be ignored.

Chapter 8
Conclusions and Contributions

This research was primarily focused on the preferred colour reproduction of skin colours, and then the methodology of skin colour modelling and skin colour enhancement were applied to study the colour preference of green foliage and blue sky. The conclusions and major contributions of the research are presented below.

8.1 Skin Colour Modelling for Skin Colour Detection

An effective method was developed to create different databases that were applied to model skin colours, green foliage colours, and blue sky colours. The consistent results of skin colour ellipses trained with two different databases verify that the method to construct databases is reliable for skin colour modelling.

Elliptical models were proposed to model the skin colour region and were used for skin colour detection and skin colour enhancement in this research. A single-ellipse model (lightness-independent model), a multi-ellipse model (lightness-dependent model), and an ellipsoid model were developed. Modelling skin colours with a single-ellipse is simple in training, and is efficient in computation. However, to cover high chroma skin colours in the mid-tone region, a sufficient large ellipse must be determined, which limits the overall detection accuracy. To improve the skin colour detection accuracy, a lightness-dependent ellipse model was developed. A set of skin colour ellipses to fit skin colours in different lightness was trained, and then their model coefficients were fitted with lightness-dependent functions. Although the model achieves very high detection accuracy, it is more complex to formulated and less efficient in computation. A third model, an ellipsoid skin colour model is a compromise among modelling complexity, computation efficiency, and detection accuracy. Unlike single-ellipse modelling, it adapts skin gamut boundary to different lightness. Although the gamut adaptation to different lightness is not as accurate as that of the lightness-dependent ellipse model, the ellipsoid modelling is simpler to train and more efficient in computation. In terms of detection accuracy among three models, all perform about the same when high false skin detection rates are acceptable. If high true skin detection rates and low false skin detection rates are vital, the lightness-dependent ellipse model is the best choice and the next is the ellipsoid model.

A separate training of Caucasian, Oriental, and African skin colours of digital photographic images demonstrates that the Caucasian skin colour gamut and the Oriental skin colour gamut are very similar; the Oriental skin colours are slightly more yellowish and slightly more chromatic than the Caucasian skin colours; the lightness ranges of the Caucasian and Oriental skin types are about the same. Comparing to the other two skin types, the African skin colour region is slightly darker, its centre is more chromatic, its chroma variation is higher, and its hue range is within those of the other two skin types.

Both CIELAB and CAM02-UCS were applied for skin colour modelling. The results of the skin colour ellipsoids trained in CIELAB and CAM02-UCS reveal that CAM02-UCS is slightly more uniform in the skin colour region. With the ellipsoid modelling, the skin colour detection is slightly more accurate in CAM02-UCS than in CIELAB colour space.

Elliptical skin colour models of the skin colour distribution of colorimetric skin colours are trained and compared with those of digital photographic images. Due to the colour rendering from the scene-referred state to the output-referred state, the contrast and chroma of digital photos are typical boosted. Combining with other factors, such as under-exposure or over-exposure, and illuminant detection inaccuracy, the skin colour gamut of digital photographic images is considerably larger than that of the colorimetric skin colours.

While the colorimetric skin colour gamut may be used for skin/face detection and illuminant detection for scene-referred images, the rendered skin colour gamut generated from output-referred digital images may be used for skin/face detection and preferred skin colour reproduction of digital photographic images.

A more general approach to model a colour region by constructing a convex hull for the region and fitting the convex hull with formulae was proposed. The method can be used to model any individual object colour gamut. Three examples were presented for skin colour modelling.

8.2 Preferred Skin Colours for Skin Colour Enhancement

Although there is a consistent conclusion from different studies that preferred skin colours are different from actual skin colours, preferred skin colours found from different studies are somewhat different. In order to have a solid understanding of skin colour preference, a series of the psychophysical experiments were conducted. They confirm that preferred skin colours are more chromatic than real skin colours.

In Experiment I, portrait photos were displayed on regular LCD displays for observers with various culture backgrounds to judge their skin colour preferences. A summary of the findings are: the preferred skin colour centre for mixed culture backgrounds is about (21, 24) for CIE a*b* in D50 illuminant with a hue angle of about 49°; the preferred Caucasian skin colour might be slightly more yellowish than average real Caucasian skin colour; preferred Oriental and African skin colours are slightly more reddish than their real skin colours; observer variances in skin colour preference are larger in chroma than in hue, i.e. hue tolerance is tighter than chroma tolerance; the inter-observer variation is about 2 ΔE^*_{ab} units without considering the variability in L*; and comparison of preferred skin colour ellipses between CIELAB and CAM02-UCS reveals that CAM02-UCS is a more uniform colour space.

In Experiment II, portrait photos were displayed on a wide-gamut LCD display and judged by Chinese observers for Oriental skin colour preference. The preferred Oriental skin colour judged by Chinese was found to be about (20, 23) for CIE a*b* in D50 illuminant with a hue angle of about 49°. Although the hue angle is about the same as that of the preferred Oriental skin colour judged by observers with mixed culture backgrounds, the chroma is slightly lower. The result reveals that the preferred Oriental skin colour judged by Chinese is slightly less chromatic than the preferred Oriental skin colour judged by observers with mixed culture backgrounds.

In Experiment III, African, Caucasian, and Oriental portrait photos were displayed on a CRT monitor and judged by African, Caucasian, and Oriental observer groups to study skin tone preferences by each ethnicity and across ethnicities. The skin tone preference by ethnicity (preferred African skin tone judged by Africans, preferred Caucasian skin tone judged by Caucasians, and preferred Oriental skin tone judged by Orientals) are: the preferred hue angle in CIELAB adapted to the D50 white point is about 49° in all three groups; statistical analysis of skin colour preference among African, Caucasian and Oriental culture backgrounds reveals that all three preferred skin colour cenrtes are significantly different from each other in 5% significant level; Orientals prefer slightly less chromatic skin colours than Africans and Caucasians; the inter-observer variation of the skin colour preference of Africans is larger than those of Caucasians and Orientals; Caucasian may prefer slightly more yellowish skin tones than African; and the result of Chinese skin colour preference from Experiment II agrees well with the Oriental data in Experiment III, which means high repeatability in our experiments. In cross-culture preference, Orientals prefer slight less chromatic skin colours than Caucasians and Africans, and Africans prefer more chromatic Caucasian and Oriental skin colours than Caucasians and Orientals.

Although different display types (regular LCD display, Adobe RGB LCD display, CRT display) were used to display images and different groups of observers evaluated skin tones in different psychophysical experiments, the results are consistent. Verifications using hardcopy further confirmed that the preferred skin colour centres obtained in this study were very reliable.

8.3 Skin Colour Enhancement

Preferred skin colour adjustment algorithms were developed for skin colour enhancement. The first method applies a statistical skin colour model to detect skin colours, and morphs skin colours toward a preferred skin colour centre. Psychophysical experiments validated that the method of preferred skin colour enhancement effectively identified skin colours without face recognition, improved the skin colour preference, and did not objectionably affect preferred skin colours in original images.

If skin colours are too much off from the regular skin colour distribution, applying above skin colour enhancement method may not enhance skin colours effectively. A face detection aided skin colour enhancement method was developed to resolve the limitation. With face box information, skin colour detection is more accurate, and a wider range of skin tones can be enhanced. With the skin colour model adapted to the individual image using face information, skin colours that are far away from the preferred skin colour centre are morphed toward a preferred skin colour centre more effectively.

To increase the computation efficiency, both algorithms may be implemented by pre-generating a 3-D LUT and applying 3-D interpolation to process image pixels.

Several psychophysical experiments were conducted to verify the effectiveness of the skin colour enhancement algorithms. The first part of the psychophysical experiments reveals that the preferred skin colour centre locates in a small colour region; if skin tones of an image are within the preferred skin colour region, morphing skin colours towards the preferred skin colour centre does not further improve skin colour preference; and observers may prefer slightly more chromatic skin colours in hardcopy than in display (i.e. a preferred skin colour centre for hardcopy may be slightly more chromatic than that in display).

The result from another experiment verifies that the skin colour enhancement effectively improves skin colour acceptance rates and modifying skin colours of non-skin objects is not objectionable.

8.4 Colour Modelling of Green Foliage and Blue Sky

The method to build elliptical skin colour models was applied to model colour regions of green foliage and blue sky. Studying the colour cluster of green foliage of digital photographic images revealed that clipping green foliage colours on sRGB colour space was common in sRGB images, and therefore using a larger encoding colour space (e.g. Adobe RGB) would benefit the colour encoding of green foliage colours. Ellipsoid colour models of green foliage colours in CIELAB and CAM02-UCS colour spaces using Adobe RGB images were trained for green foliage colour detection. Because blue sky colours are mostly very low in chroma and fitted well within the sRGB colour space, sRGB images were used to produce sky colour clusters in CIELAB and CAM02-UCS colour spaces that were applied to train the elliptical colour model for blue sky colours.

When studying blue sky colours, a lack of hue constancy (blue sky colours having a similar hue does not appear in constant hue angle) in CIELAB colour space was again revealed. A comparison of the blue sky colour cluster in CIELAB and CAM02-UCS reveals that CAM02-UCS has better hue constancy. CAM02-UCS should be more appropriate for gamut mapping and colour adjustment.

Comparing the ellipses and ellipsoids trained on skin colours, green foliage colours, and blue sky colours in these two colour spaces, following observations are found: 1) CAM02-UCS is slightly more uniform than CIELAB; 2) elliptical modelling in CAM02-UCS has better separation among three colour regions, which is useful for the classification of these three objects; 3) in the ellipsoid modelling, the three principal axes in CAM02-UCS have better separation between lightness and chroma , and therefore CAM02-UCS is more appropriate for modelling and detecting of these object colours if lightness is to be ignored.

8.5 Future Work

Several areas for subsequent research are listed below:

Skin Colour Preference

1. More extensive study of colour preference among different culture backgrounds (Hispanic, Sub-Asian, India, etc.);

2. Application of skin colours to establish 'Naturalness' model for evaluating the quality of preferred colour reproduction, colour image quality and quality of light sources; and

3. Further improvement of the effectiveness and efficiency of skin colour enhancement.

Colour Preference of Green Foliage and Blue Sky

1. More extensive collection of green foliage images and blue sky images to train green foliage colour models and blue sky colour models; and

2. Psychophysical experiments to study preferred colours of green foliages and blue skies.

Media Impact on Preferred Colour Reproduction

Further investigation of colour preference impacted by different media (displays and hardcopies).

References

Adobe RGB (1998) Color Image Encoding, Version 2005-5 (2005), http://www.adobe.com/digitalimag/pdfs/AdobeRGB1998.pdf.

Albio, A., Torres, L., and Delp, E.J. (2001) "Optimum Color Spaces for Skin Detection", IEEE International Conference on Image Processing, Vol. 1, 122-124.

Almohair, H.K., Ramli, A.R., Elsadig, A. M., and Hashim, S.J. (2007) "Skin Detection in Luminance Images using Threshold Technique" International Journal of the Computer, the Internet and Management, Vol. 15(1): 25-32.

Angelopoulou, E. (1999) "The Reflectance Spectrum of Human Skin", Technical Reports, Department of Computer & Information Science, University of Pennsylvania.

Angelopoulou, E. (2001) "Understanding the color of human skin", Proc. SPIE: Human vision and electronic imaging, Vol. 4299, 243-251.

Angelopoulou, E., Molana, R., and Daniilidis, K. (2001) "Multispectral Skin Color Modeling", IEEE Computer Society Conference on Computer Vision and Pattern Recognition, Vol. 2, 635-642.

Bala, R., Queiroz, R., Eschbach, R., and Wu, W. (2001) "Gamut Mapping to Preserve Spatial Luminance Variations", J. Imaging Sci. Technol., 15(5): 436-443.

Barnard, K. (1999) "Practical Color Constancy", Ph.D. dissertation, Simon Fraser University, School of Computing.

Bartleson, C.J. (1959) "Some Observations on the Reproduction of Flesh Colors", Photographic Science and Engineering, 3(3): 114-117.

Bartleson, C.J. (1960) "Memory Colors of Familiar Objects", J. Opt. Soc. Am., 50(1): 73-77.

Bartleson, C.J. (1961) "Color in Memory in Relation to Photographic Reproduction", Photographic Science and Engineering, 5(6): 327-331.

Bartleson, C.J. (1968) "Color Perception and Color Television", Journal of the SMPTE, 77(1): 1-12.

Bartleson, C.J. and Bray, C. P. (1962) "On the preferred Reproduction of Flesh, Blue-Sky, and Green-Grass Colors", Photographic Science and Engineering, 6(1): 19-25.

Bartleson, C.J. and Breneman, E.J. (1967) "Brightness Perception in Complex Fields", J. Opt. Soc. Am., 57(7): 953-957.

Bartleson, C.J. and Grum, F. (1984) "Optical Radiation Measurements: Visual Measurements", Vol. 5, Academic Press, Inc.

Berns, R.S., Imai, F.H., Burns, P.D., and Tzeng, D.-Y. (1998) "Multi-spectral-based Color Reproduction Research at the Munsell Color Science Laboratory", Proc. SPIE: Electronic Imaging Conference, Vol. 3409, 14-25.

Birchfield, S. (1998) "Elliptical head tracking using intensity gradients and color histograms", IEEE Computer Society Conference on Computer Vision and Pattern Recognition, 23-25.

Bodrogi, P. and Tarczali, T. (2001) "Colour Memory for Various Sky, Skin, and Plant Colours: Effect of the Image Contest", Color Res. Appl., 26(4): 278-289.

Born, R.T. and Bradley D.C. (2005) "Structure and function of visual area MT", Annu Rev Neurosci 28: 157–89.

Boussaid, F., Chai, D., and Bouzerdoum, A. (2003) "On-chip skin detection for color CMOS imagers", IEEE International Conference on MEMS, NANO and Smart Systems, 356-361.

Boust, C., Brettel, H., Vienot, F., Berche, S., and Alquie, G. (2006) "Color Enhancement of Digital Images by Experts and Preference Judgments by Observers", J. Imaging Sci. Technol. 50(1): 1-11.

Boynton, R. M. (1979), "Human Color Vision", Holt Rinehart and Winston.

Braddick, O.J., O'Brian, J.M.D., Wattam-Bell, J., Atkinson, J. Hartley, T. and Turner, R. (2001) "Brain areas sensitive to visual motion", Perception 30(1): 61–72.

Brainard, D.H. and Wandell, B.A., (1986) "Analysis of the retinex theory of color vision", J. Opt. Soc. Am. A., 3(10):1651-1661.

Brand, J. and Mason, J.S. (2000) "A Comparative Assessment of Three Approaches to Pixel-Level Human Skin-Detection", IEEE 15th International Conference on Pattern Recognition Vol. 1, 1056-1059.

Braun, K.M. (2006) "Memory Color Enhancement Algorithm", International Congress of Imaging Science, 227-229.

Braun, K.M., Balasubramanian, R., and Harrington S.J. (1999) "Gamut-Mapping Techniques for Business Graphics", IS&T 7th Color Imaging Conference, 149-154.

Brill, M.H., and Süsstrunk, S. (2008) "Repairing gamut problems in CIECAM02: A progress report", Color Res. Appl. 33(5): 424-426.

Brown, D.A., Craw, I., and Lewthwaite, J. (2000) "A SOM Based Approach to Skin Detection with Application in Real Time System", Proc. International Conference on Pattern Recognition, Vol. 1, 1056-1059.

Buzuloiu, V.V., Ciuc, M., Rangayyan, R.M., and Kij, L. (1999) "Histogram equalization of color images using the adaptive neighborhood approach", Proceed. SPIE: Nonlinear Image Processing X, Vol. 3646, 330-338.

Caetano, T.S., Olabarriaga, S.D., and Barone, D.A.C. (2002) "Performance evaluation of single and multiple-Gaussian models for skin color modelling", IEEE Brazilian Symposium on Computer Graphics and Image Processing XV, 275-282.

Chai, D. and Bouzerdoum, A. 2000 "A Bayesian approach to skin color classification in YCbCr color space", IEEE TENCON, Vol. 2, 24-27.

Chai, D. and Ngan, K.N. (1999) "Face segmentation using skin-color map in videophone applications", IEEE Transactions on Circuits and Systems for Video Technology, 9(4): 551-564.

Cai, J., Goshtasby, A., and Yu, C. (1998) "Detecting Human Faces in Color Images", IEEE International Workshop on Multi-Media Database Management Systems, 124-131.

Chen, Q., Wu, H., and Yachida, M. (1995) "Face detection by fuzzy pattern matching", IEEE 5th International Conference on Computer Vision, 591-596.

Chien, S.H.-L., Teller, D.Y., and Palmer, J. (2000), "The transition from scotopic to photopic vision in 3-month-old infants and adults: an evaluation of the rod dominance hypothesis", Vision Research, 40(28): 3853-3871.

Choi ,S. Y., "Modelling Colour and Imaging Appearance under Flat Pannel Display Viewing Conditions", PhD thesis, University of Leeds, 2008.

Chorin, M.B., Eliav, D., Roth S. (2007) "Multi-Primary Spectral Display for Soft Proofing", J. Imaging Sci. Technol., 51(6): 492-501.

Choudhury, A., Rogers, M., and Gillam, B. (2008) "A Novel Skin Tones Detection Algorithm for Contraband Image Analysis", IEEE 3rd International Workshop on Systematic Approaches to Digital Forensic Engineering, 3-9.

CIE (1995) Publication 116-1995, Industrial Colour-Difference Evaluation, Vienna.

CIE (2003) TC 8-01, A Color Appearance Model for Color Management Systems: CIECAM02.

CIE (2004a) Colorimetry, CIE Publication 15: 2004, Central Bureau of the CIE, Vienna, Austria.

CIE (2004b) A Color Appearance Model for Color Management Systems: CIECAM02, CIE Publication 159: 2004, Central Bureau of the CIE, Vienna, Austria.

Cui, G., Luo, M.R., and Rigg, B. (2001), "Investigation of the 'Crispening Effect' on Lightness Differences", 9th Congress of the International Colour Association (AIC).

Derhak, M.W. and Rosen, M.R. (2006) "Spectral colorimetry using LabPQR : an interim connection space", J. Imag. Sci. & Techno., 50(1): 53-63.

Doi, M., Tanaka, N., and Tominaga, S. (2004), "Spectral Reflectance Estimation of Human Skin and Its Application to Image Rendering", J. Imaging Sci. Technol. 49 (6): 574-582.

Ebner, M. (2007) "Color Constancy", John Wiley & Son Ltd.

Eysenck, M. W. and Keane, M. T. (2005) Cognitive Psychology: a student's handbook. 5th Edition, Psychology Press Ltd (East Sussex).

Fairchild, M. D., (1998) "Color Appearance Models", Addison Wesley Longman, Inc.

Fairchild, M.D. and Johnson, G.M. (2002) "Meet iCAM: A Next-Generation Color Appearance Model", IS&T/SID 10th Color Imaging Conference, 33-38.

Fairchild, M.D., Rosen, M.R., and Johnson, G.M. (2001), "Spectral and Metameric Color Imaging", Technical Report, Munsell Color Science Laboratory.

Felleman, D.J. and Van Essen, D.C. (1991) "Distributed hierarchical processing in the primate cerebral cortex", Cereb Cortex 1 (1): 1–47.

Fernandez, S.R., Fairchild, M.D. (2001) "Preferred Color Reproduction of Images with Unknown Colorimetry", Proc IS&T/SID 9th Color Imaging Conference, 274-279.

Fernandez, S.R., Fairchild, M.D., and Braun, K. (2005) "Analysis of Observer and Cultural Variability while Generating "Preferred" Color Reproductions of Pictorial Images", J. Imaging Sci. Technol., 49(10): 96-104.

Finlayson, G.D. (1996) "Color in Perspective", IEEE Transactions on Pattern Analysis and Machine Intelligence, 18(10): 1034-1038.

Finlayson, G.D. and Hordley, S.D. (2000) "Improving Gamut Mapping Color Constancy", IEEE Transactions on Image Processing, 9(10): 1774-1782.

Finlayson, G.D., Hordley, S.D., and Hubel, P.M. (2001) "Unifying Color Constancy", J. Imaging Sci. Technol., 45(2), 107-116.

Forsyth, D.A. (1990) "A Novel Algorithm for Color Constancy", J. Computer Vision, 5(1): 3-36.

Fredembach, C., Estrada, F., and Susstrunk, S. (2008) "Segmenting memory colors", 16th Color Imaging Conference, 315-319.

Fredembach, C., Barbuscia, N., and Susstrunk, S. (2009) "Combining visible and near-infrared images for realistic skin smoothing", Proc. IS&T/SID 17th Color Imaging Conference (IS&T, Springfield, VA), 242-247.

Fulton, J. T. 2005, http://sightresearch.net/files/adaptation.htm.

Gallagher, A.C., Luo, J., and Hao, W. (2004) "Improved blue sky detection using polynomial model fit", IEEE International Conference on Image Processing, Vol. 4, 2367–2370.

Gallagher, A.C., Luo, J., and Hao, W. (2008) "Detection of Sky in Digital Color Images", US Patent 7,336,819.

Gasparini, F., Corchs, S., and Schettini, R. (2008) "Recall or precision-oriented strategies for binary classification of skin pixels", J. Electronic Imaging, 17(2): 023017.

Gasparini, F. and Schettini, R. (2006) "Skin segmentation using multiple thresholding", Proc. SPIE: Internet Imaging VII, Vol. 6061, pp. 60610F.1-8.

Gill, G.W. (2008) "A resolution to CIE CMA02 numerical and range issues", 16th IS&T/SID Color Imaging Conference (IS&T, Springfield, VA), 327-331.

Goldstein, E. B. (2007), " Sensation and perception, (7th edition). Thompson & Wadsworth.

Gomez, G. (2002) "On selecting color components for skin detection", IEEE 16th International Conference on Pattern Recognition, Vol. 2, 961-964.

Gomez, G. and Morales, E.F. (2002) "Automatic Feature Construction and a Simple Rule Induction Algorithm for Skin Detection", Proc. ICML Workshop on Machine Learning in Computer Vision, 31-38.

Hardeberg, J. Y. (2001) "Acquisition and Reproduction of Color Images: Colorimetric and Multispectral Approaches", ISBN: 1-58112-135-0, USA.

Harrar, M. and Vienot, F. (2005) "Regulation of chromatic induction by neighboring images", J. Opt. Soc. Am A. 22(10): 2197-2206.

Hassanpour, R., Shahbahrami, A., and Wong, S. (2008) "Adaptive Gaussian Mixture Model for Skin Color Segmentation", Proc. World Academy of Science, Engineering and Technology, Vol. 31, 1-6.

Helmholtz, H. (1850), "Über die Theorie der zusammengesetzten Farben", Archiv für Anatomie, Physiologie und wissenschaftliche Medizin, Berlin, 461-482.

Hering, E. (1872) "Zur Lehre vom Lichtsinne". Sitzungsberichte der Mathematisch–Naturwissenschaftliche Classe der Kaiserlichen Akademie der Wissenschaften LXVI. Band (III Abtheilung).

Hering, E. (1964), "Outlines of a Theory of the Light Sense", translated by Leo M. Hurvich, Harvard University Press, Cambridge, Mass.

Herman, S., Janssen, J., Bellers, E., and Wendorf, J. (2004) "Automatic Segmentation-Based Grass Detection for Real-time Video", US Patent 6,832,000.

Holm, J.M. (2003) "Pictorial Digital Image Processing Incorporating Image and Output Device Modifications", US Patent 6,563,945.

Hsu, R.-L., Abdel-Mottaleb, M., and Jain, A.K. (2002) "Face detection in color images", IEEE Transactions on Pattern Analysis and Machine Intelligence, 24 (5): 696-706.

ICC Website: http://www.color.org/

Hu, G.-H., Bu, J.-J., and Chen, C. (2003) "A novel Bayesian framework for indoor-outdoor image classification", IEEE CNF II, 785-788.

Huang, P-C. and Berns, R. S. (1995), "Determination of constant Hue Loci for a CRT gamut and their predictions using color appearance spaces", Col. Res. Appl., 20(5): 285-295.

Huang, R., Jiang, X., Li, H.-T. (2010), "Image Processing Method and System of Skin Color Enhancement", International Application PCT, WO 2010/071738.

Hunt, R.W.G. (1952) "Light and dark adaptation and the reception of colour", J. Opt. Soc. Am., 42: 190-199.

Hunt, R.W.G. (1998), "Measuring Colour", 3rd Edition, Fountain Press, England.

Hunt, R.W.G. (2006) "Reproduction of Colour", 6th Edition, John Wiley & Sons, Ltd..

Hunt, R.W.G., Pitt, I.T., and Winter, L.M. (1974) "The Preferred Reproduction of Blue Ski, Green Grass and Caucasian Skin in Colour Photography", J. Photographic Science, 22: 144-149.

Huynh-Thu, Q., Meguro, M., and Kaneko, M. (2002) "Skin-color extraction in images with complex background and varying illumination", 6th IEEE Workshop on Applications of Computer Vision, 280-285.

Imai, F.H., Tsumura, N., Haneishi, H. and Miyake, Y. (1996), "Principal Component Analysis of Skin Color and Its Application to Colorimetric Color Reproduction on CRT Display and Hardcopy", J. Imaging Sci. Technol., 40 (5): 422-430.

ISO 22028-1 (2004), Photography and graphic technology -- Extended color encodings for digital image storage, manipulation and interchange -- Part 1: Architecture and requirements.

Janssen, T.J.W.M. and Blommaert, F.J.J. (2000) "Predicting the Usefulness and Naturalness of Color Reproductions", J. Imaging Sci. Technol. 44(2): 93-104.

Jiang, X. and Fairchild M.R. (2005) "Illuminant Estimation for Multi-channel Images", Proc. SPIE/IS&T Color Imaging X: Processing, Hardcopy, and Application, 118-127.

Jones, M.J. and Rehg, J.M. (2002) "Statistical color models with application to skin detection", International Journal of Computer Vision, 46(1): 81-96.

Jordao, L., Perrone, M., Costeira, J.P., Santos-Victor, J. (1999) "Active face and feature tracking", IEEE International Conference on Image Analysis and Processing, 572–576,.

Kakumanu, P., Makrogiannis, S., and Bourbakis, N. (2007) "A survey of skin-color modeling and detection methods", Pattern Recognition, 40(3): 1106-1122.

Kawazoe, D., Takase, K., Tsumura, N., Nakaguchi, T., and Miyake, Y. (2005) "Simulation of skin spectral reflectance based on an empirical model", IEEE Pacific Rim Conference on Lasers and Electro-Optics, 659-661.

Kim, D.-H., Do, H.-C., and Chien, S.-I. (2005) "Preferred Skin Color Reproduction Based on Adaptive Affine Transform", IEEE Transactions on Consumer Electronics, Vol. 51 (1), 191-197.

Kim, Y.H., Jang, H.S., Kim, K.S., and Nam, B.D. (1998) "Region-based histogram specification for dynamic range expansion", Proc. SPIE: Digital Solid State Cameras: Designs and Applications, Vol. 3302, 90-97.

Koh, C.C., Foley, J.M., and Mitra, S.K. (2006) "Color Preference and Perceived Color Naturalness of Digital Videos", Proc. SPIE: Human Vision and Electronic Imaging XI, Vol. 6057.

Koh, C.C., Foley, J.M., and Mitra, S.K. (2007) "Color Preference, Color Naturalness, and Annoyance of Compressed and Color Scaled Digital Videos", Proc. SPIE: Human Vision and Electronic Imaging XII, Vol. 6492.

Kovac, J., Peer, P., and Solina, F. (2003), "2D versus 3D color space face detection", IEEE 4th EURASIP Conference focused on Video/Image Processing and Multimedia Communications, Vol. 2, 449-454.

Krauskopf J., Zaidi Q., and Mandler M.B. (1986), "Mechanisms of simultaneous color induction", J. Opt. Soc. Am A., 3(10):1752-1757.

Kuang, J. and Fairchild, M.D. (2007) "iCAM06, HDR, and Image Appearance", IS&T/SID 15th Color Imaging Conference, 249-254.

Kuang, J., Jiang, X., Quan, S., and Chiu, A. (2005) "A psychophysical study on the influence factors of color preference in photographic color reproduction", Proc. SPIE/IS&T Electronic Imaging: Image Quality and System Performance II, Vol. 5668, 12-19.

Lamme, V., Supper H., and Spekreijse H. (1998) "Feedforward, horizontal, and feedback processing in the visual cortex", Current Opinion in Neurobiology 8(4): 529-535.

Land, E. H. (1977), 'The Retinex Theory of Color Vision', Scientific American, vol. CCXXXVII, 108–28.

Lee, E.-J. and Ha, Y.-H. (1997) "Automatic Flesh Tone Reappearance for Color Enhancement in TV", IEEE Transactions on Consumer Electronics, 43(4): 1153-1159.

Lee, J.Y. and Yoo, S.I. (2002) "An Elliptical Boundary Model for Skin Color Detection", Proceedings of the International Conference on Imaging Science, Systems, and Technology.

Luo, J. and Etz, S.P., "A physical model-based approach to detecting sky in photographic images", IEEE Transactions on Image Processing, 11(3): 201-212 (2002).

Luo, J., Etz, S., and Singhal, A., (2001) "Method for Automatic Determination of Main Subject in Photographic Images", US Patent 6,282,317.

Luo, M.R., Gao, X.W., Scrivener, S.A.R., (1995) "Quantifying colour appearance. part V. simultaneous contrast", 20(1): 18-28.

M. R. Luo, A. A. Clarke, P. A. Rhodes, A. Schappo, Schappo, A., Scrivener, S.A.R., Tait, C.J. (1991), "Quantifying colour appearance. Part II. Testing colour

models performance using lutchi colour appearance data", Col. Res. Appl., 16(3): 181–197.

Luo, M.R., Cui, G., and Li, C. (2006) "Uniform colour spaces based on CIECAM02 colour appearance model", Col. Res. Appl., 31(4): 245-370.

Luo, M.R., Cui, G., Rigg, B. (2001) "The development of the CIE 2000 colour-difference formula: CIEDE2000", Col. Res. Appl., 26(5), 340-350.

Luo, M.R. and Hunt, R.W.G. (1998) "The structure of the CIE 1997 colour appearance model (CIECAM97s)", Col. Res. Appl., 23, 138-146.

Luo, M.R. and Hunt, R.W.G. (1998), "A chromatic adaptation transform and a colour inconstancy index". Col. Res. Appl., 23: 154-158.

Luo, M.R., Rigg B., (1986) "Chromaticity-discrimination ellipses for surface colour", Col. Res. Appl., 11(1): 25-42.

Macadam, D.L. (1942) "Visual Sensitivities to Color Differences in Daylight", J. Opt. Soc. Am. 32, 247-273.

Macadam, D.L. (1950) "Quality of Color Reproduction", J. SMPTE, 56: 487-512.

Mahmoud, T.M. (2008) "A New Fast Skin Color Detection Technique", Proc. World Academy of Science, Engineering and Technology, Vol. 33, 518-522.

Martinkauppi, B. (2002) "Face Color under Varying Illumination − Analysis and Applications", PhD dissertation, University of Oulu.

McCann, J., (2001) "Calculating lightness in a single depth plane", J. Electronic Imaging, 10(1), 110-122.

Menser, B. and Wien, M. (2000) "Segmentation and tracking of facial regions in color image sequences", Proc. SPIE: Visual Communications and Image Processing, Vol. 4067, 731-740.

Meylan, L. and Süsstrunk, S., (2006) "High Dynamic Range Image Rendering with a Retinex-Based Adaptive Filter", IEEE Transactions on Image Processing, 15(9): 2820-2830.

Montag, ED. (2006) "Empirical formula for creating error bars for the method of paired comparison", J Electronic Imaging, 15: 010502.

Moroney N. (2000) "Local Color Correction Using Non-Linear Masking", IS&T/SID 8th Color Imaging Conference, 108-111.

Moroney, N. and Tastl, I., (2004) "Comparison of Retinex and iCAM for scene rendering", J. Electronic Imaging, 13(1): 139-145.

Morovic, J. (2008) Color Gamut Mapping, John Wiley and Sons.

Morovic, J. and Wang, Y. (2003) "A Multi–Resolution, Full–Color Spatial Gamut Mapping Algorithm", 11th Color Imaging Conference, 282-287.

Murakami, Y. and Ishii, J. (2004) "Color conversion method for multi-primary display for spectral color reproduction", J. Electronic Imaging, 13: 701.

Naccari, F. Battiato, S., Bruna, A., Capra, A., Castorina, A. (2005) "Natural Scenes Classification for Color Enhancement", IEEE Trans. On Consumer Electronics, 51(1), 234-238.

Nachlieli, H., Bergman, R., Greig, D., Staelin, C., Oicherman, B., Ruckenstein, G., and Shaked, D. (2009) "Skin-Sensitive Automatic Color Correction", SIGGRAPH, New Orleans.

Nakai, H., Manabe, Y., and Inokuchi, S. (1998) "Simulation and analysis of spectral distributions of human skin", Proceedings of IEEE Fourteenth International Conference on Pattern Recognition, Vol. 2, 1065-1067.

Nallaperumal, K., Subban, R., Krishnaveni, K., Fred, L., and Selvakumar, R.K. (2006) "Human Face Detection in Color Images Using Skin Color and Template Matching Models for Multimedia on the Web", IEEE IFIP International Conference on Wireless and Optical Communications Networks.

Nayatani, Y. and Nakajima, M. (1996), "Prediction of the Helmholtz-Kohlrausch Effect Using the CIELUV Formula", Col. Res. Appl., 21(4): 252-268.

Newhall, S.M, Burnham, R.W., and Clark, J.R. (1957), "Comparison of Successive with Simultaneous Color Matching", J. Opt. Soc. Am., 47(1):43-54.

Nielsen, M., and Stokes, M. (1998), "The Creation of the sRGB ICC Profile," Proc. IS&T/SID 6th Color Imaging Conference (IS&T, Springfield, VA), 253-257.

Park, D.-S., Kim, S.K., Kim, C.-Y., Choi, W.-H., Lee, S.-D., Seo, Y.-S. (2003) "User-preferred color temperature conversion for video on TV or PC", Proc. SPIE: Device-Independent Color, Color Hardcopy, and Graphic Arts VIII, Vol. 5008, 285-293.

Park, D.-S., Kwak, Y., Ok, H., and Kim, C.Y. (2006) "Preferred skin color reproduction on the display", J. Electronic Imaging, 15(4): 041203.

Phung, S.L., Bouzerdoum, A., and Chai, D. (2002) "A novel skin color model in YCbCr color space and its application to human face detection", International Conference on Image Processing, Vol. 1(I), 289-292.

Prabhakar, S., Cheng, H., Handley, J.C., Fan, Z., and Lin, Y.-W. 2002 "Picture-Graphics Color Image Classification", IEEE ICIP II, 785-788.

Qian, R., (2001) "System for Detecting Skin-Tone Regions within an Image", US Patent 6,332,033.

Quach, N.T., Zafarifar, B., and Gaydadjiev, G.N. (2007) "Real-time FPGA-implementation for blue-sky Detection", IEEE International Conf. on Application-Specific Systems, Architectures and Processors, 76-82.

Quan, S., Chiu, A., and Jiang, X. (2005) "Sensor-Dependent Skin Color Detection and Skin Tone Prioritized 3A Control", 13th Color Imaging Conference, pp 319.

Quan, S., and Jin, E. (2008) "Memory Color Based Preferred Color Reproduction with Psychophysical Evaluation", 16th Color Imaging Conference, 304-308.

RIT Munsell Website:
http://www.cis.rit.edu/mcsl/online/Spectral/SpectralData/HumanFace/Spectral_Data /

Rosa, M.G.P. and Tweedale, R. (2000) "Visual areas in lateral and ventral extrastriate cortices of the marmoset monkey", J Comp Neurol 422(4): 621-51.

Rybicki, G. and Lightman, A. (1976), Radiative Processes In Astrophysics, J. Wiley and Son.

Rybicki, G. B., Lightman, A. P. (1979), Radiative Processes in Astrophysics, New York: John Wiley & Sons.

Sanders, C. L. (1959) "Color Preferences for Natural Objects", Illum. Eng. 54: 452-456.

Sanger, D., Asada, T., Haneishi, H., and Miyake, Y. (1994) "Facial Pattern Detection and Its Preferred Color Reproduction", IS&T/SID 2nd Color Imaging Conference, 149-153.

Sanger, D., Miyake, Y., Haneishi, H., and Tsumura, N. (1997) "Algorithm for Face Extraction Based on Lip Detection", J. Imaging Sci. Technol. 41(1): 71.

Sharma, G. (2003) Digital Color Imaging Handbook, CRC Press.

Shin, M.C., Chang, K.I., Tsap, L.V. (2002) "Does Colorspace Transformation Make Any Difference on Skin Detection?", 6th IEEE Workshop on Applications of Computer Vision, 275–279.

Sigal, L., Sclaroff, L., and Athitsos, V. (2000) "Estimation and prediction of evolving color distributions for skin segmentation under varying illumination", IEEE Conference on Computer Vision and Pattern Recognition, Vol. 2, 152-159.

Sincich L.C., Park K.F. (2004) Wohlgemuth M.J., Horton J.C., "Bypassing V1: a direct geniculate input to area MT.". Nat Neurosci 7 (10): 1123–8.

Skaff, S. and Clark, J.J. (2007) "Maximum Entropy Spectral Models for Color Constancy", IS&T/SDI 15th Color Imaging Conference, 100-105.

Skarbek, W. and Koschan, A., (1994) "Color Image Segmentation – a Survey", Technical University of Berlin, Berlin.

Spaulding, K.E., Ellson, R.N., and Sullivan, J.R., "UltraColor: A new gamut mapping strategy", Proceedings SPIE Vol. 2414: Device-Independent Color Imaging II, 61-68 (1995).

Stevens, J.C. and Stevens S.S. (1963) "Brightness functions: Effects of Adaptation", J. Opt. Soc. Am., 53: 375-385.

Stoke, M. Anderson, M., Chandrasekar, S., and Motta, R. (1996) "A Standard Default Color Space for the Internet – sRGB", http://www.w3.org/Graphics/Color/sRGB.

Storring, M., Andersen, H.J., and Granum E. (2004) "A multispectral approach to robust human skin detection", CGIV: 2nd European Conference on Color Graphics, Iaging and Vision, 110-115.

Storring, M. and Graunum, E. (2002) "Adapting a Statistical Skin Color Model to Illumination Changes", CGIV: 1st European Conference on Color Graphics, Imaging, and Vision, 16-21.

Sun, Q. and Fairchild, M.D. (2002) "Statistical characterization of face spectral reflectances and its application to human portraiture spectral estimation", J. Imaging Sci. Technol., Vol. 46(6): 498-506.

Süsstrunk, S., Holm, J., and Finlayson, G.D. (2001) "Chromatic Adaptation Performance of Different RGB Sensors". Proc. SPIE: Color Imaging: Device-Independent Color, Color Hardcopy, and Graphic Arts VI, Vol. 4300, 172-183.

Szummer, M. and Picard, R.W. (1998) "Indoor-outdoor image classification", IEEE CNF, 42-51.

Takahashi, Y. and Hirata, K. (2006) "Segmented-Region Based Approach Using Object Components Database to Detect Sky Region", IEEE International Conference on Image Processing, 2733-2736.

Tastl, I., Bhachech, M, and Moroney, N. (2005) "ICC Color Management and CIECAM02", IS&T/SID 13th Color Imaging Conference (IS&T, Springfield, VA), 217-223.

Terrillon, J.-C., Shirazi, M.N., Fukamachi, H., and Akamatsu S. (2000) "Comparative performance of different skin chrominance models and chrominance spaces for the automatic detection of human faces in color images", 4th IEEE International Conference on Automatic Face and Gesture Recognition, 54-61.

Tian, Y., Wan, Q., and Wu, F. (2007) "Local Histogram Equalization Based on the Minimum Brightness Error", IEEE 4th International Conference on Image and Graphics, 58-61.

Tomaz, F., Candeias, T., and Shahbazkia, H. (2003) "Improved Automatic Skin Detection in Color Images", Proc. 7th Digital Image Computing: Techniques and Applications, Sydney, 419-427.

Topfer, K, Jin E., O'Dell, S., Ribeiro, J. (2006) "Regional Preference for the Rendition of People", International Congress of Imaging Science, 245-248.

Tsumura, N., Haneishi, H., and Miyake, Y. (2000) "Independent Component Analysis of Spectral Absorbance Image in Human Skin", Optical Review, Vol. 7 (6): 479-482.

Tzeng, D.-Y. and Berns, R.S. (1999) "Spectral Based Ink Selection for Multiple-Ink Printing II. Optimal Ink Selection", IS&T 7th Color Imaging Conference, 182-187.

Tzeng, D.-Y. and Berns, R.S. (2000) "Spectral-Based Six-Color Separation Minimizing Metamerism", IS&T 8th Color Imaging Conference, 342-347.

Ungerleider L.G., Desimone R. (1986) "Cortical connections of visual area MT in the macaque", J. Comp Neurol 248 (2): 190-222.

Vezhnevets, V., Sazonov, V., and Andreeva, A. (2003) "A Survey on Pixel-Based Skin Color Detection Techniques", http://graphics.cs.msu.ru.

Viola, P., and Jones, M. (2004) "Robust real-time face detection," International J. Computer Vision, 57 (2): 137-154.

Wright, W.D. (1941) "The sensitivity of the eye to small color differences", Proc. Physical Society, 53: 93-112.

Wyszecki, G., Fielder, G.H. (1971). "New Color-Matching Ellipses". J. Opt. Soc. Am. 61 (9): 1135–1152.

Wyszecki, G. and Stiles, W.S. (1982), Color Science: Concepts and Methods, Quantitative Data and Formulae, 2nd ed., John Wiley & Sons, New York.

Xiong, W. and Funt, B. (2006) "Color Constancy for Multiple-Illuminant Scenes Using Retinex and SVR", IS&T/SDI 4th Color Imaging Conference, 304-308.

Xu, X, and Pan, H. (2000) "Skin and Sky Color Detection and Enhancement System", United State Patent Application, US 2010/0322513 A1.

Yamamoto, S., Tsumura, N., Nakaguchi, T., Miyake, Y., "Development of a multi-spectral scanner using LED array for digital color proof", J. Imaging Sci. Technol., 51(1): 61-69 (2007).

Yang, M.-H. and Ahuja, N. (1998) "Detecting human faces in color images", IEEE International Conference on Image Processing, Vol. 1, 127-130.

Yano, T. and Hashimoto, K. (1997) "preference for Japanese Complexion Color under Illumination", Col. Res. Appl., 22(4): 269-274.

Yendrikhovskij, S.N (1999) "Image Quality: Between Science and Fiction", IS&T's PICS Conference, 173-178.

Yendrikhovskij, S.N., Blommaert, F.J.J., and Ridder, H. (1998) "Optimizing color reproduction of natural images", IS&T 6th Color Imaging Conference, 140-145.

Yendrikhovskij, S.N., Blommaert, F.J.J., Ridder, H. (1999) "Color Reproduction and the Naturalness Constraint", Col. Res. Appl. 24(1): 54-67.

You, J.-Y., and Chien, S.-I. (2008) "Saturation Enhancement of Blue Sky for Increasing Preference of Scenery Images", IEEE Transactions on Consumer Electronic, 54(2): 762-768.

Young, T. (1802), "On the theory of light and colors", Philosophical transactions of the Royal Society of London, 92: 12-48.

Young, T. and Kelland, P. (1845), "A Course of Lectures on Natural Philosophy and the Mechanical Arts", Taylor and Walton, London.

Zarit, B.D., Super, B.J., and Quek, F.K.H. (1999) "Comparison of Five Color Models in Skin Pixel Classification", International Workshop on Recognition, Analysis, and Tracking of Faces and Gestures in Real-Time Systems, 58-63.

Zeng, H. (2000) "Gray Component Replacement by Direct Colorimetric Mapping", Proc. SPIE: Device-Independent Color, Color Hardcopy, and Graphic Arts V, Vol. 3963, 317-322.

Zeng, H. (2000) "Gamut Mapping in Multiple Color Spaces", Proc. SPIE: Device-Independent Color, Color Hardcopy, and Graphic Arts V, Vol. 3963, 301-306.

Zeng, H. (2001) "Gamut Mapping in a Composite Color Space", IS&T NIP17: International Conference on Digital Printing Technologies, 797-800.

Zeng, H. (2001) "Ink Limit Control for Inkjet Printer Color Calibration", Proc. SPIE: Device-Independent Color, Color Hardcopy, and Graphic Arts VI, Vol. 4300, 93-96.

Zeng, H. (2002) "Color Accuracy in ICC Color Management System", Proc IS&T PICS; 175-180.

Zeng, H. (2003) "Neutral Gray Adjustment for Printer ICC Profiles", Proc. SPIE: Color Imaging: Device-Independent Color, Color Hardcopy, and Graphic Arts VIII, Vol. 5008, 341-348.

Zeng, H. (2006) "Spring-Primary Mapping: Combining Primary Adjustment and Gamut Mapping for Pictorials and Business Graphics", Proc. IS&T/SID 9th Color Imaging Conference, 240-245.

Zeng, H. and Luo, M.R. (2009) "Modelling Skin Colours for Preferred Colour Reproduction", Proc IS&T/SID 17th Color Imaging Conference, 175-180.

Zeng, H. and Luo, M.R. (2010) "Modelling Memory Colour Region for Preference Colour Reproduction", Proc. SPIE: Color Imaging: Device-Independent Color, Color Hardcopy, and Graphic Arts XV, Vol. 7528, 752808 1-11.

Zeng, H. and Luo, M.R. (2010) "Colour and Tolerance for Preferred Skin Colours", Proc IS&T/SID 18th Color Imaging Conference, 190-195.

Zeng, H. and Luo, M.R. (2011) "Skin Color Modeling of Digital Photographic Images", J Imaging Sci Tech, 55(3): 030201 – 1-12.

Zeng, H. and Luo, M.R. (2011) "A Preferred Skin Color Enhancement Method for Photographic Color Reproduction", Proc. SPIE: Color Imaging: Device-Independent Color, Color Hardcopy, and Graphic Arts, 786613 1-9.

Zhang, X., Jones, R.W., Baharav, I., and Reid, D.M. (2006) "System and Method for Digital Image Tone Mapping Using an Adaptive Sigmoidal Function Based on Perceptual Preference Guidelines", US Patent 7,023,580.

Zolliker, P. and Simon, K., (2007) "Retaining Local Image Information in Gamut Mapping Algorithms", IEEE Transactions on Image Processing, 16(3): 664-672.

Appendices

Appendix A: Training Result of Lightness-Independent Skin Colour Ellipse Model of Digital Photographic Images in CIELAB Colour Space (Adapted to D50 White Point)

Ellipse a*b* centre: (18.7, 19.6)

$$\Lambda = \begin{pmatrix} 327.871 & 211.271 \\ 211.271 & 613.479 \end{pmatrix}$$

$$\Lambda^{-1} = \begin{pmatrix} \lambda_{00} & \lambda_{01} \\ \lambda_{10} & \lambda_{11} \end{pmatrix} = \begin{pmatrix} 0.00392 & -0.00135 \\ -0.00135 & 0.002095 \end{pmatrix}$$

$$\begin{pmatrix} u_0 \\ u_1 \\ u_2 \end{pmatrix} = \begin{pmatrix} 0.00392 \\ -0.0027 \\ 0.002095 \end{pmatrix}$$

Orientation of the major axis from the horizontal axis: -62° (negative means rotating counter-clockwise)

Semi-major and semi-minor axes: (26.9, 14.7)

$\rho=1$ for 95% coverage rate

Appendix B: Training Result of Lightness-Dependent Skin Colour Ellipse Model of Digital Photographic Images in CIELAB Colour Space (Adapted to D50 White Point)

Ellipse centres:

L* Bucket	a*	b*
0 to 10	-	-
10 to 20	15.7	16.2
20 to 30	16.7	19.9
30 to 40	19.9	21.3
40 to 50	20.7	20.8
50 to 60	20.0	21.3
60 to 70	19.2	20.1
70 to 80	17.8	18.2
80 to 90	12.8	14.7
0 to 10	7.4	8.9

Orientation (degrees) of the major axis from the horizontal axis (negative means rotating counter-clockwise), and Semi-major and semi-minor axes:

L* Bucket	Orientation	Semi-major axis	Semi-minor axis
0 to 10	-	-	-
10 to 20	-46.6°	12.43	5.92
20 to 30	-59.4°	19.62	7.65
30 to 40	-59.2°	26.84	9.22
40 to 50	-56.4°	29.29	10.86
50 to 60	-57.0°	30.66	12.02
60 to 70	-65.9°	29.27	12.76
70 to 80	-68.9°	24.67	11.99
80 to 90	-66.8°	18.92	10.01
90 to 100	-87.6°	10.43	5.34

Inverse matrix $\Lambda^{-1} = \begin{pmatrix} \lambda_{00} & \lambda_{01} \\ \lambda_{10} & \lambda_{11} \end{pmatrix}$:

L* Bucket	λ_{00}	λ_{01} and λ_{10}	λ_{11}
0 to 10	-	-	-
10 to 20	0.018094	-0.02201	0.016888
20 to 30	0.013327	-0.01269	0.006351
30 to 40	0.009052	-0.00913	0.004109
40 to 50	0.006235	-0.00674	0.003408
50 to 60	0.005183	-0.00535	0.002799
60 to 70	0.005316	-0.00371	0.001997
70 to 80	0.006268	-0.00357	0.002334
80 to 90	0.008875	-0.0052	0.003906
90 to 100	0.035068	-0.00219	0.009236

u_0, u_1, u_2:

L* Bucket	u_0	u_1	u_2
0 to 10	-	-	-
10 to 20	0.0180936	-0.0220098	0.0168876
20 to 30	0.0133265	-0.0126911	0.00635143
30 to 40	0.00905222	-0.0091331	0.0041087
40 to 50	0.0062346	-0.00674206	0.00340754
50 to 60	0.00518273	-0.00534737	0.00279936
60 to 70	0.00531627	-0.00371129	0.00199713
70 to 80	0.00626773	-0.00357456	0.00233357
80 to 90	0.00887461	-0.00520429	0.0039056
90 to 100	0.0350677	-0.00219152	0.00923625

$\rho = 1$ for 90% coverage rate

Appendix C: Training Result of Ellipsoid Skin Colour Model of Digital Photographic Images in CIELAB Colour Space (Adapted to D50 White Point)

Ellipsoid colour centre: (59.0, 18.7, 19.6)

$$\Lambda = \begin{pmatrix} 1401.5 & -108.7 & -122.6 \\ -108.7 & 351.3 & 226.4 \\ -122.6 & 226.4 & 657.3 \end{pmatrix}$$

$\rho = 1$ for 90% coverage rate

$$\begin{pmatrix} u_0 \\ u_1 \\ u_2 \\ u_3 \\ u_4 \\ u_5 \end{pmatrix} = \begin{pmatrix} 0.00073397 \\ 0.000356861 \\ 0.0037019 \\ 0.000150894 \\ -0.00248318 \\ 0.00196303 \end{pmatrix}$$

Major-axis vector: (95.9, 13.5, 12.3), semi-axis length: 38.0

Medium-axis vector: (65.5, 30.7, 44.1), semi-axis length: 28.0

Minor-axis vector: (59.4, 32.3, 12.9), semi-axis length: 15.2

Appendix D: Training Result of Ellipsoid Skin Colour Model of Digital Photographic Images in CAM02-UCS (Adapted to D50 White Point)

Ellipsoid colour centre: (62.3, 12.9, 11.8)

$$\Lambda = \begin{pmatrix} 1426.5 & -87.4 & -73.7 \\ -87.4 & 135.8 & 42.6 \\ -73.4 & 42.6 & 163.7 \end{pmatrix}$$

$\rho=1$ for 90% coverage rate

$$\begin{pmatrix} u_0 \\ u_1 \\ u_2 \\ u_3 \\ u_4 \\ u_5 \end{pmatrix} = \begin{pmatrix} 0.000737474 \\ 0.000807553 \\ 0.00824084 \\ 0.000453874 \\ -0.00392184 \\ 0.00672245 \end{pmatrix}$$

Major axis vector: (100.1, 10.1, 9.6), semi-axis length: 37.9

Medium axis vector: (61.1, 5.0, 0.3), semi-axis length: 14.0

Minor axis vector: (62.1, 4.4, 17.6), semi-axis length: 10.2

Appendix E: Training Result of Lightness-Independent Ellipse Model of Colorimetric Skin Colours in CIELAB Colour Space (Adapted to D50 White Point)

Ellipse a*b* centre: (14.0, 17.1)

$$\Lambda = \begin{pmatrix} 40.7634 & 4.79288 \\ 4.79288 & 47.8878 \end{pmatrix}$$

$$\Lambda^{-1} = \begin{pmatrix} \lambda_{00} & \lambda_{01} \\ \lambda_{10} & \lambda_{11} \end{pmatrix} = \begin{pmatrix} 0.024824 & -0.00248 \\ -0.00248 & 0.021131 \end{pmatrix}$$

$$\begin{pmatrix} u_0 \\ u_1 \\ u_2 \end{pmatrix} = \begin{pmatrix} 0.024824 \\ -0.00497 \\ 0.021131 \end{pmatrix}$$

Orientation of the major axis from the horizontal axis: -63.3^{o} (negative means rotating counter-clockwise)

Semi-major and semi-minor axes: (7.1, 6.2)

$\rho = 1$ for 95% coverage rate

Appendix F: Training Result of Lightness-Independent Ellipse Model of Colorimetric Skin Colours in CAM02-UCS (Adapted to D50 White Point)

Ellipse a*b* centre: (9.5, 5.1)

$$\Lambda = \begin{pmatrix} 20.1774 & -2.82527 \\ -2.82527 & 27.9094 \end{pmatrix}$$

$$\Lambda^{-1} = \begin{pmatrix} \lambda_{00} & \lambda_{01} \\ \lambda_{10} & \lambda_{11} \end{pmatrix} = \begin{pmatrix} 0.050273 & 0.005089 \\ 0.005089 & 0.036345 \end{pmatrix}$$

$$\begin{pmatrix} u_0 \\ u_1 \\ u_2 \end{pmatrix} = \begin{pmatrix} 0.050273 \\ 0.010178 \\ 0.036345 \end{pmatrix}$$

Orientation of the major axis from the horizontal axis: 71.9^{o} (positive means rotating clockwise)

Semi-major and semi-minor axes: (5.4, 4.4)

$\rho=1$ for 95% coverage rate

Appendix G: Training Result of Ellipsoid Model of Colorimetric Skin Colours in CAM02-UCS (Adapted to D50 White Point)

Ellipsoid colour centre: (60.2, 9.5, 5.1)

$$\Lambda = \begin{pmatrix} 1571.71 & 17.1241 & -170.92 \\ 17.1241 & 51.6596 & -7.23346 \\ -170.92 & -7.23346 & 71.4556 \end{pmatrix}$$

$\rho=1$ for 99% coverage rate

$$\begin{pmatrix} u_0 \\ u_1 \\ u_2 \\ u_3 \\ u_4 \\ u_5 \end{pmatrix} = \begin{pmatrix} 0.00085994 \\ 0.00000060 \\ 0.01963580 \\ 0.00411451 \\ 0.00398986 \\ 0.0191175 \end{pmatrix}$$

Major axis vector: (20.5, 9.0, 9.6), semi-axis length: 39.9

Medium axis vector: (59.4, 14.9, -0.7), semi-axis length: 8.0

Minor axis vector: (60.6, 14.5, 9.7), semi-axis length: 6.8

Appendix H: Experiment I-1

Frequency matrices of 12 images (A, B, …, L) from paired-comparison:

A:

	0	1	2	3	4	5	6	7	8
0	10	16	8	16	18	12	19	18	15
1	4.5	10	8	12	20	11	15	18	13
2	12	12	10	17	16	17	17	20	17
3	4	8	3	10	16	11	12	14	9
4	2	0	4	4	10	9	6	12	7
5	8	9.5	3	9	11	10	10	12	12
6	1	5	3.5	8.5	14	10	10	16	9
7	2.5	2	0	6	8.5	8	4	10	7
8	5.5	7	3	11	13	8.5	11	13	10
Avg	5.5	7.67	4.72	10.39	14.06	10.67	11.44	14.67	10.89

B:

	0	1	2	3	4	5	6	7	8
0	9.5	12	11	13	15	13	12	17	12
1	7	9.5	7	9	17	12	8	15	15
2	8.5	12	9.5	10	15	17	9	17	16
3	6	10	9	9.5	13	10	12	12	9
4	4	2	4	6	9.5	7	6	12	8
5	6	7.5	2	9	12	9.5	4	9	10
6	7	11	10	7.5	13	15	9.5	16	12
7	2	4	2	7	7.5	10	3	9.5	8
8	7	4.5	3	10	11	9	7	11	9.5
Avg	6.33	8.06	6.33	9	12.56	11.33	7.78	13.11	11

C:

	0	1	2	3	4	5	6	7	8
0	9.5	14	12	13	17	14	12	16	13
1	5.5	9.5	8	9	16	15	7	16	11
2	7	11	9.5	10	11	13	7	14	15
3	6.5	10	9	9.5	16	13	7	12	9
4	2.5	3.5	8	3	9.5	8	3.5	7.5	9
5	5	4.5	6	6	11	9.5	6.5	8	8.5
6	7	12	12	12	16	13	9.5	14	13
7	3.5	3	5	7	12	11	5	9.5	11
8	6.5	8.5	4.5	10	10	11	6	8	9.5
Avg	5.89	8.39	8.22	8.78	12.94	11.78	7.06	11.61	10.83

D:

	0	1	2	3	4	5	6	7	8
0	9.5	12	11	17	17	11	13	16	12
1	7	9.5	6.5	12	18	11	9	16	12
2	8.5	13	9.5	12	15	17	11	14	17
3	2.5	7	7	9.5	16	12	11	13	8
4	2	1.5	4	3	9.5	7	4	11	9
5	8	8	2	7	12	9.5	9	11	8
6	6.5	10	8	8.5	15	10	9.5	15	10
7	3	3	5.5	6	8	8	4	9.5	5
8	7.5	7.5	2.5	11	10	11	9	14	9.5

Avg   6.06   7.89   6.17   9.5   13.33   10.72   8.72   13.22   9.89

E:

	0	1	2	3	4	5	6	7	8
0	9.5	15	12	8.5	17	13	10	13	12
1	4	9.5	6	3	13	11	4.5	10	7
2	7	13	9.5	8	11	14	5.5	8.5	8
3	11	16	11	9.5	16	14	6.5	10	8
4	2	6	8	3	9.5	8	2	3	5
5	6.5	8.5	5.5	5	11	9.5	6	7.5	7
6	9	15	14	13	17	13	9.5	15	14
7	6	9	11	9	16	12	4	9.5	9.5
8	7	12	11	11	14	12	5	9.5	9.5
Avg	6.83	11.5	9.67	7.72	13.83	11.61	5.89	9.56	8.89

F:

	0	1	2	3	4	5	6	7	8
0	10	11	8.5	18	17	12	16	17	12
1	9	10	4	10	19	14	17	19	11
2	12	16	10	15	16	18	14	19	15
3	2	10	5	10	13	9	4.5	10	7
4	3	1.5	4	7	10	6.5	3	9.5	4
5	8	6	2.5	11	14	10	13	11	7
6	4.5	3	6	16	17	7	10	13	9.5
7	3	1	1	10	11	9.5	7	10	6
8	8.5	9.5	5.5	13	16	13	11	14	10
Avg	6.61	7.56	5.17	12.17	14.61	10.94	10.5	13.56	8.89

G:

	0	1	2	3	4	5	6	7	8
0	10	15	9	18	19	15	19	18	11
1	5	10	7.5	8	18	10	12	17	12
2	11	13	10	14	18	19	17	20	18
3	2.5	12	6	10	16	12	8.5	14	11
4	1	2	2	4	10	7	4	10	7.5
5	5	10	1	8	13	10	7.5	13	9
6	1	8	3	12	16	13	10	14	11
7	2	3	0	6	10	7	6	10	9
8	9.5	8	2	9	13	11	9	11	10
Avg	5.22	8.94	4.5	9.78	14.72	11.5	10.33	14.11	10.89

H:

	0	1	2	3	4	5	6	7	8
0	9.5	15	9	17	15	13	14	18	15
1	4	9.5	8	9	19	11	11	17	13
2	10	11	9.5	11	15	17	14	17	15
3	2	10	8	9.5	15	10	9	13	9
4	4	0	4	4	9.5	6	5	13	5
5	6	8.5	2.5	9	13	9.5	9	11	12
6	5	8	5	10	14	10	9.5	14	11
7	1	2	2	6	6	8	5	9.5	7
8	4.5	6	4	10	14	7	8	12	9.5
Avg	5.11	7.78	5.78	9.5	13.39	10.06	9.39	13.83	10.67

I:

	0	1	2	3	4	5	6	7	8
0	9.5	5	5	16	12	4.5	16	11	3.5
1	14	9.5	5	13	19	5	14	17	6.5
2	14	14	9.5	17	16	15	16	17	12
3	3	6	2	9.5	9	5	14	5	3.5
4	7.5	0	3	10	9.5	6	11	11	1
5	15	14	4.5	14	13	9.5	15	12	9
6	3	5	3	5	8	4	9.5	8	3
7	8.5	2	2	14	8	7	11	9.5	3
8	16	13	7	16	18	10	16	16	9.5
Avg	9.94	7.56	4.56	12.67	12.44	7.28	13.61	11.78	5.67

J:

	0	1	2	3	4	5	6	7	8
0	9.5	12	9	14	17	11	16	17	10
1	7	9.5	6	10	15	8	13	17	5.5
2	10	13	9.5	12	16	14	14	16	11
3	5	9	7	9.5	13	9	10	12	8
4	2	4.5	3	6	9.5	7	9	10	3.5
5	8	11	5	10	12	9.5	11	13	9
6	3	6	5	9	10	8	9.5	13	9
7	2	2	3	7	9	6	6	9.5	7
8	9	14	8.5	11	16	10	10	12	9.5
Avg	6.17	8.94	6.22	9.83	12.94	9.17	10.94	13.28	8

K:

	0	1	2	3	4	5	6	7	8
0	9.5	15	11	14	16	9	13	15	9
1	4	9.5	5	10	16	6.5	9	11	3.5
2	8.5	14	9.5	11	14	14	10	13	7.5
3	5	9	8	9.5	12	7	5.5	12	9
4	3	3.5	5	7	9.5	4	4	8	5
5	10	13	5.5	12	15	9.5	7.5	9.5	5
6	6.5	10	9	14	15	12	9.5	13	9
7	4.5	8	6.5	7	11	9.5	6	9.5	6
8	10	16	12	10	14	14	10	13	9.5
Avg	6.78	10.78	7.83	10.44	13.56	9.39	8.22	11.44	7.06

L:

	0	1	2	3	4	5	6	7	8
0	10	5	4	20	15	7	20	16	6
1	15	10	2	19	19	6	19	19	12
2	16	18	10	20	20	18	19	20	18
3	0.5	1	0	10	10	3	15	7	3
4	5	1	0	10	10	2.5	16	15	1
5	13	14	2	17	18	10	17	20	8.5
6	0	1	1	5	4	3	10	6	1
7	4	1	0	13	5	0	14	10	3
8	14	8	2	17	19	12	19	17	10
Avg	8.61	6.56	2.33	14.5	13.28	6.78	16.56	14.44	6.94

Z-scores of each image (A, B, …, L) at each of nine colour centres (1, 2, …, 8):

Image	0	1	2	3	4	5	6	7	8
A	-0.7	-0.56	-0.98	0.06	0.8	0.1	0.24	0.89	0.13
B	-0.46	-0.23	-0.5	-0.07	0.45	0.28	-0.25	0.56	0.22
C	-0.52	-0.18	-0.18	-0.11	0.52	0.32	-0.34	0.32	0.19
D	-0.52	-0.27	-0.5	0	0.61	0.19	-0.12	0.54	0.07
E	-0.39	0.3	0.02	-0.27	0.67	0.29	-0.53	0	-0.08
F	-0.5	-0.42	-0.72	0.32	0.68	0.14	0.07	0.58	-0.15
G	-0.78	-0.18	-1.07	-0.01	0.73	0.25	0.1	0.81	0.14
H	-0.69	-0.49	-0.56	0.02	0.79	0.09	-0.01	0.69	0.17
I	0.05	-0.52	-0.76	0.48	0.7	-0.31	0.61	0.37	-0.62
J	-0.52	-0.1	-0.48	0.05	0.52	-0.04	0.21	0.58	-0.21
K	-0.4	0.18	-0.23	0.13	0.59	-0.02	-0.18	0.27	-0.35
L	-0.49	-0.63	-1.84	0.98	0.78	-0.67	1.27	1.12	-0.5

Appendix I: Experiment I-2

Frequency matrices of 12 images (a, b, …, l) from paired-comparison:

a:

	0	1	2	3	4	5	6	7	8
0	0.5	0.85	0.7	0.5	0.75	0.7	0.6	0.6	0.53
1	0.15	0.5	0.65	0.3	0.63	0.55	0.35	0.5	0.57
2	0.3	0.35	0.5	0.2	0.4	0.6	0.3	0.45	0.55
3	0.5	0.7	0.8	0.5	0.8	0.75	0.33	0.65	0.7
4	0.25	0.38	0.6	0.2	0.5	0.6	0.2	0.35	0.57
5	0.3	0.45	0.4	0.25	0.4	0.5	0.2	0.35	0.33
6	0.4	0.65	0.7	0.68	0.8	0.8	0.5	0.6	0.6
7	0.4	0.5	0.55	0.35	0.65	0.65	0.4	0.5	0.78
8	0.47	0.42	0.45	0.3	0.42	0.68	0.4	0.23	0.5
Avg	0.36	0.53	0.59	0.36	0.59	0.65	0.36	0.47	0.57

b:

	0	1	2	3	4	5	6	7	8
0	0.5	0.72	0.55	0.65	0.78	0.6	0.82	0.82	0.63
1	0.28	0.5	0.53	0.6	0.45	0.42	0.65	0.8	0.6
2	0.45	0.47	0.5	0.6	0.7	0.57	0.55	0.75	0.78
3	0.35	0.4	0.4	0.5	0.65	0.55	0.68	0.65	0.5
4	0.23	0.55	0.3	0.35	0.5	0.3	0.45	0.7	0.5
5	0.4	0.57	0.42	0.45	0.7	0.5	0.5	0.65	0.55
6	0.17	0.35	0.45	0.33	0.55	0.5	0.5	0.6	0.5
7	0.17	0.2	0.25	0.35	0.3	0.35	0.4	0.5	0.4
8	0.38	0.4	0.23	0.5	0.5	0.45	0.5	0.6	0.5
Avg	0.32	0.46	0.4	0.48	0.57	0.47	0.56	0.67	0.55

c:

	0	1	2	3	4	5	6	7	8
0	0.5	0.82	0.57	0.57	0.82	0.8	0.6	0.75	0.72
1	0.17	0.5	0.65	0.4	0.68	0.68	0.3	0.7	0.65
2	0.42	0.35	0.5	0.4	0.63	0.68	0.4	0.55	0.55
3	0.42	0.6	0.6	0.5	0.82	0.7	0.68	0.85	0.78
4	0.17	0.33	0.38	0.17	0.5	0.6	0.23	0.35	0.55
5	0.2	0.33	0.33	0.3	0.4	0.5	0.2	0.4	0.42
6	0.4	0.7	0.6	0.33	0.78	0.8	0.5	0.8	0.6
7	0.25	0.3	0.45	0.15	0.65	0.6	0.2	0.5	0.65
8	0.28	0.35	0.45	0.23	0.45	0.57	0.4	0.35	0.5
Avg	0.31	0.47	0.5	0.34	0.64	0.66	0.39	0.58	0.6

d:

	0	1	2	3	4	5	6	7	8
0	0.5	0.7	0.55	0.72	0.75	0.5	0.57	0.8	0.53
1	0.3	0.5	0.8	0.45	0.6	0.4	0.6	0.72	0.57
2	0.45	0.2	0.5	0.55	0.6	0.68	0.75	0.65	0.68
3	0.28	0.55	0.45	0.5	0.6	0.42	0.55	0.6	0.4
4	0.25	0.4	0.4	0.4	0.5	0.55	0.5	0.65	0.42
5	0.5	0.6	0.33	0.57	0.45	0.5	0.47	0.55	0.38
6	0.42	0.4	0.25	0.45	0.5	0.53	0.5	0.63	0.45
7	0.2	0.28	0.35	0.4	0.35	0.45	0.38	0.5	0.55
8	0.47	0.42	0.33	0.6	0.57	0.63	0.55	0.45	0.5

| Avg | 0.38 | 0.45 | 0.44 | 0.52 | 0.55 | 0.52 | 0.54 | 0.62 | 0.5 |

e:

	0	1	2	3	4	5	6	7	8
0	10	6	2	12	9	4	12	11	4
1	14	10	4	17	10	4.5	16	14	6
2	18	16	10	18	14	14	18	17	13
3	8	3	2	10	6.5	4	12	12	3
4	11	10	6	14	10	4	12	12	3
5	16	16	6	16	16	10	17	17	12
6	8	4.5	2	8	8	3	10	7	2
7	9	6	3	8	8	3.5	13	10	3.5
8	16	14	7.5	17	17	8.5	18	17	10
Avg	12.22	9.44	4.72	13.28	10.94	6.17	14.17	12.89	6.17

f:

	0	1	2	3	4	5	6	7	8
0	10	12	14	13	17	15	15	16	18
1	8.5	10	15	7.5	12	16	11	14	17
2	6	5.5	10	6	13	11	9	12	13
3	7.5	13	14	10	12	14	9	15	15
4	3	8	7	8.5	10	10	7	9.5	12
5	5	4	9	6	10	10	8	7	9
6	5.5	9	11	11	13	12	10	16	16
7	4.5	6	8	5	11	13	4	10	10
8	2	3	7.5	5	8	11	4	10	10
Avg	5.78	7.72	10.56	7.94	11.67	12.44	8.5	12.11	13.28

g:

	0	1	2	3	4	5	6	7	8
0	10	14	15	9	16	16	9	11	15
1	6.5	10	14	6	9.5	12	7	9.5	9
2	5	6	10	7	10	13	5	8.5	11
3	11	14	13	10	16	15	7.5	14	14
4	4	11	10	4	10	12	2	11	9.5
5	4	8	7	5	8.5	10	5	5	8.5
6	11	13	15	13	18	15	10	18	14
7	9	11	12	6.5	9.5	15	2	10	13
8	5	11	9	6	11	12	6	7	10
Avg	7.28	10.72	11.61	7.33	12	13.22	5.94	10.33	11.56

h:

	0	1	2	3	4	5	6	7	8
0	0.5	0.75	0.75	0.6	0.7	0.8	0.68	0.65	0.68
1	0.25	0.5	0.5	0.35	0.57	0.7	0.5	0.68	0.55
2	0.25	0.5	0.5	0.3	0.55	0.57	0.35	0.5	0.65
3	0.4	0.65	0.7	0.5	0.82	0.78	0.42	0.72	0.7
4	0.3	0.42	0.45	0.17	0.5	0.65	0.23	0.6	0.45
5	0.2	0.3	0.42	0.23	0.35	0.5	0.2	0.4	0.55
6	0.33	0.5	0.65	0.57	0.78	0.8	0.5	0.7	0.7
7	0.35	0.33	0.5	0.28	0.4	0.6	0.3	0.5	0.7
8	0.33	0.45	0.35	0.3	0.55	0.45	0.3	0.3	0.5
Avg	0.32	0.49	0.54	0.37	0.58	0.65	0.39	0.56	0.61

i:

	0	1	2	3	4	5	6	7	8
0	0.5	0.8	0.45	0.57	0.85	0.65	0.53	0.7	0.6
1	0.2	0.5	0.38	0.33	0.65	0.6	0.55	0.6	0.68
2	0.55	0.63	0.5	0.65	0.55	0.7	0.55	0.65	0.57
3	0.42	0.68	0.35	0.5	0.78	0.7	0.57	0.65	0.6
4	0.15	0.35	0.45	0.23	0.5	0.75	0.25	0.5	0.5
5	0.35	0.4	0.3	0.3	0.25	0.5	0.33	0.57	0.47
6	0.47	0.45	0.45	0.42	0.75	0.68	0.5	0.7	0.5
7	0.3	0.4	0.35	0.35	0.5	0.42	0.3	0.5	0.35
8	0.4	0.33	0.42	0.4	0.5	0.53	0.5	0.65	0.5
Avg	0.37	0.5	0.41	0.42	0.59	0.61	0.45	0.61	0.53

j:

	0	1	2	3	4	5	6	7	8
0	0.5	0.75	0.65	0.75	0.7	0.6	0.85	0.75	0.7
1	0.25	0.5	0.5	0.42	0.57	0.7	0.7	0.72	0.75
2	0.35	0.5	0.5	0.57	0.65	0.72	0.5	0.7	0.68
3	0.25	0.57	0.42	0.5	0.65	0.75	0.4	0.6	0.7
4	0.3	0.42	0.35	0.35	0.5	0.65	0.45	0.9	0.7
5	0.4	0.3	0.28	0.25	0.35	0.5	0.45	0.45	0.72
6	0.15	0.3	0.5	0.6	0.55	0.55	0.5	0.65	0.6
7	0.25	0.28	0.3	0.4	0.1	0.55	0.35	0.5	0.5
8	0.3	0.25	0.33	0.3	0.3	0.28	0.4	0.5	0.5
Avg	0.31	0.43	0.42	0.46	0.49	0.59	0.51	0.64	0.65

k:

	0	1	2	3	4	5	6	7	8
0	0.5	0.55	0.3	0.63	0.65	0.55	0.68	0.65	0.4
1	0.45	0.5	0.4	0.65	0.68	0.45	0.7	0.75	0.6
2	0.7	0.6	0.5	0.6	0.7	0.65	0.65	0.85	0.63
3	0.38	0.35	0.4	0.5	0.45	0.4	0.53	0.55	0.35
4	0.35	0.33	0.3	0.55	0.5	0.45	0.4	0.53	0.2
5	0.45	0.55	0.35	0.6	0.55	0.5	0.4	0.6	0.38
6	0.33	0.3	0.35	0.47	0.6	0.6	0.5	0.6	0.4
7	0.35	0.25	0.15	0.45	0.47	0.4	0.4	0.5	0.25
8	0.6	0.4	0.38	0.65	0.8	0.63	0.6	0.75	0.5
Avg	0.46	0.42	0.35	0.57	0.6	0.51	0.54	0.64	0.41

l

	0	1	2	3	4	5	6	7	8
0	10	14	12	12	14	12	9	11	6
1	6	10	10	10	13	11	6	6	5
2	8	10	10	8	13	14	10	8	11
3	8.5	10	12	10	15	12	10	12	12
4	6.5	7.5	7.5	5.5	10	12	3	3.5	8.5
5	8	9	6	8.5	8	10	8	7	7
6	11	14	10	10	17	12	10	15	11
7	9	14	12	8	17	13	5	10	12
8	14	15	9	8	12	13	9	8.5	10
Avg	9	11.5	9.83	8.83	12.89	12.06	7.78	9	9.11

Z-scores of each image (a, b, …, l) at each of nine colour centres (A, B, …, I):

Image	A	B	C	D	E	F	G	H	I
a	-0.37	0.1	0.25	-0.37	0.26	0.39	-0.37	-0.08	0.18
b	-0.48	-0.1	-0.26	-0.05	0.19	-0.07	0.17	0.47	0.13
c	-0.51	-0.05	0.01	-0.45	0.38	0.42	-0.31	0.24	0.27
d	-0.34	-0.14	-0.15	0.05	0.12	0.04	0.11	0.31	-0.01
e	0.33	-0.08	-0.79	0.49	0.15	-0.55	0.61	0.41	-0.57
f	-0.6	-0.32	0.08	-0.27	0.23	0.33	-0.21	0.29	0.48
g	-0.37	0.09	0.22	-0.36	0.3	0.43	-0.59	0.07	0.21
h	-0.47	-0.03	0.1	-0.36	0.22	0.41	-0.31	0.16	0.28
i	-0.35	0.02	-0.24	-0.22	0.26	0.3	-0.13	0.29	0.08
j	-0.53	-0.18	-0.2	-0.1	-0.06	0.23	0.05	0.4	0.39
k	-0.11	-0.2	-0.41	0.17	0.27	0.04	0.1	0.39	-0.24
l	-0.13	0.2	-0.02	-0.15	0.4	0.26	-0.3	-0.14	-0.12

Appendix J: Experiment II

Oobserver data from paired-comparison:

Boy

	0	1	2	3	4	5	6	7	8
0									
1	9								
2	15	13							
3	10	16	13						
4	10	10	10	5					
5	12	10	9	7	12				
6	15	19	17	19	18	16			
7	12	15	11	10	15	10	5		
8	13	12	10	11	14	12	8	15	

Girl

	0	1	2	3	4	5	6	7	8
0									
1	7								
2	6	11							
3	11	13	12						
4	5	7	8	4					
5	10	9	3	4	10				
6	17	15	18	17	17	16			
7	10	11	14	7	11	11	3		
8	10	10	8	8	10	13	5	10	

Man

	0	1	2	3	4	5	6	7	8
0									
1	5								
2	10	12							
3	15	15	13						
4	7	9	9	2					
5	10	10	8	6	13				
6	16	16	17	15	17	16			
7	11	15	14	12	15	15	5		
8	11	13	10	12	13	12	4	13	

Woman

	0	1	2	3	4	5	6	7	8
0									
1	2								
2	1	9							
3	17	17	15						
4	7	10	11	2					
5	10	10	9	1	11				
6	17	18	18	18	19	18			
7	13	16	13	10	12	16	1		
8	13	15	10	8	11	10	3	10	

Z-scores of each image (a, b, …, l) at each of nine colour centres (A, B, …, I):

	A	B	C	D	E	F	G	H	I
Boy	0.31	0.57	0.08	0.01	0.43	0.12	-1.13	-0.09	-0.30
Girl	0.02	0.19	0.16	-0.21	0.40	0.38	-0.98	0.01	0.03
Man	0.15	0.45	0.20	-0.26	0.53	0.25	-0.86	-0.27	-0.17
Woman	0.04	0.67	0.53	-0.52	0.49	0.45	-1.41	-0.19	-0.05
Average	0.13	0.47	0.24	-0.25	0.46	0.30	-1.10	-0.14	-0.12

Appendix K: Experiment III

Skin tone preference by ethnicity (African skin tone judged by Africans, Caucasian skin tone judged by Caucasians, and Oriental skin tone judged by Orientals):

Observer	*African*		*Caucasian*		*Oriental*	
	a*	b*	a*	b*	a*	b*
#1	19.8	22.5	21.2	25.8	17.9	21.1
#2	19.2	24.1	19.5	24.5	19.5	23.9
#3	21.6	25.7	19.2	24.8	17.5	21.7
#4	21.1	25.3	21.3	25.7	17.9	22.9
#5	21.6	24.7	19.3	23.2	18.1	22.1
#6	18.9	22.1	20.4	25.9	18.4	23.8
#7	20.6	22.3	20.5	24.3	18.6	22.2
#8	20.0	25.3	19.3	23.5	19.0	23.2
#9	20.5	25.5	20.5	24.0	18.1	22.3
#10	21.7	25.1	21.4	25.7	17.4	21.0
#11	21.2	25.8	21.0	25.8	18.0	21.9
#12	19.2	22.5	19.5	24.1	17.7	21.4
#13	21.7	25.6	20.3	25.6	18.6	21.3
#14	19.0	22.7	20.2	24.9	17.6	21.7
#15	20.6	23.0	19.7	25.7	17.9	21.4
#16	20.6	24.8	20.5	24.9	17.2	21.6
#17			20.2	26.1	17.4	22.0
#18			20.8	24.6	19.6	23.6
#19					19.7	23.3
#20					17.3	21.2
#21					18.4	21.2

The t-test result using ttest2 in MATLAB:

	p-value (a*)	p-value (b*)
Caucasian, African	0.536	0.068
Caucasian, Oriental	$1.030*10^{-10}$	$1.287*10^{-11}$
African, Oriental	$2.624*10^{-9}$	$5.321*10^{-6}$

Multivariate Analysis of Variance of African and Caucasian Data Sets Using SAS:

Characteristic Roots and Vectors of: E Inverse * H, where

H = Type III SSCP Matrix for group

E = Error SSCP Matrix

Characteristic   Characteristic Vector V'EV=1

Root	Percent	astar	bstar
0.31688810	100.00	-0.22517369	0.20351292
0.00000000	0.00	0.16553339	0.04090971

MANOVA Test Criteria and Exact F Statistics for the Hypothesis of No Overall group Effect

H = Type III SSCP Matrix for group

E = Error SSCP Matrix

S=1   M=0   N=14.5

Statistic	Value	F Value	Num DF	Den DF	Pr > F
Wilks' Lambda	0.75936596	4.91	2	31	0.0140
Pillai's Trace	0.24063404	4.91	2	31	0.0140
Hotelling-Lawley Trace	0.31688810	4.91	2	31	0.0140
Roy's Greatest Root	0.31688810	4.91	2	31	0.0140

Appendix L: Training Result of Lightness-Independent Ellipse Modelling of Green Foliage Colours of Digital Photographic Images

Training in CIELAB colour space (adapted to D50 white point):

Ellipse a*b* centre: (-24.7, 34.2)

$$\Lambda = \begin{pmatrix} 321.467 & -216.722 \\ -216.722 & 1020.86 \end{pmatrix}$$

$$\Lambda^{-1} = \begin{pmatrix} \lambda_{00} & \lambda_{01} \\ \lambda_{10} & \lambda_{11} \end{pmatrix} = \begin{pmatrix} 0.00363 & 0.000771 \\ 0.000771 & 0.001143 \end{pmatrix}$$

$$\begin{pmatrix} u_0 \\ u_1 \\ u_2 \end{pmatrix} = \begin{pmatrix} 0.00363 \\ 0.00154 \\ 0.00114 \end{pmatrix}$$

Orientation of the major axis from the horizontal axis: 74.1^0)

Semi-major and semi-minor axes: (32.9, 16.1)

$\rho=1$ for 97% coverage rate

Training in CAM02-UCS (adapted to D50 white point):

Ellipse AB centre: (-16.3, 19.5)

$$\Lambda = \begin{pmatrix} 95.6833 & -28.2173 \\ -28.2173 & 210.662 \end{pmatrix}$$

$$\Lambda^{-1} = \begin{pmatrix} \lambda_{00} & \lambda_{01} \\ \lambda_{10} & \lambda_{11} \end{pmatrix} = \begin{pmatrix} 0.010881 & 0.001457 \\ 0.001457 & 0.004942 \end{pmatrix}$$

$$\begin{pmatrix} u_0 \\ u_1 \\ u_2 \end{pmatrix} = \begin{pmatrix} 0.010881 \\ 0.002915 \\ 0.004942 \end{pmatrix}$$

Orientation of the major axis from the horizontal axis: 76.9^o)

Semi-major and semi-minor axes: (14.79.4)

$\rho=1$ for 97% coverage rate

Appendix M: Training Result of Ellipsoid Modelling of Green Foliage Colours of Digital Photographic Images

Training in CIELAB colour space (adapted to D50 white point):

Ellipsoid colour centre: (49.7, -16.3, 19.5)

$$\Lambda = \begin{bmatrix} 2061.3 & -285.2 & 982.6 \\ -285.2 & 421.1 & -283.9 \\ 982.6 & -283.9 & 1337.1 \end{bmatrix}$$

$\rho=1$ for 97% coverage rate

$$\begin{pmatrix} u_0 \\ u_1 \\ u_2 \\ u_3 \\ u_4 \\ u_5 \end{pmatrix} = \begin{pmatrix} 0.000755838 \\ 0.00032089 \\ 0.00280571 \\ -0.0010427 \\ 0.000955474 \\ 0.00123239 \end{pmatrix}$$

Major-axis vector: (36.5, -14.9, 0.729), semi-axis length: 36.7

Medium-axis vector: (76.5, -22.5, 25.1), semi-axis length: 30.0

Minor-axis vector: (48.3, -7.01, 39.5), semi-axis length: 18.4

Training in CAM02-UCS (adapted to D50 white point):

Ellipsoid colour centre: (48.0, -24.7, 34.2)

$$\Lambda = \begin{bmatrix} 2074.55 & -46.807 & 366.647 \\ -46.807 & 125.545 & -37.0237 \\ 366.647 & -37.0237 & 276.408 \end{bmatrix}$$

$\rho=1$ for 97% coverage rate

$$\begin{pmatrix} u_0 \\ u_1 \\ u_2 \\ u_3 \\ u_4 \\ u_5 \end{pmatrix} = \begin{pmatrix} 0.000629658 \\ -2.40587e-005 \\ 0.00829304 \\ -0.00167367 \\ 0.00225355 \\ 0.00487879 \end{pmatrix}$$

Major-axis vector: (77.7, -9.11, 17.5), semi-axis length: 29.0

Medium-axis vector: (51.9, -20.7, 34.5), semi-axis length: 15.8

Minor-axis vector: (49.2, -6.00, 22.7), semi-axis length: 10.8

Appendix N: Training Result of Lightness-Independent Ellipse Modelling of Blue Sky Colours of Digital Photographic Images

Training in CIELAB colour space (adapted to D50 white point):

Ellipse a*b* centre: (-5.6, -28.5)

$$\Lambda = \begin{pmatrix} 172.729 & -132.317 \\ -132.317 & 831.558 \end{pmatrix}$$

$$\Lambda^{-1} = \begin{pmatrix} \lambda_{00} & \lambda_{01} \\ \lambda_{10} & \lambda_{11} \end{pmatrix} = \begin{pmatrix} 0.006593 & 0.001049 \\ 0.001049 & 0.001369 \end{pmatrix}$$

$$\begin{pmatrix} u_0 \\ u_1 \\ u_2 \end{pmatrix} = \begin{pmatrix} 0.006593 \\ 0.002098 \\ 0.001369 \end{pmatrix}$$

Orientation of the major axis from the horizontal axis: 79.1^0)

Semi-major and semi-minor axes: (29.3, 12.1)

$\rho=1$ for 95% coverage rate

Training in CAM02-UCS (adapted to D50 white point):

Ellipse AB centre: (-10.1, -20.3)

$$\Lambda = \begin{pmatrix} 69.179 & 18.958 \\ 18.958 & 255.85 \end{pmatrix}$$

$$\Lambda^{-1} = \begin{pmatrix} \lambda_{00} & \lambda_{01} \\ \lambda_{10} & \lambda_{11} \end{pmatrix} = \begin{pmatrix} 0.014755 & -0.00109 \\ -0.00109 & 0.00399 \end{pmatrix}$$

$$\begin{pmatrix} u_0 \\ u_1 \\ u_2 \end{pmatrix} = \begin{pmatrix} 0.014755 \\ -0.00219 \\ 0.00399 \end{pmatrix}$$

Orientation of the major axis from the horizontal axis: -84.3^o)

Semi-major and semi-minor axes: (16.1, 8.2)

$\rho=1$ for 95% coverage rate

Appendix O: Training Result of Ellipsoid Modelling of Blue Sky Colours of Digital Photographic Images

Training in CIELAB colour space (adapted to D50 white point):

Ellipsoid colour centre: (62.8, -5.6, -28.5)

$$\Lambda = \begin{bmatrix} 1467.1 & -229.8 & 518.8 \\ -229.8 & 203.2 & -155.6 \\ 518.8 & -155.6 & 978.1 \end{bmatrix}$$

$\rho=1$ for 95% coverage rate

$$\begin{pmatrix} u_0 \\ u_1 \\ u_2 \\ u_3 \\ u_4 \\ u_5 \end{pmatrix} = \begin{pmatrix} 0.000934281 \\ 0.00154247 \\ 0.00624211 \\ -0.000745766 \\ 0.00116825 \\ 0.00131317 \end{pmatrix}$$

Major-axis vector: (33.1 -2.33 -21.3), semi-axis length: 30.8

Medium-axis vector: (59.5, 6.41, -47.4), semi-axis length: 22.6

Minor-axis vector: (63.2, 5.89, -21.3), semi-axis length: 13.6

Training in CAM02-UCS (adapted to D50 white point):

Ellipsoid colour centre: (65.0, -10.1, -20.3)

$$\Lambda = \begin{bmatrix} 1462.95 & -46.9651 & 315.443 \\ -46.9651 & 81.0449 & -37.0237 \\ 315.443 & 22.2099 & 299.734 \end{bmatrix}$$

$\rho=1$ for 95% coverage rate

$$\begin{pmatrix} u_0 \\ u_1 \\ u_2 \\ u_3 \\ u_4 \\ u_5 \end{pmatrix} = \begin{pmatrix} 0.000935748 \\ 0.00165794 \\ 0.013329 \\ -0.00209243 \\ -0.00372016 \\ 0.00457517 \end{pmatrix}$$

Major-axis vector: (32.3, -5.69, -20.8), semi-axis length: 33.0

Medium-axis vector: (65.7, -3.41, -6.91), semi-axis length: 15.0

Minor-axis vector: (64.6, -17.9, -16.3), semi-axis length: 8.7